DISSERTATION

GENE-TARGETED MOUSE MODELS PROVIDE NOVEL INSIGHTS INTO STRAIN DIVERSITY AND INTERSPECIES TRANSMISSION OF CHRONIC WASTING DISEASE

Submitted by

Julianna Sun

Graduate Degree Program in Cell and Molecular Biology

In partial fulfillment of the requirements

For the Degree of Doctor of Philosophy

Colorado State University

Fort Collins, Colorado

Fall 2022

Doctoral Committee:

Advisor: Glenn Telling

Eric Ross
Soham Chanda
Rushika Perera

ABSTRACT

GENE-TARGETED MOUSE MODELS PROVIDE NOVEL INSIGHTS INTO STRAIN DIVERSITY AND INTERSPECIES TRANSMISSION OF CHRONIC WASTING DISEASE

Prion diseases are fatal, transmissible neurodegenerative diseases that affect humans and other animals and are caused by the aberrant misfolding of the prion protein (PrP) to a disease-causing form. The term ‘prion’ was coined in 1982 by Stanley Prusiner to denote a small proteinaceous infectious particle which is now known to be the cause of scrapie in sheep, transmissible mink encephalopathy (TME), bovine spongiform encephalopathy (BSE) in cattle, and chronic wasting disease (CWD) in cervids such as deer and elk. Additionally, humans can develop prion diseases via multiple routes – spontaneously in the case of sporadic Creutzfeldt-Jakob disease (CJD), inherited in the cases of fatal familial insomnia (FFI) and Gerstmann-Straussler-Scheinker (GSS) syndrome, or acquired in the cases of variant CJD and Kuru. In addition to classical prion diseases, neurodegenerative diseases such as Alzheimer’s disease, Parkinson’s disease, and Frontotemporal dementia have recently been classified as prion-like diseases due to similar protein misfolding mechanisms critical to these disease pathogeneses. Thus, the exploration of prion disease mechanisms has implications for a variety of neurodegenerative diseases.

The main focus of this thesis will be the characterization of CWD strains and pathogenesis using mouse models of CWD. The disease was first described in Colorado in the 1960s in mule deer and rocky mountain elk and since then has expanded in has expanded in both geographical range and host species range including white-tailed deer, moose, red deer and reindeer. In North America, CWD has now been documented in 30 American states and three provinces in Canada. In addition to cases in North America, CWD has been identified in South Korea as a result of accidental transmission of subclinically infected cervids from Canada.

In 2015, Norway reported a case of CWD in a herd of reindeer, and shortly after also reported cases of CWD in three free-ranging moose, marking the first cases of CWD in Europe. As a result, surrounding countries increased CWD surveillance, and Finland reported two cases of CWD in moose, and Sweden reported four cases of CWD in moose. At the time of writing, 20 reindeer, 11 moose, and two red deer in Norway, four moose in Sweden, and two moose in Finland have been diagnosed as CWD positive in Europe. The persistent spread of CWD raises both ecological and economical concerns thus the characterization of CWD pathogenesis is of utmost importance.

Prions are unlike viral and bacterial pathogens in that their infectious component is entirely proteinaceous. The templated conversion of PrP^{C} to PrP^{Sc} is driven by PrP^{Sc} imposing its infectious conformation onto PrP^{C}. In other words, there are no primary structural differences between PrP^{C} and PrP^{Sc} and thus higher order structural differences between PrP^{C} and PrP^{Sc} must account for infectivity of PrP^{Sc}. This is confirmed by recently solved cryogenic-electron microscopy structures of PrP^{Sc} which show an insoluble, β-sheet rich protein structure, as opposed to the soluble, α-helical rich PrP^{C} conformation. Though all heritable information is encoded in protein conformation, prions can exhibit strain characteristics similar to other pathogens. Strains are operationally defined by characteristics such as time to disease onset, clinical signs, and neuropathology. While these characteristics can be defined in the natural disease host, the use of the mouse bioassay has facilitated the ease of strain typing.

Since the primary structure of mouse PrP is slightly different than cervid PrP, transmission of CWD to mice is generally inefficient. Our and other labs combat this by the design of transgenic mice expressing cervid-PrP. Specifically, the Telling lab designed prototype transgenic overexpressing cervid-PrP mice, expressing either glutamate (E) or glutamine (Q) at residue 226 of PrP. This is the only primary structural difference between CWD susceptible cervid species: North American elk express E226, while deer, moose, and reindeer express Q226.

Our lab then designed gene-targeted mice which express endogenous levels of cervid-PrP, either E226 or Q226 expressing. These mice serve as a proxy to characterize CWD strain characteristics and lend insight into the pathogenesis of CWD. The work included in this thesis largely utilizes these mice to answer fundamental questions pertaining to CWD. These questions include: 1. What effect does the polymorphism at residue 226 of cervid PrP have on CWD pathogenesis? 2. How do the strain profiles of emergent cases of Nordic CWD compare to well-characterized cases of North American CWD? 3. Did CWD originate from a cross species transmission, and what is the potential for further cross species transmission of CWD?

ACKNOWLEDGEMENTS

This work represents the culmination of my time here at CSU and would not have been possible without the support of the following members of the Telling lab: Jifeng Bian, Sehun Kim, Jenna Crowell, Bailey Webster, Emma Raisley and Sarah Kane. I would like to personally thank each individual for their contribution to the data generated in this dissertation. The entire Telling lab has provided unwavering support to me throughout the years, and I would not have reached this point without their company. The Prion Research Center provided comradery and a sounding board for new ideas and collaboration and generally fostered an environment that has encouraged my growth as a scientist. I would also like to thank Drs. Eric Ross, Soham Chanda and Rushika Perera for serving as my committee members and providing insightful input throughout my years here. I also acknowledge Dr. Carol Wilusz, CMB program director, who has fielded my endless questions and gone above and beyond for me as a student.

I would next like to thank family and friends who have shown me unwavering support. The endless encouragement has surely shaped me into the person I am today. Thank you to my parents who have patiently listened to scientific ramblings over the years and have always supported me in all my endeavors, scientific or otherwise. Thank you to all the friends I've made in Colorado throughout this journey and who have become family along the way. I would also like to thank Wyatt Beyers who has provided much needed emotional support during this thesis writing process and who also has never forgone a late-night scientific discussion.

I would additionally like to thank all of my educators and mentors over the years. My teachers, even from elementary school instilled in me a curiosity for knowledge and inspired in me a love for learning. I thank Dr. Weihong Lin and the entire Lin Lab at the University of Maryland, Baltimore County who mentored me as an undergraduate student in the lab. Without this first lab experience I may have never pursued research as a career.

Finally, I acknowledge my thesis mentor Dr. Glenn Telling. I thank him for graciously taking a chance on me and demonstrating what a life-long passion for science should look like. I am the scientist I am today because of him and I thank him for believing in me.

DEDICATION

To all of the mice whose lives were given

to further our scientific understanding.

TABLE OF CONTENTS

LIST OF TABLES

LIST OF FIGURES

CHAPTER 1 - INTRODUCTION

A Historical Perspective

In the mid-eighteenth century, sheep farmers in Great Britain noted behavioral changes in their animals including pruritus, or an itchiness leading to scraping off their wool, tremors, and locomotor incoordination that slowly progressed to recumbency and death (1). The disease was termed “scrapie” and though not discovered for more than two centuries, the race to determine the cause began.

In the 1920s, Drs. Hans Gerhard Creutzfeldt and Alfons Maria Jakob first described an unusual neurological disease in humans that would later be attributed to the same class of pathogen as sheep scrapie (2,3). Initially, the disease was coined “spastic pseudosclerosis” due to the characteristic muscular atrophy and slowly deteriorating mental state of patients (4). Creutzfeldt first diagnosed a 23 year old patient who presented with an unprecendented neurological disease to which she succumbed two and a half years later (2). Postmortem analysis of her brain revealed previously undocumented alterations in the subcortical nuclei and grey matter of the cerebral cortex. Three more diagnoses of the same disease phenotype were made the following year by Jakob (3). Later, the disease came to be recognized as Creutzfeldt-Jakob disease (CJD) for the discovering pathologists.

Shortly after, in 1947, mink farmers in Wisconsin documented a neurological disease which manifested as mink having difficulty eating coupled with a general decline in grooming behaviors (5,6). It later was named transmissible mink encephalopathy (TME), and has been attributed to farmed mink consuming foodstuffs contaminated with diseased cattle or sheep (7). Across the globe in 1957 and working with the Fore people of Papau New Guinea, Dr. Carlton Gadjusek documented a related fatal, human neurodegenerative disease – Kuru, meaning to tremble from fever or cold. A linguistic group comprised of multiple tribes, the Fore people participated in cannibalistic funeral rituals which Gadjusek hypothesized resulted in the spread

of Kuru (8). This was confirmed by experiments done in his laboratory in which he and his colleague Joseph Gibbs inoculated chimpanzees with human brains infected with Kuru, and in turn, the chimpanzees succumbed to Kuru (9). Gajusek later was awarded the nobel prize in 1976 for his work on Kuru.

In a northern Colorado research facility in the late 1960s, researchers noted a fatal wasting syndrome in mule deer (*Odocoileus hemionus hemionus*) later coined chronic wasting disease (CWD) (10,11). Retrospective studies also revealed CWD infection in mule deer and black-tailed deer (*Odocoileus hemionus columbianus*) at the Toronto Zoo starting in 1973 (12). At the time, the leading hypothesis for the etiology of these similar yet diverse group of diseases was a slow-acting virus as the unknown diseases shared a variety of characteristics with already characterized viral diseases. However, it was not until a meticulously designed experiment from Stanley Prusiner's laboratory in 1982 revealed that the infectious agent in scrapie was solely proteinaceous, that these diseases were conclusively linked (13). Prusiner coined the term 'prion' to denote a small proteinaceous infectious particle that we now recognize to be the cause of scrapie, CJD, TME, Kuru, and CWD (see table 1.1 for exhaustive list of prion diseases). Prion diseases, also known as transmissible spongiform encephalopathies (TSEs), are pathologically characterized by fatal neurodegeneration caused by the misfolding of the prion protein (PrP) which results in spongiform degeneration, astrocytic gliosis, and amyloidgenic plaques.

A neurological aberration in cattle was noted in 1986 in the United Kingdom (UK), and another prion disease was discovered: bovine spongiform encephalopathy (BSE), colloquially known as mad cow disease (14). BSE-contaminated central nervous system (CNS) matter was fed to cattle and those cattle were distributed for consumption by humans. As a result, strict regulations about feeding rendered meat and bone meal to cattle were put in place, and BSE has virtually been eliminated in the UK (https://www.gov.uk/government/publications/bse-in-england-epidemiology-report-2021).

Table 1.1 Prion Diseases. Table of prion diseases, affected species, year described, and the known causes

Disease	Species Affected	First described (year)	Cause
Classical Scrapie	Sheep, goats	1732 (1)	Acquired, sporadic
Atypical Scrapie	Sheep, goats	2003 (174)	Sporadic
Classical Bovine Spongiform Encephalopathy	Cattle, exotic ungulates	1986 (14)	Acquired, sporadic
Atypical H-type Bovine Spongiform Encephalopathy	Cattle	2004 (175)	Sporadic
Atypical L-type Bovine Spongiform Encephalopathy	Cattle	2004 (58)	Sporadic
Feline Spongiform Encephalopathy	Felines (domestic and zoo)	1990 (176)	Acquired
Transmissible Mink Encephalopathy	Mink	1947 (5,6)	Acquired
Chronic Wasting Disease	Cervids (deer, elk, moose, reindeer etc)	1967 (10)	Acquired, sporadic
Camelid Prion Disease	Dromedary camels	2015 (177)	Acquired
Sporadic Creutzfeldt-Jakob Disease	Human	1920 (2)	Sporadic
Variant Creutzfeldt-Jakob Disease	Human	1996 (178)	Acquired
Iatrogenic Creutzfeldt-Jakob Disease	Human	1974 (179)	Iatrogenic
Familial Creutzfeldt-Jakob Disease	Human	1924 (180)	Inherited
Kuru	Human	1957 (8,9)	Acquired
Fatal Familial Insomnia	Human	1986 (181)(181)	Inherited
Gerstmann–Straussler–Scheinker syndrome	Human	1936 (182)	Inherited
Variable Proteinase-sensitive Proteinopathy (VPSPr)	Human	2008 (183)	Sporadic

In 1996, the first case of variant CJD (vCJD) was reported and linked to consumption of BSE-contaminated meat (15). Despite the number of BSE cases in cattle totaling 100,000 in 1992, BSE has transmitted to and killed a relatively small number of humans, ~230, but not unexpectedly, mass hysteria ensued as the public learned of an invariably fatal, infectious neurological disease (16). Had swift regulations not been put in place, the repercussions for

public health could have been much greater. Cross-species transmission of BSE to humans also powerfully demonstrated the unpredictable nature of prions, and the economic, sociopolitical and animal and public health consequences.

A Proteinaceous Infectious Agent

The experimental discovery of a novel class of infectious agent led Stanley Prusiner to win the Nobel Prize in 1997, but his work built on the foundation of others and was initially met with controversy. Prusiner argued that the disease causing agent must be proteinaceous whilst other leading groups like the Gadjusek lab promoted the slow-acting virus theory (13,17,18). However nonconformist, Prusiner was not the first to posit a proteinaceous component – other lab groups also noted strange characteristics, atypical of viruses, such as failure to inactivate with formalin fixation when working with scrapie agents (19). Experiments to inactivate the scrapie agent including ionizing and UV irradiation, high temperatures, and high pressures were unsuccessful, all pointing toward a non-viral and non-bacterial origin (13,19–22).

Following these studies, Griffith was the first to definitively speculate self-replicating proteins devoid of host machinery in 1967, though not without pause (23). The central dogma of biology, put forth by Francis Crick just 10 years earlier, clearly states 'the transfer of information from nucleid acid to nucleic acid, or from nucleic acid to protein may be possible, but transfer from protein to protein, or from protein to nucleic acid is impossible' (24). As Griffith put it: the occurrence of a protein agent would not necessarily be embarrassing although it would be most interesting (23).

To build upon this, the Prusiner lab iteratively tested the response of the scrapie agent to a myriad of chemicals and conventional treatments to inactivate other infectious agents and additionally determined the agent's size to be smaller than a virus (13). Though the ideas were not entirely new, Prusiner's experiments convincingly showed the requirement of protein for infection (13). Thus, came the term 'prion' to denote a small *pro*teinaceous *in*fectious particle.

Follow up studies by Bolton, McKinley and Prusiner then showed the amount of scrapie agent in a sample directly correlated with the amount of infection, akin to titer in viral infection (25). Further, they showed a converse relationship between digestion of a sample with proteinase K (PK) which is a protease that digests protein. PK digestion of the scrapie agent reduced prion titer and therefore reduced infectivity in hamsters. With the nature of the scrapie agent determined to be protein, the hunt for the specific disease-causing protein began. Building on the work of the Prusiner lab, more clues came from Bruce Chesebro and Richard Race in 1985 when they identified a mRNA transcript specific to prion protein (PrP) 27-30, named for the size of the protein after gel electrophoresis (26). In the same year, Oesch showed that a host-encoded gene, later named *PRNP*, is responsible for the scrapie agent, rather than a foreign entity (27). Further implication of the cellular prion protein (PrP^{C}) came in 1993 with the advent of the first knockout PrP mouse model (28). Mice devoid of PrP were no longer susceptible to infection with prions, underscoring the requirement of PrP in prion disease pathogenesis (28). Further, the PrP knockout could be rescued by crossing the PrP-null mice with mice expressing the Syrian hamster PrP gene and these mice were then susceptible to hamster prions (28). These arduous, seminal studies coupled with the advances in molecular biology techniques laid the groundwork for the field to exponentially expand at the turn of the millennium.

The Prion Protein: Structure

Since the discovery of the *PRNP* gene and the associated prion protein, the structure of PrP has remained a focus of the field. As the protein-only hypothesis posits, prions self-replicate by conveying the infectious protein conformation (PrP^{Sc}) onto its normally folded counterpart (PrP^{C}) in an iterative fashion (29). The exact mechanism by which this occurs is still an active area of research and aims to address the question of how a change in protein conformation can confer infectivity. In humans, PrP^{C} is encoded by the gene *PRNP* which is located on chromosome 20 and contains 3 exons (30). Exon 3 contains the entire open reading frame

(ORF) and the subsequent protein product (30). *PRNP* and PrP^C is ubiquitously expressed in almost all tissue types but is more highly expressed in CNS tissues (31).

The structure of mouse PrP^C was solved by Riek et al in 1996 using nuclear magnetic resonance (NMR) (32). Shortly following, the entire structure of human PrP^C was solved also by NMR in 2000 by Kurt Wuthrich, contributing to his nobel prize, and the third nobel prize awarded in regard to prion biology (33). These studies showed that the N-terminal domain is largely unstructured, consisting of the signal peptide and copper-binding octapeptide repeats (Figure 1.1A) (32). In humans, the octapeptide repeats consists of the amino acid motif P(H/Q)GGG(−/G)WGQ repeated five times normally, but extra copies of can result in CJD phenotypes (34–40). The globular C-terminal is more structured and its secondary structure comprises largely of three alpha helices and two anti-parallel beta-sheets. The alpha helices span residues 144-154, 173-194, and 200-228 while the anti-parallel beta sheets are located at residues 128-131 and 161-164 (human PrP numbering) (41). Importantly, a polymorphism in the first beta sheet, has a profound bearing on susceptibility to vCJD and sCJD. Humans can express either methionine (M), valine (V) or both at residue 129 of PrP. Of the ~230 cases of vCJD caused by BSE, all but one patient, who was heterozygous MV129, expressed homozygous MM129 suggesting a protective effect of valine at residue 129 (42).

The C-terminal domain structure also accomodates multiple post-translational modifications. PrP^C can exist in three states of glycosylation based on the occupancy of two N-linked glycan sites at asparagine residues 181 and 197 (human PrP numbering) or 180 and 196 (mouse PrP numbering) (43,44). When both glycan sites are occupied, PrP is diglycosylated, or hyperglycosylated. If just one site is occupied (either 181/180 or 197/196), PrP is monoglycosylated. Last, if neither glycan site is occupied, PrP is unglycosylated. Additionally, a disulfide bond exists between cysteine residues 179 and 214 (32). PrP^C is bound via its C-terminus to the cholesterol-rich lipid raft regions of outer leaflet of the plasma membrane by a glycophosphatidylinositol (GPI) anchor (45). Depletion of the GPI anchor in mice results in a

prion disease devoid of spongiosis with unique clinical signs and dense PrP^{Res} plaque deposits (46).

PrP^{C} exists as a primarily alpha helical, monomeric unit that is non-infectious, soluble, and sensitive to digestion with proteinases (Figure 1.1B) (47). In stark contrast, PrP^{Sc} is rich in anti-parallel beta sheets, has a propensity to aggregate into fibrils, and is infectious, insoluble, and relatively resistant to proteinase digestion (41). Because of its insolubility and non-

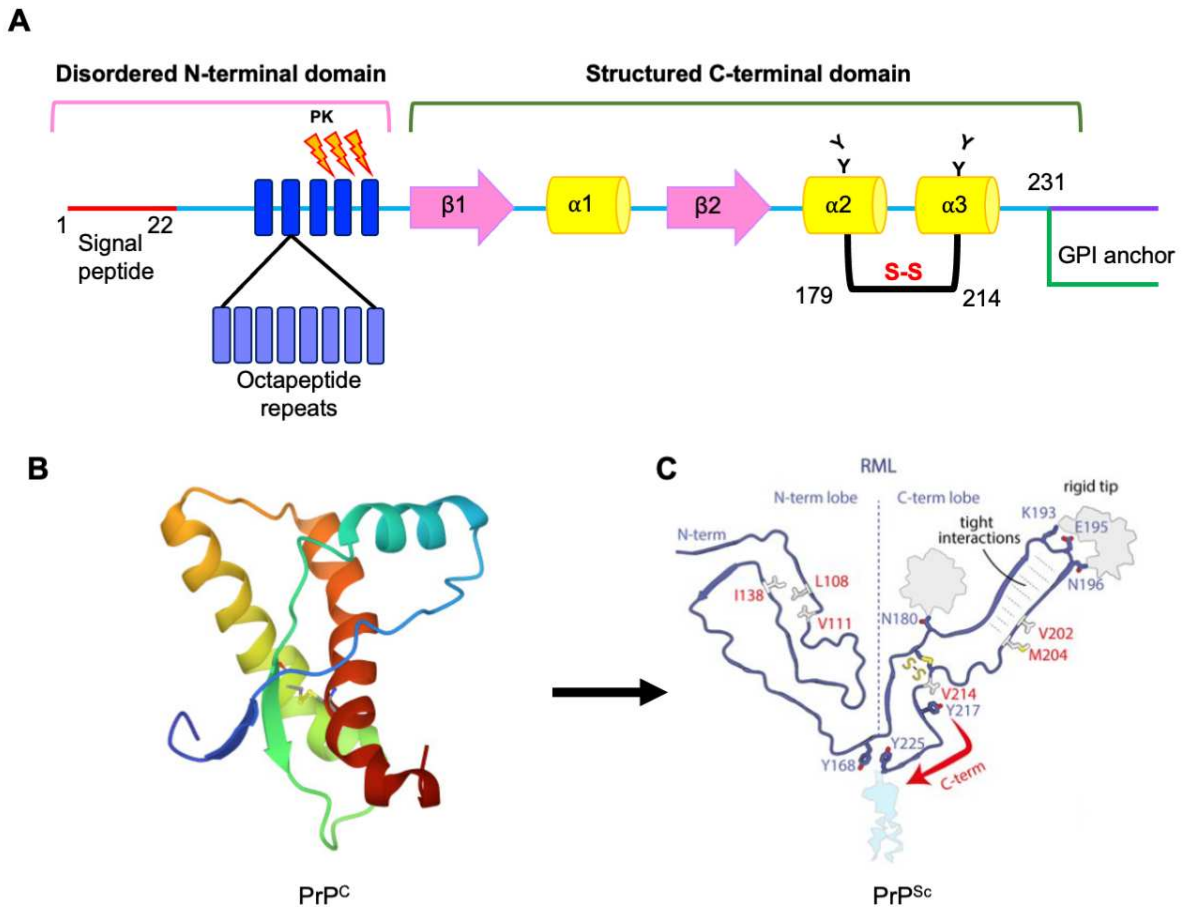

Figure 1.1 Structure of PrP^{C} and PrP^{Sc}. In humans, *PRNP* is encoded on chromosome 20 and contains three exons, the third of which contains the entire PrP coding sequence. (A) Residues 1-22 encode the signal peptide, which is cleaved from the full length protein after processing. The disordered N-terminal domain also contains the octapeptide repeat region. The C-terminal domain is structured and contains three alpha helices and two anti-parallel beta sheets. PrP can be glycosylated at residues 181 and 197, and a disulfide bond exists between cysteine residues 179 and 214. The GPI anchor, existing at the C-terminus, secures PrP to the outer leaflet of the plasma membrane. (B) 3-D reconstruction of mouse PrP 121-231 derived from NMR; PDB: 1AG2. (C) Recent cryo-EM structure of RML mouse prions from Manka et el 2022.

homogenous population of monomers, oligomers and fibrils, the structure of PrP^{Sc} has been refractory to resolution by conventional structural biology methods such as x-ray crystallography and NMR spectroscopy. Though some progress on characterization of PrP^{Sc} from *in vitro* sources such as recombinant PrP has shown promise, specific-infectivities are generally too low to be meaningful (48–51).

Recent advances in cryogenic-electron microscopy (cryo-EM) have allowed multiple labs to obtain structures of ex-vivo bonafide prions. Kraus et al. published the first high-resolution cryo-EM structure, a near atomic structure of hamster 263K prions revealing a parallel in-register intermolecular beta-sheet (PIRIBS) structure comprised of single protofilaments (52). Shortly after, Manka et al. solved the cryo-EM structure of mouse RML prions, also showing a PIRIBS structure comprised of single, paried protofilaments (Figure 1.1C) (53). Hoyt et. al also recently described the cryo-EM structure of anchorless RML, showing a GPI anchor and N-linked glycan deficient structure (54). Though these prions lack GPI anchors and posttranslational modifications, the core amyloidgenic fibril structure is the same of the wildtype RML structure. The first human PrP^{Sc} cryo-EM structure comes from Hallinan et al, where they show Gerstmann-Straussler-Scheinker (GSS) disease prions are amyloidgenic and are comprised of dimeric, trimeric and tetrameric left-handed protofilaments (55). These recent publications offer a new avenue of exploring an aspect of prion disease that not only has eluded prion biologists since the inception of the field, but will have ramifications for the future directions of the field, particularly in relation to strain typing.

Methods for Prion Detection

One of the more difficult aspects of studying prion diseases is the detection of prions in suspect positive samples. Because infectious prions (PrP^{Sc}) share their primary DNA sequence with normal PrP^{C}, discrimination between the two protein conformations is of utmost importance. Historically, reserachers have used proteinase K (PK) to do this. Digestion of a sample

containing prions with PK at a concetration between 10 -100 μg/mL and temperature between 37 - 60° C for 30 –120 minutes will result in PK-resistant core of PrP^{Sc}, deemed PrP^{Res}, which does not exist in PrP^{C} (56). Variation in digestion conditions exists because various prion species are differentially senstitive to digestion with PK (57). The remaining core fragment can be detected via western blotting and can be used to discrimate between prion species depending on the immunoblot profile and reactivity with species specific PrP antibodies (16,58). In addition to detection of PrP^{Sc} in frozen samples, immunohistochemistry and PrP^{Sc} staining technniques are commonly used to look at the distribution of PrP^{Sc} in the both the CNS and non-CNS materials (59,60). Distribution of PrP^{Sc} across a variety of brain regions is fairly consistent within each prion disease, and can be used as a diagnostic tool postmortem. High magnification micrographs can reveal minute amounts of PrP^{Sc}. Staining fixed slides with hematoxylin and eosin (H&E) allows for visualization of tissue architecture and identification of spongiosis (61). Lesion profile scoring, initially developed by Fraser and Dickinson, can then be done to assess the severity of neurodegeneration (62). While western blotting and immunohistology are useful tools for determining whether a sample contains PrP^{Sc}, and in humans can help differentiate between prion diseases and other neurodegenerative diseases with similar clinical presentation such as Alzheimer's disease, these methods require an abundance of PrP^{Sc} which may not be present in small sample sizes or subclinically infected animals.

To address this, in 2001, the Soto lab developed a technique to detect small amounts of PrP^{Sc} called protein misfolding cyclic amplification (PMCA) which capitalizes on the ability of PrP^{Sc} to convert PrP^{C} in an iterative fashion (63). In this assay, a substrate of PrP^{C} is provided to a prion seed to amplify *in vitro*. PMCA utilizes a repetitive sonication at 37° C to amplify a mixture of perfused brain homogenates from mice overexpressing PrP^{C} with a seed of infected brain homogenate. 24-72 cycles of 30 seconds of sonication followed by ~30 minutes of rest time will result in conversion of the uninfected substrate to infectious PrP^{Sc}. The sonication step

breaks up already existing PrP^{Sc} oligomers and fibrils to smaller oligomers. The rest time allows for those smaller oligomers to seed conversion of the substrate and create larger oligomers and fibrils. Repetition of this process eventually results in exponential amplication of the original seed. After rounds of amplification, samples are analyzed for PrP^{Res} via western blotting. For samples with small amounts of initial PrP^{Sc}, serial rounds of PMCA can be performed. PMCA offers a diagnostic answer on a timescale of days versus transmission in the natural host, which can take years (64).

A similar method was developed by the Caughey lab in 2010 and further characterized by the Nishida lab (65,66). Coined real-time quaking induced conversion (RT-Quic), this method uses soluble recombinant PrP as the substrate that is amplified by an infectious prion seed. RT-Quic is even less time consuming than PMCA and does not require the use of uninfected mouse brain homogenates. RT-Quic has allowed detection of low titer prions in non-CNS materials such as urine and feces (67).

The enzyme-linked immunosorbent assay (ELISA) can also be used to detect prions in a sample in an antibody based format. Preliminary studies used from the Collinge lab showed differential glycosylation patterns between PrP^{C} and PrP^{Sc} and further differential glycosylation patterns between PrP^{Sc} strains (68). Our lab also developed a monoclonal PrP antibody that recognizes undergylcosylated PrP, which can be used in an ELISA format to differentiate between uninfected and infected samples (69). Overall, the ELISA offers a quantitative method to detect prions and strain type using glycosylation state-dependent PrP antibodies.

One of the most useful techniques for studying prion disease is the bioassay using lab animals. This capitalizes on the infectious nature of prions and transmissibility between animals. Studying smaller models in a lab, rather than studying disease in the natural host offers a tool to perform large scale experiments in small physical space. The cost of maintaining a mouse colony is also far cheaper than maintaining a deer herd. Mice, hamsters and bank voles have been used as the primary models for the bioassay (70,71). The first mouse models to study

prion disease involved adapting sheep scrapie prions through iterative passage to efficiently infect wildype mice after intracerebral inoculation (72). Mice also offer ease of genetic manipulation, which will be discussed in the context of CWD later. Hamsters and bank voles rapidly propagate multiple prion strains and thus can offer quicker results than mouse models without the need for genetic manipulation (73).

Prion Strains and the Species Barrier

Unlike viruses and bacteria, prions are devoid of any encoding nucleic acid component but still exhibit heritable strain characteristics in a similar manner. Even before the prion hypothesis was brought forth, researchers had noticed and begun to investigate apparent strain differences manifesting as clinical differences in sheep and goats infected with the same preparation of sheep scrapie (74,75). Using hamsters as a model, Bessen and March showed that when inoculated with TME, hamsters displayed two distinct phenotypes in response to infection (76). Some hamsters displayed hyperactivity and succumbed to disease at a mean time of 65 days post inoculation. Other hamsters showed a more lethargic behavioral phenotype and succumbed to disease much later at a mean time of 168 days post inoculation. They coined the two phenotypes hyper-TME (HY-TME) and drowsy-TME (DY-TME). Further investigation showed the PrP27-30 species constituting HY-TME was distinct from the protein conformation causing DY-TME (77).

Strains arise in viruses and bacteria by mutations in their DNA sequence (78). Early studies on scrapie strains provided evidence for a viral etiology rather than proteinaceous since no difference exists in the primary structure between PrP^{C} and PrP^{Sc} (79). Since disproven, prion strain information is inferred to then be encoded in the higher order conformations of the protein (80). Glenn Telling showed in 1996 that the PrP^{Sc} species in fatal familial insomnia, had a transmissible, protease resistant core with a size of 19kD, and was a distinct size from other forms of human prion diseases which have protease resistant cores around 21kD (80). As the

first cryo-EM structure of PrP^{Sc} was published less than one year ago at the time of writing, prion strains have historically had to be defined by operational properties. These include time to disease onset, clinical signs, neuropathological features such as distribution of PrP^{Sc}, and conformational stability in response to denaturation with chaotropic agents (81).

The emergence of multiple different phenotypes resulting from infection with the same original prion preparation can be explained by the conformational selection model of prion strains (48). This hypothesis posits that in a prion infected animal, multiple different conformations of PrP^{Sc} may exist, but the recipient animal may be more susceptible to one conformation over the others. In turn, the recipient animal's PrP^{C} will be converted to PrP^{Sc} by the dominant infecting conformation, and this becomes the conformation that will propagate thus more. The conformational selection model can also help to describe the species barrier that prevents facile transmission of prions between species (82). One single conformation out of all of the conformations in a prion infected animal could be optimal for conversion of another species' PrP. Subsequent passaging through the new animal host allows for the original prion to adapt and optimize infection in a new host. In this model, prions behave as quasispecies, and a strain represents a pool of different prion species under control of the host (83).

In addition to conformational differences denoting strains, posttranslational modifications and host factor interactions could contribute to prion strain differentiation. For example, it has been shown using PMCA, undersialylated PrP^{C} is more readily converted than oversialylated PrP^{C} (84,85). Sialylation referes to the addition of sialic acid to an N-linked glycan (86). Additionally, Kang, Bian and Kane et al. showed that while PrP^{C} primarily exists in the fully glycosylated state, PrP^{Sc} is relatively underglycosylated (69). The role of sialylation and glycosylation in PrP conversion are still open areas of investigation in the field. Much work has also been done in exploring the role of host factors in prion conversion (87). Cellular cofactors such as RNA and lipids have been shown to influence prion tropism (88–90). The importance of cofactors in prion genesis is underscored by the generation of lower titer, less infectious

recombinant prions by removing cofactors from PMCA (91). Further investigation into structural differences between prion strains can help to predict the transmissibility, both inter- and intraspecies, of newly emergent prion strains.

Prion-like Diseases

In recent years, multiple other neurodegenerative diseases have earned the designation of 'prion-like diseases' (92). Several other disease-causing host proteins have been documented to have amyloid seeding activity. For example, in Alzheimer's disease, amyloid-beta forms extracellular amyloidgenic plaques while tau forms intracellular tangles (93). α-synuclein in Parkinson's Disease (PD), TDP-43 and SOD1 in Amyotrophic lateral sclerosis (ALS), and the huntingtin protein in Huntington's disease (HD) all have prion-like qualities in their propensity to aggregate (94,95). Furthermore, α-synuclein exhibits strain properties similar to prion disease strains (96). The unifying theme is the propensity for a protein to misfold, causing neuronal aberrations. Whether or not protein misfolding is the cause of disease, or a downstream effect of the real etiology of these neurodegenerative diseases, using prion diseases as a proxy for other neurodegenerative diseases can give insight into the mechanisms behind them.

Chronic Wasting Disease

Etiology

CWD was first identified in 1967 in mule deer (*Odocoileus hemionus hemionus*) at a research facility owned by Colorado State University, located in Northern Colorado (10,11). The mystery disease was classified as a prion disease based on neuropathological similarities to other previously characterized prion diseases. Afflicted deer display gradual loss of good body condition including severe weight loss, generalized depressive behavior, and loss of fear of

humans (97). The clinical course can extend between three and four months in mule deer, and terminal clinical signs include polydipsia, polyuria, sialorrhea and generalized incoordination. After the initial discovery, CWD was also found at a research facility in Wyoming in mule deer and also in captive Rocky Mountain elk (*Cervus elaphus nelsoni*) in both the Colorado and Wyoming facilities. Surveillance additionally revealed CWD cases in free-ranging mule deer and elk in Colorado and Wyoming (11). Since there was no surveillance prior to its identification at the research facilities, it is likely that CWD was present in the endemic region years before its recognition (98). In addition to geographical spread in North America, CWD has spread in affected cervid species. CWD has been identified in both captive and wild North American moose (*Alces alces shirasi*) and on a red deer farm in Quebec, Canada (99–101). Experimental transmission to Canadian caribou, or reindeer (*Rangifer tarandus tarandus*) from elk or white-tailed deer via the oral route has also been shown (102) The Mathiason lab has also shown successful experimental transmission to Reeves' Muntjac Deer (*Muntiacus reevesi*) (103). The Richt lab showed intracerebral transmission of white tail deer CWD caused disease in 4 out of 13 fallow deer (*dama dama*) (104). However, when cohoused with infected mule deer, no disease occurred in fallow deer (105).

Unique to CWD, the disease exists in both captive farmed and wild animals; all other animal prion diseases have only been identified in farmed or domestic animals, like BSE in livestock cattle, scrapie in sheep and goat herds, TME in farmed mink and FSE in domestic and zoo cats. Even more worrisome, the prevalence of CWD in free-ranging cervids has been recorded to be as high as 30% in some areas, in accordance with the extraordinary contagiousness of the disease (97). Efforts to eradicate CWD are largely unsuccessful, with CWD now present in 30/50 states and 3 Canadian provinces (Figure 1.2A). Additionally, subclinically infected animals were shipped to South Korea from a Canadian farm and now South Korean deer farms cannot eradicate CWD from their farmed animals (106,107).

In 2016, for the first time, CWD was detected in Europe, specifically Norway. As a team approached a herd of free-ranging reindeer (*Rangifer tarandus tarandus*) in southern Norway to radio-collar them as part of a larger study on reindeer, they found one reindeer separated from the herd (108). The animal left tracks in the snow indictive of uneven gait, and later the reindeer was found recumbent and died shortly after discovery. Confirmatory diagnosis was made using a commercially available Enzyme-Linked Immunosorbent Assay (ELISA) test for detection of PrP^{Res}, or protease-resistant PrP. National surveillance further revealed evidence of CWD in more reindeer from the same herd, three European moose (*Alces alces alces*) and one red deer (*Cervus elaphus*) (109,110). Additional mandatory surveillance in European Union states with moose and reindeer populations led to detection of CWD in two moose in Finland, and four moose in Sweden (Figure 1.2B) (111). Continual survelliance in Norway has revealed ~ 20 reindeer, 11 moose, and 3 red deer with CWD (Figure 1.2B). Initial immunohistochemistry and western blots suggested Nordic moose and red deer CWD are of a distinct etiology from the

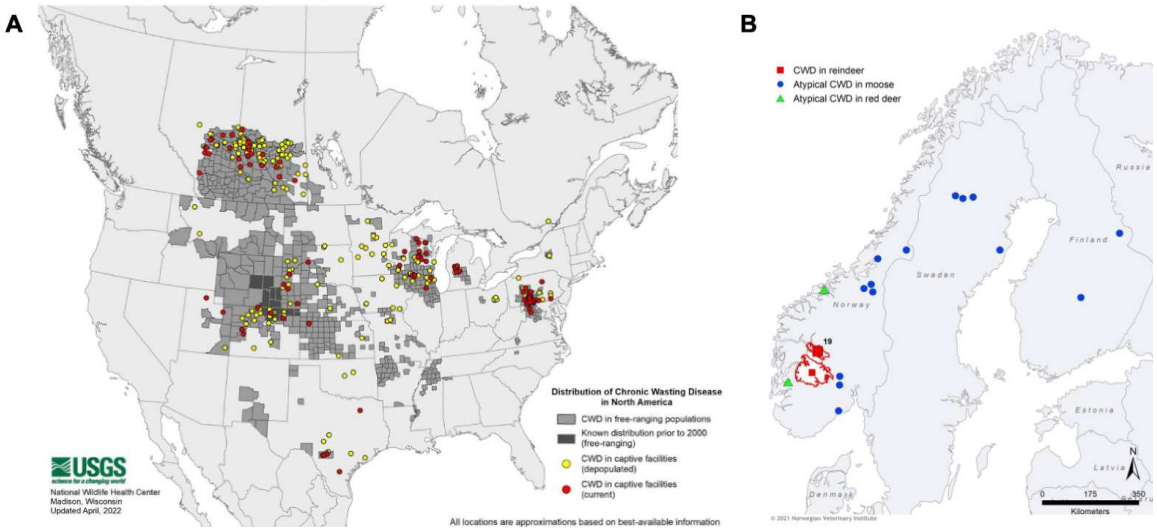

Figure 1.2 Maps depicting CWD distribution. (A) Map of North America updated April 2022 indicating CWD cases in counties prior to 2000 (dark grey) and after 2000 (light grey). Yellow dots indicate CWD in captive facilities that have been depopulated while red dots indicate active CWD cases in captive facilities. Source: https://www.usgs.gov/media/images/distribution-chronic-wasting-disease-north-america-0 (B) Map of Norway, Sweden and Finland updated November 2021 indicating newly discovered CWD cases in reindeer (red squares), moose (blue circles) and red deer (green triangles). Source: Tranulis et. al 2021 (112).

endemic North American CWD (112). Complimentary analyses by the Telling lab using mouse bioassay and the Nonno lab using bank vole bioassay confirmed the distinct etiology and postulated a new origin for Nordic cases of CWD (113,114).

Transmission and Pathogenesis

Similar to other animal prion diseases, CWD is experimentally transmissible between cervids after intracerebral inoculation (11). Depending on the species, the latent incubation period can last up to two years (11). However, it is highly unlikely that wild cervids are transmitting CWD to each other via intracerebral inoculation. Instead, transmission via shedding of CWD into the environment poses the more likely infection route. In North American cervids, PrP^{Sc} has been detected in abundance in lymphoid tissue starting early in disease pathogenesis; North American CWD is thus considered lymphotropic prion (115). In addition to lymphoid tissue, CWD has been detected in skeletal muscle, cardiac muscle, pancreas, and adrendal gland tissue (116–119). By bioassay, CWD prions have also been detected in saliva, blood, urine, antler velvet, spleen and muscle (120–123). Multiple research groups have also shown that infectious CWD prions can be detected in fecal material even from subclinically infected deer (121,124). Taken together, the likelihood that infected cervids shed CWD into the environment is fairly high. Further evidence points to the ability of CWD to bind soil and plants, persist in the environment for years and remain infectious (125,126).

The contagiousness of CWD is unparalleled among other prion diseases (10,97,98). This is demonstrated by a captive mule deer population of which 90% developed CWD in a two year span (10). Lateral transmission, either directly from animal to animal or indirectly from the environment is thought to be the primary mode of transmission (127). It was however recently shown in Muntjac deer that vertical transmission, from mother to offspring, is also a possible

route of transmission (128). Further, via PMCA, CWD prions can be detected in fetal tissue in white tail deer (128,129).

As evidenced by the transmission of BSE from cattle to humans, animal prion diseases have the potential to cross species barriers with tremendous repercussions. The transmissibility of CWD between cervids raises concerns for spillover to other animal species, particularly because of the close proximity of farmed species to both wild and farmed cervids and their shared grazing lands. Perhaps of greater concern is the potential for humans to develop prion disease resulting from the consumption of CWD contaminated meat. In Colorado alone, Colorado Parks and Wildlife sold ~345,000 cervid hunting licences for the 2021 hunting season (https://cpw.state.co.us/Documents/Hunting/BigGame/Statistics/Deer/2021StatewideDeerHarvest.pdf). Our lab has shown that CWD can be detected in skeletal muscle of deer, and the Chesebro lab has detected CWD in fat, so the likelihood that hunters are consuming CWD prions is extremely high (117,130). Additionally, CWD has been detected in antler velvet, raising concern for the large demand for use in traditional Asian medicine (122). Studies using transgenic mice expressing human PrP^{C} have largely failed to show any conversion of CWD (131–133). The Gilch lab has recently shown intracerebral transmission of white-tailed deer CWD to M129-human PrP 6x overexpressing mice (134). While these mice exhibited clinical signs and passaged brain material showed high amplification, western blotting and histology failed to readily detect hallmark PrP^{Sc}. Using CWD as a seed, Barria et. al showed human PrP can be converted via PMCA if the CWD seed has been stabilized either *in vitro* or *in vivo* prior to amplification (135). Additonally, CWD transmission to squirrel monkeys (*Saimiri sciureus*), a nonhuman primate, was showed via the intracerebral inoculation route (136,137). Transmission results of CWD to macaques, the closest tested relative to humans, are mixed (138). In 2018, Race et. al showed no transmission of CWD from deer or elk to cynomolgus macaques (139). Yet, ongoing studies show potential transmission, with some macaques showing clinical signs

including evidence of wasting (140). Evenso, there has not been shown to be any definitive CWD transmission to humans (141,142).

Studies with transgenic mice overexpressing ovine or bovine mice inoculated with CWD prions have not shown convincing interspecies transmission (133). However, the Greenlee lab recently showed oronasal transmission from mule deer to Suffolk sheep resulted in subclinical disease in one of seven inoculated sheep (143). Additionally, domestic cats succumb to feline-adapted CWD after multiple passages (144). Concern for predators that hunt and consume cervids has also been increasing with the spread of CWD. After consumption and passage through the digestive tract of mountain lions, detectable CWD decreases by >96% (145). Yet, passage through digestive tracts of coyotes, crows and earthworms does not affect infectivity, and CWD prions remain infectious (146–148).

CWD Strains

While CWD has spread across the United States and into Canada, the strain variation across North America is quite low. To address the effect of cervid species and geographic location on CWD strains, the Telling lab generated transgenic mice expressing cervid PrP, Tg(CerPrP)1536$^{+/-}$, and isolates from captive and wild mule deer, white-tailed deer and elk were intracerebrally inoculated into the mice (149). Angers and Kang et al showed the emergence of two distinct CWD prion strains, termed CWD1 and CWD2 (149). The two strains, when passaged in mice produce different neuropathological and clinical features. Further, transmissions of CWD from elk produced either the CWD1 or CWD2 phenotype, while transmissions of CWD from deer sometimes produced a mixed phenotype between CWD1 and CWD2, suggesting that deer brains may harbor strain mixtures more readily than elk brains. Strain differences between deer and elk may exist due to a polymorphism expressed at residue 226 of cervid PrP. Elk express glutamate (E), while deer, moose, and reindeer express

glutamine (Q) (150). Red deer are polymorphic and can express either E or Q or both E and Q at residue 226 (150).

Since it is known the origin of CWD in South Korea is importation of subclinically infected animals from Canada, the CWD strains in South Korea are largely identical to North American strains, CWD1 and CWD2 (unpublished data from the Telling lab). The discovery of CWD in Norway, Sweden and Finland raises questions about the emergence of new CWD strains in these regions. Studies in bank voles revealed different incubation times, PrP^{Sc} profiles, neuropathology and deposition between Norwegian and North American CWD strains (114). Bioassays in gene-targeted mice also reveal stark differences in the transmission properties of Norwegian reindeer, Norwegian moose, and North American CWD (113).

Transgenic Mouse Models

Which much research has been done in CWD in the natural cerivd hosts, long incubation times and the expense of housing cervids present challenges for using the natural host as an experimental host (120). Due to the species barrier, wildtype mice are largely resistant to infection with CWD (151). To eliminate the species barrier, a variety of transgenic mouse models expressing cervid-PrP have been developed. Additionally, to facilitate the study of other prion diseases, transgenic mice expressing bovine, ovine, mink and human PrP were created and provided evidence that CWD could be studied using a similar approach (152–160). The Telling lab designed the first prototype transgenic cervid mice expressing deer PrP (Q226), $Tg(CerPrP)1536^{+/-}$ (151). These mice, when intracerebrally incolated with CWD, were able to recapitulate diseae pathogenesis and the resulting neuropathological hallmarks. Shortly after, comparable mouse models expressing either deer or elk PrP from the Telling lab along with multiple other labs confirmed the success of the mouse bioassay to study CWD (122,133,161–163). The advent of CWD-susceptible mice has allowed a means to study existing strain properties and generate novel cervid prion strains (164–166). In addition to strain properties,

cervid mouse assays have been able to parse the mechanism of transmission of CWD between deer and elk such as through excretion and exchange of bodily fluids (120,121,124,167) Transgenic cervid mice also provide a facile way to assess interspecies transmission of CWD prions, especially risk to humans (117,122,130).

Transgenic mouse models also give researchers the ability to study PrP polymorphisms and their effects on CWD susceptibility and transmission. For example, the elk PrP sequence is polymorphic at residue 132 and either methionine (M) or leucine (L) can be expressed (168,169). The allele is equivalent to codon 129 in human PrP, which harbors the M/V polymorphism that has bearing on susceptibility to CJD. Studies in the natural host show that L132 confers partial resistance to CWD (170–172). To further explore the mechanism of resistance conferred by L132, the Telling lab created transgenic elk PrP mice expressing either M132 or L132 (173). As expected, CerPrP-L132 mice were partially resistant to inoculation with CWD. However, when inoculated with SSBP/1 sheep scrapie prions, disease developed efficiently in the L132 mice, indicative of strain specific resistance conferred by the 132 polymorphism (173).

Though the transgenic cervid mice have increased understanding about the pathogenesis of CWD, uncontrolled insertion of an overexpressed transgene could lead to an artificial system. Additionally, a key feature of CWD is its ability to replicate in the periphery of cervids and infiltrate the lymphatic system. Tg(CerPrP) mice do not recapitulate the lymphotropic qualities of natural CWD and PrP^{Sc} is not detected in peripheral tissue (123). To combat this, the Telling lab designed the next generation of cervid-PrP mice in which a gene-targeted approach was used to replace the coding sequence of mouse *Prnp* with cervid *PRNP* via homologous recombination in embryonic stem cells (123). Since homologous recombination was used, expression of cervid PrP is driven by the endogenous mouse promoter and thus wild type levels of cervid PrP are expressed. Additionally, CWD prions are detectable in lymphoid tissue such as spleen, and also skeletal muscle in the infected mice, indicating recapitulation of

peripheral replication. Further evidence of lymphoid accumulation is shown by the ability of CWD prions to cause disease in gene-targeted mice via intraperitoneal inoculation, rather than intracerebral. In order to more fully assess the effects of the E/Q226 polymorphism of cervid PrP on disease pathogenesis, the Telling lab created gene-targeted mice expressing either E226 or Q226. Inoculation of these mice with multiple CWD isolates show distinct strain characteristic when propagated through each mouse line (123).

Summary

Prion diseases have been documented for hundreds of years. Yet, advancements in the past ~50 years have greatly improved our cellular and molecular understanding of prion disease pathogenesis; however, many unanswered questions remain. This dissertation will aim to answer three major questions. 1. How does CWD accumulate over time during disease, and what bearing does the E/Q 226 polymorphism have on this? 2. What is the etiology of CWD emerging in Nordic countries and just how different is it from North American CWD? 3. What is the potential for interspecies transmission of CWD, and could the origin of CWD, either North American or Nordic be from interspecies transmission?

REFERENCES

1. M'Gowan JP. Investigation into the Disease of Sheep called" Scrapie"(Traberkrankheit; La Tremblante) with Especial Reference to its Association with Sarcosporidiosis. Edinburgh: William Blackwood & Sons; 1914.

2. Creutzfeldt HG. Über eine eigenartige herdförmige Erkrankung des Zentralnervensystems (vorläufige Mitteilung). Gesamte Neurol Psy. 1920;57:1–18.

3. Jakob AM. Über eigenartige Erkrankungen des Zentralnervensystems mit bemerkenswertem anatomischen Befund (spastische Pseudosklerose-Encephalomyelopathie mit disseminierten Degenerationsherden). Dtsch Z Nervenheilkd. 1921;

4. Davison C. Spastic Pseudoschlerosis (Disseminated Encephalomyelopathy; corticopallidospinal Degeneration). Arch Neurol Psychiatry. 1940;44(3):578–98.

5. Hartsough GR, Burger D. Encephalopathy of mink. I. Epizootiologic and clinical observations. J Infect Dis [Internet]. 1965;115(4):387–92. Available from: https://www.ncbi.nlm.nih.gov/pubmed/5891240

6. Burger D, Hartsough GR. Encephalopathy of mink. II. Experimental and natural transmission. J Infect Dis [Internet]. 1965;115(4):393–9. Available from: https://www.ncbi.nlm.nih.gov/pubmed/5837893

7. Robinson MM, Hadlow WJ, Huff TP, Wells GAH, Dawson M, Marsh RF, et al. Experimental infection of mink with bovine spongiform encephalopathy. Journal of General Virology. 1994;75(9):2151–5.

8. Liberski PP. Kuru: A journey back in time from papua new guinea to the Neanderthals' extinction. Vol. 2, Pathogens. 2013. p. 472–505.

9. Gajdusek DC, Zigas V. Kuru. Clinical, pathological and epidemiological study of an acute progressive degenerative disease of the central nervous system among natives of the Eastern Highlands of New Guinea. Vol. 26, The American Journal of Medicine. 1959. p. 442–69.

10. Williams ES, Young S. Chronic wasting disease of captive mule deer: a spongiform encephalopathy. J Wildl Dis. 1980;16(1):89–98.

11. Williams ES, Young S. Spongiform encephalopathies in Cervidae. Revue Scientifique et Technique. 1992;11(2):551–67.

12. Dubé C, Mehren KG, Barker IK, Peart BL, Balachandran A. Retrospective investigation of chronic wasting disease of cervids at the Toronto Zoo, 1973-2003. Canadian Veterinary Journal. 2006;47(12):1185–93.

13. Prusiner SB. Novel proteinaceous infectious particles cause scrapie. Science (1979). 1982;216(4542):136–44.

14. Wells GA, Scott AC, Johnson CT, Gunning RF, Hancock RD, Jeffrey M, et al. A novel progressive spongiform encephalopathy in cattle. Vet Rec. 1987;121(18):419–20.

15. Wilesmith JW, Ryan JB, Atkinson MJ. Bovine spongiform encephalopathy: epidemiological studies on the origin. Vet Rec. 1991;128(9):199–203.

16. Hill AF, Desbruslais M, Joiner S, Sidle KCL, Gowland I, Collinge J, et al. The same prion strain causes vCJD and BSE. Vol. 389, Nature. 1997. p. 448–50.

17. Gajdusek DC, Gibbs CJ. Slow, latent and temperate virus infections of the central nervous system. Res Publ Assoc Res Nerv Ment Dis. 1968;44:254–80.

18. Field EJ. Slow virus infections of the nervous system. Vol. 8, International Review of Experimental Pathology. 1969. p. 129–239.

19. Pattison IH. Resistance of the scrapie agent to formalin. J Comp Pathol. 1965;75(2):159–64.

20. Hunter GD, Millson GC. Studies on the heat stability and chromatographic behaviour of the scrapie agent. J Gen Microbiol. 1964;37:251–8.

21. Alper T, Haig DA, Clarke MC. The exceptionally small size of the scrapie agent. Biochem Biophys Res Commun. 1966;22(3):278–84.

22. Alper T, Cramp WA, Haig DA, Clarke MC. Does the agent of scrapie replicate without nucleic acid? Nature. 1967;214(5090):764–6.

23. Griffith JS. Self-replication and scrapie. Nature. 1967;215(5105):1043–4.

24. Crick F. Central dogma of molecular biology. Nature. 1970;227(5258):561–3.

25. Bolton DC, Mckinley MP, Prusiner SB. Identification of a protein that purifies with the scrapie prion. Science (1979). 1982;218(4579):1309–11.

26. Chesebro B, Wehrly K, Nishio J, Bloom M, Lechner D, Bergstrom S, et al. Identification of scrapie prion protein-specific mRNA in scrapie-infected and uninfected brain. Nature. 1985;315(6017):331–3.

27. Oesch B, Westaway D, Wälchli M, McKinley MP, Kent SBH, Aebersold R, et al. A cellular gene encodes scrapie PrP 27-30 protein. Cell. 1985;40(4):735–46.

28. Büeler H, Aguzzi A, Sailer A, Greiner RA, Autenried P, Aguet M, et al. Mice devoid of PrP are resistant to scrapie. Cell. 1993;73(7):1339–47.

29. Ma J, Wang F. Prion disease and the “proteinonly hypothesis.” Essays Biochem. 2014;56(1):181–91.

30. Westaway D, Cooper C, Turner S, da Costa M, Carlson GA, Prusiner SB. Structure and polymorphism of the mouse prion protein gene. Proc Natl Acad Sci U S A. 1994;91(14):6418–22.

31. Uhlén M, Fagerberg L, Hallström BM, Lindskog C, Oksvold P, Mardinoglu A, et al. Tissue-based map of the human proteome. Science (1979). 2015;347(6220):1260419.

32. Riek R, Hornemann S, Wider G, Billeter M, Glockshuber R, Wuthrich K. NMR structure of the mouse prion protein domain PrP(121-231). Nature. 1996;382(6587):180–2.

33. Zahn R, Liu A, Lührs T, Riek R, von Schroetter C, Garcia FL, et al. NMR solution structure of the human prion protein. Proc Natl Acad Sci U S A. 2000;97(1):145–50.

34. Pietrini V, Puoti G, Limido L, Rossi G, di Fede G, Giaccone G, et al. Creutzfeldt-Jakob disease with a novel extra-repeat insertional mutation in the PRNP gene. Neurology. 2003;61(9):1288–91.

35. Goldfarb LG, Brown P, McCombie WR, Goldgaber D, Swergold GD, Wills PR, et al. Transmissible familial Creutzfeldt-Jakob disease associated with five, seven, and eight extra octapeptide coding repeats in the PRNP gene. Proc Natl Acad Sci U S A. 1991;88(23):10926–30.

36. Krasemann S, Zerr I, Weber T, Poser S, Kretzschmar H, Hunsmann G, et al. Prion disease associated with a novel nine octapeptide repeat insertion in the PRNP gene. Molecular Brain Research. 1995;34(1):173–6.

37. Campbell TA, Palmer MS, Will RG, Gibb WRG, Luthert PJ, Collinge J. A prion disease with a novel 96-base pair insertional mutation in the prion protein gene. Neurology. 1996;46(3):761–6.

38. Capellari S, Vital C, Parchi P, Petersen RB, Ferrer X, Jarnier D, et al. Familial prion disease with a novel 144-bp insertion in the prion protein gene in a Basque family. Neurology. 1997;49(1):133–41.

39. Yanagihara C, Yasuda M, Maeda K, Miyoshi K, Nishimura Y. Rapidly progressive dementia syndrome associated with a novel four extra repeat mutation in the prion protein gene. J Neurol Neurosurg Psychiatry. 2002;72(6):788–91.

40. Lewis V, Collins S, Hill AF, Boyd A, McLean CA, Smith M, et al. Novel prion protein insert mutation associated with prolonged neurodegenerative illness. Neurology. 2003;60(10):1620–4.

41. Cohen FE, Fletterick RJ, Serban A, Gasset M, Baldwin M, Mehlhorn I, et al. Conversion of alpha-helices into beta-sheets features in the formation of the scrapie prion proteins. Proc Natl Acad Sci U S A. 1993;90(23):10962–6.

42. Kaski D, Mead S, Hyare H, Cooper S, Jampana R, Overell J, et al. Variant CJD in an individual heterozygous for PRNP codon 129. The Lancet. 2009;374(9707):2182.

43. Locht C, Chesebro B, Race R, Keith JM. Molecular cloning and complete sequence of prion protein cDNA from mouse brain infected with the scrapie agent. Proc Natl Acad Sci U S A. 1986;83(17):6372–6.

44. Liao YU, Cheng J., Lebo R v., Clawson GA, Smuckler EA. Human prion protein cDNA: Molecular cloning, chromosomal mapping, and biological implications. Science (1979). 1986;233(4761):364–7.

45. Stahl N, Borchelt DR, Hsiao K, Prusiner SB. Scrapie prion protein contains a phosphatidylinositol glycolipid. Cell. 1987;51(2):229–40.

46. Chesebro B, Race B, Meade-White K, LaCasse R, Race R, Klingeborn M, et al. Fatal transmissible amyloid encephalopathy: a new type of prion disease associated with lack of prion protein membrane anchoring. PLoS Pathog. 2010;6(3):1000800.

47. Pergami P, Jaffe H, Safar J. Semipreparative chromatographic method to purify the normal cellular isoform of the prion protein in nondenatured form. Anal Biochem. 1996;236(1):63–73.

48. Collinge J, Clarke AR. A general model of prion strains and their pathogenicity. Vol. 318, Science. 2007. p. 930–6.

49. Diaz-Espinoza R, Soto C. High-resolution structure of infectious prion protein: The final frontier. Vol. 19, Nature Structural and Molecular Biology. 2012. p. 370–7.

50. Schmidt C, Fizet J, Properzi F, Batchelor M, Sandberg MK, Edgeworth JA, et al. A systematic investigation of production of synthetic prions from recombinant prion protein. Open Biol. 2015;5(12):150–65.

51. Collinge J. Mammalian prions and their wider relevance in neurodegenerative diseases. Vol. 539, Nature. 2016. p. 217–26.

52. Kraus A, Hoyt F, Schwartz CL, Hansen B, Artikis E, Hughson AG, et al. High-resolution structure and strain comparison of infectious mammalian prions. Mol Cell. 2021;81(21):4540–51.

53. Manka SW, Zhang W, Wenborn A, Betts J, Joiner S, Saibil HR, et al. 2.7 Å cryo-EM structure of ex vivo RML prion fibrils. Nat Commun. 2022 Jul 13;13(1):4004.

54. Hoyt F, Standke HG, Artikis E, Schwartz CL, Hansen B, Li K, et al. Cryo-EM structure of anchorless RML prion reveals variations in shared motifs between distinct strains. Nat Commun. 2022;13(1):4005.

55. Hallinan GI, Ozcan KA, Hoq MR, Cracco L, Vago FS, Bharath SR, et al. Cryo-EM structures of prion protein filaments from Gerstmann-Sträussler-Scheinker disease. Acta Neuropathol. 2022 Jul 12;144(3):509–20.

56. Sajnani G, Requena JR. Prions, proteinase K and infectivity. Vol. 6, Prion. 2012. p. 430–2.

57. Safar J, Wille H, Itri V, Groth D, Serban H, Torchia M, et al. Eight prion strains have PrP(Sc) molecules with different conformations. Nat Med. 1998;4(10):1157–65.

58. Casalone C, Zanusso G, Acutis P, Ferrari S, Capucci L, Tagliavini F, et al. Identification of a second bovine amyloidotic spongiform encephalopathy: Molecular similarities with sporadic Creutzfeldt-Jakob disease. Proc Natl Acad Sci U S A. 2004;101(9):3065–70.

59. Kovács GG, Head MW, Hegyi I, Bunn TJ, Flicker H, Hainfellner JA, et al. Immunohistochemistry for the prion protein: Comparison of different monoclonal antibodies in human prion disease subtypes. Brain Pathology. 2002;12(1):1–11.

60. Budka H, Aguzzi A, Brown P, Brucher J -M, Bugiani O, Gullotta F, et al. Neuropathological Diagnostic Criteria for Creutzfeldt-Jakob Disease (CJD) and Other Human Spongiform Encephalopathies (Prion Diseases). Brain Pathology. 1995;5(4):459–66.

61. Fischer AH, Jacobson KA, Rose J, Zeller R. Hematoxylin and eosin staining of tissue and cell sections. CSH Protoc. 2008 May 1;2008:pdb.prot4986.

62. Fraser H, Dickinson AG. The sequential development of the brain lesions of scrapie in three strains of mice. J Comp Pathol. 1968;78(3):301–11.

63. Saborio GP, Permanne B, Soto C. Sensitive detection of pathological prion protein by cyclic amplification of protein misfolding. Nature. 2001;411(6839):810–3.

64. Peden AH, Suleiman S, Barria MA. Understanding Intra-Species and Inter-Species Prion Conversion and Zoonotic Potential Using Protein Misfolding Cyclic Amplification. Vol. 13, Frontiers in Aging Neuroscience. 2021. p. 716452.

65. Atarashi R, Sano K, Satoh K, Nishida N. Real-time quaking-induced conversion: A highly sensitive assay for prion detection. Vol. 5, Prion. 2011. p. 150–3.

66. Wilham JM, Orrú CD, Bessen RA, Atarashi R, Sano K, Race B, et al. Rapid end-point quantitation of prion seeding activity with sensitivity comparable to bioassays. PLoS Pathog. 2010;6(12):1001217.

67. John TR, Schätzl HM, Gilch S. Early detection of chronic wasting disease prions in urine of pre-symptomatic deer by real-time quaking-induced conversion assay. Prion. 2013;7(3):253–8.

68. Khalili-Shirazi A, Summers L, Linehan J, Mallinson G, Anstee D, Hawke S, et al. PrP glycoforms are associated in a strain-specific ratio in native PrPSc. Journal of General Virology. 2005;86(9):2635–44.

69. Kang HE, Bian J, Kane SJ, Kim S, Selwyn V, Crowell J, et al. Incomplete glycosylation during prion infection unmasks a prion protein epitope that facilitates prion detection and strain discrimination. J Biol Chem. 2020;10420–33.

70. Watts JC, Prusiner SB. Mouse models for studying the formation and propagation of prions. Vol. 289, Journal of Biological Chemistry. 2014. p. 19841–9.

71. Arshad H, Bourkas MEC, Watts JC. The utility of bank voles for studying prion disease. In: Progress in Molecular Biology and Translational Science. 2020. p. 179–211.

72. Chandler RL. Encephalopathy in mice produced by inoculation with scrapie brain material. The Lancet. 1961;277(7191):1378–9.

73. Kimberlin RH, Walker CA. Characteristics of a short incubation model of scrapie in the golden hamster. Journal of General Virology. 1977;34(2):295–304.

74. Cuille JCP. Investigations of scrapie in sheep. Investigations of scrapie in sheep Vet Med. 1938;34:417–8.

75. Pattison IH, Jones KM. The possible nature of the transmissible agent of scrapie. Vet Rec. 1967;80(1):2–9.

76. Bessen RA, Marsh RF. Identification of two biologically distinct strains of transmissible mink encephalopathy in hamsters. Journal of General Virology. 1992;73(2):329–34.

77. Bessen RA, Marsh RF. Distinct PrP properties suggest the molecular basis of strain variation in transmissible mink encephalopathy. J Virol. 1994;68(12).

78. Ryu WS. Discovery and Classification. In: Molecular Virology of Human Pathogenic Viruses. 2017. p. 3–20.

79. Bruce ME, Dickinson AG. Biological evidence that scrapie agent has an independent genome. Journal of General Virology. 1987;68(1):79–89.

80. Telling GC, Parchi P, DeArmond SJ, Cortelli P, Montagna P, Gabizon R, et al. Evidence for the conformation of the pathologic isoform of the prion protein enciphering and propagating prion diversity. Science (1979). 1996;274(5295):2079–82.

81. Bessen RA, Kocisko DA, Raymond GJ, Nandan S, Lansbury PT, Caughey B. Non-genetic propagation of strain-specific properties of scrapie prion protein. Nature. 1995;375(6533):698–700.

82. Supattapone S. What makes a prion infectious? Vol. 327, Science. 2010. p. 1091–2.

83. Weissmann C, Li J, Mahal SP, Browning S. Prions on the move. Vol. 12, EMBO Reports. 2011. p. 1109–17.

84. Katorcha E, Makarava N, Savtchenko R, d′Azzo A, Baskakov I v. Sialylation of Prion Protein Controls the Rate of Prion Amplification, the Cross-Species Barrier, the Ratio of PrPSc Glycoform and Prion Infectivity. PLoS Pathog. 2014;10(9):1004366.

85. Makarava N, Chang JCY, Molesworth K, Baskakov I v. Posttranslational modifications define course of prion strain adaptation and disease phenotype. Journal of Clinical Investigation. 2020;140(8):4382–95.

86. Bhide GP, Colley KJ. Sialylation of N-glycans: mechanism, cellular compartmentalization and function. Vol. 147, Histochemistry and Cell Biology. 2017. p. 149–74.

87. Bartz JC. Environmental and host factors that contribute to prion strain evolution. Vol. 142, Acta Neuropathologica. 2021. p. 5–16.

88. Saá P, Sferrazza GF, Ottenberg G, Oelschlegel AM, Dorsey K, Lasmézas CI. Strain-Specific Role of RNAs in Prion Replication. J Virol. 2012;86(19):10494–504.

89. Burke C, Walsh D, Steele A, Agrimi U, di Bari MA, Watts JC, et al. Full restoration of specific infectivity and strain properties from pure mammalian prion protein. PLoS Pathog. 2019;15(3):1007662.

90. Burke CM, Walsh DJ, Mark KMK, Deleault NR, Nishina KA, Agrimi U, et al. Cofactor and glycosylation preferences for in vitro prion conversion are predominantly determined by strain conformation. PLoS Pathog. 2020;16(4):1008495.

91. Deleault NR, Walsh DJ, Piro JR, Wang F, Wang X, Ma J, et al. Cofactor molecules maintain infectious conformation and restrict strain properties in purified prions. Proc Natl Acad Sci U S A. 2012;109(28):1938–46.

92. Frost B, Diamond MI. Prion-like mechanisms in neurodegenerative diseases. Vol. 11, Nature Reviews Neuroscience. 2010. p. 155–9.

93. Reiniger L, Lukic A, Linehan J, Rudge P, Collinge J, Mead S, et al. Tau, prions and Aβ: The triad of neurodegeneration. Vol. 121, Acta Neuropathologica. 2011. p. 5–20.

94. Hasegawa M, Nonaka T, Masuda-Suzukake M. Prion-like mechanisms and potential therapeutic targets in neurodegenerative disorders. Vol. 172, Pharmacology and Therapeutics. 2017. p. 155–9.

95. Sibilla C, Bertolotti A. Prion properties of SOD1 in amyotrophic lateral sclerosis and potential therapy. Cold Spring Harb Perspect Biol. 2017;9(10):a024141.

96. Malfertheiner K, Stefanova N, Heras-Garvin A. The Concept of α-Synuclein Strains and How Different Conformations May Explain Distinct Neurodegenerative Disorders. Vol. 12, Frontiers in Neurology. 2021. p. 737195.

97. Williams ES. Review article - Chronic Wasting Disease. Vet Pathol. 2005;42(5):530–49.

98. Miller MW, Williams ES, McCarty CW, Spraker TR, Kreeger TJ, Larsen CT, et al. Epizootiology of chronic wasting disease in free-ranging cervids in Colorado and Wyoming. J Wildl Dis. 2000;36(4):676–90.

99. Kreeger TJ, Montgomery DL, Jewell JE, Schultz W, Williams ES. Oral transmission of chronic wasting disease in captive Shira's moose. J Wildl Dis. 2006;42(3).

100. Baeten LA, Powers BE, Jewell JE, Spraker TR, Miller MW. A natural case of chronic wasting disease in a free-ranging moose (Alces alces shirasi). J Wildl Dis. 2007;43(2):309–14.

101. Gagnier M, Laurion I, Denicola AJ. Control and surveillance operations to prevent chronic wasting disease establishment in free-ranging white-tailed deer in Québec, Canada. Animals. 2020;10(2):283.

102. Mitchell GB, Sigurdson CJ, O'Rourke KI, Algire J, Harrington NP, Walther I, et al. Experimental oral transmission of chronic wasting disease to reindeer (Rangifer tarandus tarandus). PLoS One. 2012;0039055.

103. Nalls A v., McNulty E, Powers J, Seelig DM, Hoover C, Haley NJ, et al. Mother to Offspring Transmission of Chronic Wasting Disease in Reeves' Muntjac Deer. PLoS One. 2013;8(8):0071844.

104. Hamir AN, Kunkle RA, Nicholson EM, Miller JM, Hall SM, Schoenenbruecher H, et al. Preliminary Observations on the Experimental Transmission of Chronic Wasting Disease (CWD) from Elk and White-Tailed Deer to Fallow Deer. J Comp Pathol. 2008;138(2–3):121–30.

105. Rhyan JC, Miller MW, Spraker TR, Mccollum M, Nol P, Wolfe LL, et al. Failure of fallow deer (dama dama) to develop chronic wasting disease when exposed to a contaminated environment and infected mule deer (odocoileus hemionus). J Wildl Dis. 2011;47(3):739–44.

106. Sohn HJ, Kim JH, Choi KS, Nah JJ, Joo YS, Jean YH, et al. A case of chronic wasting disease in an elk imported to Korea from Canada. Journal of Veterinary Medical Science. 2002;64(9):855–8.

107. Kim TY, Shon HJ, Joo YS, Mun UK, Kang KS, Lee YS. Additional cases of Chronic Wasting Disease in imported deer in Korea. Journal of Veterinary Medical Science. 2005;67(8):753–9.

108. Benestad SL, Mitchell G, Simmons M, Ytrehus B, Vikøren T. First case of chronic wasting disease in Europe in a Norwegian free-ranging reindeer. Vet Res. 2016;88.

109. Pirisinu L, Tran L, Chiappini B, Vanni I, di Bari MA, Vaccari G, et al. Novel type of chronic wasting disease detected in moose (Alces alces), Norway. Emerg Infect Dis. 2018;2210–8.

110. Vikøren T, Våge J, Madslien KI, Røed KH, Rolandsen CM, Tran L, et al. First detection of chronic wasting disease in a wild red deer (Cervus elaphus) in Europe. J Wildl Dis. 2019;55(4):970–2.

111. Ågren EO, Sörén K, Gavier-Widén D, Benestad SL, Tran L, Wall K, et al. First detection of chronic wasting disease in moose (Alces alces) in Sweden. J Wildl Dis. 2021;57(2):461–3.

112. Tranulis MA, Gavier-Widén D, Våge J, Nöremark M, Korpenfelt SL, Hautaniemi M, et al. Chronic wasting disease in Europe: new strains on the horizon. Vol. 63, Acta Veterinaria Scandinavica. 2021.

113. Bian J, Kim S, Kane SJ, Crowell J, Sun JL, Christiansen J, et al. Adaptive selection of a prion strain conformer corresponding to established North American CWD during propagation of novel emergent Norwegian strains in mice expressing elk or deer prion protein. PLoS Pathog. 2021;17(7):1009748.

114. Nonno R, di Bari MA, Pirisinu L, D'Agostino C, Vanni I, Chiappini B, et al. Studies in bank voles reveal strain differences between chronic wasting disease prions from Norway and North America. Proc Natl Acad Sci U S A. 2020;117(49):31417–26.

115. Sigurdson CJ, Williams ES, Miller MW, Spraker TR, O'Rourke KI, Hoover EA. Oral transmission and early lymphoid tropism of chronic wasting disease PrP(res) in mule deer fawns (Odocoileus hemionus). Journal of General Virology. 1999;80(10):2757–64.

116. Jewell JE, Brown J, Kreeger T, Williams ES. Prion protein in cardiac muscle of elk (Cervus elaphus nelsoni) and white-tailed deer (Odocoileus virginianus) infected with chronic wasting disease. Journal of General Virology. 2006;87(11):3443–50.

117. Angers RC, Browning SR, Seward TS, Sigurdson CJ, Miller MW, Hoover EA, et al. Prions in skeletal muscles of deer with chronic wasting disease. Science (1979). 2006;311(5764):1117.

118. Sigurdson CJ, Spraker TR, Miller MW, Oesch B, Hoover EA. PrPCWD in the myenteric plexus, vagosympathetic trunk and endocrine glands of deer with chronic wasting disease. Journal of General Virology. 2001;82(10):2327–34.

119. Fox KA, Jewell JE, Williams ES, Miller MW. Patterns of PrPCWD accumulation during the course of chronic wasting disease infection in orally inoculated mule deer (Odocoileus hemionus). Journal of General Virology. 2006;87(11):3451–61.

120. Mathiason CK, Powers JG, Dahmes SJ, Osborn DA, Miller K v., Warren RJ, et al. Infectious prions in the saliva and blood of deer with chronic wasting disease. Science (1979). 2006;314(5796):133–6.

121. Haley NJ, Mathiason CK, Zabel MD, Telling GC, Hoover EA. Detection of sub-clinical CWD infection in conventional test-negative deer long after oral exposure to urine and feces from CWD+ deer. PLoS One. 2009;4(11):7990.

122. Angers RC, Seward TS, Napier D, Green M, Hoover E, Spraker T, et al. Chronic wasting disease prions in eik antler velvet. Emerg Infect Dis. 2009;15(5):696–703.

123. Bian J, Christiansen JR, Moreno JA, Kane SJ, Khaychuk V, Gallegos J, et al. Primary structural differences at residue 226 of deer and elk PrP dictate selection of distinct CWD prion strains in gene-targeted mice. Proc Natl Acad Sci U S A. 2019;12478–87.

124. Tamgüney G, Miller MW, Wolfe LL, Sirochman TM, Glidden D v., Palmer C, et al. Asymptomatic deer excrete infectious prions in faeces. Nature. 2009;461(7263):529–32.

125. Wyckoff AC, Kane S, Lockwood K, Seligman J, Michel B, Hill D, et al. Clay components in soil dictate environmental stability and bioavailability of cervid prions in mice. Front Microbiol. 2016;7(NOV):01885.

126. Rasmussen J, Gilroyed BH, Reuter T, Dudas S, Neumann NF, Balachandran A, et al. Can plants serve as a vector for prions causing chronic wasting disease? Prion. 2014;8(1):136–42.

127. Williams ES, Miller MW. Chronic wasting disease in deer and elk in North America. OIE Revue Scientifique et Technique. 2002;21(2):305–16.

128. Nalls A v., McNulty EE, Mayfield A, Crum JM, Keel MK, Hoover EA, et al. Detection of chronic wasting disease prions in fetal tissues of free-ranging white-tailed deer. Viruses. 2021;13(12):2430.

129. Bravo-Risi F, Soto P, Eckland T, Dittmar R, Ramírez S, Catumbela CSG, et al. Detection of CWD prions in naturally infected white-tailed deer fetuses and gestational tissues by PMCA. Sci Rep. 2021;11(1):18385.

130. Race B, Meade-White K, Race R, Chesebro B. Prion Infectivity in Fat of Deer with Chronic Wasting Disease. J Virol. 2009;83(18):9608–10.

131. Wadsworth JDF, Joiner S, Linehan JM, Jack K, Al-Doujaily H, Costa H, et al. Humanized Transgenic Mice Are Resistant to Chronic Wasting Disease Prions From Norwegian Reindeer and Moose. J Infect Dis. 2021;jiab033.

132. Sandberg MK, Al-Doujaily H, Sigurdson CJ, Glatzel M, O'Malley C, Powell C, et al. Chronic wasting disease prions are not transmissible to transgenic mice overexpressing human prion protein. Journal of General Virology. 2010;91(10):2651–7.

133. Tamgüney G, Giles K, Bouzamondo-Bernstein E, Bosque PJ, Miller MW, Safar J, et al. Transmission of Elk and Deer Prions to Transgenic Mice. J Virol. 2006;80(18):9104–14.

134. Hannaoui S, Zemlyankina I, Chang SC, Arifin MI, Béringue V, McKenzie D, et al. Transmission of cervid prions to humanized mice demonstrates the zoonotic potential of CWD. Acta Neuropathol. 2022 Aug 22;

135. Barria MA, Telling GC, Gambetti P, Mastrianni JA, Soto C. Generation of a new form of human PrPScin vitro by interspecies transmission from cervid prions. Journal of Biological Chemistry. 2011;286(9):7490–5.

136. Marsh RF, Kincaid AE, Bessen RA, Bartz JC. Interspecies Transmission of Chronic Wasting Disease Prions to Squirrel Monkeys (Saimiri sciureus) . J Virol. 2005;79(21):13794–6.

137. Race B, Meade-White KD, Miller MW, Barbian KD, Rubenstein R, LaFauci G, et al. Susceptibilities of nonhuman primates to chronic wasting disease. Emerg Infect Dis. 2009;15(9):1366–76.

138. Hayasaka K, Gojobori T, Horai S. Molecular phylogeny and evolution of primate mitochondrial DNA. Mol Biol Evol. 1988;5(6):626–44.

139. Race B, Williams K, Orrú CD, Hughson AG, Lubke L, Chesebro B. Lack of Transmission of Chronic Wasting Disease to Cynomolgus Macaques. J Virol. 2018;92(14):00550–18.

140. Czub S, SSW, SHC, BM, SH, MD. First Evidence of Intracranial and Peroral Transmission of Chronic Wasting Disease (CWD) into Cynomolgus macaques: A Work In Progress. From Prion. Prion 2017. 2017.

141. Belay ED, Maddox RA, Williams ES, Miller MW, Gambetti P, Schonberger LB. Chronic wasting disease and potential transmission to humans. Vol. 10, Emerging Infectious Diseases. 2004. p. 977–84.

142. MaWhinney S, Pape WJ, Forster JE, Anderson CA, Bosque P, Miller MW. Human prion disease and relative risk associated with chronic wasting disease. Emerg Infect Dis. 2006;12(10):1527–35.

143. Cassmann ED, Jo Moore S, Greenlee JJ. Experimental oronasal transmission of chronic wasting disease agent from white-tailed deer to Suffolk sheep. Emerg Infect Dis. 2021;27(12):3156–8.

144. Mathiason CK, Nalls A v., Seelig DM, Kraft SL, Carnes K, Anderson KR, et al. Susceptibility of Domestic Cats to Chronic Wasting Disease. J Virol. 2013;87(4):1947–56.

145. Baune C, Wolfe LL, Schott KC, Griffin KA, Hughson AG, Miller MW, et al. Reduction of Chronic Wasting Disease Prion Seeding Activity following Digestion by Mountain Lions. mSphere. 2021;6(6):0081221.

146. Nichols TA, Fischer JW, Spraker TR, Kong Q, VerCauteren KC. CWD prions remain infectious after passage through the digestive system of coyotes (Canis latrans). Prion. 2015;9(5):367–75.

147. VerCauteren KC, Pilon JL, Nash PB, Phillips GE, Fischer JW. Prion Remains Infectious after Passage through Digestive System of American Crows (Corvus brachyrhynchos). PLoS One. 2012;7(10):45774.

148. Pritzkow S, Morales R, Camacho M, Soto C. Uptake, retention, and excretion of infectious prions by experimentally exposed earthworms. Emerg Infect Dis. 2021;27(12):3151–4.

149. Angers RC, Kang HE, Napier D, Browning S, Seward T, Mathiason C, et al. Prion strain mutation determined by prion protein conformational compatibility and primary structure. Science (1979). 2010;328(5982):1154–8.

150. Arifin MI, Hannaoui S, Chang SC, Thapa S, Schatzl HM, Gilch S. Cervid prion protein polymorphisms: Role in chronic wasting disease pathogenesis. Vol. 22, International Journal of Molecular Sciences. 2021. p. 2271.

151. Browning SR, Mason GL, Seward T, Green M, Eliason GAJ, Mathiason C, et al. Transmission of Prions from Mule Deer and Elk with Chronic Wasting Disease to Transgenic Mice Expressing Cervid PrP. J Virol. 2004;78(23):13345–50.

152. Scott M, Foster D, Mirenda C, Serban D, Coufal F, Wälchli M, et al. Transgenic mice expressing hamster prion protein produce species-specific scrapie infectivity and amyloid plaques. Cell. 1989;59(5):847–57.

153. Telling GC, Scott M, Hsiao KK, Foster D, Yang SL, Torchia M, et al. Transmission of Creutzfeldt-Jakob disease from humans to transgenic mice expressing chimeric human-mouse prion protein. Proc Natl Acad Sci U S A. 1994;91(21):9936–40.

154. Telling GC, Scott M, Mastrianni J, Gabizon R, Torchia M, Cohen FE, et al. Prion propagation in mice expressing human and chimeric PrP transgenes implicates the interaction of cellular PrP with another protein. Cell. 1995;83(1):79–90.

155. Scott MR, Safar J, Telling G, Nguyen O, Groth D, Torchia M, et al. Identification of a prion protein epitope modulating transmission of bovine spongiform encephalopathy prions to transgenic mice. Proc Natl Acad Sci U S A. 1997;94(26):14279–84.

156. Buschmann A, Pfaff E, Reifenberg K, Müller HM, Groschup MH. Detection of cattle-derived BSE prions using transgenic mice overexpressing bovine PrPC. Archives of Virology, Supplement. 2001;(16):75–86.

157. Crozet C, Flamant F, Bencsik A, Aubert D, Samarut J, Baron T. Efficient Transmission of Two Different Sheep Scrapie Isolates in Transgenic Mice Expressing the Ovine PrP Gene. J Virol. 2001;75(11):5328–34.

158. Vilotte JL, Soulier S, Essalmani R, Stinnakre MG, Vaiman D, Lepourry L, et al. Markedly Increased Susceptibility to Natural Sheep Scrapie of Transgenic Mice Expressing Ovine PrP. J Virol. 2001;75(13):5977–84.

159. Castilla J, Gutiérrez Adán A, Brun A, Pintado B, Ramírez MA, Parra B, et al. Early detection of PrPres in BSE-infected bovine PrP transgenic mice. Arch Virol. 2003;148(4):677–91.

160. Windl O, Buchholz M, Neubauer A, Schulz-Schaeffer W, Groschup M, Walter S, et al. Breaking an Absolute Species Barrier: Transgenic Mice Expressing the Mink PrP Gene Are Susceptible to Transmissible Mink Encephalopathy. J Virol. 2005;79(23):14971–5.

161. Kong Q, Huang S, Zou W, Vanegas D, Wang M, Wu D, et al. Chronic wasting disease of elk: Transmissibility to humans examined by transgenic mouse models. Journal of Neuroscience. 2005;25(35):7944–9.

162. LaFauci G, Carp RI, Meeker HC, Ye X, Kim JI, Natelli M, et al. Passage of chronic wasting disease prion into transgenic mice expressing Rocky Mountain elk (Cervus elaphus nelsoni) PrPC. Journal of General Virology. 2006;87(12):3773–80.

163. Meade-White K, Race B, Trifilo M, Bossers A, Favara C, Lacasse R, et al. Resistance to Chronic Wasting Disease in Transgenic Mice Expressing a Naturally Occurring Allelic Variant of Deer Prion Protein. J Virol. 2007;81(9):4533–9.

164. Green KM, Castilla J, Seward TS, Napier DL, Jewell JE, Soto C, et al. Accelerated high fidelity prion amplification within and across prion species barriers. PLoS Pathog. 2008;4(8):1000139.

165. Meyerett C, Michel B, Pulford B, Spraker TR, Nichols TA, Johnson T, et al. In vitro strain adaptation of CWD prions by serial protein misfolding cyclic amplification. Virology. 2008;382(2):267–76.

166. Kurt TD, Telling GC, Zabel MD, Hoover EA. Trans-species amplification of PrPCWD and correlation with rigid loop 170N. Virology. 2009;387(1):235–43.

167. Haley NJ, Seelig DM, Zabel MD, Telling GC, Hoover EA. Detection of CWD prions in urine and saliva of deer by transgenic mouse bioassay. PLoS One. 2009;4(3):4848.

168. Schätzl HM, Wopfner F, Gilch S, von Brunn A, Jäger G. Is codon 129 of prion protein polymorphic in human beings but not in animals? Lancet. 1997;349(9065):1603–4.

169. O'Rourke KI, Baszler T v., Miller JM, Spraker TR, Sadler-Riggleman I, Knowles DP. Monoclonal antibody F89/160.1.5 Defines a conserved epitope on the ruminant prion protein. J Clin Microbiol. 1998;36(6):1750–5.

170. O'Rourke KI, Besser TE, Miller MW, Cline TF, Spraker TR, Jenny AL, et al. PrP genotypes of captive and free-ranging Rocky Mountain elk (Cervus elaphus nelsoni) with chronic wasting disease. Journal of General Virology. 1999;80(10):2765–79.

171. Hamir AN, Gidlewski T, Spraker TR, Miller JM, Creekmore L, Crocheck M, et al. Preliminary observations of genetic susceptibility of elk (Cervus elaphus nelsoni) to chronic wasting disease by experimental oral inoculation. Journal of Veterinary Diagnostic Investigation. 2006;18(1):110–4.

172. O'Rourke KI, Spraker TR, Zhuang D, Greenlee JJ, Gidlewski TE, Hamir AN. Elk with a long incubation prion disease phenotype have a unique PrPd profile. Neuroreport. 2007;18(18):1935–8.

173. Green KM, Browning SR, Seward TS, Jewell JE, Ross DL, Green MA, et al. The elk PRNP codon 132 polymorphism controls cervid and scrapie prion propagation. Journal of General Virology. 2008;89(2):598–608.

174. Benestad SL, Sarradin P, Thu B, Schönheit J, Tranulis MA, Bratberg B. Cases of scrapie with unusual features in Norway and designation of a new type, Nor98. Veterinary Record. 2003;153(7):202–8.

175. Biacabe AG, Laplanche JL, Ryder S, Baron T. Distinct molecular phenotypes in bovine prion diseases. EMBO Rep. 2004;5(1):110–5.

176. Fraser H, Pearson GR, McConnell I, Bruce ME, Wyatt JM, Gruffydd-Jones TJ. Transmission of feline spongiform encephalopathy to mice. Vet Rec. 1994;134(17):449.

177. Babelhadj B, di Bari MA, Pirisinu L, Chiappini B, Gaouar SBS, Riccardi G, et al. Prion disease in dromedary camels, Algeria. Emerg Infect Dis. 2018;1029–36.

178. Will RG, Ironside JW, Zeidler M, Cousens SN, Estibeiro K, Alperovitch A, et al. A new variant of Creutzfeldt-Jakob disease in the UK. Lancet. 1996;

179. Duffy P, Wolf J, Collins G, DeVoe AG, Streeten B, Cowen D. Possible Person-to-Person Transmission of Creutzfeldt-Jakob Disease. New England Journal of Medicine. 1974;290(12):692–3.

180. WR K. Zwei eigenartige Erkrankung des Zentralnervensystems nach Art der spatischen Pseudosklerose (Jakob). Z Neurol Pyschiatry. 1924;92:175–220.

181. Lugaresi E, Medori R, Montagna P, Baruzzi A, Cortelli P, Lugaresi A, et al. Fatal Familial Insomnia and Dysautonomia with Selective Degeneration of Thalamic Nuclei. New England Journal of Medicine. 1986;315(16):997–1003.

182. Gerstmann J SESI. Über eine eigenartige hereditär-familiäre Erkrankung des Zentralnervensystems. Zugleich ein Beitrag zur Frage des vorzeitigen lokalen Alterns". Zeitschrift für die gesamte Neurologie und Psychiatrie. 1936;154:736–62.

183. Gambetti P, Dong Z, Yuan J, Xiao X, Zheng M, Alshekhlee A, et al. A novel human disease with abnormal prion protein sensitive to protease. Ann Neurol. 2008;63(6):697–708.

CHAPTER 2 - DETAILED INVESTIGATION OF THE ROLE PLAYED BY RESIDUE 226 OF PRP IN CHRONIC WASTING DISEASE PATHOGENESIS AND STRAIN SELECTION

Introduction

Prions diseases are fatal, neurodegenerative diseases which affect humans and other animals and are caused by the templated misfolding of the cellular prion protein (PrP^{C}) into an infectious, aberrant form (PrP^{Sc}) (1). The potential for prion diseases to cross species barriers and cause great economic and public health repercussions is demonstrated by the emergence of variant Creutzfeldt-Jakob disease (vCJD) in humans resulting from the consumption of cattle infected with bovine spongiform encephalopathy (BSE) (2). Chronic wasting disease (CWD) is a prion disease of relatively unknown zoonotic potential affecting deer, elk, moose and other members of the cervid family (3–5). CWD was first described in captive mule deer at a Colorado State University facility in the 1960s and since then, cases in either free-ranging and captive animals have been documented in 30 US states, three provinces in Canada, South Korea, and most recently, some Nordic countries (6–9). The unrelenting spread of CWD in not only geographical terms, but also host species range, necessitates immediate concern.

Prions differ from all other pathogens - they do not contain any nucleic acid, thus their infectious nature stems from the conversion of PrP^{C} to PrP^{Sc} (10). Similar to other pathogens, prions exhibit strain properties which can be operationally defined by features such as time to disease onset, clinical signs, and neuropathological hallmarks (11–13). Since PrP^{C} and PrP^{Sc} have indistinguishable primary structures, strain property information is inferred to be enciphered in higher order protein structure (13). In addition to strain properties, similarity between the primary structure of infectious PrP^{Sc} and the recipient PrP^{C} that is to be converted, plays a role in the efficiency of both intra- and interspecies transmissions (14). For interspecies transmissions, the ease of crossing the species barrier correlates to the homology of PrP between species (14). For intraspecies transmissions, it has been shown previously that

naturally occurring polymorphisms in PrP can influence disease susceptibility and dictate strain selection (15). In white-tail deer, the expression of serine (S) at residue 96 of PrP confers resistance to infection as opposed expression of glycine (G) at residue 96 (16). In elk, the expression of leucine (L) at residue 132 rather than methionine (M) also confers resistance to CWD infection (17). Interestingly, residue 132 of elk PrP is equivalent to residue 129 of human PrP, at which the expression of valine (V) confers significant resistance to CJD over the expression of M (18). A plethora of other polymorphisms in cervid PrP have been identified but not yet explored in the context of susceptibility to prion disease.

Across CWD susceptible cervids, the wildtype coding sequences are identical except for residue 226 where deer, moose and reindeer express glutamine (Q) at residue 226 of PrP, while North American elk express glutamate (E) (19). Red deer can express either Q, E, or both at 226 (19). Previously, the Telling lab created gene-targeted (Gt) mice in which the mouse coding sequence of *Prnp* was replaced via homologous recombination with cervid coding sequences of *Prnp*, to detail the polymorphic effects of residue 226 on disease pathogenesis (20). When inoculated with CWD prions from North American deer or elk, Gt mice expressing Q at residue 226 (GtQ) present with longer time to disease onset than mice expressing E at residue 226 (GtE) (20). Additionally, the neuropathology and conformational stability in response to denaturation agents varied depending on which allele was expressed at residue 226. Differential phenotypes propagated in the GtE and GtQ mice could lend insight into how the susceptibility of species to CWD in the wild is dictated by the distribution of PrP polymorphisms in populations.

The Telling lab previously used a longitudinal study using wildtype FVB mice inoculated with RML prions to show increasing proteinase K (PK)-resistant PrP^{Sc} over disease course (21). Additionally, prion titers and hypoglycosylated, PRC7-reactive PrP^{Sc} increased in conjunction with each other and PK-resistant PrP^{Sc} (21). To fully understand the mechanism underlying the differences in disease phenotypes dictated by the polymorphism at 226 of cervid PrP, we

conducted a longitudinal analysis in the GtQ and GtE mice in which we intracerebrally inoculated GtQ and GtE mice with North American elk CWD and sacrificed mice every 15 days until terminal disease. Here, we detail the progression of CWD infection in Gt cervid-PrP mice and further explore the role of residue 226 over disease time course.

Materials and Methods

Ethics Statement

All animal work was performed in an Association for Assessment and Accreditation of Laboratory Animal Care International accredited facility in accordance with the Guide for the Care and Use of Laboratory Animals. All procedures used in this study were performed in compliance with and were approved by the Colorado State University Institutional Animal Care and Use Committee.

CWD Inocula

The elk isolate used to originally inoculate mice transgenic overexpressing cervid-PrP mice and referred to as E-US1 represents a diseased Rocky Mountain elk, 99w12389 with genotype MM132 99w, that has been previously described (17,22).

Animal work

The development and characterization of TgQ226, TgE226, GtQ226, and GtE226 mice has been previously described (20,23,24). For inoculation of mice, 10% homogenates of brain tissue from transgenic overexpressing cervid-PrP CWD affected mice, were prepared by mechanical disruption (MP Biomedical) in phosphate-buffered saline (PBS) lacking calcium and magnesium ions. For each collection timepoint, equal numbers of male and female mice between the ages of five to eight weeks were anaesthetized with halothane and intracerebrally (ic) inoculated freehand with 30 μl of 1% brain tissue homogenates into the right parietal lobe

using a 26-gauge needle at a depth of ~ 2 mm. Regardless of planned collection timepoint, all animals were subsequently monitored three times a week for the development of neurological signs consistent with prion disease phenotypes. These signs included truncal ataxia, loss of extensor reflex, slowed movement, unsteady or flattened gait, plastic tail, dorsal kyphosis, head bobbing, rough coat and weight loss or gain. The time to disease onset, aka incubation period, is defined as the time between inoculation and the first day on which subsequently progressive clinical signs were identified. Six mice were humanely sacrificed at 15-day intervals until terminal stages of disease.

Analysis of PrP^{Sc} by Western Blotting

Protein concentrations of 10% brain homogenates were determined by bicinchoninic acid assay (BCA) (Pierce Biotechnology). Homogenates were treated with 50 μg/mL PK (Roche) in the presence of 2% sarkosyl for 1 hour at 37 °C. PK digestion was terminated with phenylmethylsulfonyl fluoride (PMSF) at a final concentration of 2 mM. Prior to electrophoresis, samples were boiled at 100 °C for 5 minutes in XT-sample buffer (Bio-Rad Laboratories) in the absence of reducing agents. Samples were loaded onto precast 12% discontinuous Bis-Tris gels (Bio-Rad Laboratories). Proteins were then transferred overnight to PVDF-FL membranes (Millipore). Membranes were blocked for 1 hour in 5% nonfat milk in TBST, probed with monoclonal antibody (mAb) PRC5 at a dilution of 1:5000, followed by incubation with horseradish peroxidase (HRP)-conjugated anti-mouse IgG secondary antibody at a dilution of 1:5000 (Cytiva). Membranes were developed using ECL 2 western blot substrate (Thermo Scientific). Chemiluminescent signal was quantified using ImageJ software (25).

Analysis of PrP^{Sc} by Dot Blot Assay

Protein concentrations of 10% brain homogenates were determined by BCA (Pierce Biotechnology). 1 μg of protein was transferred to a nitrocellulose membrane (GE Healthcare) in a 96 well format using a dot blot manifold (GE Whatman) and dried onto the membrane for 1 hour. Membranes were digested with 5 μg/mL PK for 1 hour at 37 °C, then digestion was stopped with 2 mM PMSF for 20 minutes. To expose the PRC5 epitope, membranes were incubated with 3 M guanidine isothiocyanate for 10 minutes at room temperature, then blocked for 1 hour with 5% nonfat milk at room temperature. Next, membranes were incubated overnight with primary antibody PRC5 at a dilution of 1:5000 at 4 °C, then incubated for 1 hour with secondary antibody HRP-conjugated anti-mouse IgG at a dilution of 1:5000 (Cytiva). Membranes were developed using ECL 2 western blot substrate (Thermo Scientific). Membranes were imaged with a GE ImageQuant LAS 4000, and signal was quantified using ImageQuant software.

Analysis of underglycosylated PrP by 7-5 sandwich ELISA

7-5 ELISA samples were prepared and analyzed as previously described (21). 96-well plates were coated with 1μg of mAb PRC7 in carbonate-bicarbonate buffer at 4 °C. Prior to capture with PRC7, brain homogenates were solubilized in 1% Triton X-100/PBS. Samples were treated with guanidine hydrochloride at a final concentration of 5 M for 15 minutes at 37 °C with mixing on an orbital heat block shaker. Prior to addition of brain samples, wells were blocked with 3% bovine serum albumin (BSA) in PBS for 1 hour at 37 °C. Samples were then incubated on the plates overnight at 4 °C with capture antibody. Next, the detection antibody PRC5 was added and incubated for 1 hour at 37 °C. Wells were washed, then incubated with HRP-conjugated IgG2a secondary antibody for 1 hour at 37 °C (Alpha Diagnostics). Plates were then developed with 2,2'-azino-di(3-ethylbenzathiazoline-6-sulfonate) (ABTS) substrate

(Seracare Life Sciences) at room temperature, and reactions were stopped with ABTS Stop Solution (Seracare Life Sciences) after 15 minutes. Absorbance was read at 405 nm using a ThermoFisher Multiskan SkyHigh plate reader with SkanIt software.

Cell maintenance and cell-based prion titration

The establishment of RK-E and RK-D cells is previously described (26,27). RK13 cells were stably transfected with deer PrP (D) or elk PrP (E) constructs. RK-D and RK-E cells were cultured in Dubecco's Modified Eagle Medium (DMEM) containing 10% (v/v) fetal bovine serum (FBS), 1 μg/mL penicillin/ 100 U/ml streptomycin and 1 μg/mL puromycin. Cells were passaged using 0.05% trypsin at a ratio of 1:10 every five days. RK-E and RK-D cells were infected with CWD prions in an adapted scrapie cell assay (SCA) format termed the cervid prion cell assay (CPCA) (28–30). The top row of 96-well plates were coated with 1% brain homogenate. This was serially diluted 1:3 down each row of the plate for a final concentration of 0.00046% brain homogenate. Plates were coated for 3 hours in a biosafety cabinet, then washed twice with PBS and stored at 4 °C overnight. Either 20,000 RK-E or RK-D cells were seeded onto coated 96-well plates. Fresh DMEM was given every 5 days during a 4-week infection. At the end of the 4-week infection, 20,000 cells were filtered onto ethanol-activated Multiscreen IP 96-well 0.45-μm filter plates (enzyme-linked immunospot [ELISPOT]) assay plates (Millipore) and dried at 50 °C for ~ 1 hour. ELISPOT plates were stored at -20 °C overnight. ELISPOT plates were digested with 5μg/ml PK for 90 minutes at 37 °C. Digestion was terminated with 2mM PMSF for 20 minutes at room temperature. To expose the PrP 27-30 epitope, cells were incubated with 3 M guanidinium thiocyanate for 10 minutes at room temperature. ELISPOT plate membranes were blocked with 5% superblock for 1 hour at room temperature (Thermo Fisher). Plates were then incubated with primary antibody PRC5 at a concentration of 1:5000 overnight with rotation at 4 °C. Alkaline phosphatase (AP)-conjugated goat anti mouse IgG (Southern Biotech) was then

incubated on plates for 1 hour at room temperature at a dilution of 1:5000. ELISPOT plates were developed using 5-bromo-4-chloro-3-indolyl phosphate (BCIP)/nitro blue tetrazolium (NBT) tablets (Sigma Aldrich) for 15 minutes. Images were scanned and infection spots counted with ImmunoSpot S6-V Analyzer (Cellular Technology Ltd).

Histoblot Analysis

Histoblots were prepared and analyzed as previously described (31). Whole brains were snap frozen on dry ice. Ten μm coronal cryostat sections on slides were transferred to nitrocellulose membranes using lysis buffer. Membranes were treated with 0.2 mg/ml PK for 1 hour at 37 °C then incubated with 2 mM PMSF for 15 minutes. Membranes were incubated with 3 M guanidine isothiocyanate for 10 minutes at room temperature and then blocked in 5% nonfat milk for 30 minutes. Next, membranes were incubated overnight at 4°C with mAb PRC5 at a dilution of 1:5000. AP-conjugated goat anti mouse IgG (Southern Biotech) was then incubated for 1 hour at room temperature at a dilution of 1:5000. Membranes were developed using BCIP/NBT tablets (Sigma Aldrich) for 5-15 minutes. Micrographs were captured using a Nikon Z1000 microscope.

Immunohistochemical Analyses

Immunohistochemistry (IHC) was performed as previously described (32). In brief, brains were fixed in 10% formalin. Paraffin embedded brain slices were mounted on slides and heated to 60°C for 30 minutes prior to xylene and graduated ethanol treatment followed by treatment with 88% formic acid for 30 minutes. Antigen retrieval was performed in the 2100 Retriever (ProteoGenix) using citrate buffer followed by endoperoxidase quenching in 3% hydrogen peroxide. Slides were blocked in 5% nonfat milk for 30 minutes at room temperature before overnight incubation at 4°C with primary antibody D18 at a 1:2500 dilution. Slides were

incubated with biotin labelled goat Fab anti-human IgG secondary antibody (Southern Biotech) at a dilution of 1:5000 for 1 hour at room temperature. Slides were developed with avidin-conjugated HRP with diaminiobenzidine (DAB) as a substrate for 30 minutes at room temperature (Vector Laboratories). Slides were counterstained with hematoxylin, run through graduated ethanol treatment, cover slipped and imaged at 4x or 100x under oil immersion.

Statistical Information

Statistical analyses were performed using Graphpad Prism software (San Diego). Statistical significance between survival curves of inoculated groups was assessed by comparing median times of survival of various inoculated groups using the log rank (Mantel-Cox) test. One-way ANOVA was used to compare glycosylation states.

Results

Residue 226 of cervid PrP affects kinetics of CWD disease course

To fully assess the impact of residue 226 of cervid-PrP on CWD disease course, we intracerebrally challenged GtE and GtQ mice with CWD prions. GtE mice were inoculated with CNS material from a transgenic overexpressing E226 cervid-PrP mouse elk originally inoculated with 99w CWD prions. GtQ mice were inoculated with CNS material from a transgenic overexpressing Q226 cervid-PrP mouse elk originally inoculated with 99w CWD prions. The starting inoculum was genotype matched at residue 226 to eliminate any transmission effects of mismatching alleles at residue 226. Six mice were sacrificed, and tissues collected every 15 days until terminal disease (Figure 2.1B, 2.1D). For every CWD inoculated GtE and GtQ mouse, an aged-matched control was inoculated with uninfected brain homogenate and collected at the same time (Figure 2.1A, 2.1C). In all GtE and GtQ mice inoculated with uninfected brain homogenate, no clinical disease was noted (Figure 2.1A, 2.1C). At 180 days post inoculation (DPI) in the GtE background, 2/6 mice were diagnosed with clinical signs of prion disease,

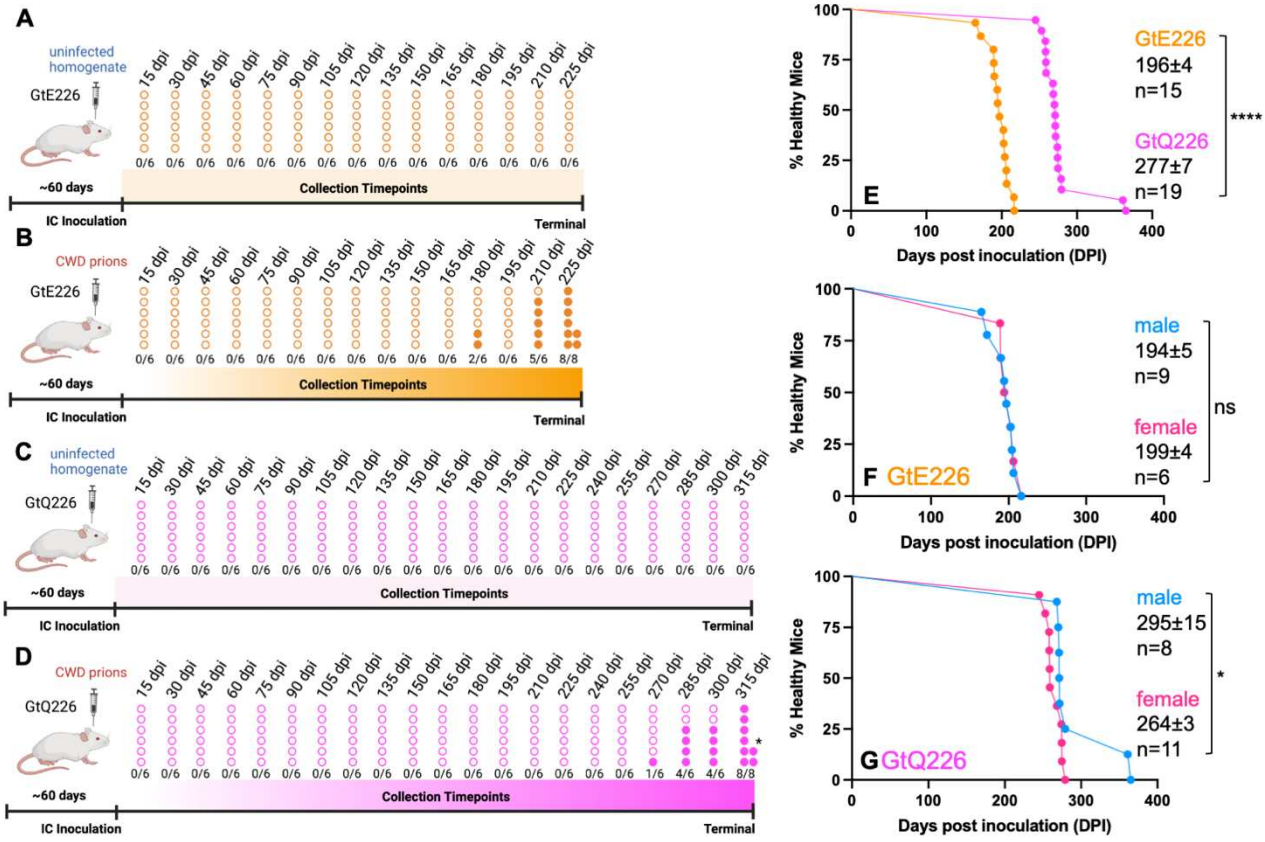

Figure 2.1 Transmission of North American CWD prions in mice expressing Q226 and E226 cervid-PrP. (A-D) Figure created using BioRender.com. Experimental design describing planned collection timepoints. Circles represent individual mice. Open circles – no disease, closed circles – clinically diagnosed (A) uninfected homogenate → GtE mice, (B) CWD homogenate → GtE mice, (C) uninfected homogenate → GtQ mice, (D) CWD homogenate → GtQ. * indicates 2 mice that were not diagnosed at 315 DPI, but developed delayed disease ~375 DPI. (E) Survival curves of GtE and GtQ mice following transmission of CWD infected homogenate, ****$p < 0.0001$. (F) Survival curve of GtE mice separated by sex, ns. (G) Survival curve of GtQ mice separated by sex, *$p < 0.05$. log-rank (Mantel-Cox) test.

marking the first collection timepoint with clinical disease (Figure 2.1B). For GtQ mice, the first collection timepoint with clinically diagnosed mice was 270 DPI, which was 90 days after the GtE mice (Figure 2.1D). The last GtE collection timepoint was at 225 DPI, with 8/8 mice developing disease before that time (Figure 2.1B), while the last GtQ collection timepoint was at 315 DPI, where 6/8 mice had developed disease at that time (Figure 2.1D). In CWD inoculated mice that were allowed to progress to the clinical stage, the kinetics of disease onset were more

rapid in GtE mice (196±4 DPI, n=15) than in GtQ mice (277±7 DPI, n=19, ****p < 0.0001) (Figure 2.1E). This is in accordance with the well characterized more rapid transmission of North American CWD in cervid mice expressing the E226 allele, regardless of host allele at residue 226 (20). Since our knock-in cervid-PrP mice are syngeneic except at residue 226 of PrP, we can conclude that differences in disease kinetics are due to the polymorphism at residue 226 of PrP.

For each timepoint, 3 male and 3 female mice were collected. It has been shown in wild populations, males are 1.5 - 3 times more likely to be infected with CWD than females in white-tailed deer, mule deer, and reindeer (33–35). Thus, we sought to determine whether sex played a role in time to disease onset as a potential explanation of CWD infecting male cervids more readily. In clinically sick GtE mice, there was no significance in time to disease onset between male mice (194±5 DPI) and female mice (199±54 DPI, ns, p = 0.81) (Figure 2.1F). For clinically sick GtQ mice, male mice had a delayed time to disease onset (295±15 DPI) when compared to female mice (264±3 DPI, *p < 0.05) (Figure 2.1G). However, this likely due to two male mice that had a significantly delayed time to disease onset, and when an outlier test was performed, they were determined to be outliers (Figure 2.1G). Thus, we cannot conclude that time to disease onset has an effect on likelihood of CWD infection dependent on sex. Rather, many wildlife biologists speculate that sex-specific behavior, such as fighting in males, has a larger bearing on likeliness of contracting CWD (35). Overall, we reconfirm GtE mice develop disease at a more rapid rate than GtQ mice and sex has little bearing on time to clinical disease.

Steady increase in PrP^{Sc} over disease course in GtE and GtQ mice, with delay in GtQ mice

We examined CNS material from both GtE and GtQ mice via western blotting to monitor accumulation of PK-resistant PrP^{Sc} over disease course. Equivalent amounts of protein were loaded onto bis-tris gels for each timepoint and we observed detectable and quantifiable PrP^{Sc}

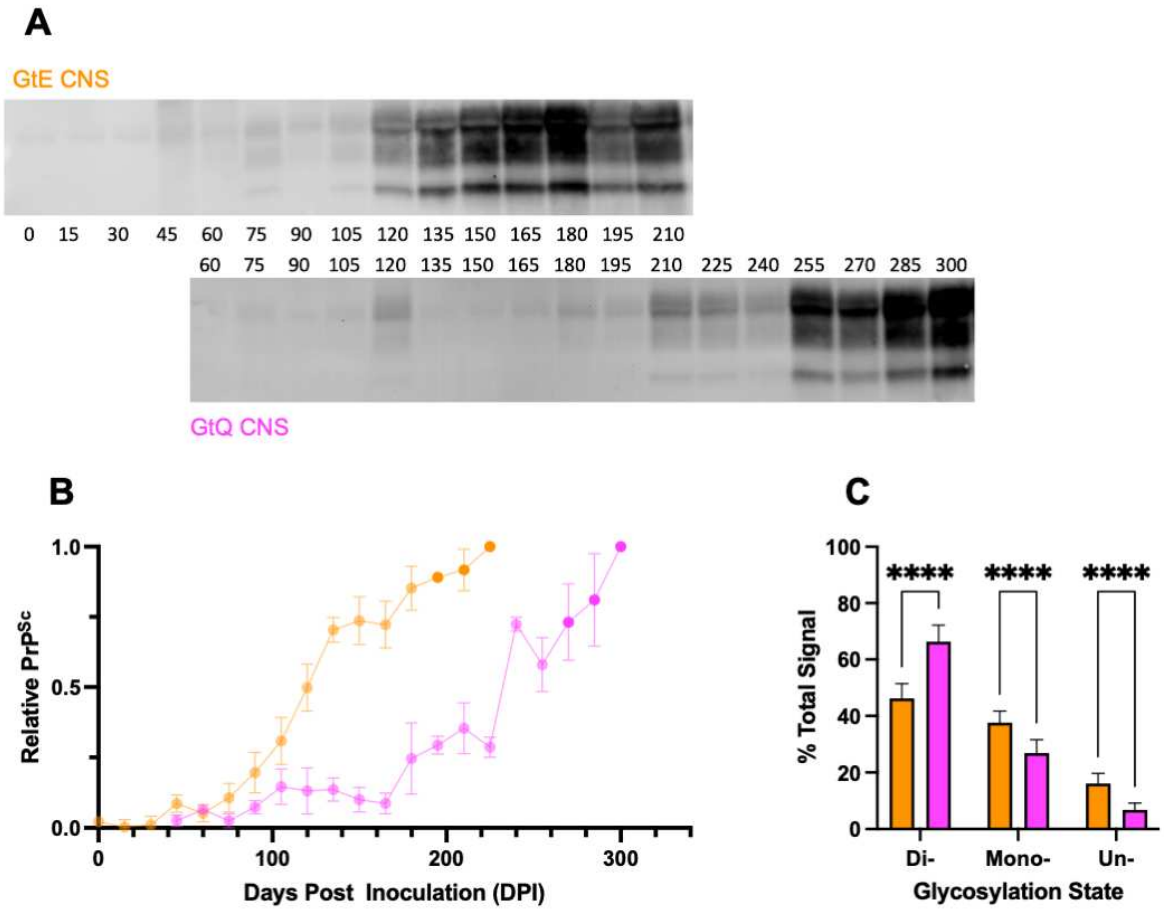

Figure 2.2 PrP^{Sc} accumulation in GtE and GtQ mice via western blotting (A) Representative western blots of PK-resistant PrP^{Sc} at each timepoint for both GtE and GtQ mice. (B) Quantification of A. Each point represents n = 4, mean ± standard error of the mean. (C) Quantification of glycosylation state (di-, mono- or un-) for GtE and GtQ mice. ****p < 0.0001. GtE = orange, GtQ = pink, transparent circles = no clinical disease, filled circles = clinically diseased.

signal in GtE mice around 75 DPI, ~120 days before clinical signs are observed (Figure 2.2A, 2.2B). In GtQ mice, PrP^{Sc} signal was detected around 120 dpi, ~150 days before clinical disease onset (Figure 2.2A, 2.2B). In both mouse lines, after detectable PrP^{Sc} was observed, PrP^{Sc} increased in a relatively linear fashion until the terminal stage of disease (Figure 2.2B). The delay in detectable PrP^{Sc} in GtQ mice when compared to GtE mice is consistent with the delay in disease onset in GtQ mice when inoculated with North American CWD prions.

PrP contains two conserved N-linked glycan sites at asparagine residues 180 and 196 (mouse numbering) – meaning a total of three glycosylation states can exist for PrP – both

glycan sites are occupied (di- or hyperglycosylated), only residue 180 or only residue 196 is occupied (monoglycosylated), or neither glycan site is occupied (hypo- or underglycosylated). The mechanism by which PrP^{C} is able to misfold into the PrP^{Sc} conformation is complicated by posttranslational modifications on PrP including N-linked glycosylation. It has been shown that relative to PrP^{C}, PrP^{Sc} is underglycosylated (21), but in relation to other species' PrP^{Sc}, CWD prions are more heavily diglycosylated (36). Thus, we sought to parse glycosylation differences in PrP^{Sc} in relation to the polymorphism at residue 226. ~46% of total PrP^{Sc} signal in the GtE mice was a result of the diglycosylated species (Figure 2.2C). In contrast, we report ~66% of

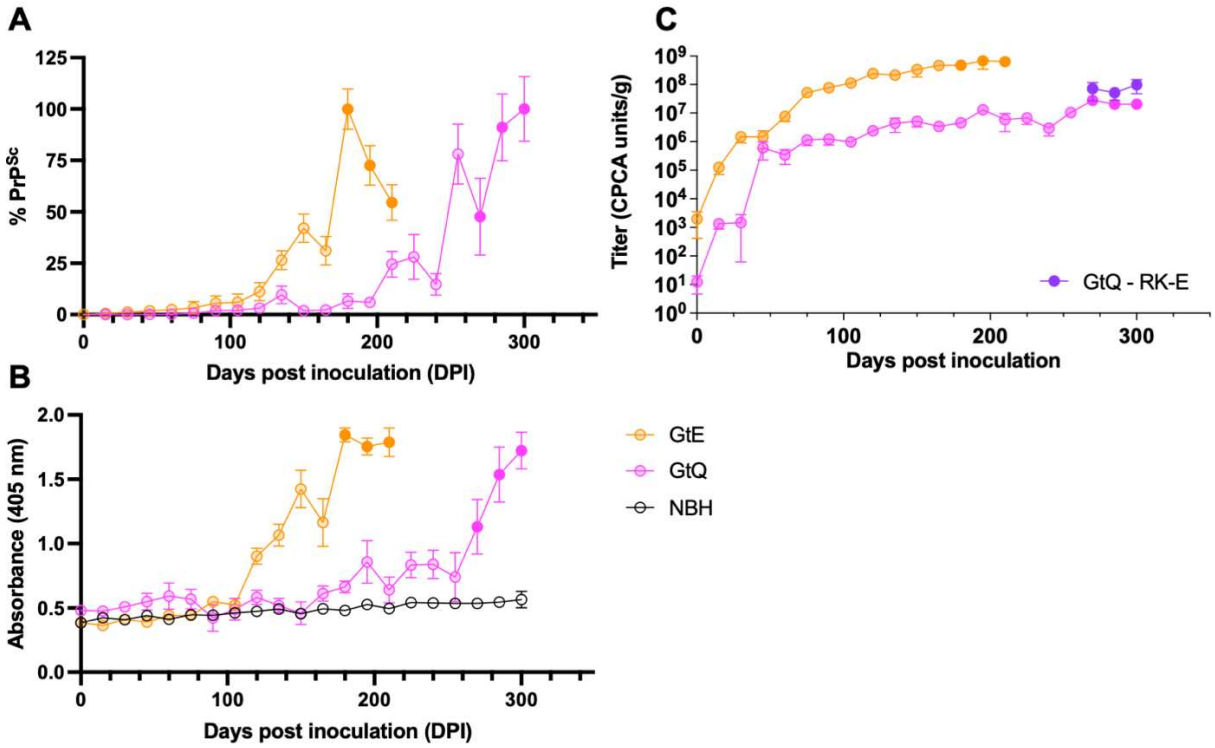

Figure 2.3 Evolution of protease-resistant and PRC7-reactive hypoglycosylated PrP^{Sc} correlate to prion titers over time in CWD infected cervid-PrP mice. (A) levels of protease-resistant PrP^{Sc} in infected mice normalized to the highest detected level of PrP^{Sc} in each mouse line. PRC5 (B) levels of hypoglycosylated PrP^{Sc} detected by PRC7 in the 7-5 ELISA format (C) CWD prion titers determined by the CPCA using RK-E and RK-D cells. PRC5. GtQ-RK-E cells = purple, GtE = orange, GtQ = pink, normal brain homogenate (NBH) = black, transparent circles = no clinical disease, filled circles = clinically diseased; n = 4 mice per timepoint

total PrP^{Sc} in GtQ mice results from diglycosylated PrP^{Sc}, significantly more than in GtE (****p < 0.0001) (Figure 2.2C). The ratio of hypoglycosylated (mono- and unglycosylated) PrP^{Sc} from GtE mice was significantly higher compared to GtQ mice (****p < 0.0001) (Figure 2.2C).

Similar to assessment by western blot, using dot blotting, PrP^{Sc} increased over the disease course (Figure 2.3A). Data was quantified as a percent of the highest PrP^{Sc} signal, which for GtE mice, was at 180 DPI, ~30 days before terminal stage (Figure 2.3A). In contrast, the highest PrP^{Sc} signal for GtQ mice occurred at the terminal stage of 300 DPI (Figure 2.3A). In both the GtE and GtQ mice, increase in PrP^{Sc} signal was not entirely linear, with some later timepoints having less signal than the previous timepoint (Figure 2.3A).

Previously, the Telling lab has created and used a discriminatory antibody, PRC7, to detect underglycosylated PrP (21,37). The epitope for PRC7 on PrP is shielded by an N-linked glycan and since PrP^{C} is preferentially diglycosylated, it is not detected with high efficiency by PRC7 (21). Prion infection leads to reduced glycosylation, and thus PRC7 detects primarily the underglycosylated forms of PrP^{Sc} (21). In both GtE and GtQ mice, hypoglycosylated PrP increased in a similar fashion to PrP^{Sc} (Figure 2.3B), confirming that PrP^{Sc} is a primarily hypoglycosylated species. Of note, in the GtE mice there is a decrease in hypoglycosylated PrP from 150 DPI to 165 DPI, immediately before the onset of clinical signs (Figure 2.3B). This is also consistent with a drop in PK-resistant PrP^{Sc} signal as shown via dot blot at the same timepoint (Figure 2.3A). This is not observed in the GtQ mice, and thus could explain another mechanistic difference between the expression of E226 vs Q226.

To address prion titer across disease course, we used CWD susceptible cells to titrate homogenates from each timepoint. Previously, the Telling lab engineered rabbit kidney epithelial (RK13) cells to express cervid-PrP, either E226 (RK-E) or Q226 (RK-D) (27). These cells have been previously shown to be susceptible to and propagate CWD prions. The cell approach to titration studies eliminates the need to do end point titration experiments involving mice and therefore is much quicker and cost effective (27). We used RK-E cells to titrate the GtE226 brain

homogenates and RK-D cells to titrate the GtQ226 brain homogenates in order to eliminate any effects of mismatching alleles. In both RK-E and RK-D cells, titer increased exponentially during the first few timepoints of infection, then leveled out and increased minimally after ~45 DPI (Figure 2.3C). The prion titer as a result of infecting RK-E cells with GtE-passaged CWD was on average, one log higher than the RK-D cells infected with GtQ-passaged CWD. As a result we infected RK-E cells with the terminal timepoints of GtQ-passaged CWD. The resulting titers were still ~ one log lower than RK-E cells infected with GtE brains (Figure 2.3C). Thus, we conclude GtQ brains have ~one log lower titer of prions when compared to GtE brains. Overall, central nervous system (CNS) PrP^{Sc}, hypoglycosylated PrP, and prion titer increase over time in a similar fashion in both GtE and GtQ mice, with GtE mice having an accelerated disease course.

Histological features are similar during early stages of disease, but diverge over time depending on residue 226

To investigate the evolution of distribution of PrP^{Sc} in the brain with respect to the 226 polymorphism, we utilized both immunohistochemistry (IHC) and histoblotting. IHC utilizes formic acid to digest PrP^{C} followed by antigen retrieval and detection with PrP mAb D18. GtE mice infected with CWD have visible PrP^{Sc} staining in the hippocampus around 90 DPI along the corpus callosum, ~80 days before clinical diagnosis at low magnification (Figure 2.4C). Staining was diffuse and bilateral in clinically sick mice (Figure 2.4E, 2.4F). When imaged at 4x magnification, no staining was visible at 0 DPI or 45 DPI (Figure 2.4A, 2.4B). However, at 100x magnification, PrP^{Sc} staining was identifiable as early as 30 DPI and 60 DPI and was visible from that time forward (Figure 2.4G, 2.4H), exemplifying the use of IHC in early disease detection. In GtQ mice infected with CWD, staining was first visible in the hippocampus at low magnification at 75 DPI along the corpus callosum, ~200 days prior to clinical disease (Figure 2.4J). IHC staining of 150 DPI and 225 DPI show increasing, localized staining on the right side

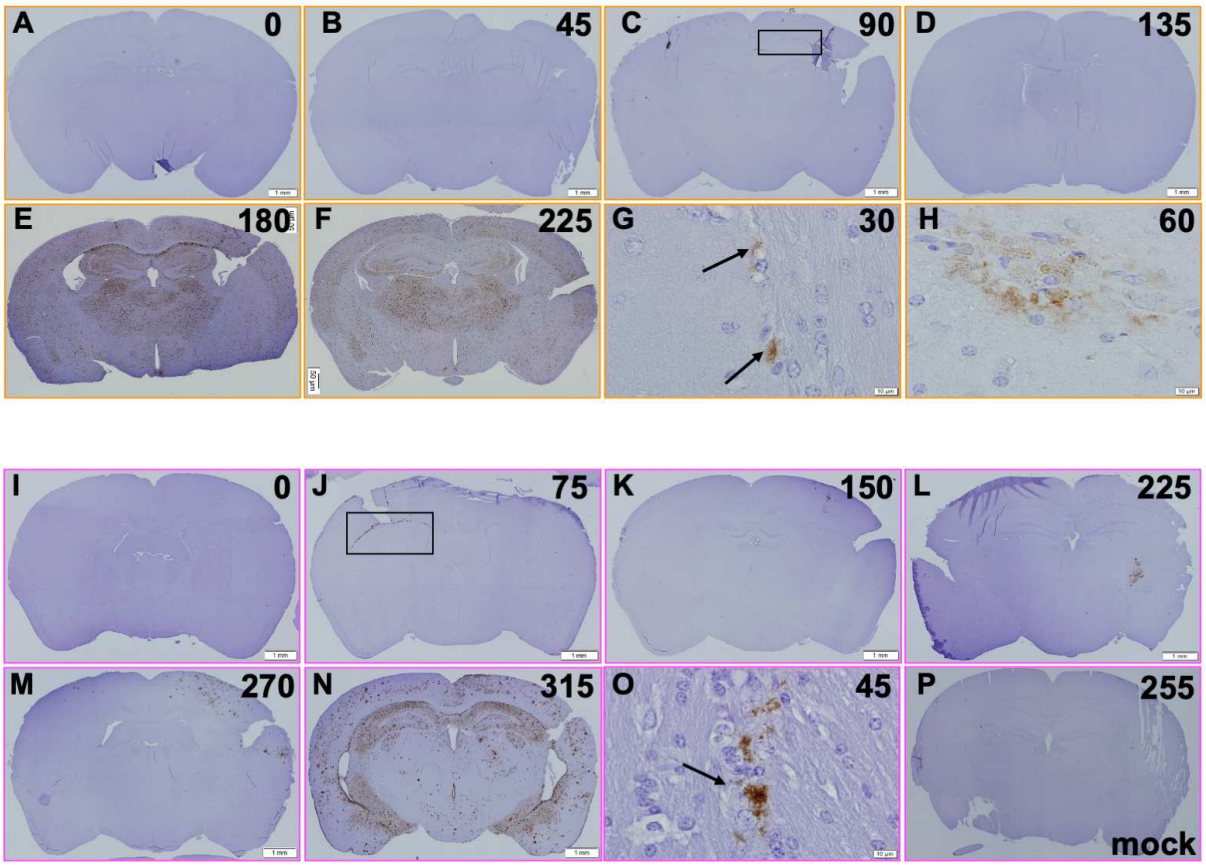

Figure 2.4 CWD distribution is similar at early timepoints but diverges as disease progresses in GtE and GtQ mice. Immunohistochemical analysis of varying timepoints of (A - H) GtE mice infected with CWD, (I - O) GtQ mice infected with CWD (P) and a mock infected GtQ mouse. Scale bar in A - F, I - N, P = 1 mm. Scale bar in G, H, O = 10μm. Boxes in C and J indicate early corpus callosum staining. Arrows in G and O indicate early PrP^{Sc} deposition only visible at higher magnification. IHC was done with mAb D18.

of the brain, the same side of which the inoculation occurred (Figure 2.4K, 2.4L). Distribution remained asymmetrical and localized at 270 DPI, when first clinical signs are noted (Figure 2.4M), but at 315 DPI, staining was distributed throughout the entire hippocampal section (Figure 2.4N). No staining was detected at 0 DPI, and residual inoculum was not detected either (Figure 2.4I). However, at 100x magnification, PrP staining was detectable starting at 45 DPI, far before any clinical signs could be noted (Figure 2.4O). A hippocampal section from a mouse

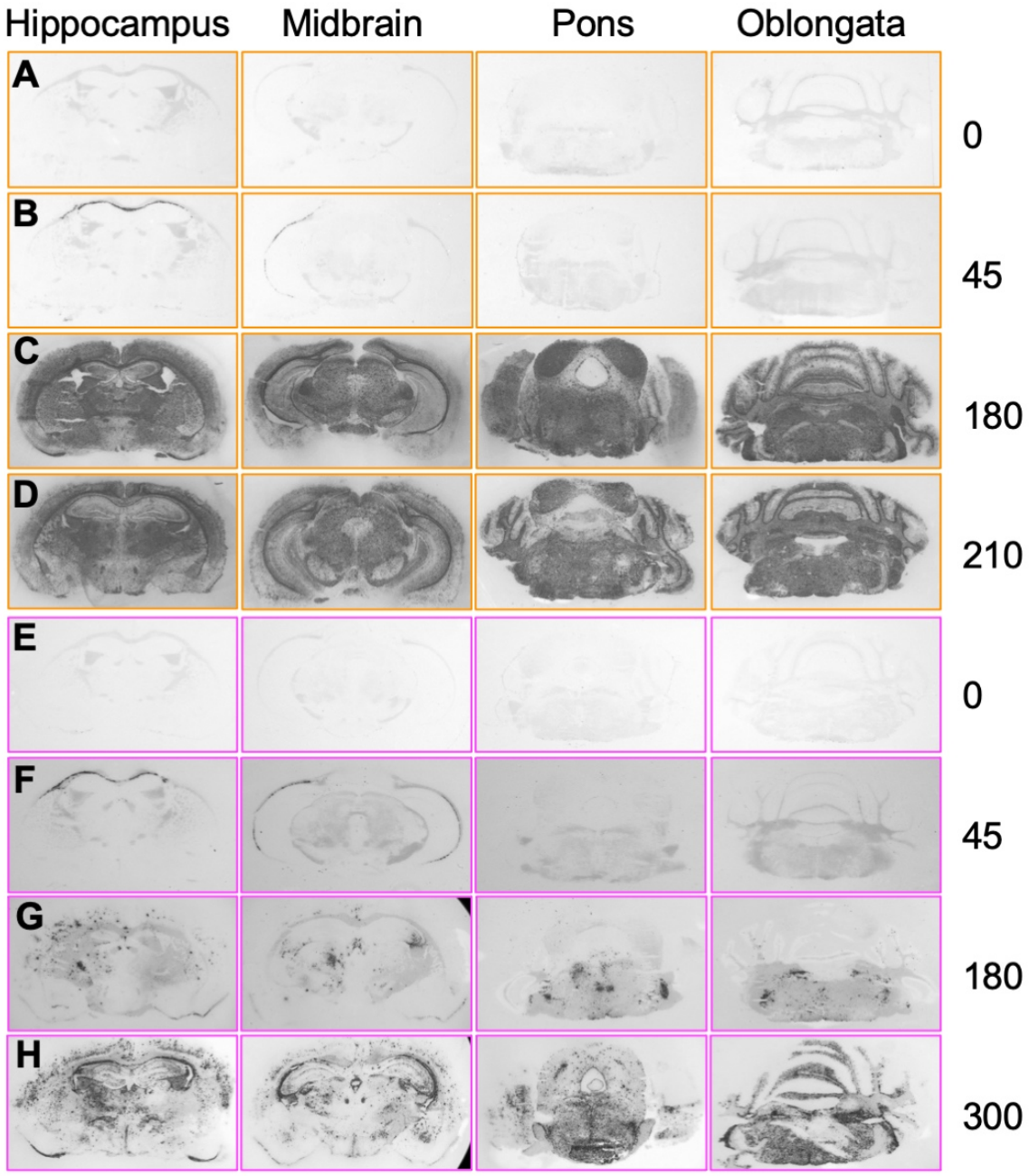

Figure 2.5 Histoblot sections of GtE and GtQ mice show similar early stage CWD distribution, but dissimilar distribution at terminal stage. Hippocampal, midbrain, pons and oblongata sections of (A - D) GtE mice infected with CWD, orange (E - H) GtQ mice infected with CWD, pink. DPI listed to the right of each row.

inoculated with uninfected brain homogenate and collected at 255 DPI is shown as a comparative negative control (Figure 2.4P). We conclude in both GtE and GtQ mice, PrP^{Sc} accumulation starts as smaller accumulations, but grow over time to show amalgamated

staining at low resolution. Interestingly, at early timepoints, staining can be detected along the corpus callosum, but no other brain regions (Figure 3.4C, 3.4J) before the GtE staining turns symmetrical and diffuse and the GtQ staining turns clumped and asymmetrical.

To further investigate protease-resistant PrP^{Sc} distribution in the brain using histoblotting, whole snap frozen brains are cut at a thickness of 10μm using a cryostat, allowing extremely precise sectioning. Using cerebral landmarks, hippocampal, midbrain, pons and oblongata sections were taken. For both infected GtE and GtQ mice, no staining was seen at 0 DPI in any of the coronal sections (Figure 3.5A, 3.5E). At 45 DPI, both GtE and GtQ mice show PrP^{Sc} distributed across the corpus callosum in the hippocampal section to the external capsule (white matter tracts) in the midbrain section (Figure 3.5B, 3.5F). However, at 180 DPI when the clinical phase starts in the GtE mice, PrP^{Sc} is diffuse across all sections and distributed widely and symmetrically (Figure 3.5C). This phenotype is maintained to the terminal timepoint of 210 DPI as PrP^{Sc} is widely distributed across the brain (Figure 3.5D). In contrast, at 180 DPI in the GtQ background, staining is disordered and more amalgamated (Figure 3.5G). The terminal timepoint of GtQ mice maintains this phenotype, just more widespread (Figure 3.5H). Concurrent with the IHC, PrP^{Sc} distribution in early disease timepoints appears to be similar in the GtE and GtQ mice, but as disease progresses, GtE PrP^{Sc} distribution remains diffuse, while GtQ PrP^{Sc} distribution compacts.

Discussion

Here we report the results of a longitudinal study of CWD pathogenesis using mice expressing endogenous levels of cervid PrP. Because the GtE and GtQ mice are syngeneic except at residue 226 of PrP, we can confidently attribute any difference in the two mouse lines to the. effect of residue 226. Though overexpression of cervid-PrP accelerates CWD disease course, comparative studies of single amino acid polymorphisms were not possible with previously used transgenic cervid-PrP mice due to uncontrollable random integration of the

transgene array and variable copy number of the transgene (38). We recapitulate the effect of residue 226 on disease kinetics published by Bian et al (20) and show that when inoculated with CWD, GtE mice succumb to disease faster than GtQ mice (Figure 2.1E). Since mice were inoculated with the same starting elk CWD isolate, the difference in disease kinetics supports the conformational selection model in that E226 elk PrP^{C} propagates a different strain than Q226 deer PrP^{C} (39).

It has been shown previously that the glycoform ratio of PrP^{Sc} species can be used to distinguish strains in human prion disease (40). Here we show in addition to disease kinetics, glycoform ratios differ with GtQ mice having a higher ratio of diglycosylated PrP^{Sc} compared to GtE mice (Figure 2.2C). Since glycans can sterically hinder proteins, a potential contributor to faster time to disease onset in the GtE mice could be the relatively hypoglycosylated PrP^{Sc} propagated by the GtE mice. We speculate that a reason GtE mice succumb to disease faster than GtQ mice could be due to the relatively less glycosylated PrP^{Sc} species that GtE mice propagate as compared to GtQ mice. We recapitulate data supporting the idea that glycosylation state may play a role in the rate of PrP conversion (41–43).

Additionally, we show delayed accumulation of PrP^{Sc} and hypoglycosylated PrP in GtQ mice compared to GtQ, correlating with longer time to disease onset in GtQ mice (Figure 2.3A, 2.3B). CWD titer in both GtE and GtQ mice increases rapidly in the first months of disease, then levels out (Figure 2.3C). CWD titer, in comparison to PrP^{Sc} seems to accumulate exponentially at early timepoints, then linearly at later timepoints. The exponential growth of titer occurs before we can detect PrP^{Sc} via western blotting or dot blotting due to the limits of detection of the assays, thus we only detect linear increase in signal with immunoblotting. Aside from delayed onset in the GtQ mice, once detectable accumulation begins, PrP^{Sc} accumulates at a similar rate in both GtE and GtQ backgrounds. A potential explanation for the exponential accumulation of titer vs the more linear accumulation of PrP^{Sc} could be the existence of multiple species of PrP^{Sc}. The Collinge lab postulates that prion propagation and toxicity occur in two

distinct phases; the former involving exponential replication of PrP^{Sc} titer with no clinical manifestation, and the later involving a plateau phase in titer with clinical manifestation (44).

Previously, the Telling lab showed distinct pathologies of elk CWD and deer CWD when inoculated into the Gt-cervid-PrP mice. GtQ mice inoculated with either CWD originating from a deer (Q226) or elk (E226) resulted in large, asymmetrical and disordered plaques (20). GtE mice inoculated with elk CWD showed diffuse, symmetrical PrP^{Sc} staining, while GtE mice inoculated with deer CWD resulted in more amalgamated, ipsilateral to the inoculation site staining (20). E226-PrP and Q226-PrP mice potentially propagate different quasispecies from the same CWD strain, and that the species propagated by E226 mice has less propensity to aggregate while the Q226 species does. This likely stems from the PrP^{Sc} structure formed from conversion of E226-PrP vs Q226-PrP. While at terminal stage, pathologies vastly differ, the initial accumulation of PrP^{Sc} is nearly identical. At early timepoints, ~45 DPI, PrP^{Sc} is distributed along the corpus callosum, the bundle of nerve fibers responsible for communication between the two hemispheres of the brain. We inoculate our mice intracerebrally into the right parietal lobe, but by end stage of disease, PrP^{Sc} is visible in all coronal sections ranging from the forebrain to hindbrain. Transport via the corpus callosum could account for the widespread distribution of CWD at end stage of disease. Since CWD prions propagated by the E226-PrP and Q226-PrP initially spread via the same corpus callosum mechanism, there must be a mechanism later in disease which dictates the diverse terminal phenotype.

Residue 226 of PrP lies in the third α-helical region of the protein, towards the C-terminal end of the protein. When folded into its final conformation, this region of the protein is known to form a discontinuous epitope with the β2–α2 loop (45,46). Interestingly, adjacent to 226, residue 225 can also be polymorphic in mule deer, either serine (S) or phenylalanine (F). Mule deer expressing SF225 were shown to have less likelihood of CWD in the wild compared to SS225 mule deer (47). Molecular dynamics studies of PrP^{C} show additional hydrogen bonding of Q226 with two carbonyl groups of the C-terminal loop with genotype F225-Q226 (48). F225-E226,

S225-Q226 or S225-Q226 did not have this additional hydrogen bonding, indicating potential structural differences stemming from polymorphisms in the α3 region. In collaboration with Witold Surewicz at Case Western University, we are currently investigating the structure of E226-PrP^{Sc} and Q226-PrP^{Sc} propagated in our Gt mice using cryogenic electron microscopy. We predict that structural differences in E226-PrP^{Sc} and Q226-PrP^{Sc} will account for the profound differences in the CWD strain propagated by each. Ongoing surveillance and sequencing of cervids in the wild is being done in the US and in Nordic countries, where novel cases of CWD have emerged, in hopes of identifying cervid-PrP polymorphisms which contribute to susceptibility to CWD. Further characterizing the residue 226 polymorphism, and other polymorphisms known to associate with susceptibility to CWD could instruct wildlife biologists of geographical areas where cervids are more or less susceptible to CWD.

REFERENCES

1. Ma J, Wang F. Prion disease and the “proteinonly hypothesis.” Essays Biochem. 2014;56(1):181–91.

2. Hill AF, Desbruslais M, Joiner S, Sidle KCL, Gowland I, Collinge J, et al. The same prion strain causes vCJD and BSE. Vol. 389, Nature. 1997. p. 448–50.

3. Williams ES. Review article - Chronic Wasting Disease. Vet Pathol. 2005;42(5):530–49.

4. Williams ES, Young S. Spongiform encephalopathy of Rocky Mountain elk. J Wildl Dis. 1982;18(4):465–71.

5. Baeten LA, Powers BE, Jewell JE, Spraker TR, Miller MW. A natural case of chronic wasting disease in a free-ranging moose (Alces alces shirasi). J Wildl Dis. 2007;43(2):309–14.

6. Kahn S, Dubé C, Bates L, Balachandran A. Chronic wasting disease in Canada: Part 1. Vol. 45, Canadian Veterinary Journal. 2004. p. 397–404.

7. Sohn HJ, Kim JH, Choi KS, Nah JJ, Joo YS, Jean YH, et al. A case of chronic wasting disease in an elk imported to Korea from Canada. Journal of Veterinary Medical Science. 2002;64(9):855–8.

8. Benestad SL, Telling GC. Chronic wasting disease: an evolving prion disease of cervids. In: Handbook of Clinical Neurology. 2018. p. 135–51.

9. Benestad SL, Mitchell G, Simmons M, Ytrehus B, Vikøren T. First case of chronic wasting disease in Europe in a Norwegian free-ranging reindeer. Vet Res. 2016;47(1):88.

10. Prusiner SB. Novel proteinaceous infectious particles cause scrapie. Science (1979). 1982;216(4542):136–44.

11. Aguzzi A, Heikenwalder M, Polymenidou M. Insights into prion strains and neurotoxicity. Vol. 8, Nature Reviews Molecular Cell Biology. 2007. p. 552–61.

12. Bessen RA, Marsh RF. Biochemical and physical properties of the prion protein from two strains of the transmissible mink encephalopathy agent. J Virol. 1992;66(4):2096–101.

13. Bessen RA, Marsh RF. Identification of two biologically distinct strains of transmissible mink encephalopathy in hamsters. Journal of General Virology. 1992;73(2):329–34.

14. Moore RA, Vorberg I, Priola SA. Species barriers in prion diseases--brief review. Archives of virology. Supplementum. 2005. p. 187–202.

15. Arifin MI, Hannaoui S, Chang SC, Thapa S, Schatzl HM, Gilch S. Cervid prion protein polymorphisms: Role in chronic wasting disease pathogenesis. Vol. 22, International Journal of Molecular Sciences. 2021. p. 2271.

16. Otero A, Duque Velásquez C, Aiken J, McKenzie D. White-tailed deer S96 prion protein does not support stable in vitro propagation of most common CWD strains. Sci Rep. 2021;11(1):11193.

17. Green KM, Browning SR, Seward TS, Jewell JE, Ross DL, Green MA, et al. The elk PRNP codon 132 polymorphism controls cervid and scrapie prion propagation. Journal of General Virology. 2008;89(2):598–608.

18. Kaski D, Mead S, Hyare H, Cooper S, Jampana R, Overell J, et al. Variant CJD in an individual heterozygous for PRNP codon 129. The Lancet. 2009;374(9707):2182.

19. Kaluz S, Kaluzova M, Flint APF. Sequencing analysis of prion genes from red deer and camel. Gene. 1997;199(1–2):283–6.

20. Bian J, Christiansen JR, Moreno JA, Kane SJ, Khaychuk V, Gallegos J, et al. Primary structural differences at residue 226 of deer and elk PrP dictate selection of distinct CWD prion strains in gene-targeted mice. Proc Natl Acad Sci U S A. 2019;12478–87.

21. Kang HE, Bian J, Kane SJ, Kim S, Selwyn V, Crowell J, et al. Incomplete glycosylation during prion infection unmasks a prion protein epitope that facilitates prion detection and strain discrimination. J Biol Chem. 2020;10420–33.

22. Miller MW, Williams ES, McCarty CW, Spraker TR, Kreeger TJ, Larsen CT, et al. Epizootiology of chronic wasting disease in free-ranging cervids in Colorado and Wyoming. J Wildl Dis. 2000;36(4):676–90.

23. Browning SR, Mason GL, Seward T, Green M, Eliason GAJ, Mathiason C, et al. Transmission of Prions from Mule Deer and Elk with Chronic Wasting Disease to Transgenic Mice Expressing Cervid PrP. J Virol. 2004;78(23):13345–50.

24. Angers RC, Seward TS, Napier D, Green M, Hoover E, Spraker T, et al. Chronic wasting disease prions in eik antler velvet. Emerg Infect Dis. 2009;15(5):696–703.

25. Schneider CA, Rasband WS, Eliceiri KW. NIH Image to ImageJ: 25 years of image analysis. Vol. 9, Nature Methods. 2012. p. 671–5.

26. Bian J, Kang HE, Telling GC. Quinacrine promotes replication and conformational mutation of chronic wasting disease prions. Proc Natl Acad Sci U S A. 2014;111(16):6028–33.

27. Bian J, Napier D, Khaychuck V, Angers R, Graham C, Telling G. Cell-Based Quantification of Chronic Wasting Disease Prions. J Virol. 2010;84(16):8322–6.

28. Klöhn PC, Stoltze L, Flechsig E, Enari M, Weissmann C. A quantitative, highly sensitive cell-based infectivity assay for mouse scrapie prions. Proc Natl Acad Sci U S A. 2003;100(20):11666–71.

29. Mahal SP, Baker CA, Demczyk CA, Smith EW, Julius C, Weissmann C. Prion strain discrimination in cell culture: The cell panel assay. Proc Natl Acad Sci U S A. 2007;104(52):20908–13.

30. Mahal SP, Demczyk CA, Smith EW, Klohn PC, Weissmann C. Assaying prions in cell culture: The standard scrapie cell assay (SSCA) and the scrapie cell assay in end point format (SCEPA). Methods in Molecular Biology. 2008;459:49–68.

31. Taraboulos A, Jendroska K, Serban D, Yang SL, Dearmond SJ, Prusiner SB. Regional mapping of prion proteins in brain. Proc Natl Acad Sci U S A. 1992;89(16):7620–4.

32. Muramoto T, DeArmond SJ, Scott M, Telling GC, Cohen FE, Prusiner SB. Heritable disorder resembling neuronal storage disease in mice expressing prion protein with deletion of an α-helix. Nat Med. 1997;3(7):750–5.

33. DeVivo MT, Edmunds DR, Kauffman MJ, Schumaker BA, Binfet J, Kreeger TJ, et al. Endemic chronic wasting disease causes mule deer population decline in Wyoming. PLoS One. 2017;12(10):0186512.

34. Mysterud A, Madslien K, Viljugrein H, Vikøren T, Andersen R, Güere ME, et al. The demographic pattern of infection with chronic wasting disease in reindeer at an early epidemic stage. Ecosphere. 2019;10(11):2931.

35. Rogers W, Brandell EE, Cross PC. Epidemiological differences between sexes affect management efficacy in simulated chronic wasting disease systems. Journal of Applied Ecology. 2022;59(4):14125.

36. Race RE, Raines A, Baron TGM, Miller MW, Jenny A, Williams ES. Comparison of Abnormal Prion Protein Glycoform Patterns from Transmissible Spongiform Encephalopathy Agent-Infected Deer, Elk, Sheep, and Cattle. J Virol. 2002;76(23):12365–8.

37. Kang HE, Weng CC, Saijo E, Saylor V, Bian J, Kim S, et al. Characterization of conformation-dependent prion protein epitopes. Journal of Biological Chemistry. 2012;287(44):37219–32.

38. Prusiner SB, Scott M, Foster D, Pan KM, Groth D, Mirenda C, et al. Transgenetic studies implicate interactions between homologous PrP isoforms in scrapie prion replication. Cell. 1990;63(4):673–86.

39. Collinge J, Clarke AR. A general model of prion strains and their pathogenicity. Vol. 318, Science. 2007. p. 930–6.

40. Hill AF, Joiner S, Beck JA, Campbell TA, Dickinson A, Poulter M, et al. Distinct glycoform ratios of protease resistant prion protein associated with PRNP point mutations. Brain. 2006;129(3):676–85.

41. Nishina KA, Deleault NR, Mahal SP, Baskakov I, Luhrs T, Riek R, et al. The stoichiometry of host PrPC glycoforms modulates the efficiency of PrPSc formation in vitro. Biochemistry. 2006;45(47):14129–39.

42. Priola SA, Lawson VA. Glycosylation influences cross-species formation of protease-resistant prion protein. EMBO Journal. 2001;20(23):6692–9.

43. Tuzi NL, Cancellotti E, Baybutt H, Blackford L, Bradford B, Plinston C, et al. Host PrP glycosylation: A major factor determining the outcome of prion infection. PLoS Biol. 2008;6(4):e100.

44. Sandberg MK, Al-Doujaily H, Sharps B, Clarke AR, Collinge J. Prion propagation and toxicity in vivo occur in two distinct mechanistic phases. Nature. 2011;470(7335):540–2.

45. Pérez DR, Damberger FF, Wüthrich K. Horse Prion Protein NMR Structure and Comparisons with Related Variants of the Mouse Prion Protein. J Mol Biol. 2010;400(2):121–8.

46. Christen B, Hornemann S, Damberger FF, Wüthrich K. Prion Protein NMR Structure from Tammar Wallaby (Macropus eugenii) Shows that the β2-α2 Loop Is Modulated by Long-Range Sequence Effects. J Mol Biol. 2009;389(5):833–45.

47. Jewell JE, Conner MM, Wolfe LL, Miller MW, Williams ES. Low frequency of PrP genotype 225SF among free-ranging mule deer (Odocoileus hemionus) with chronic wasting disease. Journal of General Virology. 2005;86(8):2127–34.

48. Angers R, Christiansen J, Nalls A v., Kang HE, Hunter N, Hoover E, et al. Structural effects of PrP polymorphisms on intra- and interspecies prion transmission. Proc Natl Acad Sci U S A. 2014;11169–74.

CHAPTER 3 - CHRONIC WASTING DISEASE IN NORDIC CERVIDS: ANALYSIS OF STRAIN VARIATION FROM CWD INFECTED MOOSE AND RED DEER

Introduction

CWD was first documented in 1967 at a Northern Colorado research facility and has been endemic to North America for at least 50 years (1,2). Specifically, the endemic region constitutes northern Colorado, southern Wyoming and western Nebraska (2–4). Initially the disease was described in mule deer (*Odocoileus hemionus hemionus*) and Rocky Mountain elk (*Cervus elaphus nelsoni*) (2). Early efforts to contain the disease failed, and now CWD has been documented in 30/50 states, though the actual incidence may be higher. CWD is also rapidly expanding in both free-ranging and farmed cervids in 3 provinces in Canada, north of the endemic region: Alberta, Saskatchewan, and Manitoba (5). Since each state has different regulations about CWD testing, the 20 states that have not yet reported any cases could be under-testing cervid populations. For example, in the endemic region in Colorado, it is mandatory to submit any hunted deer for testing by the Colorado Parks and Wildlife (https://cpw.state.co.us/learn/Pages/ResearchCWD-Submission.aspx). Yet, even though three states which border Indiana (Illinois, Ohio and Michigan) have all detected CWD, Indiana has not reported any cases, highlighting the importance of constant surveillance.

CWD in North America has also spread from the original affected cervid species, mule deer and Rocky Mountain elk, to additional susceptible cervids. It was reported in white-tailed deer (*Odocoileus virginianus*) for the first time in 2001 in free-ranging deer in South Dakota and on a farm in Nebraska (6). In Colorado, the first captive moose (*Alces alces shirasi*) was diagnosed with CWD in 2006 and the first free-ranging moose was diagnosed shortly after in Colorado (7,8). Most recently CWD cases have been reported in red deer (*Cervus elaphus*) on a farm in Quebec (9). Additionally in the early 2000s, CWD was inadvertently transported from

subclinical animals in Canada to cervid farms in South Korea (10,11). Affected species in South Korea include elk, red deer, sika deer, and crosses between red deer and sika deer (11).

Prior to 2016, other than accidental transmission to South Korea, CWD has only been reported in North America and can largely be traced to spread from the endemic region. In April of 2016, for the first time, CWD was detected in Europe. The case was in a free-ranging reindeer (*Rangifer tarandus tarandus*) in Norway (12). As a result, subsequent testing revealed evidence of CWD in additional reindeer, European moose (*Alces alces alces*) and red deer in Norway (13,14). As authorities in Norway understood the contagiousness of CWD in North America, they decided to cull the entire herd of ~2000 reindeer (about 7% of the total reindeer population in Norway) in the Nordfjella region where the CWD cases were found (15). All culled reindeer were tested, and the cull resulted in 19 total CWD positive reindeer, indicative of the beginning of an epidemic (15). The cull was done in hopes of eradicating the disease before an epidemic could happen. However, another reindeer hunted in the Hardangervidda region ~70km south of the original CWD cases, was found to be positive in 2020, indicative that the cull was not 100% effective in containing the disease and underscoring the persistence of CWD prions in the environment (16). Following the initial cull and discovery of multiple CWD positive reindeer, the European Food Safety Authority recommended six nearby countries start a three-year CWD surveillance program (17). As a result, detection of CWD occurred in two moose in Finland, and four moose in Sweden (18). To date, ~ 20 reindeer, 11 moose, and three red deer have been found to be CWD positive in Norway (16). Other than the moose in Finland and Sweden, no additional cases have been documented in surrounding countries.

The discovery of CWD in Europe raised alarms that an accidental transmission, like in the case of South Korea had occurred again. However, Norway has strict laws regarding importation, and importation of cervids is not legal. Analysis of the brain of the first reindeer CWD case revealed a western blot profile and spongiform degeneration similar to that of North American elk (12). CWD was also detected in lymph nodes, indicating reindeer CWD is

lymphotropic like North American strains of CWD. Data from the Telling lab primarily recapitulates this using passage through gene-targeted (Gt) cervid mice (19). Intracerebral transmission of retropharyngeal lymph node (RPLN) material from reindeer is able to cause disease in cervid-PrP mice. Additionally, disease is observed in cervid-PrP mice intraperitoneally inoculated with Norwegian reindeer CWD (unpublished data from the Telling lab). As deer, moose and reindeer express glutamine (Q) at residue 226 of PrP and elk express glutamate (E) at the same residue, the Telling lab designed and created gene-targeted mice, aptly named GtQ226 (GtQ) and GtE226 (GtE), to study this polymorphism and the response of multiple CWD isolates, both North American and Norwegian to the residue 226 polymorphism (see chapter 2 for extensive analysis on North American CWD). When transmitted to GtQ and GtE mice, North American isolates faithfully cause more rapid disease in the GtE mice. However, when we intracerebrally inoculated the GtQ and GtE mice with CNS material from the first three Norwegian reindeer cases, transmission efficiency was equivalent in both mouse lines (19). GtQ-passaged and GtE-passaged reindeer present similar western blotting profile and PrP^{Sc} distribution in the brains of mice compared to North American CWD (19). Yet, when challenged with increasing concentrations of guanidine hydrochloride (Gdn HCl), a denaturing chaotropic agent, Gt cervid-passaged reindeer PrP^{Sc} was less stable than Gt cervid-passaged North American CWD (19). Taken together, the strain of CWD found in Norwegian reindeer is not the same as North American CWD but exhibits fairly similar characteristics, providing more evidence for divergent origins of Norwegian reindeer CWD and North American CWD.

In addition to the CWD positive reindeer herd, three moose in Norway were subsequently diagnosed with CWD. The first moose (M-NO1) was diagnosed in May 2016 after being observed to be emaciated and having a loss of fear of humans (14). The second moose (M-NO2) tested positive after being found dead in a river also in May 2016. In October 2017, the third moose (M-NO3) was identified after showing loss of fear of humans (14). All three moose were older, female moose (Table 3.1). The three moose were found in Trøndelag County in

central Norway, ~350 km northeast of the region where the CWD positive reindeer were found. Though cervids are migratory animals, prior global positioning satellite-collared moose data have not showed migration between Trøndelag County and Nordfjella, where the reindeer were found (20–22).

PrP sequencing was done as well, and all three moose were found to have genotype KK109-MM209 (14). PrP sequencing was done at the Norwegian Veterinary Institute, and later confirmed in the Telling lab. European moose (*Alces alces alces*) but not North American moose (*Alces alces shirasi*) display a polymorphism at residue 109 of PrP where either methionine (M) or lysine (K) can be expressed. Sampling across Norway determined ~75% of moose express KK and ~25% express QQ (23). The 109KK polymorphism was distributed primarily in the northernmost and southernmost regions of Norway. North American moose, but not Norwegian moose can be polymorphic, either methionine (M) or isoleucine (I) at residue 209 of PrP, though its bearing on CWD susceptibility is unknown (24,25).

The initial confirmation of PrP^{Sc} in the moose samples was done using western blotting and immunohistochemistry (IHC). Western blotting revealed an electrophoretic mobility profile distinct from both the Norwegian reindeer and Canadian elk with Norway moose having a lower molecular weight after PK digestion, indicative of a smaller PK-resistant core (14). Concurrently, IHC revealed a diffuse, mostly intraneuronal staining pattern unlike the large, amalgamated plaques typically seen in CWD (14). As was the case with Norwegian reindeer, the Telling lab used GtQ and GtE mice to characterize the strain properties of the first three Norwegian moose cases. In contrast to North American CWD, Norwegian moose CWD transmitted with efficiency to the GtQ mice rather than the GtE mice (19). Western blot profile and histological characteristics were maintained from the original isolate (19). Additionally, all Norwegian moose isolates had a higher stability in response to increasing concentrations of Gdn HCl (19). When M-NO2 was serially passaged from a Q226 mouse brain to the E226 background, about 50% of the mice developed disease at a faster rate than the Q226 mice. Serial passaging of those E226

brains to subsequent E226 mice, caused rapid disease with a phenotype resembling North American CWD, indicative of the propensity of Norwegian moose CWD to be highly adaptable (19). We speculate the strains of CWD infecting Norwegian cervids are unstable have not yet evolved to be the steadfast conformation that infects North American cervids.

In addition to afflicted reindeer and moose, three red deer in Norway have been found to be CWD positive. The first was hunted in western Norway and did not appear to be exhibiting any clinical signs, but as a part of the national CWD surveillance program, the medulla oblongata was submitted for testing and confirmed positive (13). Red deer present an interesting case in relation to residue 226 of cervid-PrP as they can be polymorphic – EE226, EQ226 or QQ226 at this residue. Additionally, consistent with the previously characterized moose, all lymph nodes were negative for CWD.

As CWD is a lymphotropic prion disease, and the leading hypothesis for CWD transmission is through animal-to-animal transmission and environmental contamination, the etiology of non-lymphotropic CWD cases in moose and red deer are intriguing. This chapter will detail the additional cases of CWD across Norway, Sweden and Finland in moose and one Norwegian red deer to characterize newly emergent CWD strains and address the potential for these cases to be of a sporadic, atypical origin as opposed to from infection from another animal.

Materials and Methods

Ethics Statement

All animal work was performed in an Association for Assessment and Accreditation of Laboratory Animal Care International accredited facility in accordance with the Guide for the Care and Use of Laboratory Animals. All procedures used in this study were performed in compliance with and were approved by the Colorado State University Institutional Animal Care and Use Committee.

CWD Inocula

The elk isolate referred to as E-US1 represents a diseased Rocky Mountain elk, 99w12398 (99w), that has been previously described (26,27). Norwegian moose isolates M-NO1, M-NO2, M-NO3 have been previously described (14). The first moose (M-NO1) was diagnosed in May 2016 after being observed to be emaciated and having a loss of fear of humans (14). The second moose (M-NO2) tested positive after being found dead in a river also in May 2016. In October 2017, the third moose (M-NO3) was identified after showing loss of fear of humans (14). All three moose were older, female moose (Table 3.1). The three moose were found in Trøndelag County in central Norway, ~350 km northeast of the region where the CWD positive reindeer were foundThe Norwegian red deer isolate has been previously described (13). Norwegian moose isolates M-NO1 – M-NO11 and the Norwegian red deer isolate were generously provided as part of a collaboration with Dr. Sylvie Benestad at the Norwegian Veterinary Institute. M-SW1 – M-SW3 are described here (18). Swedish moose isolates were generously provided as part of a collaboration with Dr. Sylvie Benestad at the Norwegian Veterinary Institute and Maria Nöremark and Dolores Gavier-Widen at the Swedish National Veterinary Institute. M-F1 was also generously provided by Sylvie Benestad in collaboration with Sirkka-Liisa Korpenfelt at the Finnish Food Authority.

Animal work

The development and characterization of TgQ226, TgE226, GtQ226, and GtE226 mice has been previously described (28–30). For inoculation of mice, 10% homogenates of brain tissue from CWD affected moose, red deer and elk or cervid-PrP mouse brains were prepared by mechanical disruption (MP Biomedical) in phosphate-buffered saline (PBS) lacking calcium and magnesium ions. Equal numbers of male and female mice between the ages of four to six weeks were anaesthetized with halothane and intracerebrally (ic) inoculated freehand with 30 μl

of 1% brain tissue homogenates into the right parietal lobe using a 26-gauge needle at a depth of ~ 2 mm. All animals were subsequently monitored three times a week for the development of neurological signs consistent with prion disease phenotypes. These signs included truncal ataxia, loss of extensor reflex, slowed movement, unsteady or flattened gait, plastic tail, dorsal kyphosis, head bobbing, rough coat and weight loss or gain. The time to disease onset, aka incubation period, is defined as the time between inoculation and the first day on which subsequently progressive clinical signs were identified. Unless otherwise stated, all animals for which a clinical diagnosis was made were confirmed to have died as a result of prion infection by analysis of PrP^{Sc} in central nervous system (CNS) material by various means. Studies for which no clinical signs were noted were terminated ~ 600 days post inoculation as the healthy life span of the mice was reached.

Analysis of PrP^{Sc} by Western Blotting

Protein concentrations of 10% brain homogenates or 20% spleen homogenates were determined by bicinchoninic acid assay (BCA) (Pierce Biotechnology). Brain homogenates were treated with 50 μg/mL PK (Roche) in the presence of 2% sarkosyl for 1 hour at 37 °C. PK digestion was terminated with phenylmethylsulfonyl fluoride (PMSF) at a final concentration of 2 mM. Spleen homogenates were treated with 100 U/ml benzonase (Sigma) for 1 hour at 37 °C and 300 rpm, then incubated at room temperature for 30 minutes in the presence of 10% sarkosyl. Samples were ultracentrifuged at 22,000 x g for 15 minutes at 10 °C and the pellet was discarded. The supernatant was treated with 50 μg/mL PK for 1 hour at 37 °C and 500 rpm. Digestion was stopped with PMSF at final concentration of 2 mM. Samples were ultracentrifuged at 100,000 x g for 45 minutes at 10 °C and the supernatant was discarded. Pellets were resuspended in PBS. Prior to electrophoresis, both brain and spleen samples were boiled at 100 °C for 5 minutes in XT-sample buffer (Bio-Rad Laboratories) in the absence of

reducing agents. Samples were loaded onto precast 12% discontinuous Bis-Tris gels (Bio-Rad Laboratories). Proteins were then transferred overnight to PVDF-FL membranes (Millipore). Membranes were blocked for 1 hour in 5% nonfat milk in TBS-T, probed with monoclonal antibodies (mAbs) PRC5 and PRC1 (31) followed by horseradish peroxidase (HRP)-conjugated anti-mouse IgG secondary antibody (Cytiva). Membranes were developed using ECL 2 western blot substrate (Thermo Scientific).

Histoblot Analysis

Histoblots were prepared and analyzed as previously described (32). Whole brains were snap frozen on dry ice. Ten μm coronal cryostat sections on slides were transferred to nitrocellulose membranes using lysis buffer. Membranes were treated with 0.2 mg/ml PK for 1 hour at 37 °C then incubated with 2 mM PMSF for 15 minutes. Membranes were incubated with 3 M guanidine isothiocyanate for 10 minutes at room temperature and then blocked in 5% nonfat milk for 30 minutes. Next, membranes were incubated overnight at 4 °C with mAb PRC5 at a dilution of 1:5000. Alkaline phosphatase conjugated goat anti mouse IgG (Southern Biotech) was then incubated for 1 hour at room temperature at a dilution of 1:5000. Membranes were developed using 5-bromo-4-chloro-3-indolyl phosphate (BCIP)/nitro blue tetrazolium (NBT) tablets (Sigma Aldrich) for 5-15 minutes. Micrographs were captured using a Nikon Z1000 microscope.

Immunohistochemical Analyses

Immunohistochemistry (IHC) was performed as previously described (33). In brief, brains were fixed in 10% formalin. Slides with paraffin embedded brain slices were heated to 60 °C for 30 minutes prior to xylene and graduated ethanol treatment followed by treatment with 88% formic acid for 30 minutes. Antigen retrieval was then performed in the 2100 Retriever

(ProteoGenix) using citrate buffer followed by endoperoxidase quenching in 3% hydrogen peroxide. Slides were blocked in 5% nonfat milk for 30 minutes at room temperature before overnight incubation at 4 °C with primary antibody D18 at a 1:2500 dilution. Slides were incubated with biotin labelled goat Fab anti-human IgG secondary antibody (Southern Biotech) at a dilution of 1:5000 for 1 hour at room temperature. Slides were developed with avidin-conjugated HRP with diaminiobenzidine (DAB) as a substrate for 30 minutes at room temperature (Vector Laboratories). Slides were counterstained with hematoxylin, run through graduated ethanol treatment, cover slipped and micrographs captured at 4x or 100x under oil immersion using an Olympus microscope.

Conformational stability assay

The conformational stability assay was conducted as previously described (19,30,34,35). Briefly, brain homogenates containing 2.5 μg to 30 μg protein were incubated with various concentrations of guanidine hydrochloride (GdnHCl) in 96-well plates for 1 hour at room temperature. Samples were adjusted with PBS to 0.5 M GdnHCl and transferred onto nitrocellulose membrane (Whatman GmbH, Dassel, Germany) using a dot blot apparatus. After two PBS washes, the membrane was air-dried for 1 hour, then incubated with 5 μg/ml PK in cell lysis buffer (50 mM Tris-HCl, pH 8.0, 150 mM NaCl, 0.5% sodium deoxycholate, 0.5% Igepal CA-630) for 1 hour at 37 °C. PK was inactivated with 2 mM PMSF. Membranes were denatured in 3 M guanidine thiocyanate in Tris-HCl, pH 7.8 for 10 minutes at room temperature. After four washes with PBS, the membrane was blocked with 5% non-fat milk in TBST for 1 hour and probed overnight at 4 °C with mAb PRC5 at a dilution of 1:5000, followed by HRP-conjugated goat anti-mouse IgG secondary antibody at a dilution of 1:5000. The membrane was developed with ECL 2 western blot substrate and scanned with an ImageQuant LAS 4000 (GE Healthcare), and signals quantified with ImageQuant TL 7.0 software (GE Healthcare).

Lesion Profiling

For the construction of lesion profiles, vacuolar changes were scored in nine gray-matter areas of the brain of hematoxylin and eosin-stained sections. 1. medulla, 2. cerebellar cortex, 3. cortex of the superior colliculus, 4. hypothalamus, 5. thalamus, 6. hippocampus, 7. cerebral cortex at the level of the hippocampus, 8. septal nuclei of the paraterminal body, and 9. cerebral cortex at the level of the septum (36). Vacuolation scores are derived from at least four individual mice per group and are reported as mean ± standard error of the mean.

Statistical Information

Statistical analyses were performed using Graphpad Prism software (San Diego). Statistical significance between survival curves of inoculated groups was assessed by comparing median times of survival of various inoculated groups using the log rank (Mantel-Cox) test. For the conformation stability assay, sigmoidal dose-response curves were plotted using a four-parameter algorithm and nonlinear least-square fit. Error bars, ± standard error of the mean of data from analyses of three animals per group. Significance calculated by pairwise analysis of $GdnHCl_{1/2}$ values from best fit curves.

Results

Norwegian moose isolates preferentially transmit to gene targeted GtQ226

All Norwegian moose isolates were samples from the brain from Dr. Sylvie Benestad from the Norwegian Veterinary Institute. To first measure relative levels of PrP^{Sc} in the inoculum, samples were run on western blot (Figure 3.1A, 3.1B). Equivalent amounts of protein were loaded for each sample. PK-resistant material from M-NO4, M-NO5 and M-NO7 were faintly detected, consistent with reports from Dr. Benestad that these cases were borderline positive CWD cases. Since the same amount of protein was loaded in each lane, we can infer that in

general, Nordic moose isolates contain less PrP^{Sc}/gram than North American isolates. With mAb PRC5, in all detectable Norwegian cases except for M-NO6, migration profiles were more rapid, indicative of a lower molecular weight (Figure 3.1A). This suggests the PK cleavage site is located closer to the C-terminal end in the Nordic moose cases (Figure 3.1C). To further explore this, the same isolates were probed with mAb PRC1, since its epitope lies in the PK-cleavage region of PrP. In corroboration, in addition to the North American elk isolate (E-US1), only M-NO6 showed reactivity with PRC1, suggesting the PRC1 epitope was cleaved by PK in the rest of Norwegian moose isolates (Figure 3.1B).

Table 3.1 Nordic moose CWD cases. Table detailing age, sex and genotype of Norway, Sweden, and Finland moose CWD cases

Moose ID	Age	Sex	Genotype
Norway			
M-NO1	13	Female	KK109-MM209
M-NO2	14	Female	KK109-MM209
M-NO3	13	Female	KK109-MM209
M-NO4	15	Female	QQ109-MM209
M-NO5	20	Female	KK109-MM209
M-NO6	12	Female	QQ109-MM209
M-NO7	17	Female	KK109-MM209
M-NO8	13	Male	KK109-MM209
M-NO9	17	Female	KK109-MM209
M-NO10	20	Female	KK109-MM209
M-NO11	19	Female	KK109-MM209
Finland			
M-F1	15	Female	KK109-MM209
M-F2	18	Female	No Data
Sweden			
M-SW1	16	Female	KK109-MM209
M-SW2	16	Female	KK109-MM209
M-SW3	10	Female	KK109-MM209
M-SW4	14	Female	KK109-MM209

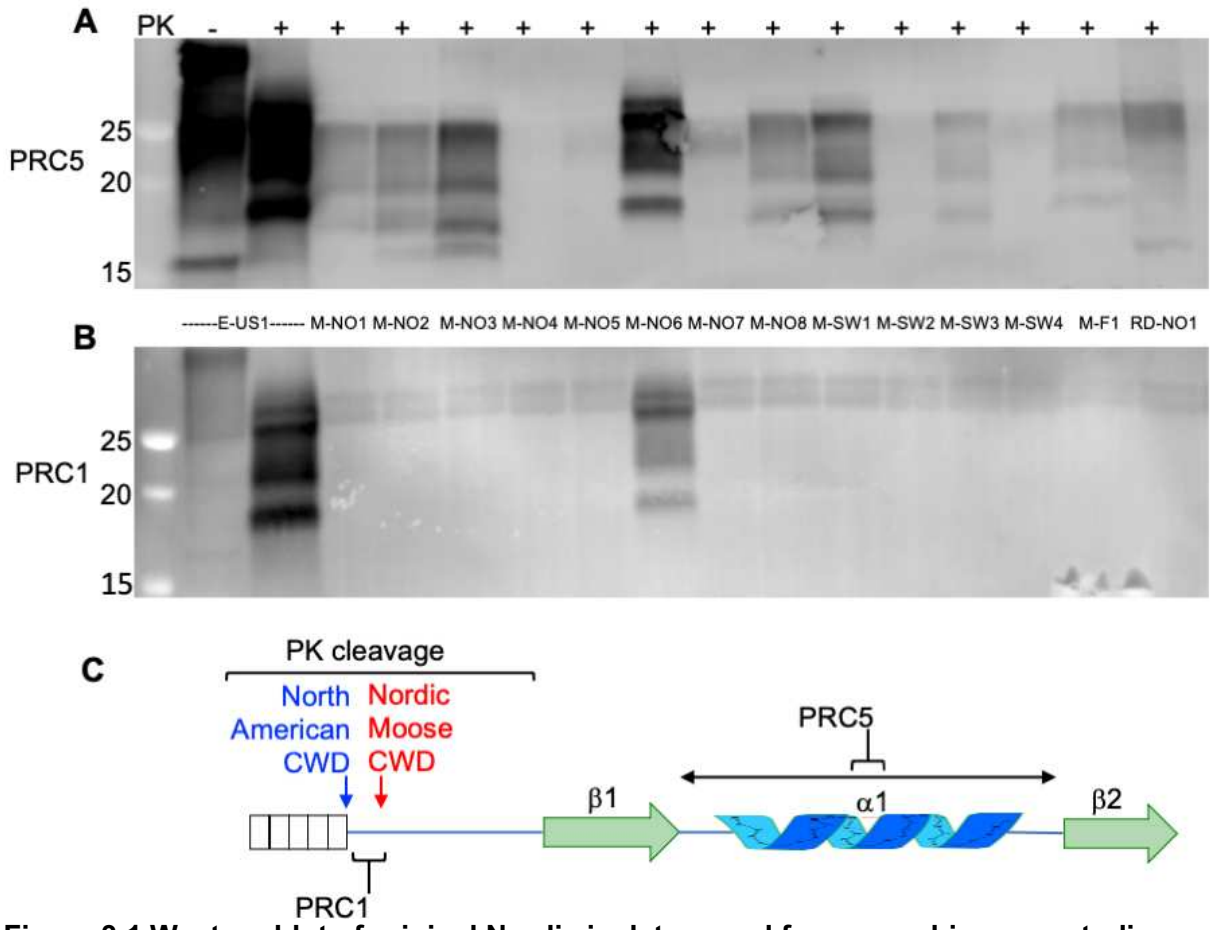

Figure 3.1 Western blot of original Nordic isolates used for mouse bioassay studies. Immunoblots showing PK-resistant profiles of Nordic isolates used for transmissions to cervid mouse models. (A) mAb PRC5 (B) mAb PRC1. Uninfected brains were included for PK digestion control. Samples were digested with 50 μg/ml of PK and ~55μg of protein was loaded onto the gel. Molecular weight markers are indicated to the left of blots. (C) Location of PrP epitopes for mAbs PRC5 and PRC1 and inferred PK cleavage sites for North American and Nordic moose CWD.

To investigate transmission properties of Norwegian moose CWD, we intracerebrally inoculated GtQ226 (GtQ) and GtE226 (GtE) mice with CNS material from all 11 Norwegian moose, At the time of writing, M-NO9, M-NO10, and M-NO11 were diagnosed with CWD less than one year ago, and thus transmissions to GtQ and GtE mice are ongoing and are not shown. Transmission of M-NO1 resulted in a 100% attack rate and mean survival time of 440±4 days post inoculation (DPI) in the GtQ mice (Figure 3.2A, Table 3.2). No transmission was recorded in the GtE background (****$p < 0.0001$) (Figure 3.2A, Table 3.2). Similarly, M-NO2

Table 3.2 Transmission of Norwegian moose isolates to GtQ and GtE mice. Survival times are reported as mean time to disease onset ± standard error of the mean (number of diagnosed mice/total number of mice). Ongoing studies at the time of writing are denoted by > days.

Inoculum	GtQ226	GtE226
M-NO1	440±4 (13/13)	552 (0/8)
M-NO2	486±9 (13/13)	608 (0/9)
M-NO3	451±16 (4/4)	422-611 (0/7)
M-NO4	508-584 (0/6)	500-584 (0/5)
M-NO5	272 (1/8)	520-650 (0/6)
M-NO6	487-520 (0/8)	524-600 (0/6)
M-NO7	>311 (0/5)	>462 (0/6)
M-NO8	122±30 (6/10)	>462 (0/5)

(486±9 DPI) and M-NO3 (451±16 DPI) were more efficiently transmitted into the GtQ background with no transmission into the GtE background (M-NO2: ****$p < 0.0001$, M-NO3: **$p < 0.0013$) (Figure 3.2B, 3.2C, Table 3.2). M-NO4 did not result in transmission to either background (ns, $p > 0.99$) (Figure 3.2D, Table 3.2). This could be due to the low amount of PrP^{Sc} in the inoculum (Figure 3.1A). Serial transmission of this isolate may be necessary to see clinical disease. M-NO5 caused disease in just one GtQ animal at 272 DPI which was confirmed to have PrP^{Sc} in the CNS via western blotting and immunohistochemistry; no evidence of PrP^{Sc} accumulation was found in mice surviving past 272 DPI (Figure 3.2E, Table 3.2). The brain of the one clinically diseased mouse was used for serial transmission that is currently ongoing. Not surprisingly, no disease was noted from the transmission of M-NO5 to GtE mice (Figure 3.2E, Table 3.2). Similar to M-NO4, M-NO6 did not cause clinical disease in either GtQ or GtE mice (ns, $p > 0.99$) (Figure 3.2F, Table 3.2). This is perplexing since the PrP^{Sc} immunoblot profile of M-NO6 is similar to North American CWD with a more N-terminal PK cleavage site resulting in retainment PRC1 reactivity. Transmission of M-NO7 is currently ongoing, with transmission in

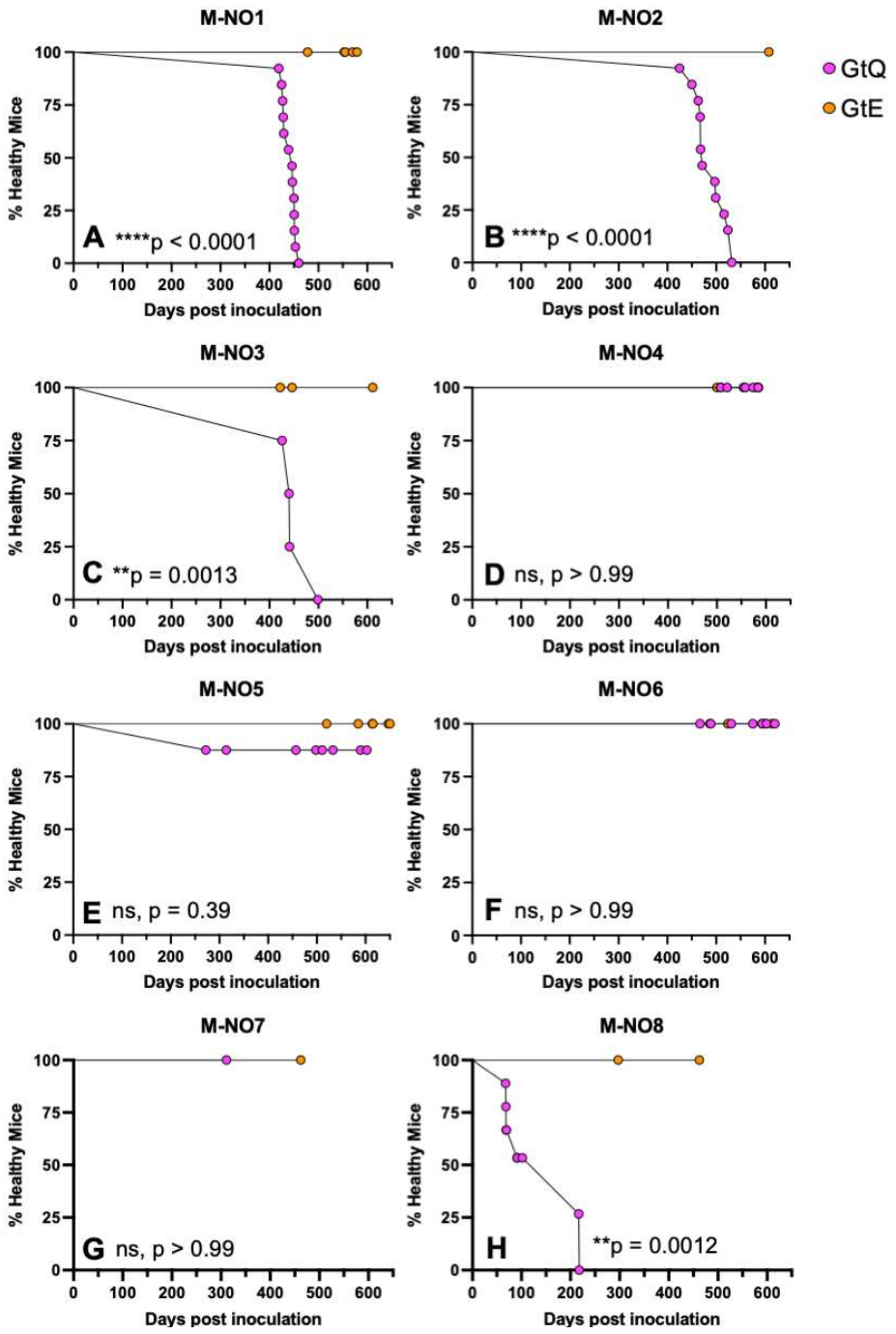

Figure 3.2 Transmission of Norwegian moose CWD isolates to GtQ and GtE mice. Survival curves of GtQ (pink circles) and GtE (orange circles) mice resulting from intracerebal inoculation with (A) M-NO1, (B) M-NO2, (C) M-NO3, (D) M-NO4, (E) M-NO5, (F) M-NO6, (G) M-NO7 and (H) M-NO8. p-values comparing survival curves as determined by the Log-rank (Mantel-Cox) test are listed at the bottom of each graph.

the GtQ mice >311 DPI and GtE mice >462 DPI at the time of writing (ns, p > 0.99) (Figure 3.2G, Table 3.2). As with the other Norwegian moose, we do not expect any disease in the GtE mice. Inoculation of M-NO8 resulted in an extremely rapid transmission of 122±30 DPI in the 6/10 of the GtQ mice (Figure 3.2H, Table 3.2). Transmission into the GtE background is ongoing at >462 DPI (**p = 0.0012) (Figure 3.2H, Table 3.2). The four GtQ mice that were not clinically diagnosed were either found dead or euthanized for unrelated illnesses. 4/6 clinically sick mice had extremely long prodromal phases of disease at an average of 102 days from time to diagnosis to terminal stage. As the transmission properties of M-NO8 are uncharacteristically

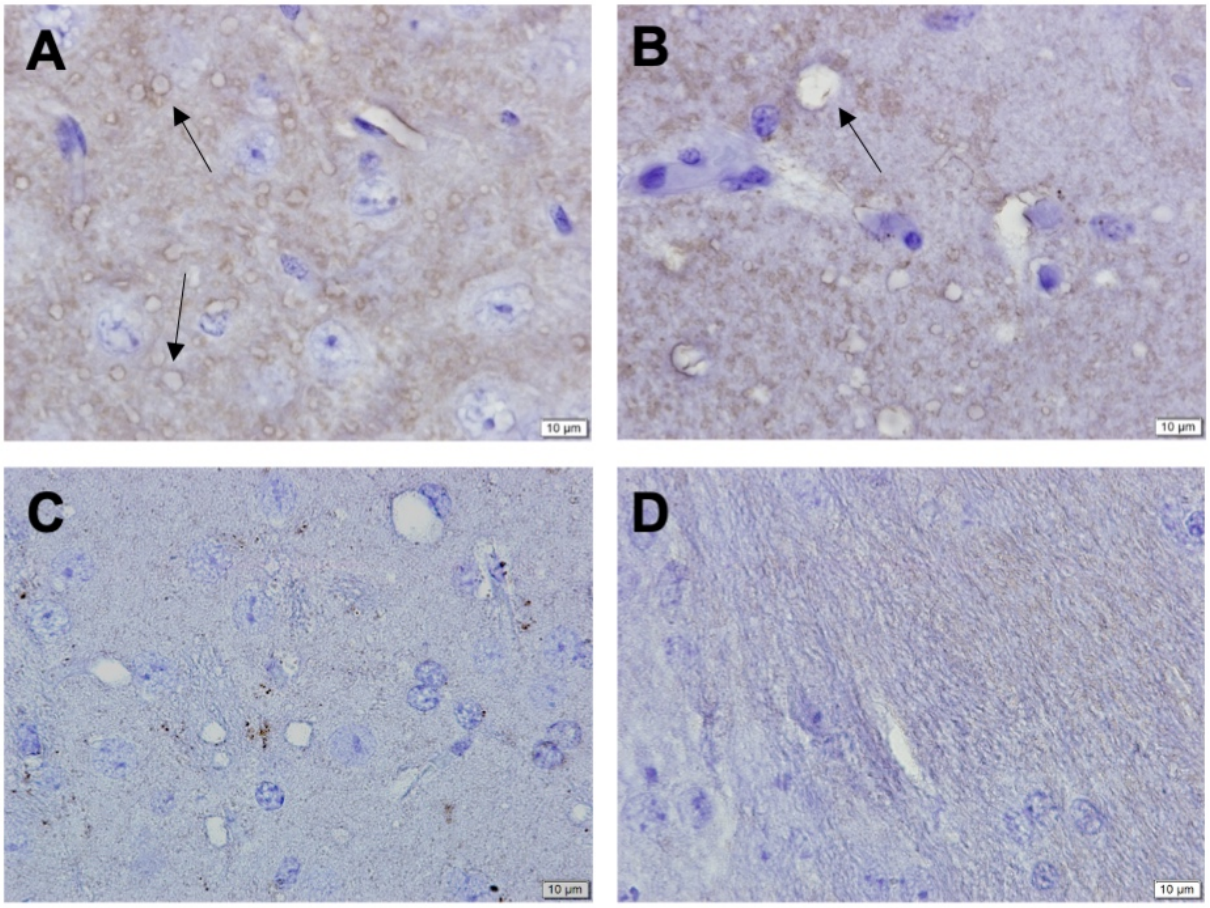

Figure 3.3 IHC staining of GtQ mice infected with M-NO8 show diffuse staining and vacuolation. IHC analysis of PrP^{Sc} distribution in the hippocampus of GtQ mice infected with (A, B) M-NO8 (C) M-NO1 and (D) an uninfected homogenate. Arrows in A indicates sites of pre-vacuole formation. Arrow in B indicate fully formed vacuole. IHC sections were probed with Fab D18. Scale bar indicates 10μm.

fast with an unusually long clinical phase, the experiment is being repeated. Confirmation of PrP^{Sc} was done using IHC coupled with high magnification microscopy. In GtQ mice infected with M-NO8, PrP^{Sc} distribution was diffuse and only visible at 100x magnification (Figure 3.3A, 3.3B) similar to distribution of M-NO1 (Figure 3.3C). An age-matched uninfected brain is shown to provide visualization of background staining (Figure 3.3D). One mouse was euthanized at 68 DPI due to poor body condition prior to clinical diagnosis, yet pre-vacuoles, indicated by the black arrows are abundant and are indicative of early neurodegeneration (Figure 3.3A) (37). Fully formed autophagic vacuoles, indicative of neurodegeneration, can be seen in another mouse, diagnosed at 68 DPI but not euthanized at terminal stage until 134 DPI, 66 days after initial diagnosis (Figure 3.3B). Overall, Norwegian moose CNS material transmits more efficiently into GtQ mice rather than GtE mice, maintaining strain differences when compared with North American CWD. Further characterization of all transmitted isolates is ongoing.

The Norwegian red deer isolate transmits with low efficiency to cervid mice and exhibits strain properties divergent from Norwegian moose

As with the Norwegian moose isolates, we sought to further characterize the first case of CWD in Norwegian red deer (RD-NO1) by using cervid-PrP mouse models. As red deer can be polymorphic at residue 226, we also did PrP sequencing and this particular animal was EE at residue 226. CNS material from the red deer was transmitted to both E226 and Q226 transgenic overexpressing (Tg) and endogenously expressing gene-targeted (Gt) mice. Transmission to the TgE mice caused disease in 3/7 mice with a mean incubation time of 478±18 DPI (Figure 3.4A, Table 3.3). Similarly, transmission to the GtE background resulted in disease 3/7 with a mean incubation time of 452±74 DPI (Figure 3.4D, Table 3.3). In contrast to Norwegian moose transmissions, transmission to either of the Q226 backgrounds, TgQ or GtQ, did not result in any clinical disease (Figure 3.4A, 3.4D, Table 3.3).

Table 3.3 Transmission of Norwegian red deer isolates to TgQ, TgE, GtQ and GtE mice. Survival times are reported as mean time to disease onset ± standard error of the mean (number of diagnosed mice/total number of mice). Ongoing studies at the time of writing are denoted by > days.

Inoculum	Passage	TgQ	TgE	GtQ	GtE
RD-NO1	p1	626-639 (0/7)	478±18 (3/7)	439-609 (0/5)	452±74 (3/7)
TgE	p2	428-594 (0/6)	544±27 (4/6)	453-570 (0/7)	518±3 (2/7), >526
TgQ	p2	564-597 (0/9)	525 (1/8)	484-562 (0/10)	454±12 (2/5), >526
GtE	p2			540±9 (3/9), >584	545±7 (5/5)

We have previously shown that serial passage of CWD prions can often decrease time to disease onset, likely due to low titer in CWD field isolates (19,30,38). In other words, inoculating cervid-PrP mice with the brain of a CWD-infected cervid-PrP mouse results in faster time to disease onset than inoculation with the original cervid brain sample. To see whether this phenomenon would improve efficiency of transmission of RD-NO1, we serially passaged CNS material from one clinically diagnosed TgE mouse, one clinically diagnosed GtE and one sub-clinically infected TgQ mouse. TgE-passaged RD-NO1 serially inoculated into TgQ or GtQ mice did not cause any clinical disease, similar to primary transmission to either Q226 background (Figure 3.4B, Table 3.3). TgE-passaged RD-NO1 inoculated into TgE mice caused disease in 4/6 mice, with a mean incubation time of 544±27 DPI (Figure 3.4B, Table 3.3). At the time of writing, serial transmission into the GtE background is still ongoing at >526 DPI, but 2/7 mice have developed disease at 518±3 DPI (Figure 3.4B, Table 3.3). When transmitted to TgQ or GtQ mice, TgQ passaged RD-NO1 did not cause clinical disease in any mice (Figure 3.4C, Table 3.3). When passaged to TgE mice, one mouse developed clinical disease at 525 DPI. Serial passage to GtE mice is ongoing at >526 DPI, but thus far, 2/5 mice have developed clinical disease at 454±12 DPI (Figure 3.4C, Table 3.3). Transmission to the GtQ background

from the GtE background resulted in clinical disease in 3/9 mice at a mean time of 540±9 (Figure 3.4E, Table 3.3). Similarly, serial transmission through GtE mice to GtE mice had a mean incubation time of 545±7 and a 100% attack rate (Figure 3.4E, Table 3.3). Overall, secondary transmission from either TgE or TgQ mice did not increase transmission efficiency

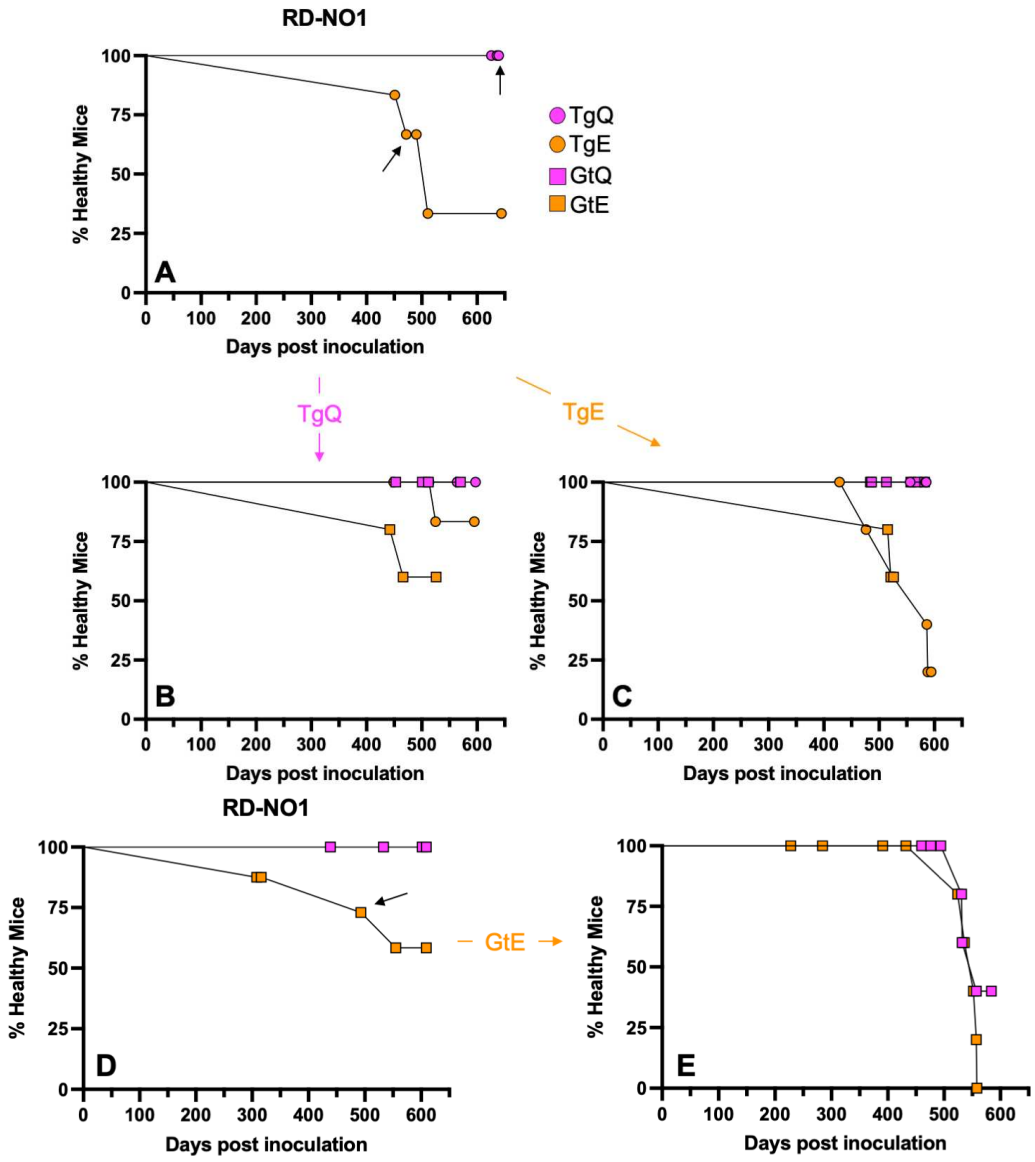

Figure 3.4 Transmission of the Norwegian red deer CWD isolate to TgQ, TgE, GtQ and GtE mice. Survival curves resulting from ic inoculation with RD-NO1 in (A) TgQ (pink circles) and TgE (orange circles), (D) GtQ (pink squares) and GtE (orange squares) mice. Secondary transmission survival curves of (B) TgE-passaged, (C) TgQ-passaged, (E) and GtE-passaged RD-NO1. Black arrows in A and D indicate individual brains used for serial passage.

into TgE, TgQ, GtE, or GtQ mice while transmission from the GtE background resulted in slightly more efficient transmission upon secondary passage.

Confirmation of clinical diagnosis by detection of PrP^{Sc} does not correlate with clinical disease

All brains, regardless of clinical disease were then examined via western blotting, IHC or histoblotting for confirmatory scrapie diagnosis. Via western blot detection, upon initial transmission of RD-NO1, two additional TgQ, one additional GtQ and four additional GtE animals terminated at the end of study had detectable PrP^{Sc} but had no clinical signs of prion disease. Surprisingly, subclinical GtE mice (indicated by *) have equivalent amounts of PrP^{Sc}

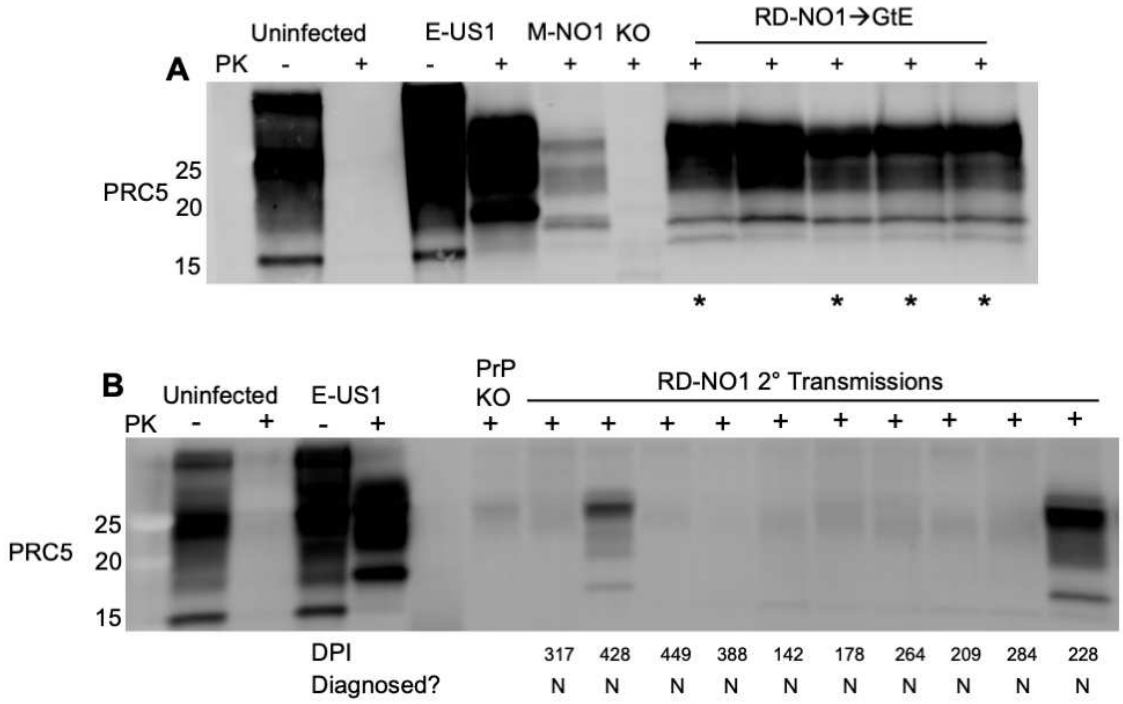

Figure 3.5 Western blots of PK-resistant PrP^{Sc} from primary and secondary transmissions of RD-NO1. Immunoblots showing PK-resistant profiles of (A) GtE mice infected with RD-NO1, * indicate mice euthanized at end of study with no clinical signs. (B) Secondary transmissions of RD-NO1. DPI on which the mouse was euthanized, and clinical status are listed below. Uninfected brains were included for PK digestion control. E-US1 is representative of a North American elk CWD isolate passaged in GtE mice. Samples were digested with 50 μg/ml of PK and ~55 μg of protein were loaded onto the gel. Blots were probed with mAb PRC5. Molecular weight markers are indicated to the left of blots.

when compared to a clinically sick GtE mouse (Figure 3.5A). Additionally, all GtE mice inoculated with RD-NO1 qualitatively have higher levels PrP^{Sc} than a GtQ mouse inoculated with M-NO1 (Figure 3.5A). We have previously shown that cervid-PrP mice inoculated with Norwegian moose CWD isolates have ~10x less PrP^{Sc} in their brains when compared to mice inoculated with North American CWD (19). As the convention in the field is that PrP^{Sc} load correlates directly to infectivity, high loads of PrP^{Sc} in a subclinical mouse is somewhat contradictory (39).

Due to the high levels of PrP^{Sc} in sub-clinically infected GtE mice upon primary passage of RD-NO1, all available brains from secondary transmissions, regardless of clinical status were examined for PrP^{Sc} via western blotting. Surprisingly, numerous mice were found to have evidence of PrP^{Sc} prior to disease onset. Figure 3.5B presents an example of subclinical accumulation via western blotting. For example, one female GtE mouse infected with GtE passaged RD-NO1, that was found dead in the cage at 228 DPI had high levels of PrP^{Sc} in the brain (Figure 3.5B, last lane) roughly ~300 days prior to the average time to disease onset of 545 ± 7 DPI for that transmission. The discovery of a prion strain originating in Norwegian red deer that is accumulating PrP^{Sc} but is non-lethal has many implications for the spread of CWD across Nordic countries.

To further determine PrP^{Sc} load and distribution in cervid-PrP mice inoculated with RD-NO1 and to compare to existing profiles resulting from inoculation with North American and Norwegian moose CWD, we used IHC to stain formic acid-treated slides with Fab D18 (α-PrP). Coronal sections of the septum, hippocampus, midbrain and cerebellum were taken. Transmission of RD-NO1 to GtE mice resulted in localized amalgamations of PrP^{Sc} in the molecular layer of the dentate gyrus of the hippocampus (Figure 3.6A). All three clinically sick and four subclinical GtE animals displayed the same phenotype. At high magnification, spongiosis due to vacuolation and large plaque formation is clear (Figure 3.6B) and reminiscent

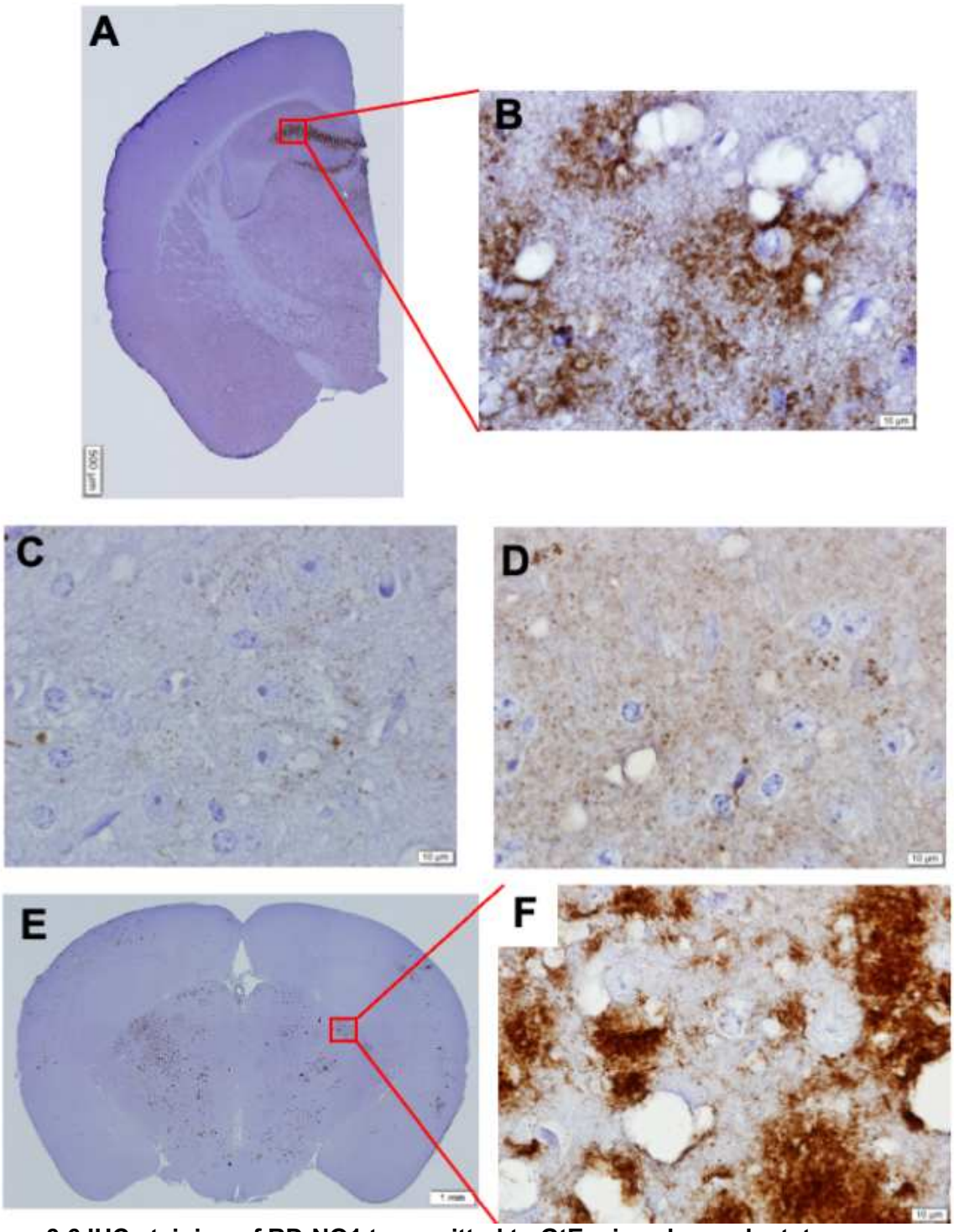

Figure 3.6 IHC staining of RD-NO1 transmitted to GtE mice shows dentate gyrus staining in the hippocampus. IHC analysis of PrP^{Sc} distribution in the hippocampus of (A, B, C) GtE mice infected with RD-NO1 (D) TgE mouse infected with TgE-passaged RD-NO1, (E, F) GtE mouse infected with North American moose CWD. IHC sections were probed with Fab D18. (A, E) Scale bar indicates 500 μm. (B, C, D, F) Scale bar indicates 10 μm.

of GtE mice infected with North American moose CWD (Figure 3.6F). However, plaque formation in GtE mice infected with North American moose CWD is distributed all over the hippocampal section, rather than confined to the dentate gyrus (Figure 3.6E). In other regions of the brain such as the septum, PrP^{Sc} staining was diffuse and similar to Norwegian moose distribution of PrP^{Sc} (Figure 3.6C). Dentate gyrus specific stain was only observed in GtE mice infected with RD-NO1. Secondary passage of TgE-passaged RD-NO1 to TgE mice resulted in a small, diffuse puncta profile of PrP^{Sc}, only visible at higher magnifications (Figure 3.6D). Plaque

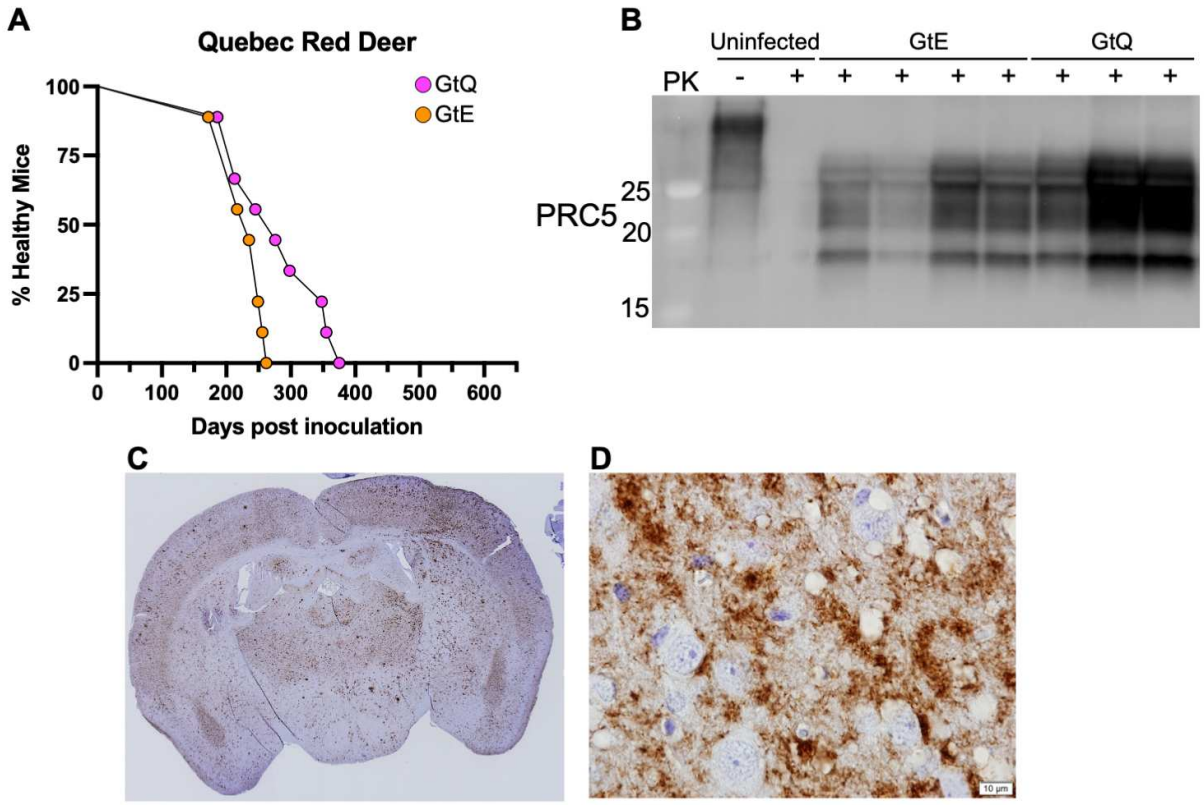

Figure 3.7 A case of CWD in a Quebec red deer has similar strain properties to other North American isolates when inoculated in Gt-cervid mice. (A) Survival curve of GtE (orange circles) and GtQ (pink circles) mice ic inoculated with a CWD positive brain from a red deer from Quebec. (B) Immunoblot showing PK-resistant profiles of GtE and GtQ mice infected with Quebec red deer CWD. Blot was probed with mAb PRC5. Molecular weight markers are indicated to the left of blots. (C, D) IHC analysis of distribution of PrP^{Sc} in the hippocampus of a GtE mouse infected with Quebec red deer CWD. (D) Scale bar indicates 10μm.

formation in the granular layer of the dentate gyrus is a novel strain phenotype, seen only in the transmission of the first case of CWD in Norwegian red deer.

A case of CWD in a red deer from Canada does not mirror CWD in the Norwegian red deer

Cases of CWD in red deer are much less prevalent than in deer and elk in North America (40). As such, we sought to understand whether the unique transmission properties of RD-NO1 were because the CWD was found in a red deer or that the CWD was found in Norway. In collaboration with Dr. Gordon Mitchell at the Canadian Food Inspection Agency, we worked to characterize a case of CWD found on a red deer farm in Quebec. Genotyping revealed this animal was heterozygous EQ at residue 226 of PrP. We intracerebrally inoculated our GtE and GtQ mice with the brain of the red deer to examine transmission properties. Similar to all other North American CWD isolates we have characterized, and different from RD-NO1, the Quebec red deer brain transmitted more efficiently to the GtE mice (230±9 DPI) rather than GtQ mice (279±23 DPI) (Figure 3.7A). The attack rate was 100%, thus there was no possibility of detecting subclinical disease (Figure 3.7A). Western blotting of the brains of either GtE or GtQ mice infected with the Quebec red deer revealed typical North American CWD immunoblot profile (Figure 3.7B). Additionally, PrP^{Sc} distribution in infected GtE mouse brains via IHC is consistent with other North American CWD isolates with large plaques visible at low magnification and widespread across the hippocampal section (Figure 3.7C, 3.7D, Figure 3.6E, 3.6F). As the case of the Quebec red deer largely aligns with strain characteristics consistent with North American CWD in mule deer and elk, the novel strain characteristics of the Norway red deer are likely not due to the intrinsic nature of red deer genetics, but rather the variety of novel strains of CWD in Norway.

Transmission of CWD from Swedish moose 1 (M-SW1) results in subclinical disease in GtE mice with unique strain properties

In addition to the 11 moose in Norway diagnosed with CWD, Sweden has also identified CWD cases in four moose. In March 2019, an older female moose was euthanized and tested for CWD because it was observed to be emaciated and blind, walking in circles on a frozen lake (M-SW1) (18). The second case was diagnosed in May 2019, ~70km from the first case, in another older female exhibiting behavioral changes (M-SW2). The third moose was hunted in September 2019, and did not appear to have clinical signs, but was determined to be CWD positive via ELISA (M-SW3). A fourth moose was found in 2020 but will not be discussed here as analysis is still ongoing. The first three moose cases were geographically clustered, but the fourth moose was found outside the geographic cluster.

Table 3.4 Transmission of Swedish moose isolates to GtQ and GtE mice. Survival times are reported as mean time to disease onset ± standard error of the mean (number of diagnosed mice/total number of mice). Ongoing studies at the time of writing are denoted by > days.

Inoculum	Passage	GtQ226	GtE226
M-SW1	p1	344±6 (10/10)	565 (1/8)
GtQ (M-SW1)	p2	365±23 (7/7)	>478 (0/4)
GtE (M-SW1)	p2	>199 (0/9)	>442 (0/4)
M-SW2	p1	528±11 (2/9)	>530-630 (0/9)
GtQ (M-SW2)	p2	94±1 (8/8)	299±20 (6/6)
GtQ (M-SW2)	p3	95±1 (10/10)	225±2 (7/7)
GtE (M-SW2)	p3	107±3 (10/10)	No data
M-SW3	p1	377±30 (7/8)	>519-611 (0/6)
GtQ (M-SW3)	p2	280±14 (9/9)	>462 (0/5)

Preliminary biochemical analysis of the field isolates reveals western blotting and IHC profile similar to Norwegian moose, and were additionally characterized to be atypical, spontaneous CWD cases (Figure 3.1A) (18). To further assess the strain properties of Swedish moose CWD cases, we transmitted CNS material from each Swedish moose to the Gt-cervid mice. M-SW1 and M-SW3 had detectable PrP^{Sc} that was PRC5-reactive but not PRC1-reactive, similar to Norwegian moose western blot profile (Figure 3.1A, 3.1B). Intracerebral transmission of M-SW1 resulted in 100% transmission to the GtQ mice at a mean time of 344±6 DPI, faster than transmission of all Norwegian moose cases barring M-NO8. One GtE mouse exhibited clinical signs at 565 DPI, marking the first evidence of transmission to the E226 background

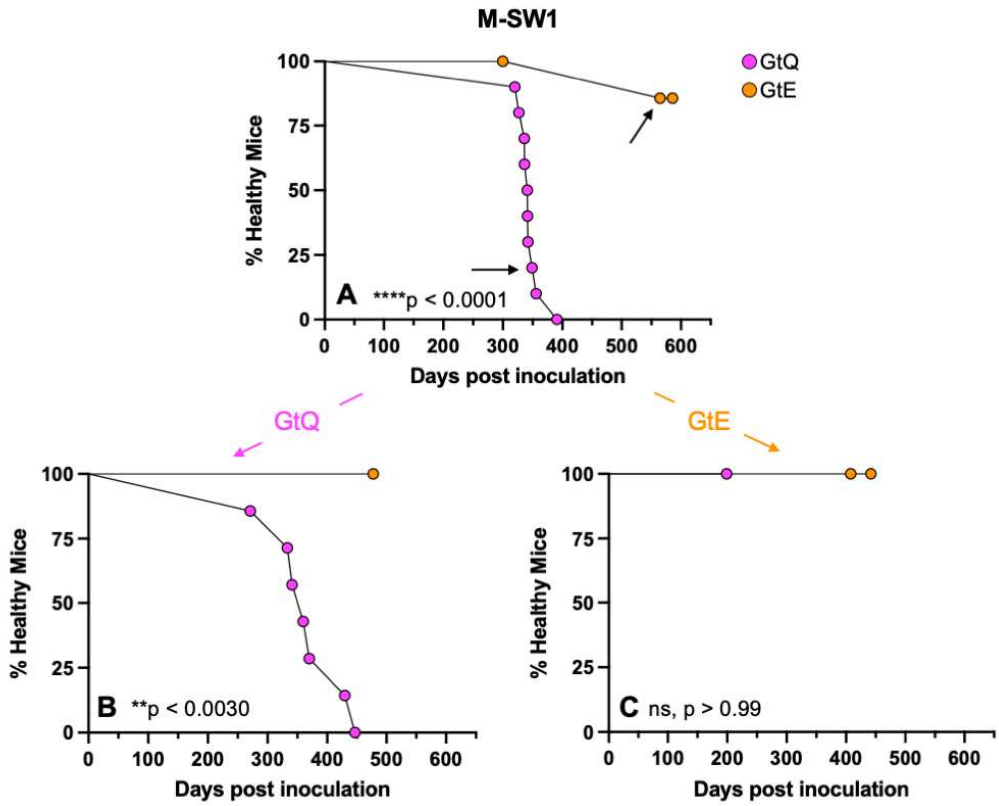

Figure 3.8 Transmission of Swedish moose CWD isolate 1 (M-SW1) to GtQ and GtE mice. Survival curves of GtQ (pink circles) and GtE (orange circles) mice resulting from ic inoculation with (A) M-SW1, (B) GtQ-passaged M-SW1, (C) GtE-passaged M-SW1. Black arrows in A indicate individual brains used for serial passage. p-values comparing survival curves as determined by the Log-rank (Mantel-Cox) test are listed at the bottom of each graph.

from a Nordic moose case upon primary transmission (Figure 3.8A, Table 3.4). All clinical disease was confirmed with either IHC or western blotting. Upon serial transmission from a clinically diseased GtQ mouse, subsequent GtQ mice succumbed to disease at 365±23 DPI, slightly slower than primary transmission, and transmission is still ongoing >478 DPI in the GtE mice with no clinical disease (**p = 0.0030) (Figure 3.8B, Table 3.4). To study the properties of Swedish moose CWD prions propagated through the E226 background, we serially transmitted CNS material from the one clinically sick GtE mouse on primary passage. Transmission in the GtQ mice is ongoing > 199 DPI, and transmission in the GtE mice is ongoing >442 DPI with no clinical signs, demonstrating the refractory nature of cervid-PrP E226 to conversion by Nordic moose CWD (Figure 3.8C, Table 3.4).

To validate clinical disease and to check for any subclinical disease, all mice were examined either via western blot, IHC or histoblotting. Histoblotting pattern of PrP^{Sc} distribution in the midbrain for M-SW1 transmitted to GtQ mice was consistent GtQ mice inoculated with Norwegian moose prions – diffuse, widely and symmetrically distributed (Figure 3.9A) (19). Using IHC, staining was only visible at higher magnification and presented as small puncta, distinct from North American moose CWD, but akin to Norwegian moose CWD (Figure 3.9B, Figure 3.3C). Unexpectedly, all seven GtE mice sacrificed at the end of study with no apparent clinical signs of prion disease were found to have positive reactivity via either IHC or histoblotting and determined to be subclinically infected. When retrospectively assessed, no subclinical disease was found in GtE mice infected with any Norwegian moose CWD cases but was detected in the case of mice infected with Norwegian red deer CWD. Of the seven subclinical mice, three had PrP^{Sc} deposition – diffuse and small puncta - similar to GtQ mice infected with M-SW1. The other four subclinical mice displayed a unique pattern, similar to the GtE mice infected with Norwegian red deer (Figure 3.9C). In the hippocampus and midbrain, dense deposition appeared specifically in the dentate gyrus, in both the granular and molecular layers (Figure 3.9C). Slightly variable from GtE mice infected with RD-NO1, at higher

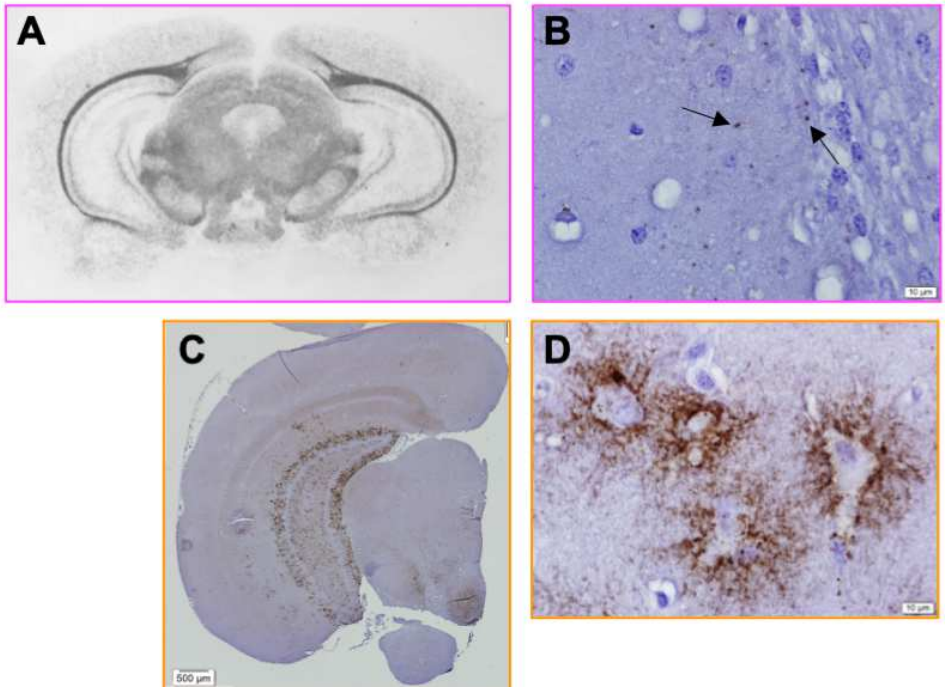

Figure 3.9 Histoblot and IHC staining of M-SW1 transmitted to GtQ and GtE shows divergent staining in the midbrain. (A) Histoblot of the midbrain section of a GtQ mouse infected with M-SW1. IHC analysis of PrP^{Sc} distribution in the midbrain of (B) GtQ mouse infected with M-SW1 (C, D) GtE mouse infected with M-SW1. Histoblot sections were probed with PRC5. IHC sections were probed with Fab D18. (B, D) Scale bar indicates 10 μm. (C) Scale bar indicates 500 μm.

magnification, staining is present surrounding cell bodies in a stellate pattern (Figure 3.9D). This is reminiscent of glial cell patterning and could indicate neuroinflammation and glial activation as a result of prion disease (41). Taken together, when transmitted to GtQ mice, M-SW1 displays similar strain properties to Norwegian moose CWD in GtQ mice. However, subclinical disease was not observed after transmission of Norwegian moose CWD to the GtE background, while it was abundantly observed with M-SW1 transmitted to GtE mice and resulted in unique deposition in the midbrain and hippocampus. Thus, we conclude GtE mice infected with M-SW1 CWD propagate a different CWD strain than GtQ and GtE mice infected with Norwegian CWD and GtQ mice infected with M-SW1.

Serial transmission of M-SW2 results in extremely rapid disease course in GtQ mice

Using the same method, we serially transmitted M-SW2 to the Gt cervid-PrP mice. Primary transmission into the GtQ mice was not efficient and resulted in 2/9 diseased mice at 528±11 DPI (Figure 3.10A, Table 3.4). No transmission or subclinical disease was noted with transmission of M-SW2 to GtE mice (ns, p = 0.1020) (Figure 3.10A, Table 3.4). However, when serially transmitted from GtQ mice to GtQ mice, all mice 8 succumbed to disease at an extremely rapid rate of 94±1 DPI (Figure 3.10B, Table 3.4). 4/8 of the mice were euthanized or found dead before clinical diagnosis could be made, but around the same time the other 4 mice were diagnosed due to the remarkably rapid clinical phase. All mice were confirmed to have evidence of PrP^{Sc} postmortem. This is the most rapid transmission of any CWD strain including establish North American strains to Gt cervid-PrP mice to date. Serial transmission from the GtQ background to the GtE background resulted in a time to disease onset of 299±20 DPI in 6/6 mice (Figure 3.10B, Table 3.4). As serial transmission of most GtQ-passaged Norwegian isolates to the GtE background resulted in either no disease, or delayed disease > 400 DPI, we consider the transmission of GtQ-passaged M-SW1 to GtE mice to be accelerated relative to the E226 background.

Upon tertiary transmission through the GtQ background, transmission time stabilized at 95±1 DPI, not significantly different from time to disease onset in secondary transmission (ns, p = 0.75) (Figure 3.10C, Table 3.4). However, two passages through the GtQ background to the GtE background resulted in a transmission time of 225±2 DPI, which is ~33% faster than the secondary transmission to the GtE background (***p = 0.0004) (Figure 3.10C, Table 3.4). Since GtE mice developed resultant disease from passage through the GtQ mice at secondary passage, we serially transmitted a brain from a clinically diseased GtE mouse. Transmission from the GtE background back to the GtQ mice resulting in a 100% attack rate and clinical disease at 107±3 DPI (Figure 3.10D, Table 3.4). Altogether, serial passaging of M-SW2 resulting in accelerated disease phenotypes in both GtQ and GtE mice.

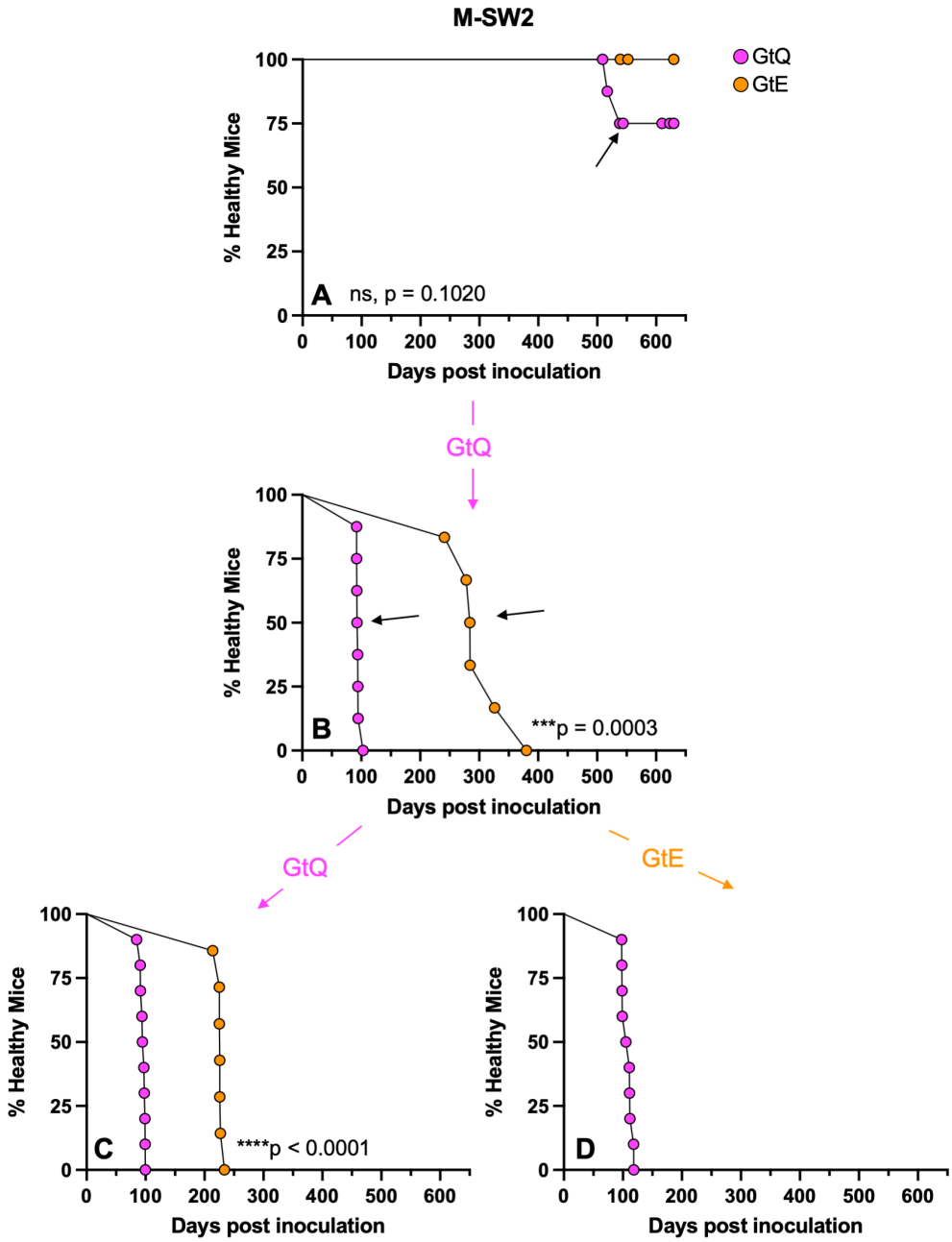

Figure 3.10 Transmission of Swedish moose CWD isolate 2 (M-SW2) to GtQ and GtE mice. Survival curves of GtQ (pink circles) and GtE (orange circles) mice resulting from ic inoculation with (A) M-SW2, (B) GtQ-passaged M-SW2, (C) GtQ-passaged GtQ(M-SW2), (D) GtE-passaged GtQ(M-SW2). Black arrows in A and B indicate individual brains used for serial passage. p-values comparing survival curves as determined by the Log-rank (Mantel-Cox) test are listed at the bottom of each graph.

To determine the mechanism behind extremely rapid transmission when adapted to the cervid-PrP mice, we used western blotting, IHC and histoblotting to define strain characteristics complimentary to the transmission profiles. Immunoblot profiles using mAb PRC5 revealed that all iterations of transmission of M-SW2 resulted in a lower migrating PK-resistant PrP^{Sc} species as seen in Norwegian moose CWD (Figure 3.11A). Additionally, though transmission led to accelerated disease, qualitatively, both GtE and GtQ-passaged M-SW2 had 10 times less PrP^{Sc} than North American CWD and ~ equivalent levels of PrP^{Sc} to Norwegian moose CWD (Figure 3.11A). Of note, tertiary transmissions of M-SW2 show weak reactivity with PRC1, indicative of an additional quasispecies present in the M-SW2 isolate with a more N-terminal PK-cleavage

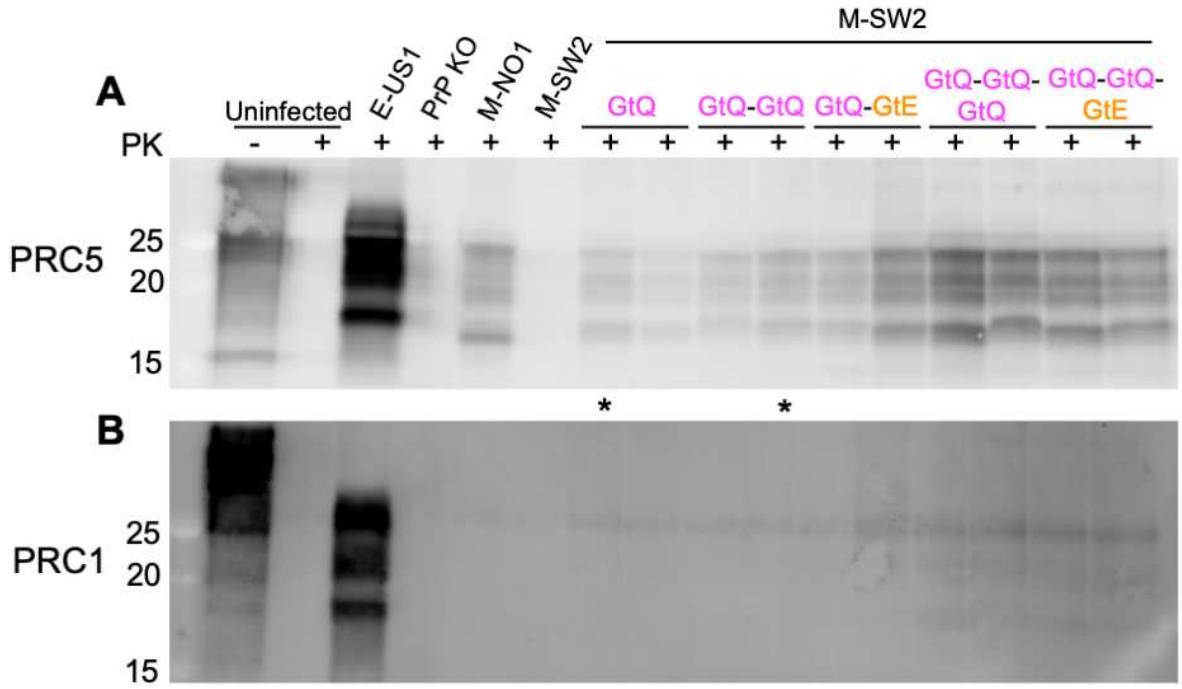

Figure 3.11 Western blots of primary, secondary and tertiary transmissions of M-SW2. Immunoblots showing PK-resistant profiles of (A, B) M-SW2 original isolate, M-SW2 passaged to GtQ mice, GtQ or GtE passaged GtQ(M-SW2), GtQ or GtE passaged GtQ(GtQ-M-SW2) * indicate mice used for serial transmission to both GtQ and GtE mice (A) mAb PRC5. (B) mAb PRC1. Uninfected brains were included for PK digestion control. Samples were digested with 50 μg/ml of PK and ~55 μg of protein were loaded onto the gel. Molecular weight markers are indicated to the left of blots.

site akin to the North American CWD cleavage site (Figure 3.11B). Immunoblot profiling did not suggest a radical difference in M-SW2 compared to other isolates that would result in the rapid transmission profile.

Next, we examined IHC and histoblot profiles of both GtQ and GtE-passaged M-SW2 to examine whether any unique PrP^{Sc} deposition was present. At low magnification, IHC staining of the hippocampal section of primary passage of M-SW2 revealed no apparent PrP^{Sc} deposition (Figure 3.12A). At high magnification, staining is diffuse and does not resemble plaques seen in North American CWD (Figure 3.12B). Puzzlingly, serial passaging of this isolate to GtQ mice resulted in transmission at 94±1 DPI. PrP^{Sc} distribution of the rapid secondary transmission, via histoblotting, presented diffuse widespread staining in the hippocampus (Figure 3.12C) with high magnification IHC showing the same (Figure 3.12D). Serial passage to the GtE mice shows fairly similar PrP^{Sc} distribution akin to GtQ mice in both low resolution histoblot sections (Figure 3.12E) and high magnification IHC (Figure 3.12F). Upon third passage, transmission time stabilized in the GtQ mice and was not different from the second passage. Consistent, IHC at both low and high magnification did not appear different than secondary passage demonstrating small diffuse punctate staining (Figure 3.12G, 3.12H). Similarly, tertiary passage to the GtE background showed no difference in PrP^{Sc} distribution when compared to other iterations of transmitted M-SW2 (Figure 3.12I, 3.12J). As with immunoblot profiles, no profound differences were noted between M-SW2 and other Nordic moose isolates which would result in expedient disease time course.

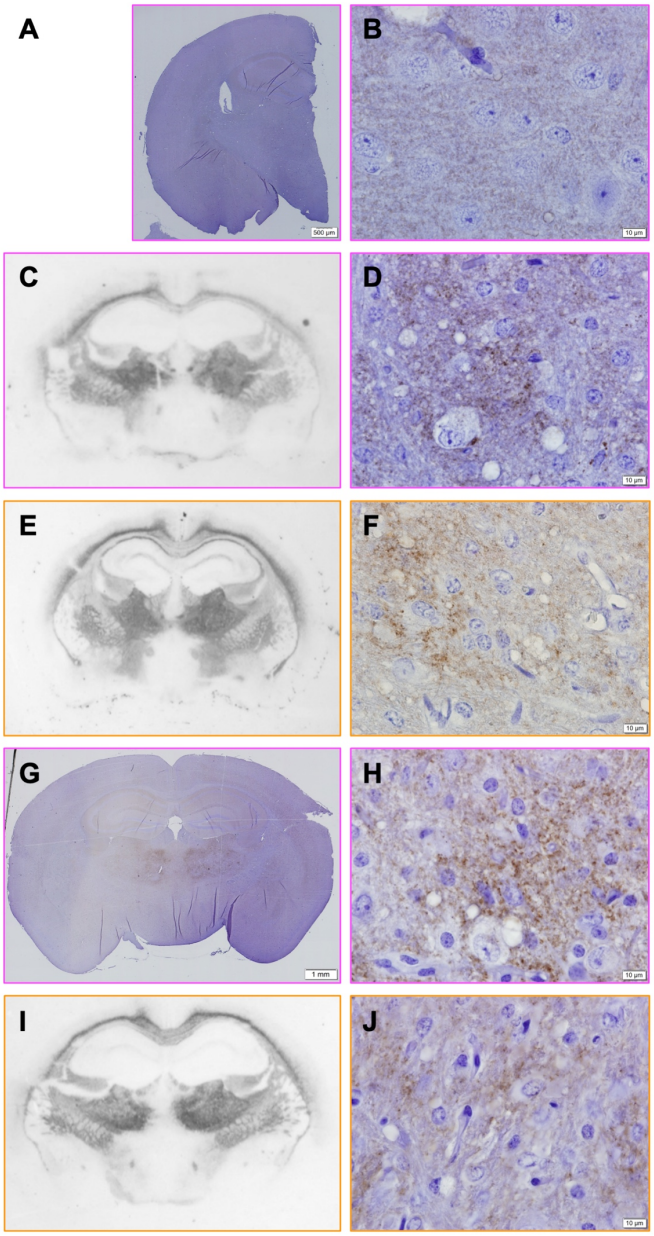

Figure 3.12 Histoblot and IHC staining of M-SW2 transmitted to GtQ and GtE shows staining consistent with mice infected with other Nordic moose isolates. (A, B) IHC of the hippocampal section of a GtQ mouse infected with M-SW2. (C) Histoblot and (D) IHC analysis of PrP^{Sc} distribution in the hippocampus of a GtQ mouse infected with GtQ-passaged M-SW2 (E) Histoblot and (F) IHC analysis of PrP^{Sc} distribution in the hippocampus of a GtE mouse infected with GtQ-passaged M-SW2. (G, H) IHC analysis of PrP^{Sc} distribution in the hippocampus of a GtQ mouse infected with GtQ-GtQ-passaged M-SW2. (I) Histoblot and (J) IHC analysis of PrP^{Sc} distribution in the hippocampus of a GtE mouse infected with GtQ-GtQ-passaged M-SW2. Histoblot sections were probed with PRC5. IHC sections were probed with Fab D18. (A) Scale bar indicates 500 μm. (B, D, F, H, J) Scale bar indicates 10 μm. (G) Scale bar indicates 1 mm.

GtQ mice infected with the third Swedish moose CWD case (M-SW3) propagate a strain distinct from M-SW1 and M-SW2

To compare the third Swedish moose case (M-SW3) to M-SW1 and M-SW2 and to previously characterized Norwegian moose cases, we inoculated Gt-cervid mice with CNS from M-SW3. Primary transmission of M-SW3 to GtQ mice caused disease in 7/8 mice at a mean of 377±30 DPI (Figure 3.13A, Table 3.4). Notably, time to disease onset ranged from 279-506 DPI, ~225 days difference between first and last diagnosis, atypical of established prion strains. On trend with the majority of Nordic moose isolates, no transmission was noted in the GtE background (**p = 0.0020) (Figure 3.13A, Table 3.4). To further examine whether time to disease would decrease with serial passaging, we transmitted a GtQ brain to both GtQ and GtE mice. Upon secondary passage, all GtQ mice succumbed to disease at a mean of 280±14, ~26% faster than the primary passage (**p = 0.0330) (Figure 3.13B, Table 3.4). Transmission to the GtE mice is ongoing > 462 DPI with no signs of clinical disease (Figure 3.13B, Table 3.4).

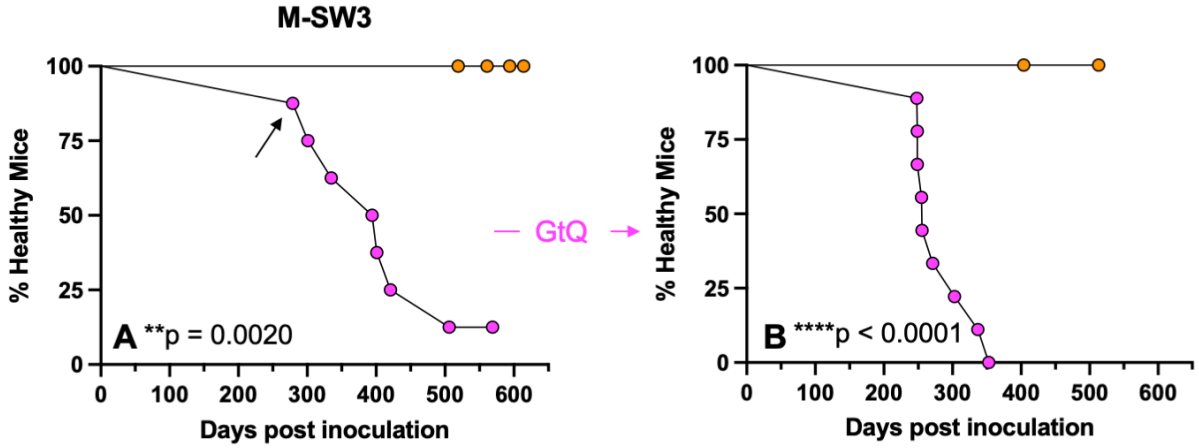

Figure 3.13 Transmission of Swedish moose CWD isolate 3 (M-SW3) to GtQ and GtE mice. Survival curves of GtQ (pink circles) and GtE (orange circles) mice resulting from ic inoculation with (A) M-SW3, (B) GtQ-passaged M-SW3. Black arrows in A indicate individual brains used for serial passage. p-values comparing survival curves as determined by the Log-rank (Mantel-Cox) test are listed at the bottom of each graph.

Overall, the transmission profile of M-SW3 does not greatly differ from Norwegian moose isolates.

To confirm the presence of PrP^{Sc} and compare the biochemical properties to established strain properties, we employed western blotting, IHC and histoblotting. Via western blotting, we determined that M-SW3 has electrophoretic migration properties akin to M-SW1 and faster than North American CWD, indicative of a more C-terminal PK cleavage site (Figure 3.14A). This is confirmed by the lack of reactivity with discriminatory antibody PRC1 (Figure 3.14B). We have previously noted Norwegian and other Swedish moose CWD cases have ~10 times less PrP^{Sc} on western blot than North American CWD cases when passaged through Gt cervid-PrP mice. This is not the case with M-SW3, and some individual mice have comparable PrP^{Sc} levels to North American CWD (Figure 3.14A). M-SW3 inoculated into GtE mice does not show any evidence of PrP^{Sc} or subclinical disease, consistent with the refractory nature of GtE mice to Nordic moose strains of CWD (Figure 3.14A).

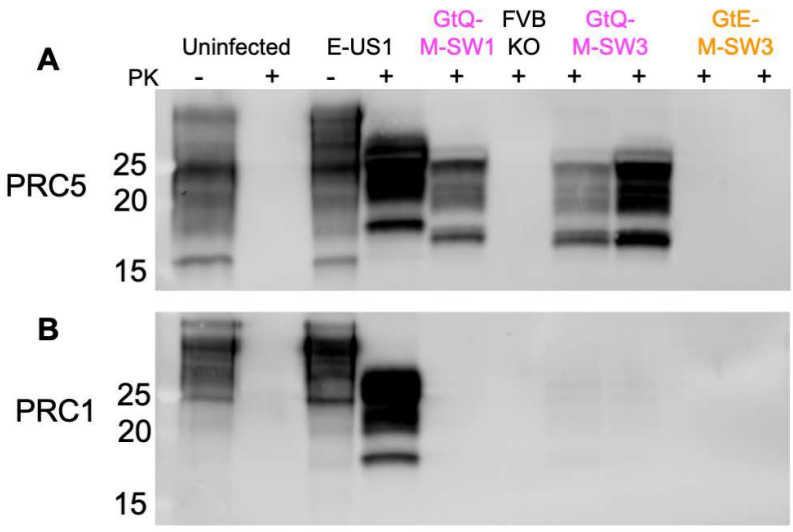

Figure 3.14 Western blots of PrP^{Sc} from transmission of M-SW3 to GtE and GtQ mice. Immunoblots showing PK-resistant profiles of (A, B) M-SW1 passaged in GtQ mice, M-SW3 passaged in GtQ mice, GtQ or GtE passaged GtQ(M-SW3) (A) mAb PRC5. (B) mAb PRC1. Uninfected brains were included for PK digestion control. Samples were digested with 50 μg/ml of PK and ~55 μg of protein were loaded onto the gel. Molecular weight markers are indicated to the left of blots.

Since M-SW3 transmissions to GtQ mice result in higher PrP^{Sc} levels in the CNS than other Swedish moose isolates, we looked for differences in distribution of PrP^{Sc} throughout the CNS. Histoblotting revealed diffuse and widely distributed PrP^{Sc} across all sections of the brain. Hippocampal section from the first passage of M-SW3 to GtQ and the midbrain section from the second passage of M-SW3 to GtQ resemble patterns seen in the Norwegian and other Swedish moose CWD cases transmitted to GtQ mice (Figure 3.15A, 3.15B). However, using IHC

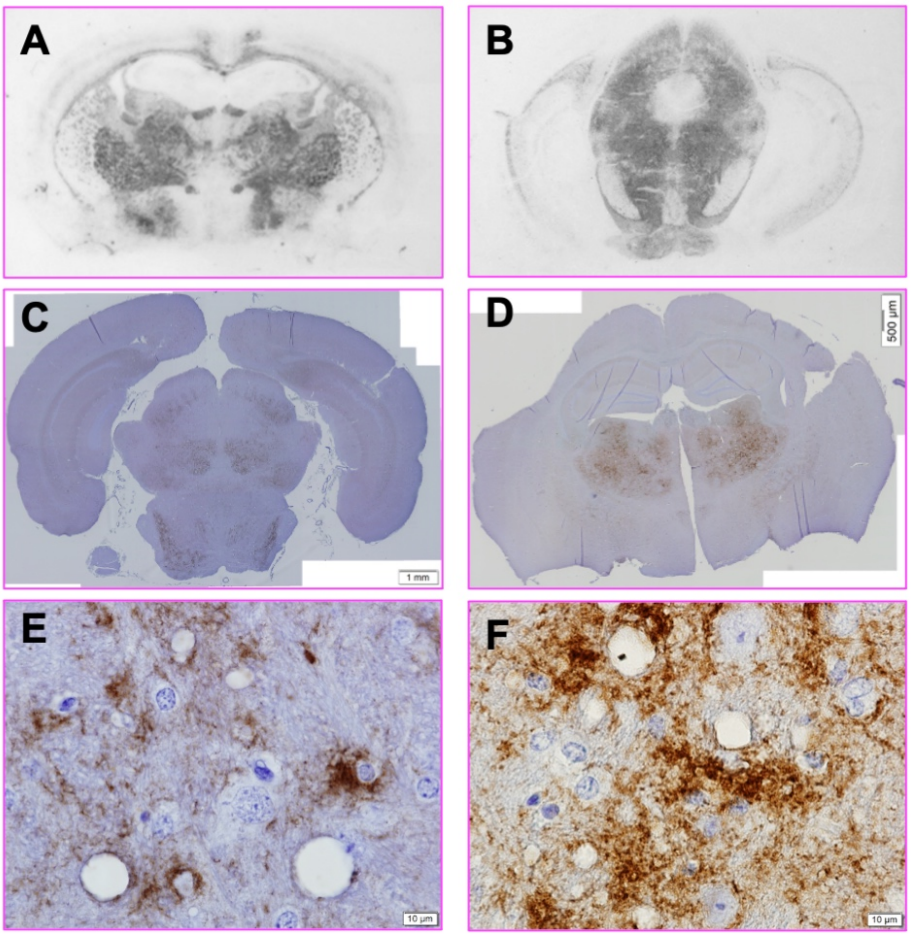

Figure 3.15 Histoblot and IHC staining of M-SW3 transmitted to GtQ and GtE mice shows unique PrP^{Sc} deposition. (A) Histoblot of the hippocampal section of a GtQ mouse infected with M-SW3. (B) Histoblot of the midbrain section of a GtQ mouse infected with GtQ-passaged M-SW3. (C, E) IHC analysis of PrP^{Sc} distribution in the midbrain of a GtQ mouse infected M-SW3 (D, F) IHC analysis of PrP^{Sc} distribution in the hippocampus of a GtQ mouse infected GtQ-passaged M-SW3. Histoblot sections were probed with PRC5. IHC sections were probed with Fab D18. (C) Scale bar indicates 1 mm. (D) Scale bar indicates 500 μm. (E, F) Scale bar indicates 10 μm.

technique, clear differences emerge between M-SW3 and the other Nordic isolates transmitted to GtQ mice. The midbrain section from a first passage and hippocampal section from the second passage of M-SW3 to GtQ mice show visible staining at low magnification (Figure 3.15C, 3.15D). Moreover, this staining is symmetrical, but not densely disordered, opposite of North American CWD pathology. High magnification of both first and second passage of M-SW3 in GtQ mice reveals staining somewhat intermediate between North American CWD pathology and Norwegian moose CWD pathology (Figure 3.15E, 3.15F). Staining is more compacted than in other Nordic CWD cases, but not quite plaque-like as North American CWD. The apparent increase in PrP^{Sc} via IHC correlates with the strong immunoblotting profile in the transmission of M-SW3. Unequivocally, GtQ mice propagate a unique CWD strain when inoculated with M-SW3. Furthermore, all 3 Swedish moose cases transmitted to the Gt cervid-PrP mice result in propagation of 3 different CWD strains that are also distinct from the already characterized North American and Norway moose CWD cases.

Another novel prion strain is responsible for chronic wasting disease in Finnish moose

In 2018, a case of CWD in an older female moose was identified in Finland (M-F1), near the Russian border as a result of increased surveillance (Table 3.1). We intracerebrally inoculated GtE and GtQ mice and their overexpressing Tg counterparts (TgE and TgQ) with homogenates of frozen CNS and lymphoreticular system (LRS) material from M-F1. CNS homogenates produced disease in 10/11 GtQ mice at 259±19 DPI and 6/8 TgQ mice at 234±27 DPI (Figure 3.16A, Figure 3.17A, Table 3.5). In contrast and consistent with other Nordic moose transmissions, all inoculated GtE mice remained free of disease for > 550 DPI, and only a single TgE mouse developed clinical signs after ~ 400 DPI (Figure 3.16A, Figure 3.17A, Table 3.5). Not surprisingly, LRS homogenates failed to produce disease in mice expressing either Q226 or E226 after elapsed times approaching 600 d (Figure 3.16B, Figure 3.17B, Table 3.5). We deduce that CWD prions failed to propagate in the LRS of Finnish moose M-F1. We also

conclude that propagation of CNS-derived M-F1 CWD prions is favored in mice expressing Q226, consistent with all previously analyzed Nordic moose CWD transmissions.

Serial propagation of M-F1 prions from the brains of two diseased GtQ mice caused disease in all inoculated GtQ mice after ~ 230 DPI (Figure 3.16C, 3.16D, Table 3.5). Similarly, iterative passages of M-F1 prions from TgQ mice elicited disease in 100% of GtQ mice after 228±3 DPI and in TgQ mice at 182±7 DPI (Figure 3.17C, Table 3.5). E226-expressing mice were less responsive. Currently, no disease has been registered in GtE mice inoculated with TgQ-passaged M-F1 after > 480 DPI, which is ~ 250 days beyond the time to disease in GtQ mice, and disease in TgE mice occurred at 388±27 DPI, ~ 180 days after the mean time to disease in TgQ mice (Figure 3.17C, Table 3.5). GtE and TgE mice were similarly poorly

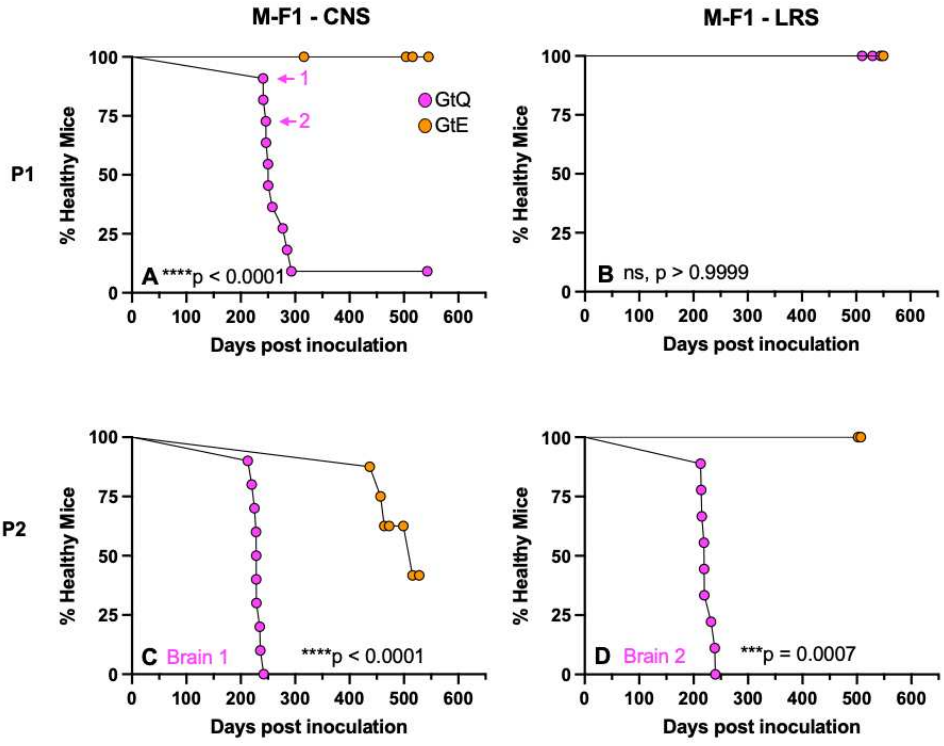

Figure 3.16 Transmission of Finnish moose CWD isolate (M-F1) to GtQ and GtE mice. Survival curves of GtQ (pink circles) and GtE (orange circles) mice resulting from ic inoculation with (A) M-F1 CNS material, (B) M-F1 LRS material, (C, D) GtQ-passaged M-F1 CNS. Pink arrows in A indicate individual brains used for serial passage. p-values comparing survival curves as determined by the Log-rank (Mantel-Cox) test are listed at the bottom of each graph.

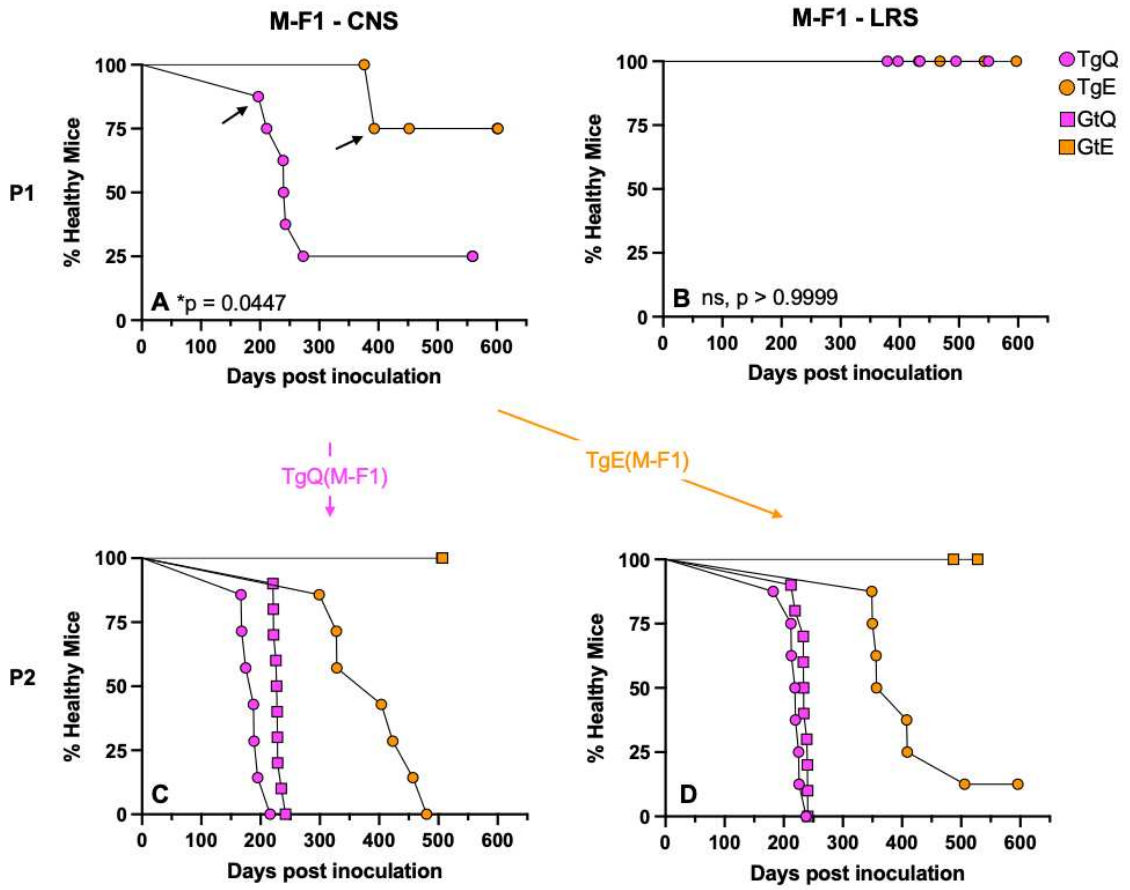

Figure 3.17 Transmission of Finnish moose CWD isolate (M-F1) to TgQ and TgE mice. Survival curves of TgQ (pink circles), TgE (orange circles), GtQ (pink squares), and TgE (orange squares) mice resulting from ic inoculation with (A) M-F1 CNS material, (B) M-F1 LRS material, (C) TgQ-passaged M-F1 CNS, and (D) TgE-passaged M-F1 CNS. Black arrows in A indicate individual brains used for serial passage. p-values comparing survival curves as determined by the Log-rank (Mantel-Cox) test are listed at the bottom of graphs.

responsive to M-F1 from the brains of two diseased GtQ mice (Figure 3.16C, 3.16D, Table 3.5). We also serially passaged prions from the CNS of the single TgE mouse which developed disease after primary passage of M-F1 (Figure 3.17D, Table 3.5). Whereas TgE-passaged M-F1 prions produced disease in GtQ mice after 232±3 DPI, they have currently failed to produce disease in GtE mice after > 500 days (Figure 3.17D, Table 3.5). Similarly, while TgE-passaged M-F1 prions produced disease in TgQ mice at 217±6 DPI, only 90 % of inoculated TgE mice developed disease after ~ 390 days, (Figure 3.17D, Table 3.5). Collectively, these serial

Table 3.5 Transmission of Finnish moose isolate CNS and LRS material to GtQ and GtE mice. Survival times are reported as mean time to disease onset ± standard error of the mean (number of diagnosed mice/total number of mice). Ongoing studies at the time of writing are denoted by > days.

Tissue	**Passage**				
		TgE	**TgQ**	**GtE**	**GtQ**
CNS	p1	393 (1/5)	234±27 (6/8)	>545 (0/9)	259±19 (10/11)
CNS (GtQ 1)	p2			>453±8 (3/7)	228±3 (10/10)
CNS (GtQ 2)	p2			>477 (0/5)	223±4 (9/9)
CNS (TgQ)	p2	388±27 (7/7)	182±7 (8/8)	>477 (0/6)	228±3 (10/10)
CNS (TgE)	p2	390±22 (7/8)	217±6 (8/8)	>498 (0/7)	232±3 (10/10)
LRS	p1	>597 (0/9)	>550 (0/9)	>550 (0/6)	>545 (0/10)

passing results support our conclusion that Q226 provides an optimized template for conversion of M-F1 CWD prions while expression of E226 restricts their transmission. Additionally, we observe that for secondary passage, the residue 226 background (Q or E) from which passage occurs, does not make a difference in time to disease onset in Q226 mice. Comparison of the transmission profiles of Finnish and Norwegian moose CWD revealed that primary and secondary transmissions of both M-F1 and Norwegian M-NO1 prions were more effective in mice expressing Q226. However, mean incubation times of M-F1 and M-NO1 to GtQ mice differed by ~ 180 days (Table 3.2, Table 3.5). These discrepant incubation times suggest that, despite their similar responses to variation at residue 226, the strain properties of these Finnish and Norwegian CWD prions are not completely concordant.

Confirmatory analyses reveal Finnish moose CWD is a distinct strain from all other Nordic moose CWD strains

Using western blotting, we compared the properties of PrP^{Sc} from M-F1 infected Tg and Gt mouse brains with those of North American and M-NO1 CWD. We show that the electrophoretic migration of M-F1 was more rapid than NA CWD, and equivalent to the

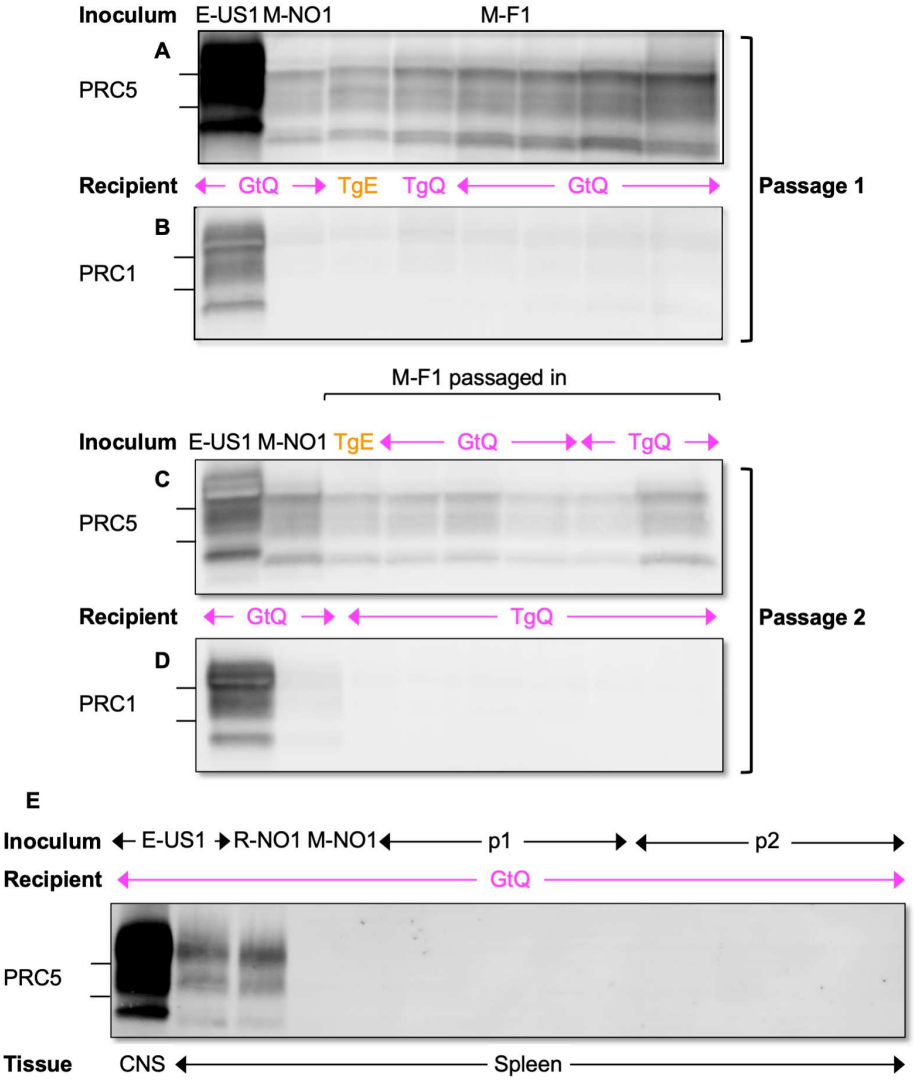

Figure 3.18 Western blots of PrP^{Sc} from primary and secondary transmissions of M-F1. Immunoblots showing PK-resistant profiles of (A, B) M-F1 passaged to TgE, TgQ, and GtQ mice (C, D) Secondary passages of M-F1 in GtQ and TgQ mice. (E) Splenic tissues of M-F1 passaged through GtQ mice (A, C, E) mAb PRC5. (B, D) mAb PRC1. Samples were digested with 50 μg/ml of PK and ~55 μg of brain or ~500 μg of spleen were loaded onto the gel. Molecular weight markers 25 kDa and 20 kDa are indicated to the left of blots.

previously reported faster migrating M-NO1 (20) (Figure 3.18A). Also in accordance with Nordic moose CWD, M-F1 was relatively refractory to detection by PRC1 (Figure 3.18B). Serial transmission of M-F1, M-NO1 and NA CWD from TgE, GtQ, and TgQ produced similar immunoblotting profiles and differential reactivity with mAb PRC1 (Figure 3.18C, 3.18D). Additionally, to confirm the non-lymphotropic properties of M-F1 were maintained after passaging to GtQ mice, we examined splenic tissue for reactivity via western blotting. As expected, no PrP^{Sc} was detected in the spleens of GtQ mice infected with M-F1, akin to spleens of GtQ mice infected with M-NO1 (Figure 3.18E). In contrast, mice infected with North American CWD and Norwegian reindeer CWD show splenic accumulation, indicative of lymphoreticular system replication (Figure 3.18E).

We then assessed the responses of M-F1, M-NO1 and North American CWD prions to denaturation with increasing concentrations of guanidine hydrochloride (GdnHCl) (Figure 3.19A). This measure of PrP^{Sc} stability is associated with conformational variation among prion strains (24). Stability profiles and concentrations of GdnHCl producing half-maximal denaturation ($GdnHCl_{1/2}$) indicate that stability of M-F1 in GtQ mice was substantially lower than M-NO1 (****$p < 0.0001$), and equivalent to NA moose CWD (Figure 3.19A). Upon second passage in the GtQ mice, conformational stability remained constant, indicative of strain stabilization (Figure 3.19B). Similar conformational stabilities of M-F1 were also observed in TgQ mice with M-F1 previously passaged in TgE or TgQ mice. Denaturation curves of these prions were overlapping (ns, 2.59 to 2.95) (Figure 3.19C). We conclude that conformational properties of M-F1 prions are distinct from those of M-NO1 prions.

Histoblotting of coronal brain sections showed that the deposition PrP^{Sc} in M-F1 infected GtQ mice was widespread, diffuse, and symmetrically distributed across both brain hemispheres (Figure 3.20A). This distribution pattern was also consistent in M-F1-infected TgQ mice (Figure 3.20B). Iterative passage to additional GtQ mice also showed the same pattern of distribution (Figure 3.20C). The distribution of M-F1 was indistinguishable from that of M-NO1 in

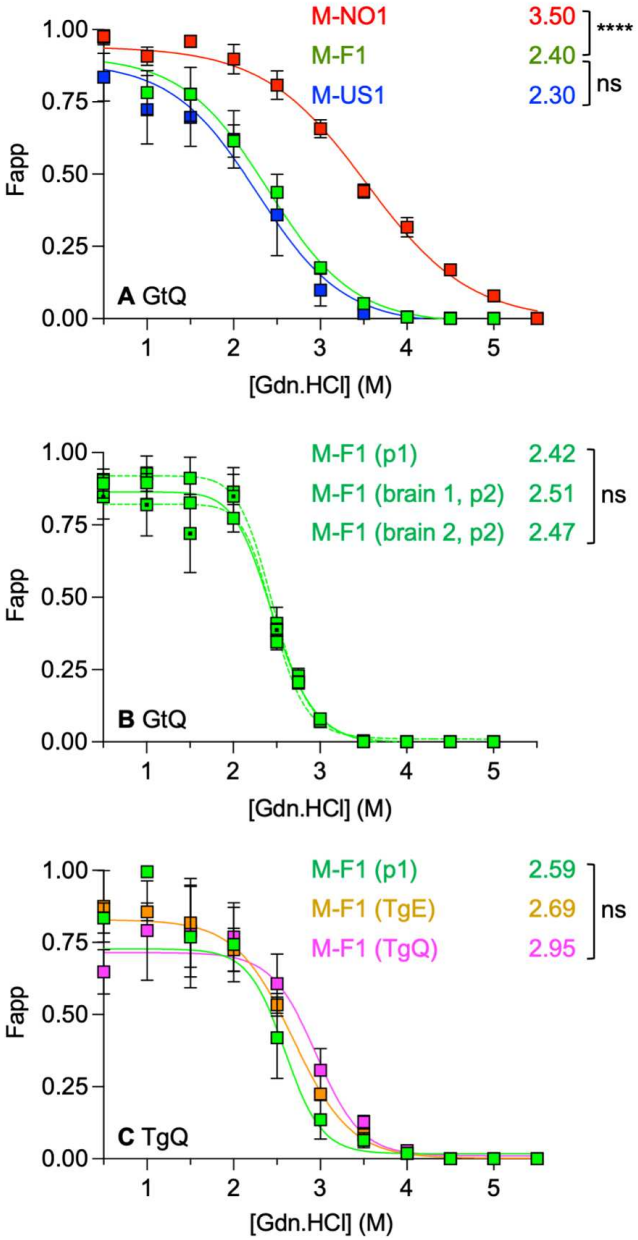

Figure 3.19 Responses of GtQ and TgQ mice infected with M-F1 to increasing concentrations of guanidine hydrochloride. (A, B) Responses of PrP^{Sc} in the CNS of diseased GtQ mice to denaturation with increasing concentrations of GdnHCl. Green = M-F1, red = M-NO1, blue = M-US1. (C) Responses of TgQ mice infected with passage of M-F1 through TgQ and TgE mice. Green = M-F1 in TgQ mice, orange = M-F1 passaged through TgE mice, magenta = M-F1 passaged through TgQ mice. PK-resistant PrP^{Sc} was quantified by densitometry of immunoprobed dot blots and plotted against GdnHCl concentration. Sigmoidal dose-response curves were plotted using a four-parameter algorithm and nonlinear least-square fit. F_{app}, fraction of apparent PrP^{Sc} = (maximum signal-individual signal)/(maximum signal-minimum signal). Error bars, ± standard error of the mean of data from analyses of three animals per group. $GdnHCl_{1/2}$ values (M) for each infection are reported on the right-hand side of each graph. Significance calculated by pairwise analysis of $GdnHCl_{1/2}$ values from best fit curves.

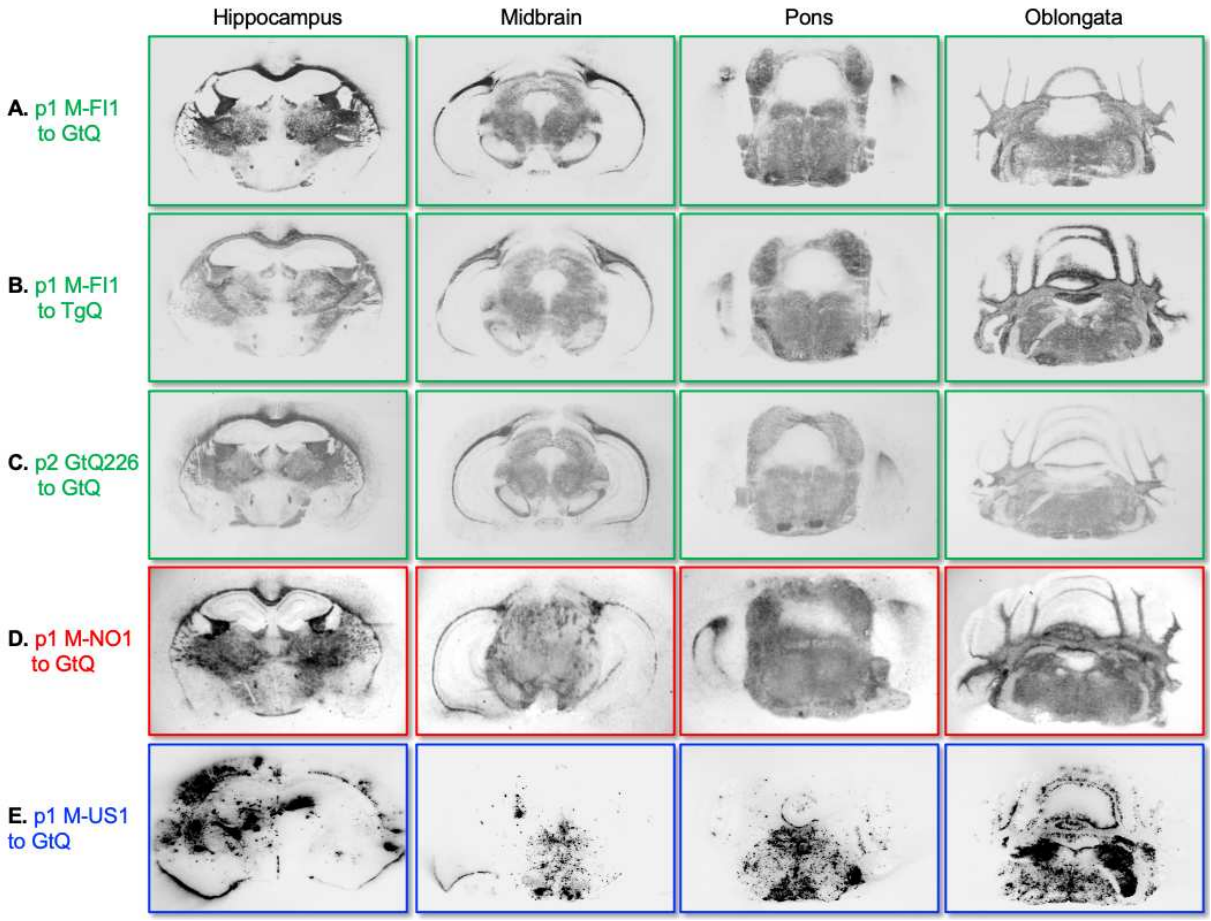

Figure 3.20 Histoblot staining of M-F1 transmitted to GtQ and TgQ. Histoblot of the hippocampal, midbrain, pons and oblongata sections of (A) a GtQ mouse infected with M-F1, (B) a TgQ mouse infected with M-F1, (C) a GtQ mouse infected with GtQ passaged M-F1 (D) a GtQ mouse infected with M-NO1, (E) a GtQ mouse infected with North American moose CWD, Histoblot sections were probed with PRC5.

GtQ mice (Figure 3.20D). Consistent with all of our other findings about Nordic moose, these M-F1 and M-NO1 patterns differed from the disorganized, asymmetrically distributed amalgamations of North American CWD in GtQ mice (Figure 3.20E).

Microscopic analysis via IHC staining of CNS sections from infected mice revealed small punctate accumulations set against a background of diffuse staining were only visible at high magnification of CNS sections from M-F1-infected GtQ mice (Figure 3.21A). M-F1-infected TgE mice revealed a similar pattern of accumulation (Figure 3.21B). Consistent with other studies, only small punctate accumulations were detected in M-NO1-infected GtQ mice (Figure 3.21C).

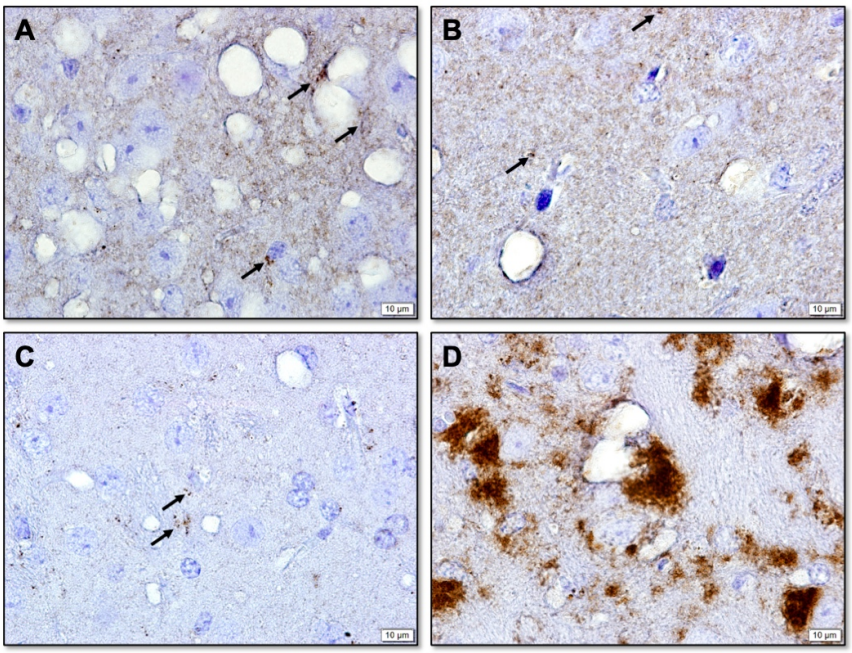

Figure 3.21 IHC staining of hippocampal sections M-F1 transmitted to GtQ and TgE mice shows PrP^{Sc} deposition akin to Norwegian CWD. IHC analysis of (A) a GtQ mouse infected with M-F1, (B) a TgE mouse infected with M-F1, (C) a GtQ mouse infected with M-NO1 and (D) a GtQ mouse infected with North American moose CWD. IHC sections were probed with Fab D18. Scale bar indicates 10 μm.

In contrast GtQ mice infected with North A merican CWD contained intensely staining, amorphous aggregates (Figure 3.21D). We also stained slides with hematoxylin and eosin (H&E) to perform lesion profiling. 9 established brain regions from hindbrain to forebrain were scored for severity of vacuolation (36). First and second passages of M-F1 in GtQ mice showed consistent vacuolation scores across all 9 brain sections (Figure 3.22A). Hindbrain sections showed similar spongiform severities between M-F1, first and second passages, and M-NO1 (Figure 3.22A). However, forebrain sections such as hippocampal and septal sections from M-F1 passages showed more severe vacuolation than sections from M-NO1 (Figure 3.22A, 3.22B, 3.22C). Differences in vacuolation adds to evidence that M-F1 CWD is a strain different than other Nordic moose isolates. Altogether, CWD infecting Finnish moose CWD is distinct from Sweden moose CWD and additionally distinct Norwegian moose CWD.

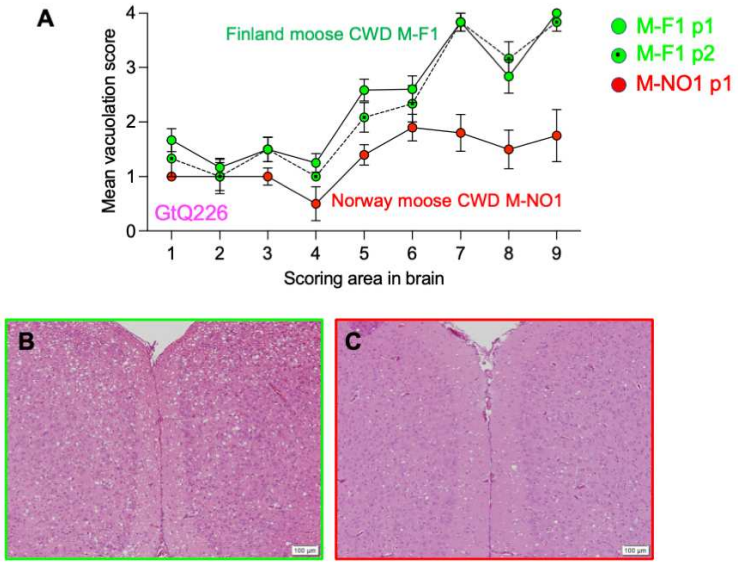

Figure 3.22 Lesion profiling of M-F1 and M-NO1 in GtQ mice shows strain differences. (A) Lesion profiles of M-F1 primarily and secondarily passaged in GtQ mice and M-NO1 passaged in GtQ mice. Brain-scoring areas: 1. medulla, 2. Cerebellum, 3. Superior colliculus, 4. Hypothalamus, 5. Thalamus, 6. Hippocampus, 7. Hippocampal cortex, 8. Septum, 9. Septal cortex. (B) Region 9 of M-F1, passage 1, (C) Region 9 of M-NO1. Scale bar indicates 100 μm.

Discussion

Norwegian moose, red deer and reindeer all propagate novel, distinct CWD strains

Here we investigate the strain properties of novel cases of CWD in European moose and red deer in Norway. Using mouse bioassay of our gene-targeted cervid-PrP expressing mice, we have previously shown that the first 3 cases of CWD found in Norwegian moose are distinct strains from North American CWD (19). In contrast to North American CWD strains, Norwegian moose CWD isolates transmit preferentially to Q226-PrP expressing mice rather than E226-PrP expressing, have a more C-terminal PK cleavage site, and create diffuse, small puncta of PrP^{Sc} in the brain rather than amalgamated plaques.

The fourth case of CWD in a Norwegian moose (M-NO4) did not cause disease in either GtQ or GtE mice (Figure 3.2D, Table 3.2). This is likely due to the low titer of prions in the initial moose brain (Figure 3.1A). To assess clinical disease using mouse bioassay, we could use PMCA to amplify the small amount of CWD in M-NO4, then reinoculated mice with increased

titer prions. We also found that only one GtQ mouse and no GtE mice succumbed to prion disease when inoculated with M-NO5 (Figure 3.2E, Table 3.2). This could also be due to the low titer of prions in the initial moose brain, and we could use PMCA to amplify then reinoculated mice here as well (Figure 3.1). A more puzzling case of no resultant disease comes from the transmission of M-NO6, which did not transmit to either GtQ or GtE mice (Figure 3.2F, Table 3.2). However, PrP^{Sc} was detectable in the original inoculum, and was reactive with both PRC5 and PRC1, indicating a PK cleavage site on PrP more similar to North American CWD (Figure 3.1).

Of the 11 Norwegian, 4 Swedish and 2 Finnish CWD positive moose, M-NO4 and M-NO6 were the only two to express glutamine (QQ) at residue 109 of PrP rather than lysine, KK109. Since CWD is new to Nordic countries, and only European moose can be polymorphic at 109, there is no data on whether the 109 polymorphism has any effect of CWD susceptibility. It could be the case that QQ109 is more refractory to CWD, similar to the 132L polymorphism in elk, resulting in low efficiency of transmission (27). Continual surveillance and diligent genotyping of subsequent CWD cases will help shed light on any polymorphisms in Nordic cervids that contribute to susceptibility to CWD.

Transmissions of M-NO7, M-NO9, M-NO10, and M-NO11 are ongoing and thus will not be discussed. Transmission of M-NO8 to the GtE mice is ongoing, but rapid disease was observed in the GtQ mice. GtQ mice intracerebrally inoculated with M-NO8 developed disease at 122±30. While only 6/10 mice developed clinical disease, the other 4 mice were all euthanized for concurrent illnesses and may have eventually developed disease. Clinically diseased mice had very little PrP^{Sc} in the brain when compared to diseased mice inoculated with other CWD prions (Figure 3.3). This could indicate a fast-replicating prion, that is extremely toxic to mice. The concept of toxic species of PrP^{Sc} is not novel (42). Many speculate that smaller oligomers, rather than large plaques are more neurotoxic to cells as they can exist intraneuronally as opposed to plaques that exist in between cells (43,44). M-NO8, when

transmitted to cervid-PrP mice, causes rapid disease, with a long clinical phase, indicative of either a rather toxic species or fast replicating, but nontoxic species. From this we can conclude that M-NO8 propagates a distinct CWD strain from the first three Norwegian moose cases. Further investigation, using amplification assays such as RT-Quic and PMCA will be done in the future to determine replicative properties of prions stemming from M-NO8.

Prions generated from the first case of CWD in red deer (RD-NO1) in Norway appear to be non-toxic. RD-NO1 upon primary transmission did not cause disease in Q226-cervid PrP mice and transmitted with low efficiency to the E226 backgrounds (Figure 3.4A). Secondary passage of TgE-passaged or TgQ-passaged RD-NO1 did not improve transmission efficiency (Figure 3.4B, 3.4C). However, upon examination of all GtE brains infected with RD-NO1, we found four subclinically infected animals that were terminated at the end of study at 609 DPI. All four animals were determined to be subclinically infected based on the strong immunoblot profile they exhibited, extremely atypical of animals with no neurological clinical signs (Figure 3.5A). All four animals, along with three clinical animals also exhibited a novel IHC pattern in the brain, with strong PrP^{Sc} accumulation in the granular layer of the dentate gyrus of the hippocampus (Figure 3.6A, 3.6B). The majority of clinical signs used to diagnose prion disease in mice correlate to cerebellar and lower brain stem dysfunction such as ataxia and loss of reflexes (45). In this study, the majority of PrP^{Sc} accumulation was detected in the dentate gyrus, which functions as part of the pathway to form episodic memories (46). Deficits in the dentate gyrus, and the hippocampus in general can be measured using hippocampal memory behavioral assays. As we did not perform these, we cannot rule out that the PrP^{Sc} accumulation the dentate gyrus led to memory deficits in the mice. Another intriguing aspect of dentate gyrus specific PrP^{Sc} is the existence of adult stem cells in the dentate gyrus. While still controversial, most agree that adult neurogenesis is possible, and originates from stem cells in the hippocampus (47). Multiple groups are using stem cells to attempt to treat prion diseases (48),

so the notion of a prion strain that specifically targets an area of the brain rich in stem cells in intriguing.

Secondary transmission of GtE-passaged RD-NO1 resulted in transmission to the GtQ background at a mean time of 540±9 in 3/9 mice (Figure 3.4D, Table 3.3). Similarly, serial transmission through GtE mice to GtE mice had a mean incubation time of 545±7 and a 100% attack rate (Figure 3.4D, Table 3.3). Analysis of PrP^{Sc} distribution is still ongoing. However, because of the unusual disease kinetics of this isolates, all isolates were examined for PrP^{Sc} via western blot. Many animals that were euthanized due to other conditions, or were found dead in their cage, were found to have PrP^{Sc} in the brain. The earliest evidence of PrP^{Sc} was found ~300 days before the first clinical diagnosis. In chapter 2, we showed that at the earliest, minimal PrP^{Sc} is detectable on western blot ~150 days before clinical disease onset. To further investigate the disease kinetics induced by RD-NO1, we are planning a longitudinal study to examine RD-NO1 PrP^{Sc} accumulation over time. We predict early replication and accumulation of PrP^{Sc} followed by stable levels of prions in the brain that do not cause clinical disease. This phenomenon is somewhat reminiscent of nonadaptive prion amplification (NAPA), coined by Bian and Telling (35). Using mouse bioassay, after interspecies transmission, serial transmission to the same new species resulted in no disease. While there is no species barrier between our cervid-PrP mice and the Norway red deer inoculum, this presents an avenue where Norway red deer CWD originated from an interspecies transmission. This will be addressed later in Chapter 4.

3 cases of Swedish moose CWD have distinct strain properties from each other when transmitted in Gt cervid-PrP mice

In a similar fashion to the examination of the strain properties of Norwegian moose CWD cases, we transmitted the first three cases of Swedish moose CWD to our GtQ and GtE mice.

Transmission of the first case (M-SW1) resulted in disease in the GtQ background (344±6 DPI), in line with the Norwegian moose cases, but more rapid (Figure 3.8A). Additionally, one GtE mouse presented with clinical signs near the end of study at 565 DPI (Figure 3.8A). However, when examined postmortem, all GtE mice terminated at end of study had evidence of PrP^{Sc} in their CNS material via western blotting or IHC analysis. Moreover, some of those mice had a staining pattern consistent with glial infection, specifically in the dentate gyrus, similar to the Norwegian red deer case (Figure 3.9C, 3.9D). If the healthy lifespan of a mouse was not the determinant of when a study is terminated, perhaps these GtE mice would exhibit clinical signs eventually. The alternative would postulate that the selected quasispecies in GtE mice has the capability to infect glial cells but not neuronal cells, and this is not sufficient to ever cause disease. Colocalization with glial markers, Iba1 and GFAP will be done in the future to confirm this. The notion that E226 cervids in Nordic countries harbor subclinical infection should be of concern. Our bioassay of the red deer, which is EE at residue 226, and the subclinical disease identified in GtE226 mice infected with M-SW1 is strong evidence that E226 cervids may be less susceptible to Nordic CWD strains but are still at risk for spreading infection. Furthermore, PrP^{Sc} deposition was largely contained to the dentate gyrus, indicative of cell type specific PrP^{Sc} accumulation. These animals, because they do not outwardly exhibit behavioral aberrations, yet harbor scrapie loads consistent with disease, could be a source of CWD spread in Nordic countries that is near impossible to detect and manage.

Transmission of M-SW2 when transmitted to GtQ and GtE mice presents another interesting CWD strain. Upon primary passage, just two GtQ mice manifested clinical disease at 528±11 DPI (Figure 3.10A). However, serial passage to GtQ mice results in transmission with a mean time to disease onset of 94±1 DPI an 82% decrease from primary passage (Figure 3.10B). Typically, an extreme reduction in time to disease onset like this, is seen with adaptation after interspecies transmission (49). Yet, the gene-targeted cervid mice were designed to abrogate the species barrier, and thus reduction in time to disease onset must be due another

factor. Western blotting and histological techniques did not lend any insight into divergence between M-SW2 and other Nordic CWD isolates. Furthermore, transmission from the GtQ mice to GtE mice resulted in 100% attack rate at 299±20 DPI which considered a rather rapid transmission for Nordic isolates serially transmitted to GtE mice (Figure 3.10B). Tertiary transmission of the M-SW2 isolate had the same time to disease onset as secondary transmission in the GtQ mice and is considered to be stabilized (Figure 3.10C) and disease was slightly more accelerated in the GtE mice. Additionally, passaging from the GtQ to GtE to GtQ background results in another rapid transmission of 107±3 DPI (Figure 3.10D). Taken together, regardless of residue 226 and serial passage number, M-SW2 causes rapid transmission but exhibits no other notable biochemical characteristics in relation to the other Nordic moose isolates. This suggests that the dominant strain in this isolate is an intensely potent one. Further experiments to study disease kinetics include a longitudinal study of disease and sciatic nerve inoculation to measure the time it takes for the prions to reach the CNS. We postulate that the conformation of PrP^{Sc} in this strain has properties that allow for usual ease of the unfolding and refolding of PrP^{C} to PrP^{Sc}. As such, in collaboration with Witold Surewicz, we plan to obtain the cryo-EM structure of these prions that we imagine to be highly toxic.

Transmission of the third Swedish moose case (M-SW3) caused disease in the GtQ mice at 377±30 DPI preferentially to the GtE mice analogous to the other Nordic moose cases (Figure 3.13A). Relative to the other Nordic moose cases however, M-SW3 displayed more PK-resistant PrP^{Sc} via western blot, more comparable to levels seen in North American CWD cases. Additionally, IHC staining produces an intermediate deposition pattern between diffuse Nordic CWD and plaque-like North American CWD. This phenotype remains consistent upon serial passaging of this isolate. The intermediate phenotype here is reminiscent of M-NO2's ability to adapt through serial passaging to exhibit characteristics more akin to North American CWD (19). Continual passaging of M-SW3 could eventually lead to adaptation to the GtE226 mice and other North American CWD strain properties. Altogether, evidence from all 3 Swedish

moose isolates indicates, just like Norway, that there exists a highly unstable strain population which can be characterized using our mouse bioassay.

CWD prions from a Finnish moose are distinct from all other Nordic moose CWD cases

Using the mouse bioassay, our analyses reveal that certain characteristics of M-F1 CWD prions overlap with those of other Nordic moose CWD cases. Like all other Nordic moose CWD isolates, propagation of M-F1 was more efficient in Q226 mice rather than E226 mice (Figure 3.16, 3.17). Western blot and histoblot profiles of M-F1 and M-NO1 in GtQ mice are indistinguishable from each other (Figure 3.18, 3.20). Unlike infection with North American CWD, GtQ mice infected with M-F1 or M-NO1 do not show any PrP^{Sc} reactivity in splenic tissue (Figure 3.18).

Despite these similarities, other assays reveal strain variation between M-F1 and M-NO1 CWD. Notably, the conformational stability of M-F1 prions in response to denaturation with GdnHcl was significantly lower than that of M-NO1 and equivalent to North American CWD (Figure 3.19). Additionally, lesion profiling reveals more severe vacuolation in the forebrain of mice infected with M-F1 as opposed to M-NO1 (Figure 3.22). These incompletely overlapping properties of Finnish and Norwegian moose CWD prions add to an increasing body of evidence for a surprising variety of strains among Nordic cervids which stands in contrast to a relatively consistent CWD strain profile among NA deer, elk and moose.

Interestingly, serial passaging of the Finnish moose CWD lends further insight into the role played by residue 226 of cervid PrP. Primary passage of M-F1 resulted in no clinically sick GtE mice and just one clinically diseased TgE mouse (Figure 3.16, 3.17). However, serial passage of CWD prions from TgQ-passaged M-F1, TgE-passaged M-F1, or GtQ-passaged M-F1 all resulted in equivalent incubation times in GtQ or TgQ mice. This indicates that there was little to no initial adaptation into the E226 background and E226 Nordic prions maintain preference for propagation in a Q226 background. This is concordant with the number of CWD

cases in Q226 cervids (moose and reindeer) and E226 cervids. In total, 37 Q226 cervids (17 moose and 20 reindeer) and 3 E226 cervids (red deer) have been diagnosed to be CWD positive.

An unstable population of CWD strains of unknown origin are prevalent in Nordic countries.

Taken all together, the prevalence and number of novel strains of CWD in Nordic countries is increasing with new cases being identified each year. Transmission of North American CWD isolates, whether from a deer, elk, red deer or moose to cervid-PrP mice generally results in similar incubation times, residue 226 tropism, immunoblot fingerprint, and PrP^{Sc} distribution in the brain. However, each isolate transmitted from a CWD positive animal in the Nordic countries results in slightly different disease outcomes. This would suggest the existence of an unstable strain population that will likely stabilize as CWD becomes endemic to the region where the most dominant strain will become the most prevalent.

Early studies by Bolton, McKinley and Prusiner showed that the amount of scrapie agent in sample is directly correlated with the amount of infection (39). Our studies with transmission of new Nordic isolates challenge this precedent. First, on average transmission of Nordic moose CWD isolates results in 10 times less PrP^{Sc} than transmission of North American CWD isolates, yet upon serial transmission, transmission times of Nordic vs North American isolates are not 10 times different from each other (19). Transmission of the Norwegian red deer CWD isolate produces high amounts of PrP^{Sc}, but little to no infection. Opposingly, transmission of Norwegian moose CWD isolate 8 and Swedish moose CWD isolate 2 does not produce more PrP^{Sc} than average, but results in rapid transmission. The convention that scrapie correlates with amount of infection does not hold true for novel Nordic isolates, lending to the unstable and unpredictable nature of these newly identified cases of CWD.

The origin of CWD in Nordic countries remains under scrutiny. It appears just one strain of CWD is infecting Norwegian reindeer based on mouse bioassay (19). This is also supported

by detection of CWD in reindeer peripheral tissue such as lymph nodes. All positive reindeer were in the same herd in the same region, so it seems likely that animal to animal transmission and a contaminated environment allowed the transmission of CWD in reindeer. Initial speculation to the origin of Nordic moose and red deer CWD pointed to an atypical, spontaneous origin (16). This was postulated due to the old age of the animals, no detection of CWD in peripheral tissue and the resulting atypical PrP^{Sc} immunoblot profile. The notion that spontaneous disease arose in 17 moose total and 3 red deer in 3 geographically connected countries have been found to be CWD positive in the past ~7 years, with the first cases emerging around the time of the first detection in reindeer seems unlikely but not impossible. Surveillance efforts in Norway, Sweden and Finland prior to 2015 existed, but were not rigorous (16). However, increased surveillance after the first cases were detected has surely led to detection of more CWD cases.

Another argument against the spontaneous origin of CWD in Nordic moose and red deer comes from evidence provided from spontaneous prion disease in other species. For example, spontaneous Creutzfeldt-Jakob disease (sCJD) cases have been characterized to 6 subtypes, but these strains are dictated by the PrP genotype at 129 (MM1, MM2, MV1, MV2, VV1, and VV2) (50,51). The importance of this polymorphism in susceptibility to prion diseases in humans is the main driver of the phenotypic differences between strains. Similarly, atypical scrapie has been described as a spontaneous prion disease in older sheep (52). Atypical scrapie has also been associated with polymorphisms in PrP (F141 and H154) and there is not a vast variety of strains associated with atypical scrapie (53). Known spontaneous diseases in other species are largely homogeneous strains, dictated by susceptibility polymorphisms on PrP. As we have not identified any novel polymorphisms associated with these Nordic moose CWD cases, they do not fit the mold of the atypical cases of prion diseases across other species. However, the novelty of these diseases warrant further investigation before a non-spontaneous origin could be determined.

A puzzling moose wasting syndrome was noted in Sweden first in 1985 and was named Älvsborg disease since the highest incidence was in that region, affecting 150-180 animals per year (54,55). These moose presented with dehydration, emaciation, impaired vision, general weakness and central nervous system disturbance (55). The etiology of the Swedish Moose Wasting Syndrome is still unknown, but environmental toxins, viral infection or trace element imbalances (56,57). The emergence of CWD across Nordic countries raises questions about Moose Wasting Syndrome having a prion origin. However, immunohistochemical analyses done in the 1990s failed to detect any spongiosis or PrP^{Sc} (54). While no PrP^{Sc} was detectable, the existence of Moose Wasting Syndrome in Sweden could have a potential link to the current CWD cases in Sweden.

Since all Nordic moose and red deer were infected with non-lymphotropic strains of CWD, the route of infection is still unknown. If these cases are not of a spontaneous origin, it is possible that CWD infected material was ingested, as was the case with the BSE epidemic (58). As such, transmission studies involving the feeding of Nordic CWD to Gt-cervid PrP are a future direction. The potential for an interspecies transmission event to be the cause of Nordic CWD will be addressed in Chapter 4.

REFERENCES

1. Williams ES. Review article - Chronic Wasting Disease. Vet Pathol. 2005;42(5):530–49.

2. Williams ES, Young S. Chronic wasting disease of captive mule deer: a spongiform encephalopathy. J Wildl Dis. 1980;16(1):89–98.

3. Williams ES, Young S. Spongiform encephalopathies in Cervidae. Revue Scientifique et Technique. 1992;11(2):551–67.

4. Williams ES, Young S. Spongiform encephalopathy of Rocky Mountain elk. J Wildl Dis. 1982;18(4):465–71.

5. Kahn S, Dubé C, Bates L, Balachandran A. Chronic wasting disease in Canada: Part 1. Vol. 45, Canadian Veterinary Journal. 2004. p. 397–404.

6. Samuel MD, Storm DJ. Chronic wasting disease in white-tailed deer: Infection, mortality, and implications for heterogeneous transmission. Ecology. 2016;97(11):ecy1538.

7. Kreeger TJ, Montgomery DL, Jewell JE, Schultz W, Williams ES. Oral transmission of chronic wasting disease in captive Shira's moose. J Wildl Dis. 2006;42(3):640–5.

8. Baeten LA, Powers BE, Jewell JE, Spraker TR, Miller MW. A natural case of chronic wasting disease in a free-ranging moose (Alces alces shirasi). J Wildl Dis. 2007;43(2):309–14.

9. Gagnier M, Laurion I, Denicola AJ. Control and surveillance operations to prevent chronic wasting disease establishment in free-ranging white-tailed deer in Québec, Canada. Animals. 2020;10(2):283.

10. Sohn HJ, Kim JH, Choi KS, Nah JJ, Joo YS, Jean YH, et al. A case of chronic wasting disease in an elk imported to Korea from Canada. Journal of Veterinary Medical Science. 2002;64(9):855–8.

11. Kim TY, Shon HJ, Joo YS, Mun UK, Kang KS, Lee YS. Additional cases of Chronic Wasting Disease in imported deer in Korea. Journal of Veterinary Medical Science. 2005;67(8):753–9.

12. Benestad SL, Mitchell G, Simmons M, Ytrehus B, Vikøren T. First case of chronic wasting disease in Europe in a Norwegian free-ranging reindeer. Vet Res. 2016;47(1):88.

13. Vikøren T, Våge J, Madslien KI, Røed KH, Rolandsen CM, Tran L, et al. First detection of chronic wasting disease in a wild red deer (Cervus elaphus) in Europe. J Wildl Dis. 2019;55(4):970–2.

14. Pirisinu L, Tran L, Chiappini B, Vanni I, di Bari MA, Vaccari G, et al. Novel type of chronic wasting disease detected in moose (Alces alces), Norway. Emerg Infect Dis. 2018;2210–8.

15. Mysterud A, Rolandsen CM. A reindeer cull to prevent chronic wasting disease in Europe. Vol. 2, Nature Ecology and Evolution. 2018. p. 1343–5.

16. Tranulis MA, Gavier-Widén D, Våge J, Nöremark M, Korpenfelt SL, Hautaniemi M, et al. Chronic wasting disease in Europe: new strains on the horizon. Vol. 63, Acta Veterinaria Scandinavica. 2021. p. 48.

17. EFSA Panel on Biological Hazards (BIOHAZ). EFSA. 2016;4667:15.

18. Ågren EO, Sörén K, Gavier-Widén D, Benestad SL, Tran L, Wall K, et al. First detection of chronic wasting disease in moose (Alces alces) in Sweden. J Wildl Dis. 2021;57(2):461–3.

19. Bian J, Kim S, Kane SJ, Crowell J, Sun JL, Christiansen J, et al. Adaptive selection of a prion strain conformer corresponding to established North American CWD during propagation of novel emergent Norwegian strains in mice expressing elk or deer prion protein. PLoS Pathog. 2021;17(7):1009748.

20. Rolandsen CM, Solberg EJ, Sæther BE, Moorter B van, Herfindal I, Bjørneraas K. On fitness and partial migration in a large herbivore – migratory moose have higher reproductive performance than residents. Oikos. 2017;126(4):oik.02996.

21. Bunnefeld N, Börger L, van Moorter B, Rolandsen CM, Dettki H, Solberg EJ, et al. A model-driven approach to quantify migration patterns: Individual, regional and yearly differences. Journal of Animal Ecology. 2011;80(2):466–76.

22. Meisingset EL, Loe LE, Brekkum Ø, Bischof R, Rivrud IM, Lande US, et al. Spatial mismatch between management units and movement ecology of a partially migratory ungulate. Journal of Applied Ecology. 2018;55(2):13003.

23. Güere ME, Våge J, Tharaldsen H, Kvie KS, Bårdsen BJ, Benestad SL, et al. Chronic wasting disease in Norway—A survey of prion protein gene variation among cervids. Transbound Emerg Dis. 2021;69(4):20–31.

24. Huson HJ, Happ CM. Polymorphisms of the prion protein gene (PRNP) in Alaskan moose (Alces alces gigas). Anim Genet. 2006;37(4):425–6.

25. Cullingham CI, Peery RM, Dao A, McKenzie DI, Coltman DW. Predicting the spread-risk potential of chronic wasting disease to sympatric ungulate species. Prion. 2020;14(1):56–66.

26. Miller MW, Williams ES, McCarty CW, Spraker TR, Kreeger TJ, Larsen CT, et al. Epizootiology of chronic wasting disease in free-ranging cervids in Colorado and Wyoming. J Wildl Dis. 2000;36(4):676–90.

27. Green KM, Browning SR, Seward TS, Jewell JE, Ross DL, Green MA, et al. The elk PRNP codon 132 polymorphism controls cervid and scrapie prion propagation. Journal of General Virology. 2008;89(2):598–608.

28. Browning SR, Mason GL, Seward T, Green M, Eliason GAJ, Mathiason C, et al. Transmission of Prions from Mule Deer and Elk with Chronic Wasting Disease to Transgenic Mice Expressing Cervid PrP. J Virol. 2004;78(23):13345–50.

29. Angers RC, Seward TS, Napier D, Green M, Hoover E, Spraker T, et al. Chronic wasting disease prions in eik antler velvet. Emerg Infect Dis. 2009;15(5):696–703.

30. Bian J, Christiansen JR, Moreno JA, Kane SJ, Khaychuk V, Gallegos J, et al. Primary structural differences at residue 226 of deer and elk PrP dictate selection of distinct CWD prion strains in gene-targeted mice. Proc Natl Acad Sci U S A. 2019;12478–87.

31. Kang HE, Weng CC, Saijo E, Saylor V, Bian J, Kim S, et al. Characterization of conformation-dependent prion protein epitopes. Journal of Biological Chemistry. 2012;287(44):37219–32.

32. Taraboulos A, Jendroska K, Serban D, Yang SL, Dearmond SJ, Prusiner SB. Regional mapping of prion proteins in brain. Proc Natl Acad Sci U S A. 1992;89(16):7620–4.

33. Muramoto T, DeArmond SJ, Scott M, Telling GC, Cohen FE, Prusiner SB. Heritable disorder resembling neuronal storage disease in mice expressing prion protein with deletion of an α-helix. Nat Med. 1997;3(7):750–5.

34. Saijo E, Kang HE, Bian J, Bowling KG, Browning S, Kim S, et al. Epigenetic Dominance of Prion Conformers. PLoS Pathog. 2013;9(10):e1003692.

35. Bian J, Khaychuk V, Angers RC, Fernández-Borges N, Vidal E, Meyerett-Reid C, et al. Prion replication without host adaptation during interspecies transmissions. Proc Natl Acad Sci U S A. 2017;114(5):1141–6.

36. Fraser H, Dickinson AG. The sequential development of the brain lesions of scrapie in three strains of mice. J Comp Pathol. 1968;78(3):301–11.

37. Liberski PP, Gajdusek DC, Brown P. How do neurons degenerate in prion diseases or transmissible spongiform encephalopathies (TSEs): Neuronal autophagy revisited. In: Acta Neurobiologiae Experimentalis. 2002. p. 141–7.

38. Angers RC, Kang HE, Napier D, Browning S, Seward T, Mathiason C, et al. Prion strain mutation determined by prion protein conformational compatibility and primary structure. Science (1979). 2010;328(5982):1154–8.

39. Bolton DC, Mckinley MP, Prusiner SB. Identification of a protein that purifies with the scrapie prion. Science (1979). 1982;218(4579):1309–11.

40. Schwabenlander MD, Culhane MR, Hall SM, Goyal SM, Anderson PL, Carstensen M, et al. A case of chronic wasting disease in a captive red deer (Cervus elaphus). Journal of Veterinary Diagnostic Investigation. 2013;25(5):573–6.

41. Carroll JA, Striebel JF, Rangel A, Woods T, Phillips K, Peterson KE, et al. Prion Strain Differences in Accumulation of PrPSc on Neurons and Glia Are Associated with Similar Expression Profiles of Neuroinflammatory Genes: Comparison of Three Prion Strains. PLoS Pathog. 2016;12(4):e1005551.

42. Harrison CF, Barnham KJ, Hill AF. Neurotoxic species in prion disease: A role for PrP isoforms? Vol. 103, Journal of Neurochemistry. 2007. p. 1709–20.

43. Simoneau S, Rezaei H, Salès N, Kaiser-Schulz G, Lefebvre-Roque M, Vidal C, et al. In vitro and in vivo neurotoxicity of prion protein oligomers. PLoS Pathog. 2007;3(8):e125.

44. Huang P, Lian F, Wen Y, Guo C, Lin D. Prion protein oligomer and its neurotoxicity. Vol. 45, Acta Biochimica et Biophysica Sinica. 2013. p. 442–51.

45. Watts JC, Prusiner SB. Mouse models for studying the formation and propagation of prions. Vol. 289, Journal of Biological Chemistry. 2014. p. 19841–9.

46. Amaral DG, Scharfman HE, Lavenex P. The dentate gyrus: fundamental neuroanatomical organization (dentate gyrus for dummies). Vol. 163, Progress in Brain Research. 2007. p. 3–22.

47. Gonçalves JT, Schafer ST, Gage FH. Adult Neurogenesis in the Hippocampus: From Stem Cells to Behavior. Vol. 167, Cell. 2016. p. 897–914.

48. Metkar SK, Girigoswami K, Girigoswami A. Stem cell-based therapeutic strategy in delaying prion disease. In: Stem Cells and Aging. 2021.

49. Angers R, Christiansen J, Nalls A v., Kang HE, Hunter N, Hoover E, et al. Structural effects of PrP polymorphisms on intra- and interspecies prion transmission. Proc Natl Acad Sci U S A. 2014;11169–74.

50. Brown P, Gibbs CJ, Rodgers-Johnson P, Asher DM, Sulima MP, Bacote A, et al. Human spongiform encephalopathy: The national institutes of health series of 300 cases of experimentally transmitted disease. Ann Neurol. 1994;35(5):513–29.

51. Bishop MT, Will RG, Manson JC. Defining sporadic Creutzfeldt-Jakob disease strains and their transmission properties. Proc Natl Acad Sci U S A. 2010;107(26):12005–10.

52. Benestad SL, Sarradin P, Thu B, Schönheit J, Tranulis MA, Bratberg B. Cases of scrapie with unusual features in Norway and designation of a new type, Nor98. Veterinary Record. 2003;153(7):202–8.

53. Greenlee JJ. Review: Update on Classical and Atypical Scrapie in Sheep and Goats. Vol. 56, Veterinary Pathology. 2019. p. 6–16.

54. Rehbinder C, Gimeno E, Belák K, Belák S, Stéen M, Rivera E, et al. A bovine viral diarrhoea/mucosal disease-like syndrome in moose (Alces alces): investigations on the central nervous system. Vet Rec. 1991;129(25–26).

55. Stéen M, Diaz R, Faber WE. An erosive/ulcerative alimentary disease of undetermined etiology in Swedish moose (AIces alces L.). Rangifer. 1993;13(4):149–56.

56. Broman E, Wallin K, Stéen M, Cederlund G. A wasting syndrome in Swedish moose (Alces alces): Background and current hypotheses. Ambio. 2002;31(5):409–16.

57. Frank A. A review of the “mysterious” wasting disease in Swedish moose (Alces alces L.) related to molybdenosis and disturbances in copper metabolism. Vol. 102, Biological Trace Element Research. 2004. p. 143–59.

58. Hill AF, Desbruslais M, Joiner S, Sidle KCL, Gowland I, Collinge J, et al. The same prion strain causes vCJD and BSE. Vol. 389, Nature. 1997. p. 448–50.

CHAPTER 4 - GENE-TARGETED AND TRANSGENIC MOUSE MODELS ALLOW EXPLORATION OF INTERSPECIES TRANSMISSION OF CWD, TME, BSE, AND SCRAPIE AND LEND INSIGHTS INTO ORIGINS OF CWD

Introduction

Chronic wasting disease (CWD) is a prion disease affecting deer, elk, moose and other cervids (1). Prion diseases are invariably fatal, neurodegenerative diseases caused by the misfolding of the cellular prion protein (PrP^{C}) to an aberrant, infectious disease-causing form (PrP^{Sc}) (2). CWD is unique from other animal prion diseases in that it is found in both free-ranging and captive populations of cervids (3). Bovine spongiform encephalopathy (BSE) is contained to cattle farms, scrapie to captive sheep flocks, and transmissible mink encephalopathy (TME) to mink farms (4–6). The existence of CWD in populations of animals that are not contained to a particular geographical area presents new challenges in terms of management which were not necessary to address with prion diseases of farmed animals. Overlap in grazing area between deer and livestock raises concern of spillover of CWD to other species that are susceptible to prion disease. Additionally, other species, such as scavengers and small rodents, which may interact with cervid carcasses, are likely exposed to CWD prions in regions where the disease is endemic.

Natural occurrences of interspecies transmission of prion diseases have primarily resulted from consumption of contaminated material. TME was first identified on a mink farm in 1947 in Wisconsin and outbreaks were identified on 5 additional farms in Wisconsin in 1961 (7). An outbreak was also recorded in Idaho in 1963 (8). Outside of the United States, outbreaks have been noted in Finland (1966), East Germany (1967), and the former Soviet Union (1979) (8–10). Retrospectively, the origin of TME has been postulated to be feed contaminated with either bovine or ovine prions (7,8). In the United States, it was common practice to use tissues from “downer” dairy cows as feed for mink farms and BSE-contaminated material is likely the

origin of TME (7,8). In the former Soviet Union, the feeding of carcasses of scrapie-infected sheep to mink has been determined to be the origin of TME (11).

In the context of human health, a strain of BSE was able to cross the species barrier and infect humans in the UK, causing variant Creutzfeldt-Jakob disease (vCJD) in the 1990s (12). Classical BSE is either from a spontaneous origin or may have arose from an interspecies transmission of sheep scrapie to cattle (13). Regardless, it is likely that young cattle were fed BSE contaminated rendered bovine meat and bone meal which subsequently infected the cattle (14). This process continued in a cyclic fashion culminating in an epizootic disease peaking in 1993 with ~1000 BSE cases per week (14). As a result of the BSE outbreak, feeding of brain, spinal cord, and other potential BSE contaminated tissues was banned and the UK reported just 2 cases of BSE in 2015. As a result of the consumption of BSE contaminated material, the first case of vCJD in humans was noted in 1996 (15). ~230 deaths have been linked to vCJD as a result of interspecies transmission of BSE. BSE can also cross the species barrier to felids and cause feline spongiform encephalopathy (FSE) in domestic and exotic cats (16) and to exotic ungulates causing exotic ungulate encephalopathy (EUE) (17).

While the natural host can be used to experimentally recapitulate the circumstances leading to cross species transmission of prion diseases, these experiments can be costly and time consuming, and in the case of transmission to humans, not legal or ethical. Instead, transgenic mouse models can be used to model transmission to better characterize properties of known interspecies transmissions and potential for other interspecies transmissions. For example, ovine-PrP expressing transgenic mice are susceptible to bovine-passaged TME, classical BSE, and L-type BSE (an atypical strain first identified in Italy) (18,19). The similarities in transmission phenotypes of bovine-passaged TME and L-type BSE suggest the origin of TME to be L-type BSE. Mice expressing human PrP have been used to study the vCJD cases caused by BSE. Two parallel studies suggest that sheep or goat-passaged BSE prions are more efficient at causing vCJD phenotypes in transgenic mice expressing human PrP than BSE

prions from cattle (20,21). Containment and elimination of any BSE cases is crucial, given the potential for classical BSE to cross multiple species' barriers.

The complicated interplay between multiple species' PrP in causing efficient interspecies transmission is critical to understand and to predict the potential for new interspecies transmission. The potential for interspecies of CWD is still somewhat murky. Successful transmission resulting from intracerebral inoculation of cattle has been shown with CWD prions from white-tailed deer, mule deer and elk (22–25). Properties of cattle prions originating from inoculation with CWD however, does not produce the classical BSE strain causing vCJD, but a novel, distinct one (22). Additionally, while intracerebral transmission to cattle has been successful, the more natural route of oral inoculation (to simulate consumption of prion contaminated material) has not produced any disease (26). Mule deer CWD has also successfully caused disease in Suffolk sheep via intracerebral inoculation (27). Additionally, oronasal transmission from mule deer to Suffolk sheep resulted in subclinical disease in one of seven inoculated sheep (28). In addition to livestock, many rodent species including meadow voles (*Microtus pennsylvanicus*), red-backed voles (*Myodes gapperi*), white-footed mice (*Peromyscus leucopus*) and deer mice (*Peromyscus maniculatus*) have shown susceptibility to CWD prions (29). Mink are susceptible to CWD, but only after intracerebral inoculation and there is likely no natural relationship between TME and CWD (30). After multiple passages, domestic cats succumb to feline-adapted CWD (31).

Predators and other scavenging animals may be naturally exposed to CWD prions as well. CWD prions remain infectious after passage through the digestive tracts of coyotes (32), crows (33), and earthworms (34). Raccoons also can accumulate PrP^{Sc} following intracerebral inoculation with CWD and additionally TME (35). Passage through the digestive tract of mountain lions appears to decrease detectable CWD by > 96% (36). The unrelenting spread of CWD across North America and the overlap in geographical area of cervids with a variety of other species warrants ecological concern.

In addition to other animals, humans likely come in contact with CWD prions, so the risk for spillover to humans has also been preliminarily assessed. At this time, there is no evidence of CWD infecting humans even after consumption of CWD contaminated meat such as in the case of hunters (37,38). As a proxy however, researchers have used squirrel monkeys to study the species barrier and after intracranial inoculation, squirrel monkeys are susceptible to CWD prions from mule deer, elk and white-tailed deer (39,40). Multiple labs have made transgenic mice expressing human PrP – either M129 or V129 – to examine the species barrier with uniformly negative transmission of CWD (38). Thus far, humanized transgenic mice are also resistant to CWD prions from Norwegian moose and reindeer (41). However, the emergence novel CWD strains in Nordic countries has raised new concern for the potential of these strains to infect humans. This chapter will aim to address the potential for CWD to have adapted from another species and the potential for further interspecies transmission of CWD.

Materials and Methods

Ethics Statement

All animal work was performed in an Association for Assessment and Accreditation of Laboratory Animal Care International accredited facility in accordance with the Guide for the Care and Use of Laboratory Animals. All procedures used in this study were performed in compliance with and were approved by the Colorado State University Institutional Animal Care and Use Committee.

CWD Inocula

The elk isolate referred to as E-US1 represents a diseased Rocky Mountain elk, 99w, that has been previously described (42). Norwegian reindeer CWD isolate R-NO1, and Norwegian moose CWD isolates M-NO1 and M-NO2 have been previously described (43). The Norwegian red deer CWD isolate (RD-NO1) has been previously described (44). Both the

uncloned and cloned TME isolates were a generous gift from Dr. Jason Bartz at Creighton University. Both the classical and L-type BSE were donated by Ed Hoover at the Prion Research Center at Colorado State University. The Nor98 atypical scrapie isolates were a generous gift from Dr. Sylvie Benestad at the Norwegian Veterinary Institute. SSBP/1 was a generous gift from Nora Hunter and originated as a homogenate of three natural scrapie brains that were subsequently passaged mostly through Cheviot sheep at the Neuropathogenesis Unit (NPU), Edinburgh UK (45,46).

Animal work

The development and characterization of TgQ226, TgE226, GtQ226, and GtE226 mice has been previously described (47–49). The development and characterization of TgOvARQ and TgOvVRQ has been previously described (50). TgBov mice were designed and created in a similar fashion by overexpression of wildtype bovine PrP. For inoculation of mice, 10% homogenates of brain tissue from CWD affected moose, reindeer and red deer, TME affected mink, BSE affected cattle or scrapie affected sheep were prepared by mechanical disruption (MP Biomedical) in phosphate-buffered saline (PBS) lacking calcium and magnesium ions. Equal numbers of male and female mice between the ages of four to six weeks were anaesthetized with halothane and either intracerebrally (IC) inoculated freehand with 30 μl or intraperitoneally (IP) inoculated with 100 μl of 1% brain tissue homogenates into the right parietal lobe using a 26-gauge needle at a depth of ~ 2 mm. All animals were subsequently monitored three times a week for the development of neurological signs consistent with prion disease phenotypes. These signs included truncal ataxia, loss of extensor reflex, slowed movement, unsteady or flattened gait, plastic tail, dorsal kyphosis, head bobbing, rough coat and weight loss or gain. The time to disease onset, aka incubation period, is defined as the time between inoculation and the first day on which subsequently progressive clinical signs were

identified. Unless otherwise stated, all animals for which a clinical diagnosis was made were confirmed to have died as a result of prion infection by analysis of PrP^{Sc} in CNS material by various means. Studies for which no clinical signs were noted were terminated ~ 600 days post inoculation as the healthy life span of the mice was reached.

Analysis of PrP^{Sc} by Western Blotting

Protein concentrations of 10% brain homogenates were determined by bicinchoninic acid assay (BCA) (Pierce Biotechnology). Homogenates were treated with 50 μg/mL PK (Roche) in the presence of 2% sarkosyl for 1 hour at 37 °C. PK digestion was terminated with phenylmethylsulfonyl fluoride (PMSF) at a final concentration of 2 mM. Prior to electrophoresis, samples were boiled at 100 °C for 5 minutes in XT-sample buffer (Bio-Rad Laboratories) in the absence of reducing agents. Samples were loaded onto precast 12% discontinuous Bis-Tris gels (Bio-Rad Laboratories). Proteins were then transferred overnight to PVDF-FL membranes (Millipore). Membranes were blocked for 1 hour in 5% nonfat milk in TBS-T, probed with monoclonal antibodies (mAbs) PRC5 or PRC1 followed by horseradish peroxidase (HRP)-conjugated anti-mouse IgG secondary antibody (Cytiva). Membranes were developed using ECL 2 western blot substrate (Thermo Scientific).

Histoblot Analysis

Histoblots were prepared and analyzed as previously described (51). Whole brains were snap frozen on dry ice. Ten μm coronal cryostat sections on slides were transferred to nitrocellulose membranes using lysis buffer. Membranes were treated with 0.2 mg/ml PK for 1 hour at 37 °C then incubated with 2 mM PMSF for 15 minutes. Membranes were incubated with 3 M guanidine isothiocyanate for 10 minutes at room temperature and then blocked in 5% nonfat milk for 30 minutes. Next, membranes were incubated overnight at 4 °C with mAb PRC5

at a dilution of 1:5000. Alkaline phosphatase conjugated goat anti mouse IgG (Southern Biotech) was then incubated for 1 hour at room temperature at a dilution of 1:5000. Membranes were developed using 5-bromo-4-chloro-3-indolyl phosphate (BCIP)/nitro blue tetrazolium (NBT) tablets (Sigma Aldrich) for 5-15 minutes. Micrographs were captured using a Nikon Z1000 microscope.

Immunohistochemical Analyses

Immunohistochemistry (IHC) was performed as previously described (52). In brief, brains were fixed in 10% formalin. Slides with paraffin embedded brain slices were heated to 60°C for 30 minutes prior to xylene and graduated ethanol treatment followed by treatment with 88% formic acid for 30 minutes. Antigen retrieval was then performed in the 2100 Retriever (ProteoGenix) using citrate buffer followed by endoperoxidase quenching in 3% hydrogen peroxide. Slides were blocked in 5% nonfat milk for 30 minutes at room temperature before overnight incubation at 4 °C with primary antibody D18 at a 1:2500 dilution. Slides were incubated with biotin labelled goat Fab anti-human IgG secondary antibody (Southern Biotech) at a dilution of 1:5000 for 1 hour at room temperature. Slides were developed with avidin-conjugated HRP with diaminiobenzidine (DAB) as a substrate for 30 minutes at room temperature (Vector Laboratories). Slides were counterstained with hematoxylin, run through graduated ethanol treatment, cover slipped and imaged at 4x or 100x under oil immersion.

Statistical Information

Statistical analyses were performed using Graphpad Prism software (San Diego). Statistical significance between survival curves of inoculated groups was assessed by comparing median times of survival of various inoculated groups using the log rank (Mantel-Cox) test.

Results

No clinical transmission of Nordic CWD isolates to mice overexpressing ovine or bovine PrP

The detection of CWD in Norway in 2015 has renewed the need to study the potential for interspecies transmissions surrounding cervid species. As such we employed transgenic overexpressing ovine-PrP (TgOvARQ and TgOvVRQ) and bovine-PrP (TgBov) mice to study the potential of Nordic CWD transmission. Sheep PrP contains 3 main polymorphisms that control susceptibility to scrapie: 136 alanine (A) or valine (V), 154 arginine (R) or histidine (H), and 171 glutamine (Q) or arginine (R). Sheep PrP with 136V, 154R, 171Q (VRQ) is considered the most susceptible, while sheep expressing PrP with 136A, 154H, 171R (AHR) are the least susceptible (53–55). The transgenic ovine-PrP mice we have express near wildtype levels of either ovine-PrP ARQ or ovine-PrP VRQ (50). We thus chose representative Nordic isolates to intracerebrally inoculate TgOvARQ, TgOvVRQ, and TgBov mice and examine the potential for Nordic prions to cross ovine and bovine species barriers.

We first chose to inoculate ovine-PrP and bovine-PrP mice with Norwegian reindeer CWD as reindeer CWD exhibits lymphotropic properties and is the most likely to be shed in the environment. Intracerebral transmission of reindeer isolate V142 (R-NO1) did not result in any clinical disease in either TgOvARQ, TgOvVRQ, or TgBov mice (Figure 4.1A, Table 4.1). Similarly, the first (M-NO1) and second (M-NO2) Norwegian CWD moose cases also did not cause any clinical disease in TgOvARQ, TgOvVRQ, or TgBov mice despite letting days post

Table 4.1 Transmission of Norwegian reindeer, moose and red deer isolates to TgOvARQ, TgOvVRQ, and TgBov mice. Survival times are reported as mean time to disease onset ± standard error of the mean (number of diagnosed mice/total number of mice).

Inoculum	Tg(OvARQ)	Tg(OvVRQ)	Tg(Bov)
R-NO1	594 (0/6)	525-588 (0/9)	478-594 (0/5)
M-NO1	484-603 (0/6)	587-607 (0/6)	494-561 (0/5)
M-NO2	452-607 (0/6)	521-607 (0/8)	589-607 (0/6)
RD-NO1	547-608 (0/6)	479-588 (0/7)	432-608 (0/5)

inoculation surpass 600 days (Figure 4.1B, 4.1C, Table 4.1). Finally, we inoculated TgOvARQ, TgOvVRQ, and TgBov mice with CNS material from the Norwegian red deer CWD case (RD-NO1) (Figure 4.1D, Table 4.1). No transmission upon primary passage of a field isolate to another species is not entirely uncommon because of the species barrier existing between various primary sequences of PrP. Additionally, we have shown Nordic CWD isolates contain ~10 times less PrP^{Sc} than North American CWD (Chapter 3), and thus titer may have been low to cause disease.

Nevertheless, we looked for evidence of PrP^{Sc} via western blotting, histoblotting and IHC staining since mice could harbor subclinical infection. All available brains from mice terminated

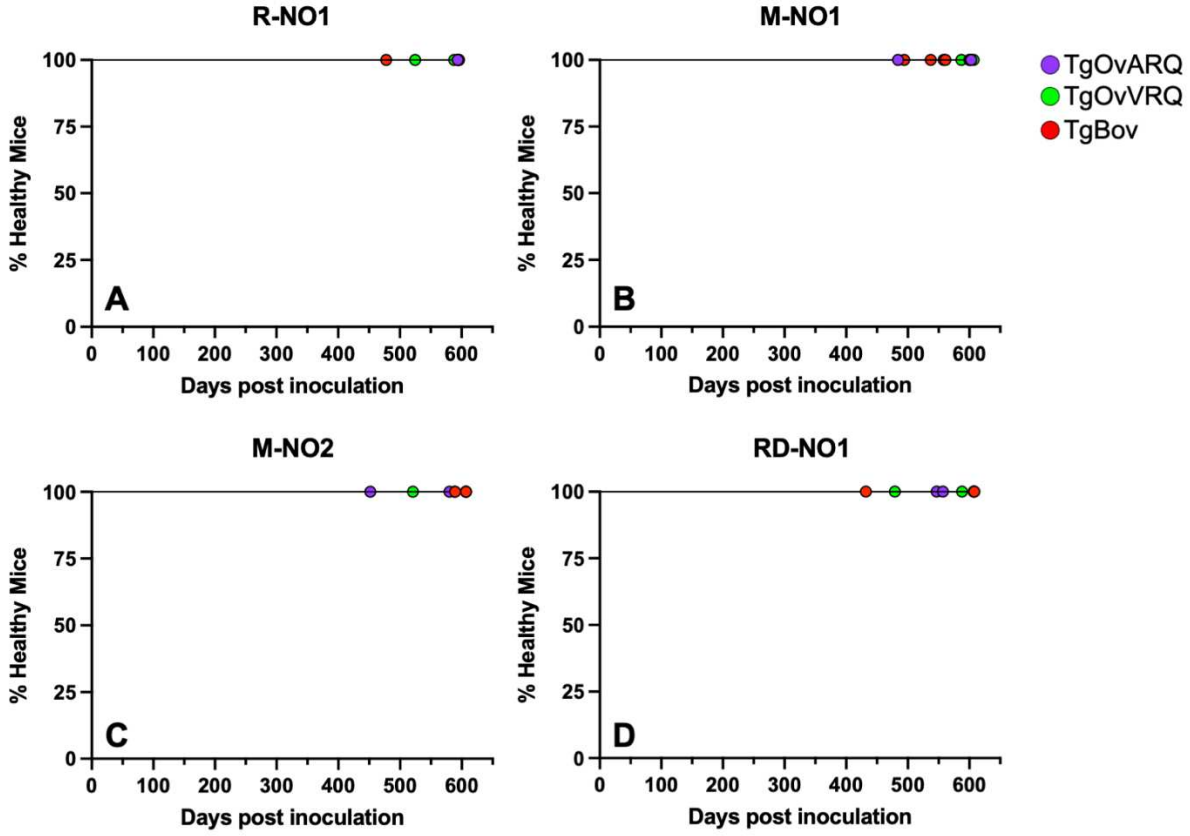

Figure 4.1 Transmission of the Norwegian reindeer, moose and red deer CWD isolates to TgOvARQ, TgOvVRQ, TgBov mice. Survival curves of TgOvARQ (purple circles), TgOvVRQ (green circles), and TgBov (red circles) mice resulting from ic inoculation with (A) R-NO1, (B) M-NO1, (C) M-NO2, (D) RD-NO1.

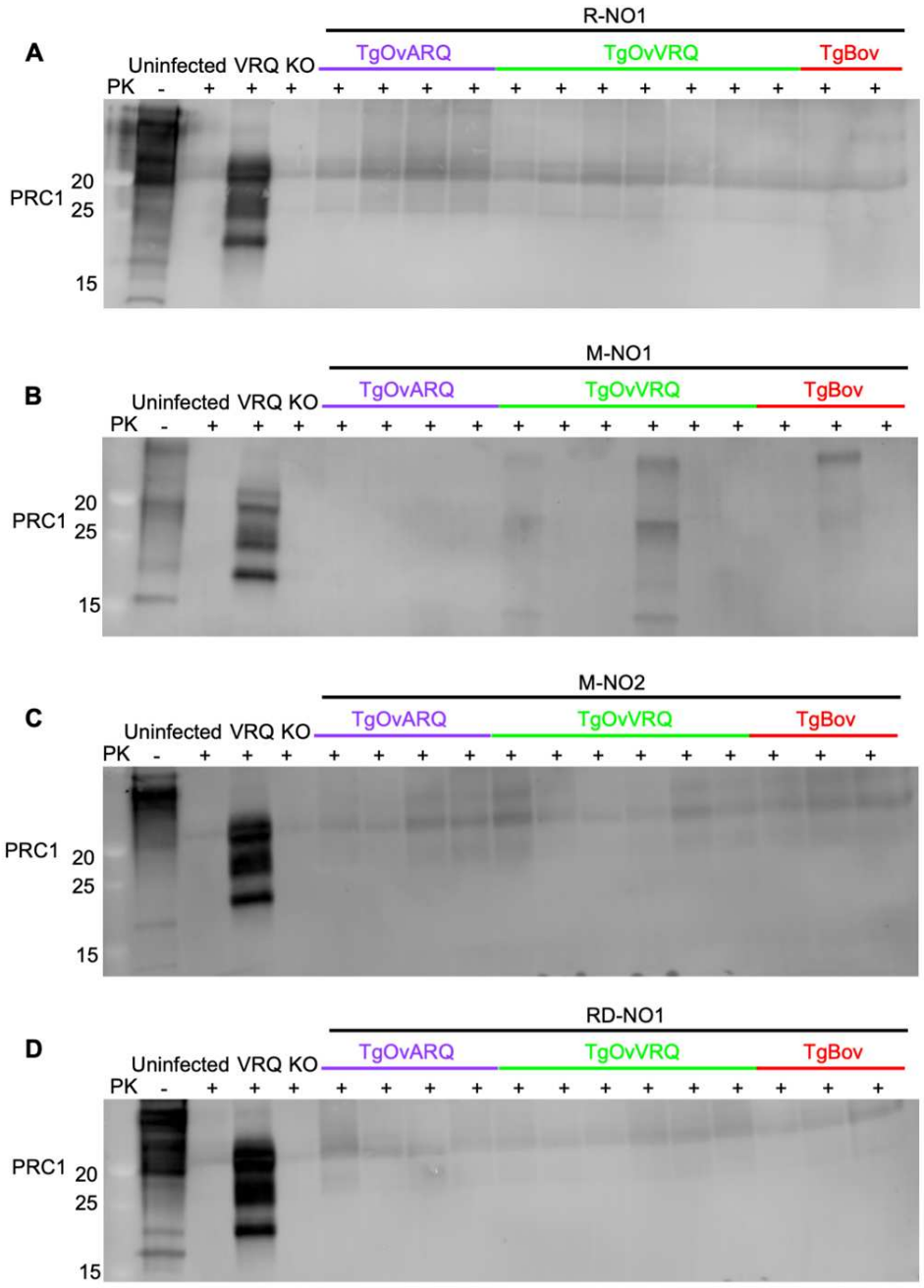

Figure 4.2 Western blots of transmissions of R-NO1, M-NO1, M-NO2, RD-NO1 to ovine-PrP and bovine-PrP mice. Immunoblots showing PK-resistant profiles of TgOvARQ, TgOvVRQ, and TgBov mice infected with (A) R-NO1 (B) M-NO1, (C) M-NO2, (D) RD-NO1. Uninfected brains were included for PK digestion control. VRQ represents a VRQ mouse infected with sheep scrapie. Samples were digested with 50 μg/ml of PK and ~55 μg of protein was loaded onto the gel. Blots were probed with mAb PRC1. Molecular weight markers are indicated to the left of blots.

at the end of the study were run on immunoblot to detect PrP^{Sc}. Western blots were probed with mAb PRC1, which is known to detect both ovine PrP and bovine PrP, rather than mAb PRC5 since its epitope detects the A136 allele but does not detect the V136 allele in ovine PrP (56). All iterations of transmission of R-NO1, M-NO1, M-NO2, and RD-NO1 to TgOvARQ, TgOvVRQ, and TgBov mice showed no PrP^{Sc} on western blot (Figure 4.2A, 4.2B, 4.2C, 4.2D). Signal seen in experimental conditions in Figure 4.2B is likely due to residual undigested PrP^{C}.

We also examined histoblots for evidence of PrP^{Sc} distributed in the brains of TgOvARQ, TgOvVRQ, and TgBov mice. When compared to an uninfected brain (Figure 4.3M), all transmissions of R-NO1, M-NO1, M-NO2, and RD-NO1 to TgOvARQ, TgOvVRQ, and TgBov

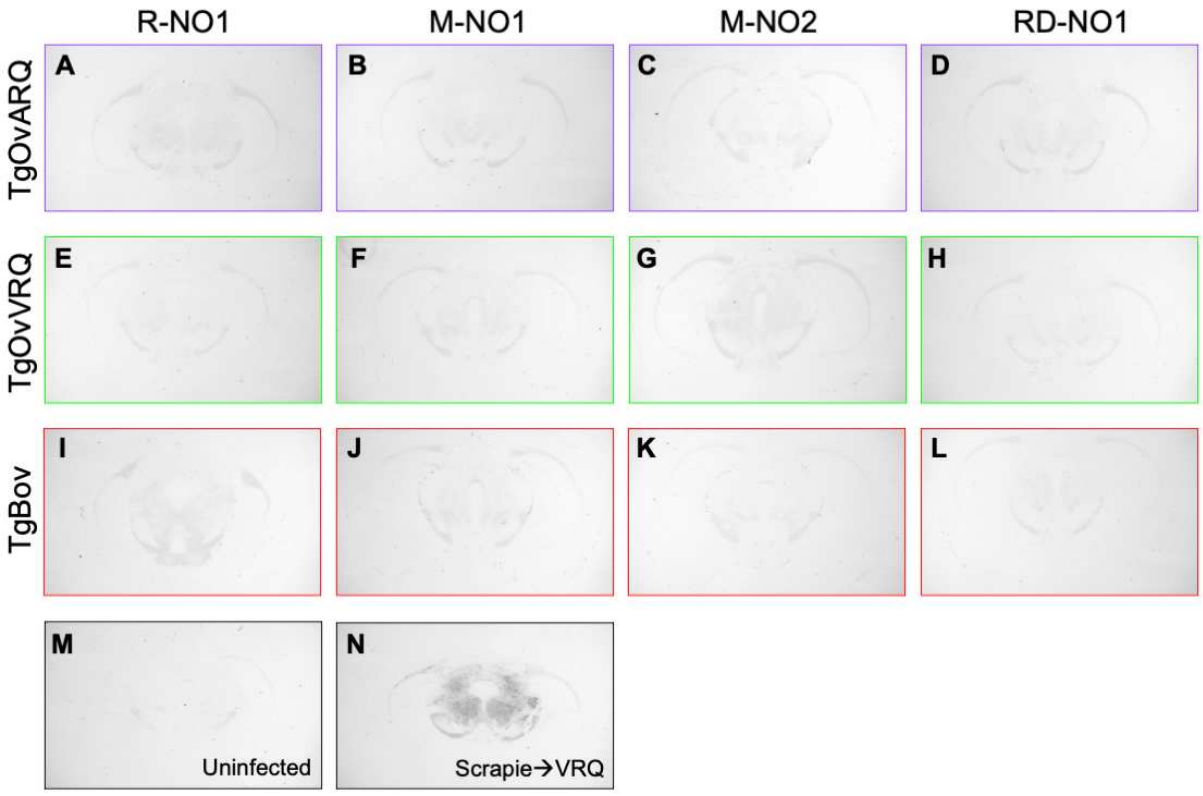

Figure 4.3 Histoblot staining of R-NO1, M-NO1, M-NO2, RD-NO1 to ovine-PrP and bovine-PrP mice. Histoblot analysis of PrP^{Sc} distribution in the midbrain of TgOvARQ mice infected with (A) R-NO1, (B) M-NO1, (C) M-NO2, (D) RD-NO1, TgOvVRQ mice infected with (E) R-NO1, (F) M-NO1, (G) M-NO2, (H) RD-NO1, TgBov mice infected with (I) R-NO1, (J) M-NO1, (K) M-NO2, (L) RD-NO1, (M) uninfected VRQ brain, (N) scrapie infected VRQ brain. Histoblots were probed with mAb PRC1.

mice had PrP^{Sc} signal slightly higher than the negative control in the midbrain section (Figure 4.3A - 4.3L). All other sections of the brain (septum, hippocampus, pons and cerebellum) all had higher signal than background but are not shown here. A positive control of a scrapie infected TgOvVRQ brain was included for reference as well, which has diffuse PrP^{Sc} distribution (Figure 4.3N). Faint staining in all transmission cases could indicate a small accumulation of PrP^{Sc} which is not sufficient to cause disease. In the future, PMCA will be used to determine whether there is any amplifiable PrP^{Sc} in brains of TgOvARQ, TgOvVRQ, and TgBov mice infected with Nordic isolates.

Gene-targeted cervid mice are susceptible to infection with sheep scrapie, but not other species' prion diseases

To parse the origin of CWD, we chose to inoculate our GtE226 and GtQ226 mice with prions from a variety of species. An advantage of the design of the gene-targeted (Gt) mice over the transgenic overexpressing mice is the ability of the Gt mice to propagate peripheral infection. Peripheral infection and propagation of prions in lymphoreticular system (LRS) tissue is specific to CWD and plays a role in dissemination of prions throughout a cervid (57). Peripheral inoculation of transgenic mice does not lead to accumulation of PrP^{Sc} in the CNS, but peripheral inoculation of the Gt mice does (49). Furthermore, PrP^{Sc} is detectable in peripheral tissue such as splenic tissue (49). As such, we intraperitoneally (IP) inoculated mice with TME, BSE and scrapie prions as the IP route is a more natural peripheral inoculation route than intracerebral inoculation.

We first IP inoculated GtE and GtQ mice with TME, both an uncloned strain and cloned strain. No clinical disease was noted in either GtE or GtQ mice (Figure 4.4A, Table 4.2). This is consistent with the poor transmission of CWD to mink only after intracerebral inoculation (30). Next, we tested the species barrier between cattle and cervids by inoculating classical BSE and

Table 4.2 Transmission of TME, BSE, and scrapie to GtQ and GtE mice. Survival times are reported as mean time to disease onset ± standard error of the mean (number of diagnosed mice/total number of mice).

Inoculum		Inoculation	GtQ	GtE
TME	Uncloned	IP	485-597 (0/8)	508-593 (0/9)
	Cloned	IP	580-593 (0/7)	507-591 (0/7)
BSE	Classical	IP	480-595 (0/8)	447-619 (0/9)
	L-type	IP	441-602 (0/7)	514-567 (0/8)
Scrapie	Classical	IC	322±38 (3/5)	353±26 (3/4)
		IP	261±3 (9/10)	403±33 (7/9)
Atypical Scrapie	Nor98-1	IP	489-587(0/8)	587-593 (0/6)
	Nor98-2	IP	464-593 (0/10)	510-582 (0/7)
	Nor98-3	IP	453-593 (0/9)	462-583 (0/8)

L-type BSE in the GtE and GtQ mice. Classical BSE is the strain of BSE characterized in the 1980s-90s which caused vCJD in humans (12). L-type BSE or bovine amyloidotic spongiform encephalopathy (BASE), is thought to be a sporadic form of BSE which has a distinct electrophoretic mobility and glycoform ratio compared to classical BSE. Not surprisingly, no transmission was noted in GtE or GtQ mice when inoculated with classical or L-type BSE (Figure 4.4B, Table 4.2). As classical BSE was first identified in the UK in the 1980s, and CWD was first identified in the 1960s in the US, it is unlikely that transmission of BSE resulted in CWD. L-type BSE has been hypothesized to be the cause of TME in the US, and thus this corroborates the lack of transmission of TME to Gt cervid-PrP mice as well (18).

Since there is evidence of transmission of scrapie to white-tailed deer via intracerebral inoculation, we first decided to intracerebrally inoculate mice with sheep scrapie strain SSBP/1 (58). SSBP/1 is not an individual field isolate, but rather originated as a homogenate of three natural scrapie brains that were subsequently passaged mostly through Cheviot sheep (45,46). Intracerebral inoculation of GtQ mice resulted in a time to disease onset of 322±38 DPI in 60% of mice inoculated (Figure 4.4C, Table 4.2). Intracerebral inoculation of GtE mice resulted in time to disease onset of 353±26 DPI in 75% of mice, not significantly different than inoculation to GtQ mice (ns, $p = 0.9449$) (Figure 4.4C, Table 4.2). To examine a peripheral route of

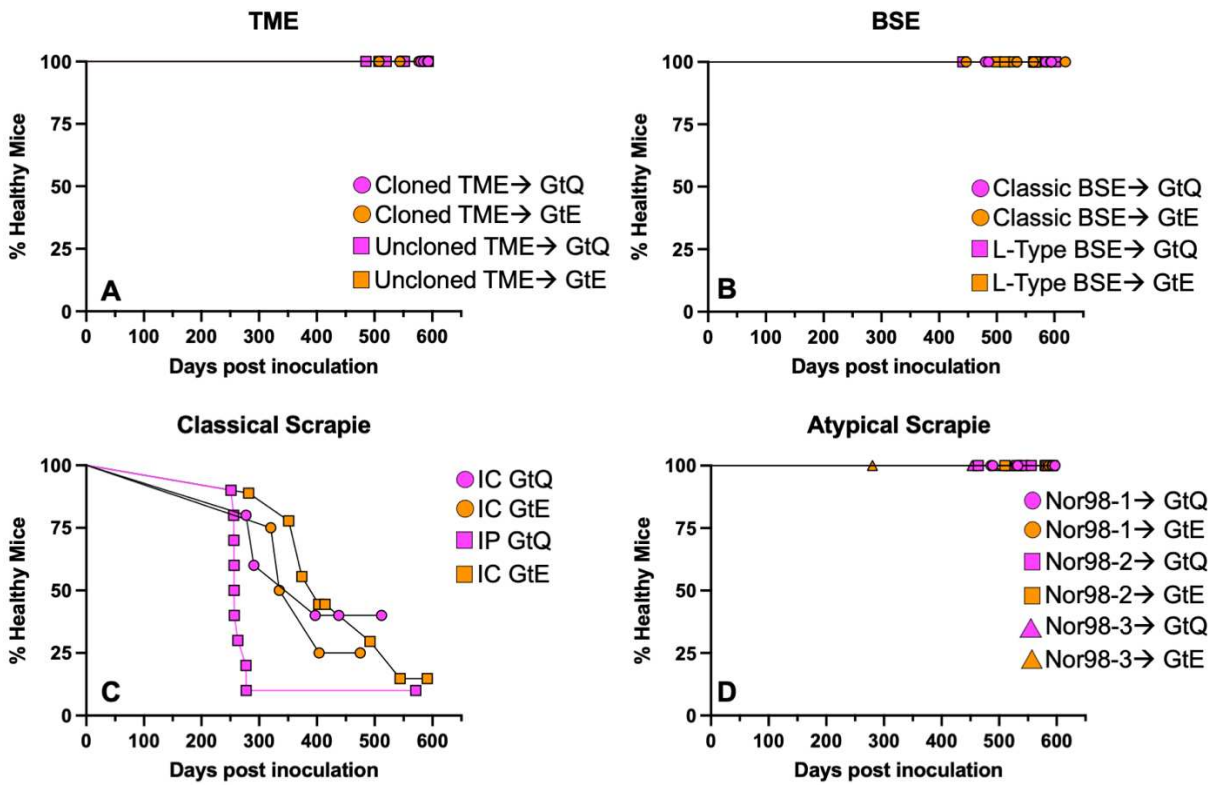

Figure 4.4 Transmission of TME, BSE and scrapie isolates to GtQ and GtE mice. Survival curves of GtQ (pink) and GtE (orange) mice resulting from IP inoculation (unless otherwise specified) with (A) TME (cloned = circles, uncloned = squares), (B) BSE (classical = circles, L-type = square), (C) classical scrapie (IC inoculation = circles, IP inoculation = squares), and (D) atypical scrapie (Nor98-1 = circles, Nor98-2 = squares, Nor98-3 = triangles).

transmission, we intraperitoneally inoculated GtQ and GtE mice with SSBP/1. Surprisingly, IP inoculation of GtQ mice resulted in disease in 90% of mice at an average of 261±3 DPI, 23% faster than IC inoculation (*p = 0.0330) (Figure 4.4C, Table 4.2). Higher efficiency with IP inoculation could be due to the importance of peripheral conversion of PrP^C in cervid species. However, IP inoculation of GtE mice at 403±33 DPI in 7/9 mice was not faster than IC inoculation of GtE mice (ns, p = 0.5049) (Figure 4.4C, Table 4.2). Via the intraperitoneal route, transmission was 54% faster in GtQ mice compared to GtE mice (*p = 0.0151) (Figure 4.4C, Table 4.2). This is intriguing given North American CWD strains cause more rapid disease in GtE mice over GtQ mice. Regardless of residue 226 tropism, classical sheep scrapie SSBP/1

transmits both IC and IP to cervid-PrP mice, indicating a weaker species barrier between classical scrapie and cervids.

Just as atypical strains of BSE exist and are likely of a spontaneous origin, atypical cases of scrapie have also been documented. Atypical scrapie was first described in Norway in 1998 and was thus coined the Nor98 strain (59). Since, atypical scrapie cases have been identified all over the world. The proximity of the discovery of Nor98 atypical scrapie to the new cases of CWD in Norwegian cervids led us to IP inoculate 3 different Nor98 isolates into GtQ and GtE mice. No clinical disease was noted from the transmission of Nor98-1, Nor98-2 or Nor98-3 into either the GtQ or GtE mice (Figure 4.4D, Table 4.2).

In order to check cervid-PrP mice for subclinical infection, we examined all brains via western blotting, histoblotting and/or IHC. All available brains from mice terminated at the end of the study were run on immunoblot to detect PrP^{Sc}. Transmission of either uncloned or cloned TME to either GtQ or GtE mice did not produce any PrP^{Sc} reactivity on western blot (Figure 4.5A, 4.5B). Similarly, both classical and L-type BSE failed to produce any PK-resistant PrP^{Sc} signal when inoculated in GtQ or GtE mice (Figure 4.5C, 4.5D). As IHC with imaging at high magnification can detect small amounts of infection, we checked for evidence of PrP^{Sc} in the GtQ and GtE mice inoculated with TME and BSE. Concurrent with western blot results, no convincing evidence was seen for transmission of uncloned and cloned TME or classical and L-type BSE to GtQ or GtE mice (Figure 4.6A-4.6G). In some micrographs, spongiosis can be seen (Figure 4.6A, 4.6D, 4.6F), but some spongiosis is typical of uninfected older mice and cannot be entirely attributed to prion disease. Therefore, we conclude that the species barrier is upheld to prevent transmission of TME or BSE to cervid-PrP mice.

We next examined the immunoblot profiles of scrapie infected GtQ and GtE mice and compared them to North American CWD transmitted to cervid-PrP mice. When transmitted to VRQ mice, SSBP/1 is not detectable with mAb PRC5 since part of the necessary PRC5 epitope is A136 (Figure 4.7A, 4.7B). The original isolate SSBP/1 is detectable with both mAb PRC5 and

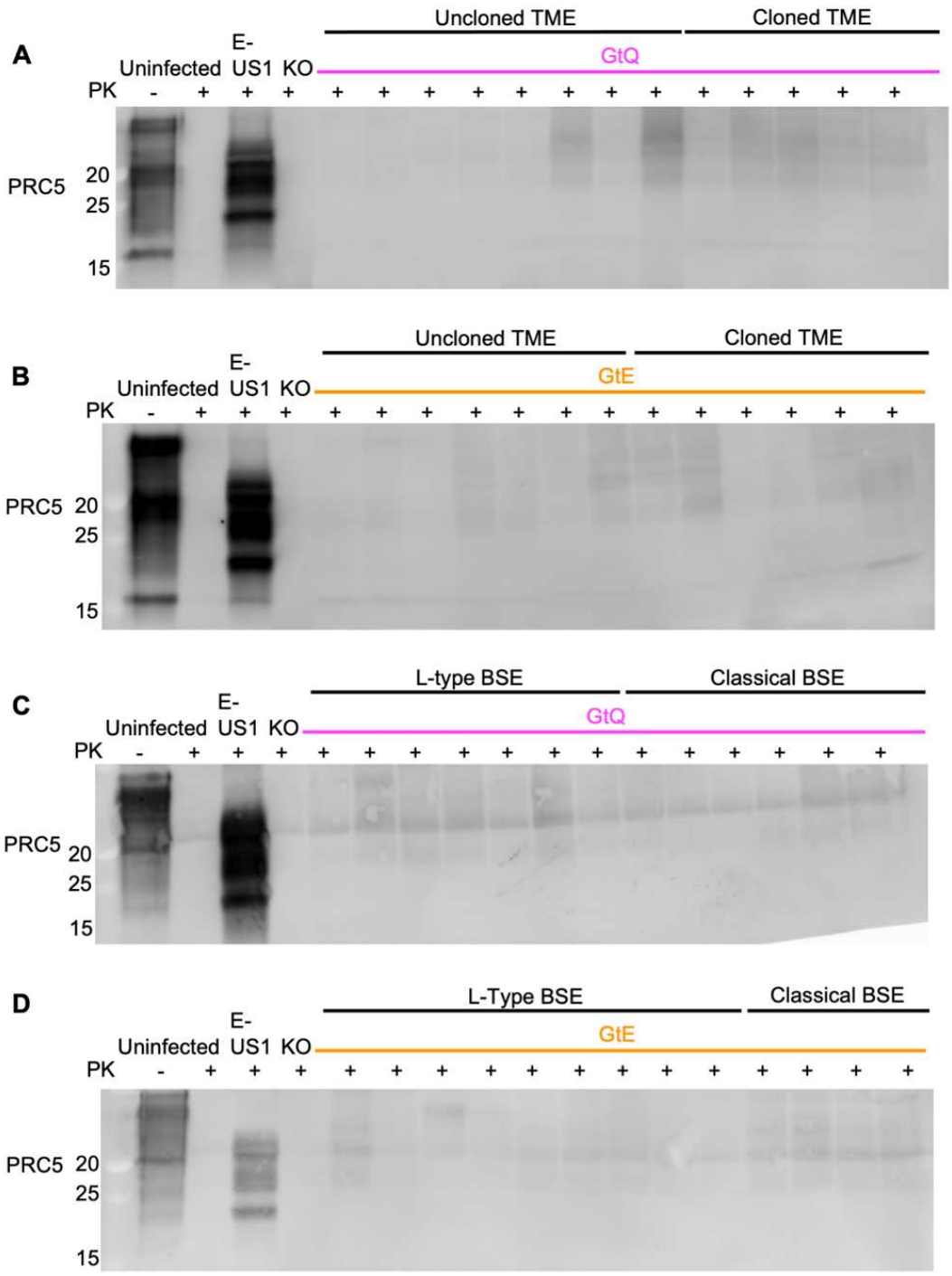

Figure 4.5 Western blots of transmissions of TME and BSE to GtQ and GtE mice. Immunoblots showing PK-resistant profiles of GtQ mice infected with (A) uncloned or cloned TME or (C) L-type BSE or classical BSE and GtE mice infected with (B) uncloned or cloned TME or (D) L-type BSE or classical BSE. Uninfected brains were included for PK digestion control. E-US1 represents a GtE mouse infected with elk CWD. Samples were digested with 50μg/ml of PK and ~55μg were loaded onto the gel. Blots were probed with mAb PRC5. Molecular weight markers are indicated to the left of blots.

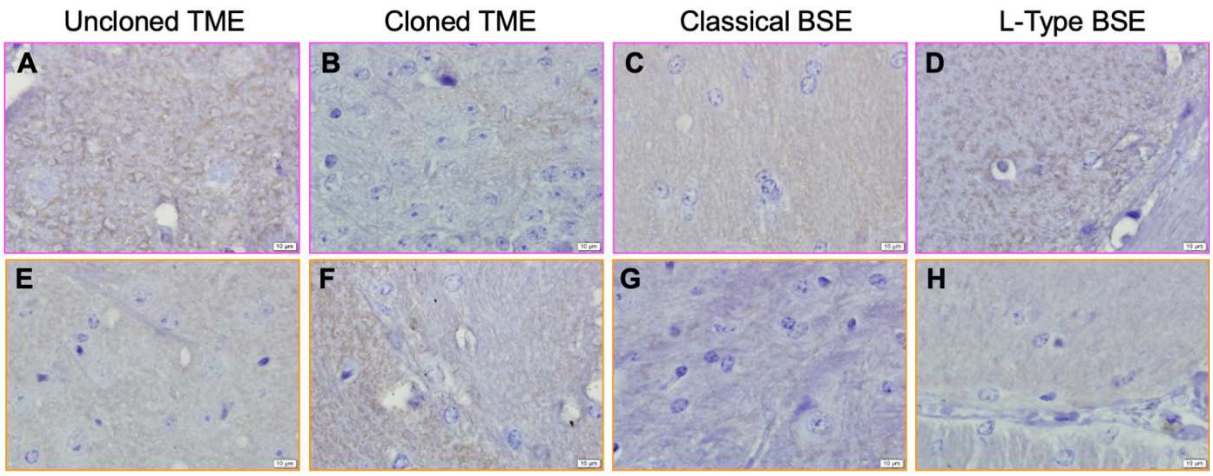

Figure 4.6 IHC staining of TME and BSE transmitted to GtE and GtQ mice. IHC analysis of PrP^{Sc} distribution in the hippocampus of GtQ mice infected with (A) uncloned TME, (B) cloned TME, (C) classical BSE, (D) L-Type BSE and GtE mice infected with (E) uncloned TME, (F) cloned TME, (G) classical BSE, (H) L-Type BSE. IHC sections were probed with Fab D18. Scale bar indicates 10 μm.

PRC1, likely lending to its origin of an amalgamation of multiple sheep scrapie isolates (Figure 4.7A, 4.7B). IP transmission to either GtQ or GtE mice and IC transmission to GtE mice results in PK-resistant PrP^{Sc} that is PRC5 reactive indicative of adaptation into the cervid-PrP mice (Figure 4.7A, 4.7B). To determine if and how PrP^{Sc} is affected by the A/V136 polymorphism, we performed histoblotting. Histoblot profiles of IP inoculated GtQ and GtE mice reveal more accumulation in the hindbrain as compared to forebrain areas (Figure 4.8A, 4.8B). This is in contrast with IC inoculated animals which show relatively equal amounts of PrP^{Sc} distribution throughout the brain (See chapter 2) (50). No drastic differences were noted between GtQ and GtE mice intraperitoneally inoculated with SSBP/1. In both cases, PrP^{Sc} accumulation was bilateral, diffuse, and preferential to the hindbrain sections (Figure 4.8A, 4.8B). Taken together, SSBP/1 sheep scrapie transmits to both GtQ and GtE mice, with no notable differences in immunoblot profile or PrP^{Sc} deposition. This is in opposition of transmission of North American CWD isolates to GtQ and GtE which was extensively discussed in Chapter 2 (49).

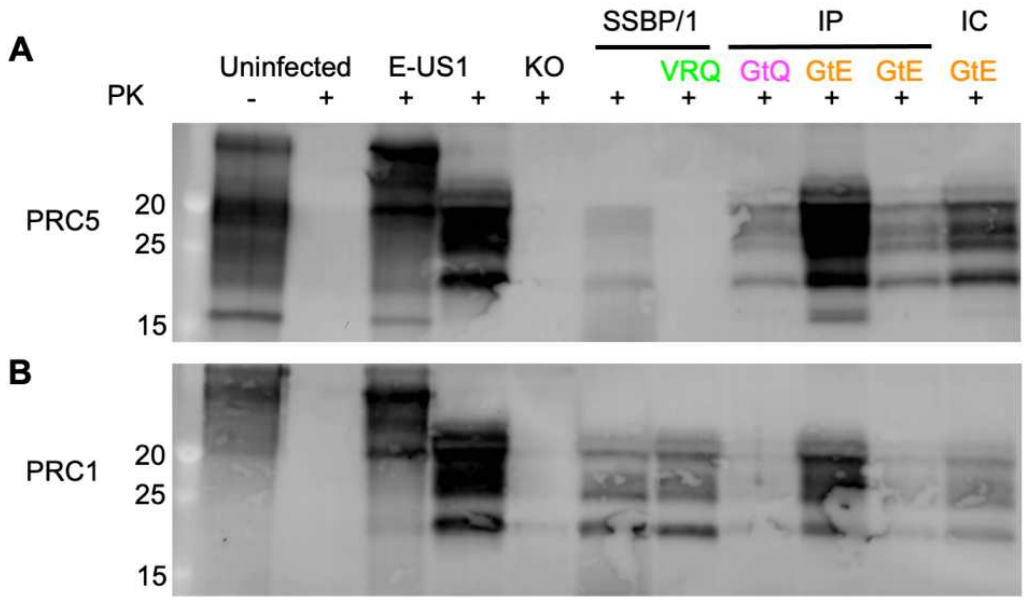

Figure 4.7 Western blots of transmissions of sheep scrapie SSBP/1 to GtQ and GtE mice. Immunoblots showing PK-resistant profiles of passages of SSBP/1 to VRQ, GtQ and GtE mice. (A) PRC5. (B) PRC1. Uninfected brains were included for PK digestion control. E-US1 represents a GtE mouse infected with elk CWD. Samples were digested with 50μg/ml of PK and ~55μg were loaded onto the gel. Molecular weight markers are indicated to the left of blots.

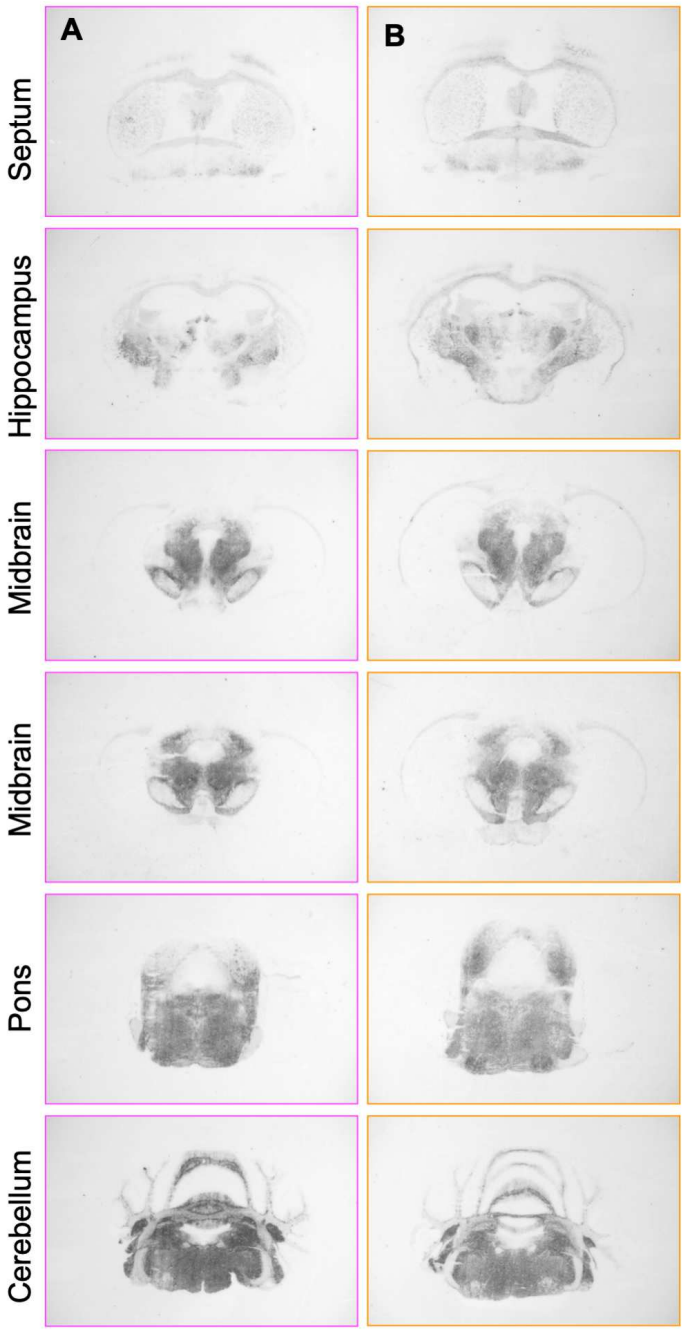

Figure 4.8 Histoblot staining of SSBP/1 sheep scrapie intraperitoneally transmitted to GtQ and GtE mice. Histoblot analysis of PrP^{Sc} distribution in the septum, hippocampus, midbrain, pons, and cerebellum of mice infected with SSBP/1 sheep scrapie. (A) GtQ mouse. (B) GtE mouse. Histoblots were probed with mAb PRC5.

Lastly, to check for any subclinical disease from transmission of 3 different atypical scrapie isolates to cervid-PrP mice, we performed either histoblotting or IHC on all terminal brains. Unsurprisingly, no convincing PK-resistant PrP^{Sc} signal was seen on histoblot for either GtQ or GtE mice inoculated with Nor98-1, Nor98-2, or Nor98-3 (Figure 4.9A, 4.9C, 4.9E, 4.9G, 4.9I, 4.9K). Accordingly, even at high magnification, no significant spongiosis or PrP^{Sc} was noted in any of the conditions (Figure 4.9B, 4.9D, 4.9F, 4.9H, 4.9J, 4.9L). The lack of transmission of Nor98 atypical scrapie, but efficient transmission of SSBP/1 classical scrapie could be due to strain differences between classical and atypical scrapie wherein classical scrapie is more optimal for converting cervid PrP^{Sc}. Overall, classical scrapie was the only non-cervid prion species that we tested to cause clinical disease and transmit to cervid-PrP mice.

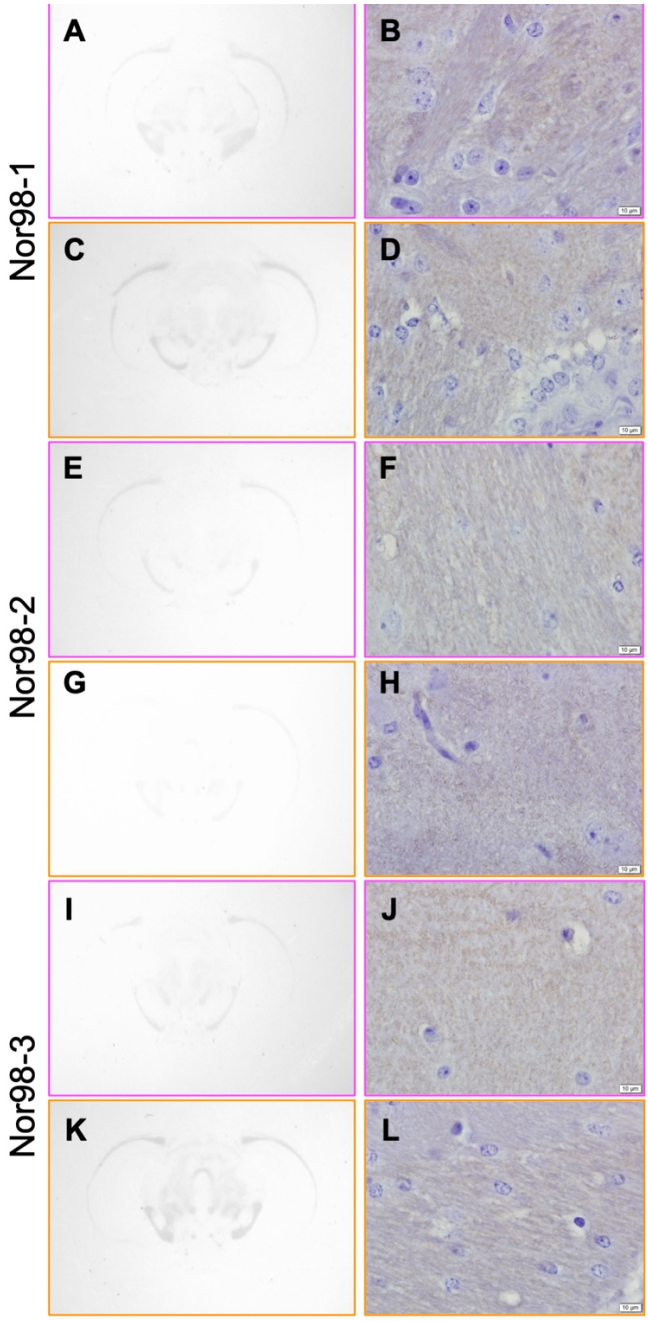

Figure 4.9 Histoblot and IHC staining in the midbrain of atypical sheep scrapie infected GtE and GtQ mice. Histoblot and IHC analysis of PrP^{Sc} distribution in the hippocampus of GtQ mice infected with (A, B) Nor98-1, (E, F) Nor98-2, (I, J) Nor98-3 and GtE mice infected with (C, D) Nor98-1, (G, H) Nor98-2, (K, L) Nor98-3. Histoblot sections were probed with PRC5. IHC sections were probed with Fab D18. (B, D, F, H, J, L) Scale bar indicates 10 μm.

Discussion

The unrelenting spread of CWD is concerning from ecological, economic and public health perspectives. As such, CWD is considered by many to be the most contagious of the animal prion diseases and spreads primarily through horizontal transmission. Direct horizontal transmission occurs from contact of two cervids (60) while indirect transmission occurs from contamination of the environment (61). Because shedding of CWD into the environment is so common, it is highly likely that other species which cohabitate in the same area are also exposed to CWD prions. We employed our transgenic and gene-targeted mice to test their susceptibility to cross species transmission of prions as a tool to estimate the probability of an interspecies transmission to be the origin of CWD and also to predict subsequent interspecies transmission of new Nordic CWD strains.

Novel Nordic CWD strains do not transmit to ovine-PrP and bovine-PrP mice

To address the latter, we employed transgenic overexpressing ovine-PrP and bovine-PrP mice to test livestock susceptibility to Norwegian CWD prions. Two separate ovine-PrP mouse lines were used: $A_{136}R_{154}Q_{171}$ (TgOvARQ) and $V_{136}R_{154}Q_{171}$ (TgOvVRQ) to simultaneously examine the effect of residue 136 of sheep PrP on susceptibility to cervid prions. We intracerebrally inoculated TgOvARQ, TgOvVRQ, and TgBov mice with a Norwegian reindeer CWD isolate (R-NO1), two Norwegian moose CWD isolates (M-NO1 and M-NO2) and a Norwegian red deer CWD isolate (RD-NO1). Inoculation of ovine-PrP and bovine-PrP mice with all of the Norwegian isolates did not result in any clinical disease (Figure 4.1A - 4.1D, Table 4.1). Confirmatory analysis with western blotting revealed no PK-resistant PrP^{Sc} in any mouse line inoculated with any Norwegian CWD isolate (Figure 4.2). Accordingly, while above background levels, minimal PrP^{Sc} was detected via histoblotting (Figure 4.3). Despite the lack of clinical disease and transmission, this does not mean the species barrier for CWD is absolute. It has been shown that iterative passage is required to induce efficient transmission in the context

of interspecies transmission. For example, primary passage of mule deer CWD via the IC route resulted in disease in 2/8 Suffolk sheep (27). Secondarily transmitting the brain of one of the two clinically sick sheep originally infected with mule deer CWD then resulted in a 100% attack rate (12/12) in Suffolk sheep(62). As such, serial passaging of TgOvARQ, TgOvVRQ and TgBov infected with Norwegian CWD isolates may result in clinical disease. Alternatively, we first could use PMCA to amplify PrP^{Sc} in the original Norwegian cervid isolates, then inoculate ovine-PrP and bovine-PrP mice with the PMCA product. Transmission of Norwegian cervid isolates has generally been inefficient with long incubation times on primary passage to Gt cervid-PrP mice (Chapter 3) (63), alluding to the low amount of PrP^{Sc} present in the original samples.

BSE, TME and atypical scrapie do not cause disease in cervid-PrP mice

To further examine the species barrier surrounding cervids and spread of CWD, we employed Gt cervid-PrP mice and probed their susceptibility to prions from other animal species. Both an uncloned and cloned strain of TME failed to cause clinical or subclinical disease in GtQ226 or GtE226 mice (Figure 4.4A, 4.5A, 4.5B, 4.6A, 4.6B, 4.6E, 4.6F). TME in mink has only been documented on mink farms, in outbreaks resulting from the feed of L-type BSE contaminated “downer” cow material. As TME is resultant from a foodborne contamination event, TME is not particularly contagious between mink and infection is not sustained in a population without constant feed of contaminated material (64,65). Temporally, TME was documented in the US around the same time we predict the CWD epidemic to have begun, yet the containment to farms and low contagiousness of TME does not point to the origin of CWD.

We also observed unsuccessful transmission and lack of detection of PrP^{Sc} with classical BSE and L-type BSE transmitted to GtQ and GtE mice (Figure 4.4B, 4.5C, 4.5D, 4.6C, 4.6D, 4.6G, 4.6H). Like TME, Classical BSE originated in the UK from feed of prion contaminated material. As such, classical BSE is not highly contagious among cattle, and was virtually eradicated once feed of contaminated material was stopped. However, classical BSE

has been shown to cause disease in humans causing variant CJD. Additionally, BSE can transmit to exotic ungulates causing exotic ungulate encephalopathy (EUE) and felines causing feline spongiform encephalopathy (FSE) (16,66). L-type BSE has been causally linked to the origin of TME (18). While it seems BSE can cause disease in a variety of species, cervids are not one of them.

Along the same lines as TME and BSE, Nor98 atypical scrapie did not cause any disease in the GtQ and GtE mice (Figure 4.4D, 4.9). We transmitted 3 individual isolates of Nor98 scrapie from Norway but no evidence of PrP^{Sc} was found with transmission of any isolate to either GtQ or GtE mice. As Nor98 atypical scrapie is thought to arise from spontaneous misfolding of PrP^{C} to PrP^{Sc}, Nor98 is not contagious like classical scrapie (59). Nevertheless, overlap in geographical region of Nor98 cases and novel CWD cases in reindeer, moose and red deer bring into question, the potential for Nor98 to adapt to cervids. Based on our lack of transmission to the GtQ and GtE mice however, it does not appear that Nor98 is the origin of CWD in Europe.

A classical sheep scrapie isolate causes prion disease in Gt cervid-PrP mice

White-tailed deer have been previously shown to be susceptible to intracerebral inoculation with sheep scrapie (58). To further characterize transmission of classical sheep scrapie to cervid-PrP animals, we both intracerebrally and intraperitoneally inoculated GtQ and GtE mice with sheep scrapie SSBP/1, a well characterized strain. Surprisingly, in GtQ mice, IP inoculation as compared to IC inoculation led to a better attack rate and faster time to disease onset (Figure 4.4C). No difference was noted in the GtE mice. On the whole, transmission to the GtQ mice was more efficient than transmission to GtE mice (Figure 4.4C). Transmission of North American CWD isolates to the GtQ and GtE mice leads to more efficient disease in the GtE background, opposite of the transmission of SSBP/1 (49). When compared via histoblotting, GtE and GtQ brains infected with SSBP/1 show a fairly similar distribution of PrP^{Sc} with more

PrP^{Sc} accumulating in the hindbrain rather than the forebrain (Figure 4.8). We have previously shown this is due to the route of inoculation (IP vs IC). When an animal is IP inoculated, prions must migrate retroactively to the brain, likely through the enteric nervous system meaning the first deposition of PrP^{Sc} is found in the hindbrain (67). With IC inoculation into the right parietal lobe, PrP^{Sc} seems to diffuse outward from the initial site of inoculation, leading to more forebrain PrP^{Sc}.

A caveat to using SSBP/1 as a model for classical scrapie, is its optimization and adaptation as a lab strain. If sheep scrapie crossed species barriers in the wild to a cervid, it is likely just one event occurred. SSBP/1 was derived from an amalgam of diseased sheep brains from the UK and was serially passaged to increase titer, and therefore no longer acts as a natural isolate. Our lab has obtained natural sheep scrapie isolates from Colorado flocks of sheep. To represent the original interspecies event more accurately, we plan to inoculate GtQ and GtE mice with natural Colorado sheep scrapie isolates, since CWD was first discovered in Colorado.

Taken together, we show that classical sheep scrapie has the potential to transmit to cervid-PrP mice. We also show that there is a strong species barrier between cervids, cattle and mink. However, as new strains of CWD are emerging in Europe, prudent surveillance of animal populations overlapping with the wild cervid populations is necessary to prevent further spread of prion diseases in the wild. Additionally, considerations for human health should be taken. Currently, no transmission to humans has been proven, and transgenic humanized mice have been shown to be resistant to infection with CWD prions for Norwegian reindeer and moose (41). However, this study used transgenic mice which were intracerebrally inoculated. As CWD is a lymphotropic disease, we cannot rule out the possibility that the lack of transmission in humanized mice is resultant from the lack of lymphotropic accumulation in transgenic mice. As such, our lab recently designed gene-targeted human-PrP mice created in the same fashion as

the gene-targeted cervid-PrP mice. With these mice, we hope to recapitulate all aspects of disease transmission, and further characterize the risk CWD poses to humans.

REFERENCES

1. Williams ES. Review article - Chronic Wasting Disease. Vet Pathol. 2005;42(5):530–49.
2. Collinge J. Prion diseases of humans and animals: Their causes and molecular basis. Vol. 24, Annual Review of Neuroscience. 2001. p. 519–50.
3. Williams ES, Young S. Spongiform encephalopathies in Cervidae. Revue Scientifique et Technique. 1992;11(2):551–67.
4. Green R, Horrocks C, Wilkinson A, Hawkins SAC, Ryder SJ. Primary isolation of the bovine spongiform encephalopathy agent in mice: Agent definition based on a review of 150 transmissions. J Comp Pathol. 2005;132(2–3):117–31.
5. Acín C, Bolea R, Monzón M, Monleón E, Moreno B, Filali H, et al. Classical and atypical scrapie in sheep and goats: Review on the etiology, genetic factors, pathogenesis, diagnosis, and control measures of both diseases. Vol. 11, Animals. 2021. p. 691.
6. Mathiason CK. Scrapie, CWD, and Transmissible Mink Encephalopathy. In: Progress in Molecular Biology and Translational Science. 2017. p. 267–92.
7. Hartsough GR, Burger D. Encephalopathy of mink. I. Epizootiologic and clinical observations. J Infect Dis [Internet]. 1965;115(4):387–92. Available from: https://www.ncbi.nlm.nih.gov/pubmed/5891240
8. Marsh RF, Hadlow WJ. Transmissible mink encephalopathy. Vol. 11, Revue scientifique et technique (International Office of Epizootics). 1992. p. 539–50.
9. Hartung J, Zimmermann H, Johannsen H. Infektiose Enzephalopathie beim Nerz 1. Mitteilung: Klinisch-eqizootiologische and experimentelle Untersuchungen. Monatsh Veterinari-med. 1970;25:385–8.
10. Dukur II, Geller VI, Chizhov VA, Roĭkhel' VM, Pogodina V v. [Clinico-morphological study of transmissible encephalopathy of mink]. Vopr Virusol. 1986;31(2):220–5.
11. Gorham JR. Viral and bacterial diseases of mink in Soviet Union. Fur Rancher. 1991;71:10–1.

12. Hill AF, Desbruslais M, Joiner S, Sidle KCL, Gowland I, Collinge J, et al. The same prion strain causes vCJD and BSE. Vol. 389, Nature. 1997. p. 448–50.
13. Huor A, Espinosa JC, Vidal E, Cassard H, Douet JY, Lugan S, et al. The emergence of classical BSE from atypical/Nor98 scrapie. Proc Natl Acad Sci U S A. 2019;116(52):26853–62.
14. Bovine spongiform encephalopathy: “Mad cow disease.” Vol. 54, Nutrition Reviews. 1996. p. 208–10.
15. Wilesmith JW, Ryan JB, Atkinson MJ. Bovine spongiform encephalopathy: epidemiological studies on the origin. Vet Rec. 1991;128(9):199–203.
16. Pearson GR, Wyatt JM, Gruffydd-Jones TJ, Hope J, Chong A, Higgins RJ, et al. Feline spongiform encephalopathy: fibril and PrP studies. Vet Rec. 1992;131(14):307–10.
17. Cullingham CI, Peery RM, Dao A, McKenzie DI, Coltman DW. Predicting the spread-risk potential of chronic wasting disease to sympatric ungulate species. Prion. 2020;14(1):56–66.
18. Baron T, Bencsik A, Biacabe AG, Morignat E, Bessen RA. Phenotypic similarity of transmissible mink encephalopathy in cattle and L-type bovine spongiform encephalopathy in a mouse model. Emerg Infect Dis. 2007;13(12):1887–94.
19. Casalone C, Zanusso G, Acutis P, Ferrari S, Capucci L, Tagliavini F, et al. Identification of a second bovine amyloidotic spongiform encephalopathy: Molecular similarities with sporadic Creutzfeldt-Jakob disease. Proc Natl Acad Sci U S A. 2004;101(9):3065–70.
20. Padilla D, Béringue V, Espinosa JC, Andreoletti O, Jaumain E, Reine F, et al. Sheep and goat BSE propagate more efficiently than cattle BSE in human PrP transgenic mice. PLoS Pathog. 2011;7(3):e1001319.
21. Plinston C, Hart P, Chong A, Hunter N, Foster J, Piccardo P, et al. Increased Susceptibility of Human-PrP Transgenic Mice to Bovine Spongiform Encephalopathy Infection following Passage in Sheep. J Virol. 2011;85(3):1174–81.

22. Hamir AN, Kehrli ME, Kunkle RA, Greenlee JJ, Nicholson EM, Richt JA, et al. Experimental interspecies transmission studies of the transmissible spongiform encephalopathies to cattle: Comparison to bovine spongiform encephalopathy in cattle. Journal of Veterinary Diagnostic Investigation. 2011;23(3):407–20.
23. Hamir AN, Kunkle RA, Cutlip RC, Miller JM, O'Rourke KI, Williams ES, et al. Experimental transmission of chronic wasting disease agent from mule deer to cattle by the intracerebral route. Journal of Veterinary Diagnostic Investigation. 2005;17(3):276–81.
24. Hamir AN, Miller JM, Kunkle RA, Hall SM, Richt JA. Susceptibility of cattle to first-passage intracerebral inoculation with chronic wasting disease agent from white-tailed deer. Vet Pathol. 2007;44(4):487–93.
25. Greenlee JJ, Nicholson EM, Smith JD, Kunkle RA, Hamir AN. Susceptibility of cattle to the agent of chronic wasting disease from elk after intracranial inoculation. Journal of Veterinary Diagnostic Investigation. 2012;24(6):1087–93.
26. Williams ES, O'Toole D, Miller MW, Kreeger TJ, Jewell JE. Cattle (Bos taurus) resist chronic wasting disease following oral inoculation challenge or ten years' natural exposure in contaminated environments. J Wildl Dis. 2018;54(3):460–70.
27. Hamir AN, Kunkle RA, Cutlip RC, Miller JM, Williams ES, Richt JA. Transmission of chronic wasting disease of mule deer to Suffolk sheep following intracerebral inoculation. Journal of Veterinary Diagnostic Investigation. 2006;18(6):558–65.
28. Cassmann ED, Jo Moore S, Greenlee JJ. Experimental oronasal transmission of chronic wasting disease agent from white-tailed deer to Suffolk sheep. Emerg Infect Dis. 2021;27(12):3156–8.
29. Heisey DM, Mickelsen NA, Schneider JR, Johnson CJ, Johnson CJ, Langenberg JA, et al. Chronic Wasting Disease (CWD) Susceptibility of Several North American Rodents That Are Sympatric with Cervid CWD Epidemics. J Virol. 2010;84(1):210–5.

30. Harrington RD, Baszler T v., O'Rourke KI, Schneider DA, Spraker TR, Liggitt HD, et al. A species barrier limits transmission of chronic wasting disease to mink (Mustela vison). Journal of General Virology. 2008;89(4):1086–96.

31. Mathiason CK, Nalls A v., Seelig DM, Kraft SL, Carnes K, Anderson KR, et al. Susceptibility of Domestic Cats to Chronic Wasting Disease. J Virol. 2013;87(4):1947–56.

32. Nichols TA, Fischer JW, Spraker TR, Kong Q, VerCauteren KC. CWD prions remain infectious after passage through the digestive system of coyotes (Canis latrans). Prion. 2015;9(5):367–75.

33. VerCauteren KC, Pilon JL, Nash PB, Phillips GE, Fischer JW. Prion Remains Infectious after Passage through Digestive System of American Crows (Corvus brachyrhynchos). PLoS One. 2012;7(10):45774.

34. Pritzkow S, Morales R, Camacho M, Soto C. Uptake, retention, and excretion of infectious prions by experimentally exposed earthworms. Emerg Infect Dis. 2021;27(12):3151–4.

35. Moore SJ, Smith JD, Richt JA, Greenlee JJ. Raccoons accumulate PrPSc after intracranial inoculation of the agents of chronic wasting disease or transmissible mink encephalopathy but not atypical scrapie. J Vet Diagn Invest. 2019 Mar;31(2):200–9.

36. Baune C, Wolfe LL, Schott KC, Griffin KA, Hughson AG, Miller MW, et al. Reduction of Chronic Wasting Disease Prion Seeding Activity following Digestion by Mountain Lions. mSphere. 2021;6(6):0081221.

37. MaWhinney S, Pape WJ, Forster JE, Anderson CA, Bosque P, Miller MW. Human prion disease and relative risk associated with chronic wasting disease. Emerg Infect Dis. 2006;12(10):1527–35.

38. Waddell L, Greig J, Mascarenhas M, Otten A, Corrin T, Hierlihy K. Current evidence on the transmissibility of chronic wasting disease prions to humans—A systematic review. Vol. 65, Transboundary and Emerging Diseases. 2018. p. 37–49.

39. Marsh RF, Kincaid AE, Bessen RA, Bartz JC. Interspecies Transmission of Chronic Wasting Disease Prions to Squirrel Monkeys (Saimiri sciureus) . J Virol. 2005;79(21):13794–6.

40. Race B, Meade-White KD, Miller MW, Barbian KD, Rubenstein R, LaFauci G, et al. Susceptibilities of nonhuman primates to chronic wasting disease. Emerg Infect Dis. 2009;15(9):1366–76.

41. Wadsworth JDF, Joiner S, Linehan JM, Jack K, Al-Doujaily H, Costa H, et al. Humanized Transgenic Mice Are Resistant to Chronic Wasting Disease Prions From Norwegian Reindeer and Moose. J Infect Dis. 2021;jiab033.

42. Miller MW, Williams ES, McCarty CW, Spraker TR, Kreeger TJ, Larsen CT, et al. Epizootiology of chronic wasting disease in free-ranging cervids in Colorado and Wyoming. J Wildl Dis. 2000;36(4):676–90.

43. Pirisinu L, Tran L, Chiappini B, Vanni I, di Bari MA, Vaccari G, et al. Novel type of chronic wasting disease detected in moose (Alces alces), Norway. Emerg Infect Dis. 2018;2210–8.

44. Vikøren T, Våge J, Madslien KI, Røed KH, Rolandsen CM, Tran L, et al. First detection of chronic wasting disease in a wild red deer (Cervus elaphus) in Europe. J Wildl Dis. 2019;55(4):970–2.

45. Onodera T, Sakudo A, Wu G, Saeki K. Bovine spongiform encephalopathy in Japan: History and recent studies on oxidative stress in prion diseases. Vol. 50, Microbiology and Immunology. 2006. p. 565–78.

46. Houston EF, Halliday SI, Jeffrey M, Goldmann W, Hunter N. New Zealand sheep with scrapie-susceptible PrP genotypes succumb to experimental challenge with a sheep-passaged scrapie isolate (SSBP/1). Journal of General Virology. 2002;83(5):1247–50.

47. Browning SR, Mason GL, Seward T, Green M, Eliason GAJ, Mathiason C, et al. Transmission of Prions from Mule Deer and Elk with Chronic Wasting Disease to Transgenic Mice Expressing Cervid PrP. J Virol. 2004;78(23):13345–50.

48. Angers RC, Seward TS, Napier D, Green M, Hoover E, Spraker T, et al. Chronic wasting disease prions in eik antler velvet. Emerg Infect Dis. 2009;15(5):696–703.

49. Bian J, Christiansen JR, Moreno JA, Kane SJ, Khaychuk V, Gallegos J, et al. Primary structural differences at residue 226 of deer and elk PrP dictate selection of distinct CWD prion strains in gene-targeted mice. Proc Natl Acad Sci U S A. 2019;12478–87.

50. Saijo E, Kang HE, Bian J, Bowling KG, Browning S, Kim S, et al. Epigenetic Dominance of Prion Conformers. PLoS Pathog. 2013;9(10):e1003692.

51. Taraboulos A, Jendroska K, Serban D, Yang SL, Dearmond SJ, Prusiner SB. Regional mapping of prion proteins in brain. Proc Natl Acad Sci U S A. 1992;89(16):7620–4.

52. Muramoto T, DeArmond SJ, Scott M, Telling GC, Cohen FE, Prusiner SB. Heritable disorder resembling neuronal storage disease in mice expressing prion protein with deletion of an α-helix. Nat Med. 1997;3(7):750–5.

53. Hunter N, Goldmann W, Foster JD, Cairns D, Smith G. Natural scrapie and PrP genotype: Case-control studies in British sheep. Veterinary Record. 1997;141(6):137–40.

54. Goldmann W, Hunter N, Foster JD, Salbaum JM, Beyreuther K, Hope J. Two alleles of a neural protein gene linked to scrapie in sheep. Proc Natl Acad Sci U S A. 1990;87(7):2476–80.

55. Hunter N, Foster JD, Benson G, Hope J. Restriction fragment length polymorphisms of the scrapie-associated fibril protein (PrP) gene and their association with susceptibility to natural scrapie in British sheep. Journal of General Virology. 1991;72(6):1287–92.

56. Kang HE, Weng CC, Saijo E, Saylor V, Bian J, Kim S, et al. Characterization of conformation-dependent prion protein epitopes. Journal of Biological Chemistry. 2012;287(44):37219–32.

57. Davenport KA, Christiansen JR, Bian J, Young M, Gallegos J, Kim S, et al. Comparative analysis of prions in nervous and lymphoid tissues of chronic wasting disease-infected cervids. Journal of General Virology. 2018;99(5):752–8.

58. Greenlee JJ, Smith JD, Kunkle RA. White-tailed deer are susceptible to the agent of sheep scrapie by intracerebral inoculation. Vet Res. 2011;42(1):107.

59. Benestad SL, Sarradin P, Thu B, Schönheit J, Tranulis MA, Bratberg B. Cases of scrapie with unusual features in Norway and designation of a new type, Nor98. Veterinary Record. 2003;153(7):202–8.

60. Miller MW, Williams ES. Horizontal prion transmission in mule deer. Nature. 2003;425(6953):35–6.

61. Miller MW, Williams ES, Hobbs NT, Wolfe LL. Environmental sources of prion transmission in mule deer. Emerg Infect Dis. 2004;10(6):1003–6.

62. Cassmann ED, Frese RD, Greenlee JJ. Second passage of chronic wasting disease of mule deer to sheep by intracranial inoculation compared to classical scrapie. Journal of Veterinary Diagnostic Investigation. 2021;33(4):711–20.

63. Bian J, Kim S, Kane SJ, Crowell J, Sun JL, Christiansen J, et al. Adaptive selection of a prion strain conformer corresponding to established North American CWD during propagation of novel emergent Norwegian strains in mice expressing elk or deer prion protein. PLoS Pathog. 2021;17(7):1009748.

64. Hanson RP, Eckroade RJ, Marsh RF, Zu Rhein GM, Kanitz CL, Gustafson DP. Susceptibility of mink to sheep scrapie. Science (1979). 1971;172(3985):859–61.

65. Hadlow WJ, Race RE, Kennedy RC. Temporal distribution of transmissible mink encephalopathy virus in mink inoculated subcutaneously. J Virol. 1987;61(10):3235–40.

66. Kirkwood JK, Cunningham AA, Wells GA, Wilesmith JW, Barnett JE. Spongiform encephalopathy in a herd of greater kudu (Tragelaphus strepsiceros): epidemiological observations. Vet Rec. 1993;133(15):360–4.

67. Natale G, Ferrucci M, Lazzeri G, Paparelli A, Fornai F. Transmission of prions within the gut and toward the central nervous system. Vol. 5, Prion. 2011. p. 142–9.

OVERALL SUMMARY

The extraordinary biology of prions and their propensity to persist has long vexed scientists. This is best reflected in the presentation of three Nobel prizes in the span of 26 years for strides made in the prion biology field. Given to Carl Gadjusek, the 1976 Nobel prize in Physiology or Medicine recognized Dr. Gadjusek's work on the documentation of Kuru. At the time, sheep scrapie, transmissible mink encephalopathy (TME), and Creutzfeldt-Jakob disease (CJD) had all been identified, yet no unifying cause had been identified. Gadjusek showed the infectious transmissibility of Kuru to chimpanzees by intracerebral inoculation of Kuru infected human brains, underscoring the neurological constituents of the scrapie agent. At the time, the assumption was the agent was a slow-acting virus.

21 years later in 1997, Dr. Stanley Prusiner was awarded the Nobel prize in Physiology and Medicine for identifying a proteinaceous component in the scrapie origin. All of these neurodegenerative diseases were linked by the term 'prion' to denote a small proteinaceous infectious particle. In the early years of the prion, work by the Prusiner lab and others identified the causative agent and recognized the importance of the prion protein (PrP) in the propagation of prion diseases.

Just 5 years later in 2002, Kurt Wuthrich was awarded the Nobel prize in Chemistry for his development of nuclear magnetic resonance (NMR) spectroscopy techniques to determine the 3-D structure of biological macromolecules in solution. This included solving the structure of the cellular prion protein (PrP^{C}). The infectious prion protein (PrP^{Sc}) is refractory to techniques such as NMR spectroscopy because of its insoluble, aggregated nature. However, recent advances in cryogenic-EM (cryo-EM), have allowed multiple groups to obtain the structure of ex-vivo infectious prions in just the last year. It is predicted that forthcoming structural prion studies in the next few years will inform the field of fundamental questions that have existed since the coining of prion.

The data in this enclosed body of work largely lends to the characterization of multiple facets of chronic wasting disease (CWD) prions. An escalating epidemic of cervids such as deer, elk and moose, CWD poses a threat to not only animal health, but also human health. Our lab uses moues models to study prion diseases and have recently designed gene-targeted cervid mice which express endogenous levels of cervid-PrP and can recapitulate CWD pathogenesis in a mouse model. In chapter 2, we extensively describe the effect of a polymorphism at residue 226 of cervid-PrP on pathogenesis. Deer, moose and reindeer express glutamine (Q) at residue 226 while elk express glutamate (E). As such we have designed two separate gene-targeted cervid-PrP mouse lines: one expressing Q at 226 (GtQ) and one expressing E at 226 (GtE). When inoculated with North American CWD prions, regardless of the host genotype, GtE mice succumb to disease at a faster rate than GtQ mice. As such, we conducted a longitudinal study to assess the disease course in GtE and GtQ mice. We found that PrP^{Sc} accumulates at a slower rate in GtQ mice compared to GtE mice. Further, we show that the initial deposition of PrP^{Sc} in GtQ and GtE mice is analogous, but somewhere during disease course, hosts expressing Q226 dictate a final PrP^{Sc} distribution of large, unorganized amalgamations of PrP^{Sc}, whereas conversion of E226 cervid-PrP leads to diffuse symmetrical PrP^{Sc} distribution. Residue 226 of cervid-PrP has a profound effect on disease pathogenesis and may have a bearing on not only the susceptibility of various cervid species to CWD, but also the CWD strains propagated in the wild.

In chapter 3, we use our GtQ and GtE mice to characterize newly emergent strains of CWD from Nordic countries. CWD was first documented Norway in 2015 in a herd of reindeer and in 3 moose. Increased surveillance in Norway and surrounding countries has now led to CWD detection in 20 reindeer, 11 moose and 3 red deer in Norway, 4 moose in Sweden and 2 moose in Finland. Using our Gt cervid-PrP mice, we show that CWD prions in moose and red deer in Nordic countries are of an entirely different origin than North American CWD prions. Responses to residue 226, immunoblot profile, CNS deposition and conformational stability

deviate from characterized North American CWD strains, but also are divergent between each Nordic animal. This is indicative of an unstable population of CWD strains which has not yet become endemic to Nordic countries. Continual characterization of newly emergent strains can instruct best practices for wildlife management and risk assessment to human and other animal health.

In chapter 4, we attempt to address the hypothesis that CWD originated from an interspecies transmission and also assess the potential for interspecies transmission of new Nordic strains to other animals. We show that a well characterized strain of sheep scrapie, SSBP/1, is able to readily infect Gt cervid-PrP mice, while TME, BSE and atypical scrapie prions are not. The temporal and geographical distribution of scrapie and CWD provide further evidence that the origin of CWD could be sheep scrapie. However, further studies using isolates of scrapie from Colorado are necessary before any conclusions can be made. Either way, the transmission of sheep scrapie to cervid-PrP mice demonstrates the permissiveness of the species barrier. While great strides have been made in understanding prion biology, the geographical spread of CWD and accompanying fast growing population of CWD strains provides a compelling argument for continual surveillance and research.

APPENDIX

CO-ACTIVATION OF SELECTIVE NICOTINIC ACETYLCHOLINE RECEPTORS IS REQUIRED TO REVERSE BETA AMYLOID-INDUCED CA^{2+} HYPEREXCITATION

A version of this appendix is published (121).
Sun JL, Stokoe SA, Roberts JP, Sathler MF, Nip KA, Shou J, et al. Co-activation of selective nicotinic acetylcholine receptors is required to reverse beta amyloid-induced Ca2+ hyperexcitation. Neurobiology of Aging. 2019 Sep

Introduction

Alzheimer's disease (AD) is a progressive neurodegenerative disorder characterized by deficits in learning and memory (1). The hippocampus plays crucial roles in learning and memory and is one of the first brain regions to display AD pathological hallmarks including beta-amyloid (Aβ) peptide-containing senile plaques (2). Despite considerable progress in deciphering the molecular pathology underlying neurodegeneration in AD over the last 3 decades, current understanding of the physiological basis of memory loss in AD remains limited (3).

Neuronal hyperexcitability and abnormal hippocampal network rewiring is strongly implicated in the early stages of AD pathogenesis (4–7). As it follows, patients with AD exhibit an increased risk for developing seizures and epilepsy (7,8). Notably, Aβ leads to both neuronal and Ca^{2+} hyperexcitation in cortical and hippocampal neurons (6,7,9–17). Although picomolar levels of Aβ can strengthen glutamatergic synapses (18), a large body of studies have shown that nanomolar levels of Aβ induce synaptic depression and impair plasticity in hippocampal excitatory synapses (2,19–21), which is inconsistent with the ability of Aβ to induce hyperexcitability. Interestingly, it has been suggested that Aβ-induced dysfunction of inhibitory interneurons contributes to hyperexcitation in hippocampal networks and cognitive decline in the AD mouse model (10,17). However, the mechanism of how Aβ disrupts interneuron function and induces hyperexcitation in hippocampal pyramidal cells is not fully understood.

Another prominent AD pathology is the loss of cholinergic neurons and nicotinic acetylcholine receptors (nAChRs) throughout the brain (22,23). Activation of neuronal nAChRs modulates neurotransmission by altering both inhibitory interneurons and pyramidal excitatory neurons in the hippocampus, thus affecting neuronal circuits at multiple levels (24,25). Notably, cholinergic signaling in GABAergic inhibitory networks is generally more impactful than direct effects on glutamatergic neurons because nAChRs are more densely expressed in inhibitory interneurons than excitatory cells in the hippocampus (26,27). Therefore, cholinergic modulation

of hippocampal synaptic activity is mainly mediated by activation of inhibitory interneurons, which act to reduce the net output of pyramidal neurons and depress plasticity mechanisms in glutamatergic cells. Accordingly, AD-associated loss of nAChRs may impair GABAergic neuron function, leading to disruption of inhibitory and excitatory balance at a circuit level, which ultimately contributes to hippocampal hyperexcitation.

Molecular interactions between Aβ and nAChRs affect receptor function in the early stages of AD (28–32). Although nearly 30 subtypes of neuronal nAChRs have been reported, the 3 major nAChR subtypes in the hippocampus are composed of α7, α4β2, and α3β4 subunits (33–35). In particular, the interaction between α7 nAChRs and Aβ has been extensively demonstrated. α7 subunits colocalize with Aβ in senile plaques of human brain slices as well as in cultured cells (36,37). Reciprocal immunoprecipitation experiments confirm Aβ physically binds to α7 nAChRs (37,38). A recent study using a quantitative time-resolved fluorescence resonance energy transfer (TR-FRET)-based binding assay also confirms the specific binding of Aβ to α7 nAChR (39). In addition, β2-containing nAChRs interact with Aβ42 in several heterologous expression systems (31,40–42). Nonetheless, the role of Aβ in the pathophysiology of AD is not yet precisely understood. In particular, the interaction between Aβ and nAChRs is still controversial. In fact, contradicting studies show Aβ produces either a functional inhibitory effect, receptor activation, or no effect (43–46). Therefore, how Aβ specifically interacts with each subtype of receptor to produce an overall impact on neuronal function, particularly in GABAergic inhibitory networks, is still unknown.

Here, we show soluble Aβ42 oligomers selectively affect both α7 and α4β2 nAChRs but not α3β4 nAChRs in hippocampal interneurons, resulting in hyperexcitation in pyramidal neurons. We further reveal co-activation of α7 and α4β2 nAChRs is required to abolish Aβ42-induced hyperexcitation. For this reason, understanding the interaction of Aβ42 with inhibitory neurons through selective nAChR inhibition may yield potential therapeutic targets for AD.

Materials and Methods

Mouse hippocampal neuron culture

Mouse hippocampal neuron cultures were prepared as described previously (47–50). Hippocampi were isolated from postnatal day 0 (P0) C57Bl6J mouse (#000664; Jackson laboratory, Bar Harbor, ME) brain tissues and digested with 10 U/mL papain (Worthington Biochemical Corp., Lakewood, NJ, USA). For Ca^{2+} Imaging and in vivo calcineurin activity assay, mouse hippocampal neurons were plated on polylysine-coated glass bottom dishes (500,000 cells) and imaged on day in vitro (DIV). For immunocytochemistry, neurons were plated on 12-mm polylysine-coated cover slips (200,000 cells) and fixed on DIV 14. For biotinylation assays, neurons were plated in 6-well dishes (500,000 cells) and biotinylated on DIV 14. Cells were grown in Neurobasal Medium (Life Technologies, Carlsbad, CA, USA) with B27 supplement (Life Technologies, Carlsbad, CA, USA), 0.5 mM GlutaMAX (Life Technologies), and 1% penicillin/streptomycin (Life Technologies). Colorado State University's Institutional Animal Care and Use Committee reviewed and approved the animal care and protocol (16e6779A).

Reagents

Soluble Aβ42 oligomers were prepared as previously described (51). 1 mg of lyophilized human Aβ42 (AnaSpec, Fremont, CA, USA) was dissolved in 1mL of 1,1,1,3,3,3-hexafluoro-2-propanol (Sigma, St. Louis, MO, USA) to prevent aggregation, portioned into 10 mg aliquots, air-dried, and stored at 80 ºC. For use in experiments, an aliquot was thawed at room temperature and then dissolved in dimethyl sulfoxide and phosphate-buffered saline (PBS) to make a 100 mM solution. The solution was incubated for 16 hours at 4 ºC and then diluted to a final concentration for use in experiments. The following antagonists were used in this study: 50 nM a-bungarotoxin (aBTx) (Alomone labs, Jerusalem, Israel), 1 mM dihydro-b-erythroidine hydrobromide (DHbE) (Tocris Bioscience, Bristol, UK), and 3 mM a-conotoxin AuIB (Alomone

labs). The following agonists were used in this study: 25 nM muscimol (MUS; MP Biomedicals, Santa Ana, CA, USA), 1 mM PNU-120596 (Alomone labs), 2 mM RJR-2403 oxalate (Alomone labs), and 1 mM carbamoylcholine chloride (carbachol) (Tocris Bioscience).

GCaMP Ca^{2+} imaging

GCaMP Ca^{2+} imaging was carried out by the previously reported method (52). DIV 4 neurons were transfected with pCMV-GCaMP5 (a gift from Douglas Kim and Loren Looger, Addgene plasmid # 31788; http://n2t.net/addgene:31788; RRID: Addgene_31788) (53) or pGP-CMV-GCaMP6f (a gift from Douglas Kim, Addgene plasmid # 40755; http://n2t.net/addgene:40755; RRID:Addgene_40755) (54) for imaging hippocampal pyramidal cells or pAAV-mDlx-GCaMP6f-Fishell-2 (a gift from Gordon Fishell, Addgene plasmid # 83899; http://n2t.net/addgene:83899; RRID:Addgene_83899) (55) for imaging interneurons by using Lipofectamine 2000 (Life Technologies) according to the manufacturer's protocol. For Ca^{2+} imaging selectively in hippocampal excitatory neurons, cells were prepared from P0 transgenic mice expressing Cre recombinase under the control of the excitatory neuron-specific alpha calcium/calmodulin-dependent protein kinase II (CaMKIIa) promoter (#005359; Jackson Laboratory), and GCaMP6f was expressed selectively in CaMKIIa-positive neurons by infection with adeno-associated virus (AAV1.CAG.Flex.GCaMP6f.WPRE.SV40; Penn Vector Core, Philadelphia, PA, USA). Neurons were imaged DIV 12-14. The transfection efficiency was around 2%, and no obvious cellular toxicity has been observed. Neurons were grown in Neurobasal Medium without phenol red (Life Technologies) and with B27 supplement (Life Technologies), 0.5 mM GlutaMAX (Life Technologies), and 1% penicillin/streptomycin (Life Technologies) for 8-10 days after transfection and during the imaging. Glass bottom dishes were mounted on a temperature-controlled stage on an Olympus IX73 microscope and maintained at 37 ºC and 5% CO2 using a Tokai-Hit heating stage and digital temperature and humidity controller. For GCaMP5, the images were captured with a 50-ms exposure time

using a 60x oil immersion objective (NA = 1.42). A total of 100 images were obtained with a 1-second interval, and Ca^{2+} activity in the cell body (excluding dendrites) was analyzed using the Olympus cellSens software. For mDlx-GCaMP6f and AAV1-GCaMP6f, the images were captured with a 10-ms exposure time and a total of 100 images were obtained with a 500-ms interval. F_{min} was determined as the minimum fluorescence value during the imaging. Total Ca^{2+} activity was obtained by 100 values of $\Delta F/F_{min} = (F_t - F_{min})/F_{min}$ in each image, and values of $\Delta F/F_{min} < 0.1$ were rejected due to bleaching. 10 to 20 neurons were used for imaging in one individual experiment, and one individual neuron was assayed in an image.

FRET-based in vivo calcineurin activity assay

In vivo calcineurin activity was determined by an FRET-based calcineurin activity sensor as shown previously (49,56). Neurons were transfected with the calcineurin activity biosensor, and FRET activity was measured at DIV 14 according to a modification of the previously described method. Neurons were pre-treated with 250 nM soluble Aβ42 oligomers or scrambled Aβ42 for 1 hour. Images were captured by using an Olympus IX73 microscope. Pseudocolor images of the emission ratio were generated by the Olympus cellSens software. The following formula was used to calculate emission ratio:

Yellow – to - cyan emission ratio (FRET channel intensity/CFP channel intensity =

$$\frac{\text{FRET channel emission intensity - FRET channel emission intensity of background}}{\text{CFP channel emission intensity - CFP channel emission intensity of background}}$$

Immunocytochemistry

Immunocytochemistry was carried out by a modification of the previously reported method (36). Cultured hippocampal neurons were fixed in 4% formaldehyde in PBS for 10 minutes, blocked in 1% bovine serum albumin, and 0.1% sapponin for

30 minutes, and then incubated overnight with an anti-choline acetyltransferase (ChAT) antibody (1:250; MilliporeSigma, Burlington, MA, USA) to identify cholinergic neurons. After 4 washes with 0.1% triton-X in PBS for 5 minutes each, cells were incubated with Alexa-Fluor-594 conjugated secondary antibody (Life Technologies 1:1000) for 1 hour, washed, and mounted in p-phenylenediamine in 90% glycerol. Neurons were imaged with a 20x objective using an Olympus BX51 microscope.

Surface biotinylation and immunoblots

Surface biotinylation was performed according to the previous studies (47–50). Equal amounts of protein were loaded on 10% SDS-PAGE gel and transferred to nitrocellulose membranes. Membranes were blotted with anti-NR1 (1:1000; Millipore), anti-GluA1 (1:2000; Millipore), anti-GluA2 (1:2000; Abcam, Cambridge, UK), anti-phosphorylated GluA1 S845 (1:1000, Millipore), and anti-actin (1:2000, Abcam) antibodies and developed with enhanced chemiluminescence (Thermo Fisher Scientific, Waltham, MA, USA). Immunoblots were at least duplicated for quantitative analysis.

Statistics

Statistical comparisons were analyzed with the GraphPad Prism7 software. Unpaired two-tailed Student t-tests were used in single comparisons. For multiple comparisons, a one-way analysis of variance followed by the Tukey test was used to determine statistical significance. Results are represented as mean ± SEM, and $p < 0.05$ was considered statistically significant.

Results

Soluble Aβ42 oligomer-induced Ca^{2+} hyperexcitation in cultured hippocampal neurons

There are contrasting findings concerning the effect of *Aβ* on neuronal excitability and synaptic function (57). This is partially due to the fact that Aβ exists in multiple forms from monomers to oligomers to fibrils and varies in conformation (58–60). Among these conformations, soluble Aβ42 oligomers appear to be the most neurotoxic species, triggering various processes that underlie AD pathogenesis including synaptic dysfunction and Ca^{2+} deregulation (61,62). We thus prepared soluble Aβ42 oligomers as described previously (51) to examine the action of Aβ on neuronal activity. As neuronal Ca^{2+} is the second messenger responsible for transmitting depolarization status and synaptic activity (63), we measured Ca^{2+} activity in cultured DIV 12-14 mouse hippocampal neurons transfected with GCaMP5 as described previously (50). We acutely treated neurons with 100 nM, 250 nM, and 500 nM soluble Aβ42 oligomers and determined Ca^{2+} activity in hippocampal neurons immediately after Aβ42 treatment. We found active spontaneous Ca^{2+} transients in both scrambled Aβ42 (sAβ42) and soluble Aβ42 oligomer (oAβ42)-treated neurons (Fig. 1A).

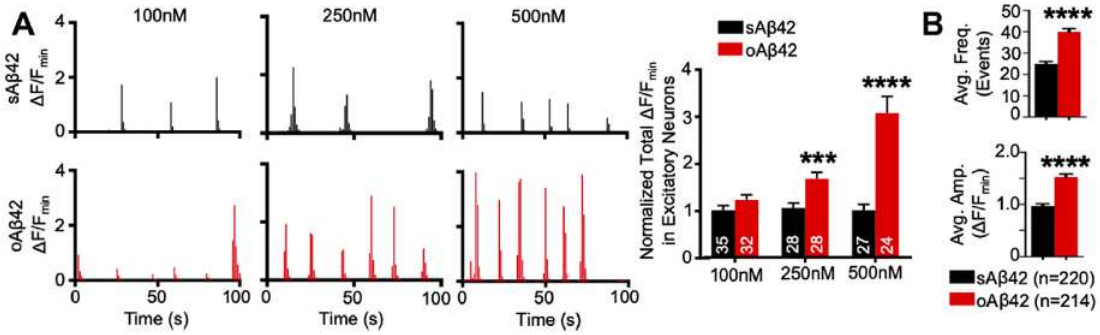

Figure 1. Soluble Ab42 oligomers induce hyperexcitability in hippocampal cells. (A) Representative traces of GCaMP5 fluorescence intensity in hippocampal cells and a summary graph of the normalized average of total Ca^{2+} activity in neurons treated with either sAβ42 (black) or oAβ42 (red) at concentrations of 100 nM, 250 nM, and 500 nM showing oAβ42 significantly increases Ca^{2+} activity at concentrations of 250 nM and 500 nM (n = number of neurons, ***p < 0.001 and ****p < 0.0001, two-tailed student's t-test). (B) Average frequency and amplitude of Ca^{2+} activity in sAβ42- or oAβ42-treated neurons showing 250 nM oAβ42 significantly elevates both frequency and amplitude of Ca2. activity in cultured hippocampal neurons (n = number of neurons, ****p < 0.0001, two-tailed Student's t-test). Abbreviations: oAβ42, soluble Aβ42 oligomer; sAβ42, scrambled Aβ42.

However, total Ca^{2+} activity in 250 nM and 500 nM oAβ42-treated cells was significantly higher than that in sAβ42-treated controls (250 nM sAβ42, 1.00 ± 0.04 $\Delta F/F_{min}$, and 250 nM oAβ42, 1.70 ± 0.13 $\Delta F/F_{min}$, $p = 0.0007$; 500 nM sAβ42, 1.00 ± 0.13 $\Delta F/F_{min}$, and 500 nM oAβ42, 3.08 ± 0.35 $\Delta F/F_{min}$, $p < 0.0001$), confirming that soluble Aβ42 oligomers at these concentrations were sufficient to increase neuronal Ca^{2+} activity, while 100 nM oAβ42 treatment slightly elevated Ca^{2+} activity but was not significantly different from control cells (100 nM sAβ42,1.00 ± 0.10 $\Delta F/F_{min}$, and 100 nM o Aβ42, 1.23 ± 0.10 $\Delta F/F_{min}$, $p = 0.112$) (Fig. 1A). We thus decided to use 250 nM soluble Aβ42 oligomers for further experiments. We also confirmed that both the average frequency (sAβ42, 24.93 ± 1.07 events, and oAβ42, 39.85 ± 1.55 events, $p < 0.0001$) and amplitude (sAβ42, 0.97 ± 0.02 DF/Fmin, and oAβ42, 1.52 ± 0.062 $\Delta F/F_{min}$, $p < 0.0001$) were significantly elevated in 250 nM oAβ42-treated neurons (Fig. 1B). Taken together, 250 nM soluble Aβ42 oligomers were sufficient to induce Ca^{2+} hyperexcitation in cultured hippocampal neurons.

Soluble Aβ42 oligomer reduces surface AMPA receptor expression

As soluble Aβ42 oligomers were sufficient to induce Ca^{2+} hyperexcitation (Fig. 1), it was possible that Aβ42 directly activated excitatory synapses. To examine the direct effect of soluble Aβ42 oligomers on excitatory synapses, we measured surface expression of synaptic glutamate receptors, including a-amino-3-hydroxy-5-methyl-4-isoxazolepropionic acid (AMPA) and N-methyl-D-aspartate (NMDA) receptors (AMPARs and NMDARs), by biotinylation after 250 nM oAβ42 was applied for one hour. Consistent with the previous findings in which Aβ induces synaptic depression at hippocampal excitatory synapses (2,19–21), 250 nM oAβ42 treatment was sufficient to reduce surface expression of AMPAR subunits GluA1 (sAβ42, 1.00, and oAβ42, 0.64 ± 0.08, $p = 0.003$) and GluA2 (sAβ42, 1.00, and oAβ42, 0.74 ± 0.08, $p = 0.0146$), an indication of decreased activity at glutamatergic synapses, yet oAβ42 treatment had no effect on NMDAR subunit NR1 surface expression (sAβ42, 1.00, and oAβ42, 0.76 ± 0.16, p =

0.182) (Fig. 2A). To further investigate how oAβ42 treatment reduced surface AMPAR levels, we measured phosphorylation of GluA1 at serine 845 (pGluA1), which is important for activity-dependent trafficking of GluA1-containing AMPARs (49). Consistent with our biotinylation data (Fig. 2A), 1 hour of 250 nM oAβ42 treatment was sufficient to reduce pGluA1 (sAβ42, 1.00, and oAβ42, 0.54 ± 0.12, p = 0.0013) (Fig. 2B). Phosphorylation of GluA1 can be regulated by kinase and phosphatase activity (64). In particular, Ca^{2+}/calmodulin-dependent protein phosphatase, calcineurin, dephosphorylates pGluA1, which enables GluA1-containing AMPARs to be endocytosed from the plasma membrane during long-term depression (65,66). Given that oAβ42 elevated Ca^{2+} activity, we hypothesized that Aβ-induced Ca^{2+} hyperexcitation enhanced calcineurin activity, resulting in reduction of pGluA1 and surface expression of AMPARs. To measure in vivo calcineurin activity directly, we employed an FRET-based calcineurin activity sensor as shown previously (47–49). As expected, oAβ42 treatment for 1 hour was sufficient to increase FRET activity (assayed by measuring the emission ratio) as compared with sAβ42 treatment (sAβ42, 1.0 ± 0.03, and oAβ42, 1.12 ± 0.04, p = 0.012) (Fig. 2C). This suggests soluble Aβ42 oligomers increase calcineurin activity, which leads a decrease in pGluA1, ultimately resulting in a reduction of surface AMPAR expression. Taken together, Aβ42-induced Ca^{2+} hyperexcitation is not solely caused by enhanced excitatory activity in cultured hippocampal neurons.

Soluble Aβ42 oligomer-induced Ca^{2+} hyperexcitation is dependent on GABAergic input

Because it has been suggested that disruption of inhibitory inputs onto hippocampal pyramidal cells contributes to network hyperexcitation and consequent cognitive decline in the AD mouse model (10,17), we acutely treated neurons with 250 nM oAβ42 together with a $GABA_A$ receptor ($GABA_AR$) agonist, MUS, to examine whether Aβ42-induced Ca^{2+} hyperexcitation is mediated by GABAergic disinhibition (Fig. 3A). To avoid affecting basal Ca^{2+} activity, we used 25 nM MUS, a concentration that had no effect on Ca^{2+} activity in control

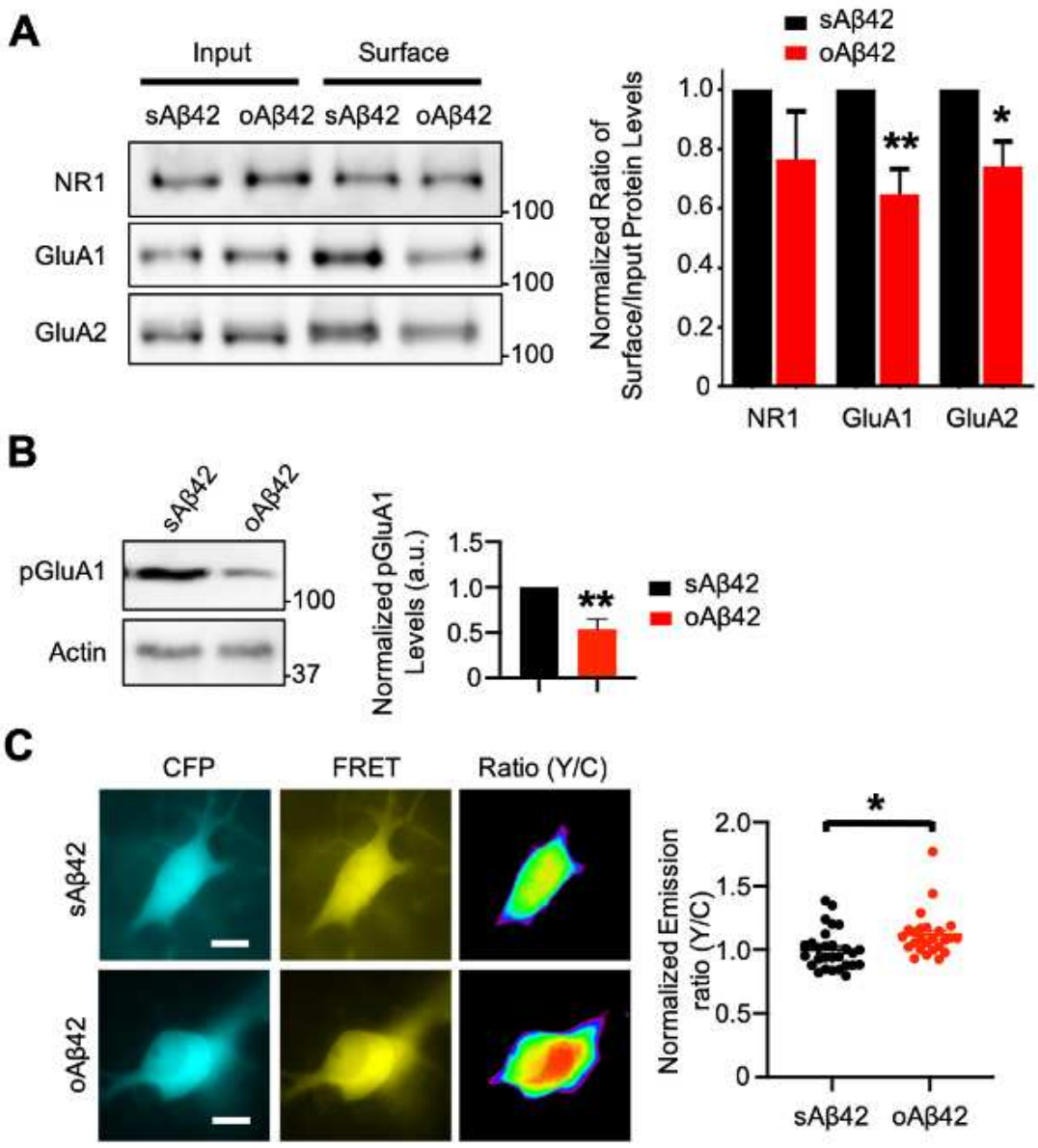

Figure 2. Soluble Aβ42 oligomer reduces surface AMPA receptor expression. (A) Representative immunoblots and quantitative analysis of surface biotinylation in each condition showing that 250nM oAβ42 is sufficient to decrease AMPAR surface expression (n = 4 independent cultures duplicated, *$p < 0.05$ and **$p < 0.01$, two-tailed student t-test). **(B)** Representative immunoblots and quantitative analysis in each condition showing that 250nM oAβ42 is sufficient to decrease pGluA1 (n = 4 independent cultures duplicated, **$p < 0.01$, two-tailed student t-test). **(C)** Representative images of CFP channel, FRET channel, and pseudocolored emission ratio (Y/C) in each condition. In pseudocolored image, blue and red represent low and high emission ratio, respectively. A scale bar indicates 5μm. A summary graph of normalized average of emission ratio (Y/C) showing that 250nM oAβ42 is sufficient to increase *in vivo* calcineurin activity (n=28 sAβ42 and 25 oAβ42 neurons, *$p < 0.05$, two-tailed student t-test).

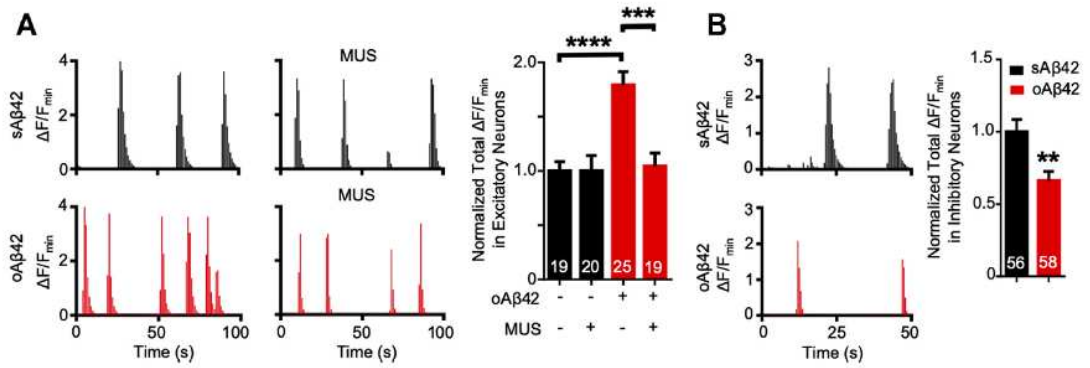

Figure 3. Soluble Aβ42 oligomer-induced hyperexcitability is mediated by GABAergic disinhibition. (A) Representative traces of GCaMP5 fluorescence intensity in hippocampal neurons and a summary graph of normalized average of total Ca^{2+} activity in each condition showing that a $GABA_AR$ agonist, 25 nM MUS, abolishes oAβ42-induced hyperexcitability (n = number of neurons, ****p < 0.0001, ***p < 0.001, one-way ANOVA, Tukey Test). (B) Representative traces of GCaMP6f fluorescence intensity and a summary graph of normalized average of total Ca^{2+} activity in hippocampal interneurons treated with 250 nM sAβ42 (black) or 250 nM oAβ42 (red) showing that oAβ42 treatment significantly reduces neuronal Ca^{2+} activity (n = number of neurons, **p < 0.01, two-tailed Student's t-test). Abbreviations: MUS, muscimol; oAβ42, soluble Aβ42 oligomer; sAβ42, scrambled Aβ42.

neurons (sAβ42, 1.00 ± 0.08 $\Delta F/F_{min}$, and sAβ42 + MUS, 1.00 ± 0.14 $\Delta F/F_{min}$, p > 0.999) (Fig. 4A), whereas 5 mM MUS treatment was sufficient to reduce activity (sAβ42, 1.0 ± 0.14 $\Delta F/F_{min}$, and sAβ42 + MUS, 0.18 ± 0.10 $\Delta F/F_{min}$, p < 0.0001) (Fig. 5). We also confirmed that 250 nM oAβ42 significantly elevated Ca^{2+} activity (sAβ42, 1.00 ± 0.08 $\Delta F/F_{min}$, and oAβ42,1.79 ± 0.12 $\Delta F/F_{min}$, p < 0.0001) (Fig. 3A). Significantly, 25 nM MUS was sufficient to abolish the oAβ42 effects on Ca^{2+} activity in hippocampal neurons (oAβ42, 1.79 ± 0.12 $\Delta F/F_{min}$, and oAβ42 + MUS, 1.04 ± 0.12 $\Delta F/F_{min}$, p = 0.0001) (Fig. 3A). This suggests the oAβ42 effects on Ca^{2+} activity are mediated by inhibitory inputs. We thus examined whether soluble Aβ42 oligomers affect Ca^{2+} activity in hippocampal interneurons by expressing GCaMP6f under the control of the GABAergic neuron-specific enhancer of the mouse Dlx gene (55). In contrast to excitatory neurons, 250 nM oAβ42 treatment significantly reduced Ca^{2+} activity in interneurons (sAβ42, 1.00 ± 0.09 $\Delta F/F_{min}$, and oAβ42, 0.66 ± 0.06 $\Delta F/F_{min}$, p = 0.0018) (Fig. 3B). To confirm whether oAβ42 induced Ca^{2+} hyperexcitation selectively in hippocampal excitatory neurons, GCaMP6f was expressed under the control of the excitatory neuron-specific CaMKIIα promoter (67,68). Indeed, we found 250 nM oAβ42 treatment was sufficient to elevate Ca^{2+} activity in CaMKIIα-

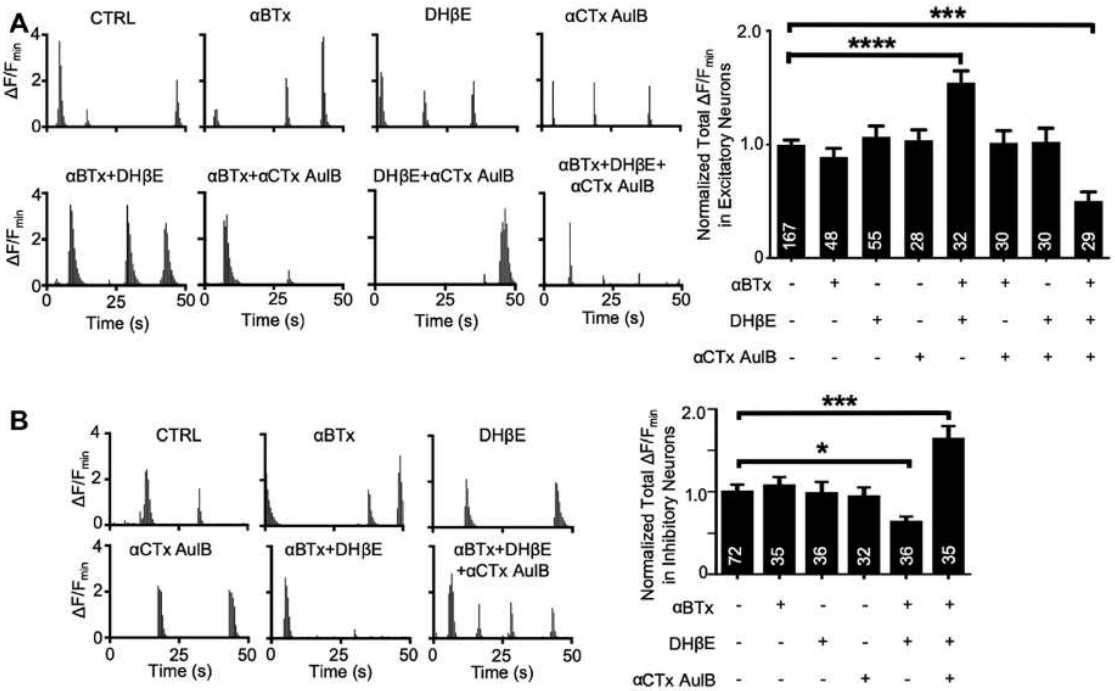

Figure 4. Selective inhibition of α7 and α4β2 nAChRs mimics Aβ42-induced hyperexcitability in hippocampal pyramidal and inhibitory neurons. (A) Representative traces of GCaMP6f fluorescence intensity and a summary graph of normalized average of total Ca2. activity in each condition showing application of 50 nM αBTX, an α7 nAChR antagonist, and 1 mM DHβE, an α4β2 nAChR antagonist, together significantly increases neuronal Ca^{2+} activity, similar to oAβ42 treatment. Opposingly, treatment of all 3 antagonists together, 50 nM αBTX, 1 mM DHβE, and 3 mM αCTX AulB, an α3β4 antagonist, significantly decreases Ca^{2+} activity. Application of each antagonist individually, 50 nM αBTX and 3 mM αCTX AulB together, or 1 mM DHβE and 3 mM αCTX AulB together had no effect on Ca^{2+} activity (n = number of neurons, ***p < 0.001, ****p < 0.0001, Tukey Test). (B) Representative traces of GCaMP6f fluorescence intensity and a summary graph of normalized average of total Ca^{2+} activity in each condition showing application of 50 nM αBTX and 1 mM DHβE together significantly decreases Ca^{2+} activity in interneurons, similar to oAβ42 treatment. Opposingly, treatment of all 3 antagonists together, 50 nM αBTX, 1 mM DHβE, and 3 mM αCTX AulB, significantly increases Ca^{2+} activity in inhibitory cells. Application of each antagonist individually had no effect on Ca^{2+} activity (n = number of neurons, *p < 0.05, ***p < 0.001, one-way ANOVA, Tukey Test). Abbreviations: αBTX, α-bungarotoxin; DHβE, dihydro-β-erythroidine hydrobromide; nAChR, acetylcholine receptor; oAβ42, soluble Aβ42 oligomer; sAβ42, scrambled Aβ42.

positive neurons (sAβ42, 1.00 ± 0.10 $\Delta F/F_{min}$, and oAβ42, 1.31 ± 0.10 $\Delta F/F_{min}$, p = 0.0347) (Fig. 6), as seen in Fig. 1A. This is consistent with the fact that the majority of cells in hippocampal cultures are excitatory neurons (69). In addition, pharmacological activation of $GABA_AR$s was able to block Aβ42-induced Ca^{2+} hyperexcitation in CaMKIIα-positive excitatory neurons (oAβ42, 1.31 ± 0.10 $\Delta F/F_{min}$, and oAβ42 + MUS, 0.73 ± 0.11 $\Delta F/F_{min}$, p = 0.0005) (Fig. 6). Taken

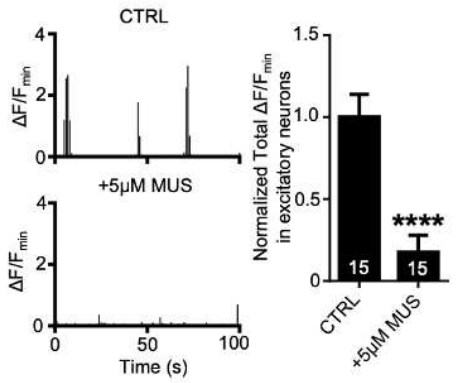

Figure 5. Higher concentration of muscimol significantly decreases Ca^{2+} activity. Representative traces of GCaMP5 fluorescence intensity and a summary graph of normalized average of total Ca^{2+} activity showing that application of a $GABA_AR$ agonist, 5μM muscimol, significantly reduces Ca^{2+} activity in hippocampal pyramidal cells (n = number of neurons, ****p < 0.0001, two-tailed student's t-test).

together, this suggests that soluble Aβ42 oligomers reduce inhibitory inputs to hippocampal excitatory neurons, indicating that network dysfunction can lead to hyperexcitability.

Selective inhibition of nAChRs mimics the oAβ42 effects on Ca^{2+} activity

Molecular interactions between Aβ and nAChRs play important roles in AD pathogenesis (28–32). It has previously reported that about 10% of neurons in primary hippocampal cultures exhibit acetylcholine (ACh) currents after rapid application of ACh, and nearly all of the responsive cells are GABAergic interneurons (43). Furthermore, there is a study showing the existence of intrinsic cholinergic interneurons in the hippocampus (70). Consistently, we also identified that cholinergic neurons were present in our culture system by immunocytochemistry using an anti-choline acetyltransferase. (ChAT) antibody (Fig. 7). Because there is conflicting evidence concerning whether Aβ42 works in an nAChR subtype-specific manner, we treated neurons with nAChR subtype-specific antagonists to identify which major subtypes of nAChRs are involved in the oAβ42 effects (Fig. 4A). Interestingly, acute treatment of 50 nM αBTx, an α7 receptor inhibitor, 1 mM DHβE, an α4β2 receptor inhibitor, or 3 mM α-conotoxin AuIB (αCTx AuIB), an α3β4 receptor inhibitor, by themselves had no effect on hippocampal Ca^{2+}

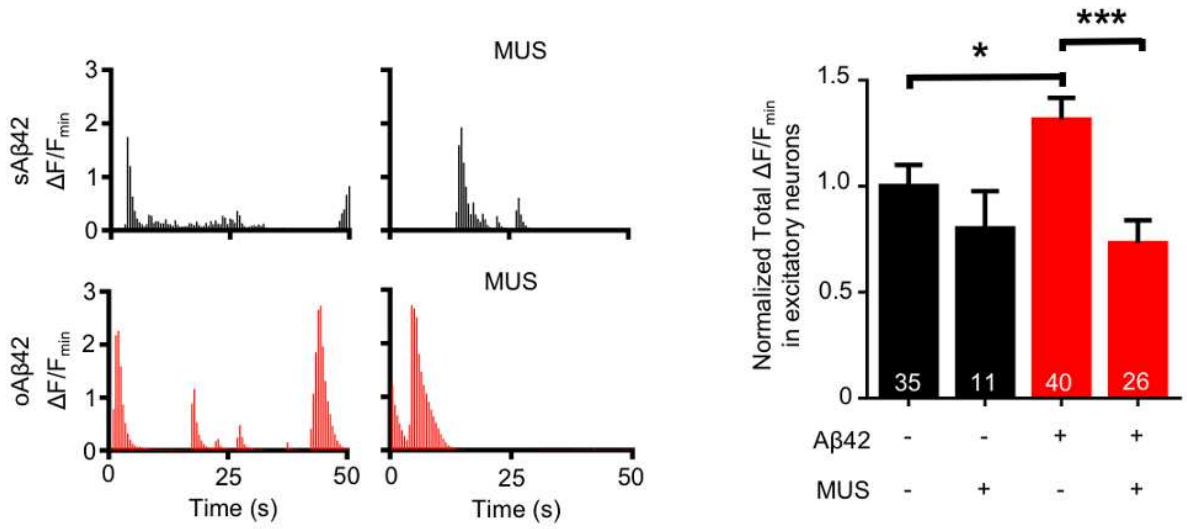

Figure 6. Soluble Aβ42 oligomer-induced hyperexcitability in CAMKIIα-positive neurons Representative traces of GCaMP6f fluorescence intensity and a summary graph of normalized average of total Ca^{2+} activity in each condition showing that oAβ42 treatment increases Ca^{2+} activity in CAMKIIα-positive neurons, which can be reduced by a $GABA_AR$ agonist, 25nM muscimol (n = number of neurons, $*p < 0.05$, $***p < 0.001$, one-way ANOVA, Tukey Test).

activity compared with control neurons (CTRL) (CTRL, 1.00 ± 0.04 $\Delta F/F_{min}$; αBTx, 0.89 ± 0.07 $\Delta F/F_{min}$, p = 0.931; DHβE, 1.06 ± 0.09 $\Delta F/F_{min}$, p = 0.995, and αCTx AuIB, 1.04 ± 0.10 $\Delta F/F_{min}$, p > 0.999) (Fig. 4A). Inhibition of α7 and α3β4 nAChRs together or α4β2 and α3β4 nAChRs together also yielded no effect on Ca^{2+} activity (CTRL, 1.00 ± 0.04 $\Delta F/F_{min}$; αBTx + αCTx AuIB, 1.02 ± 0.11 $\Delta F/F_{min}$, p > 0.999; αBTx + DHβE, 1.02 ± 0.12 $\Delta F/F_{min}$, p > 0.999). However, inhibition of both α7 and α4β2 nAChRs together significantly elevated GCaMP5 activity (αBTx + DHβE, 1.54 ± 0.10 $\Delta F/F_{min}$, p < 0.0001) (Fig. 4A) similar to oAβ42 treatment (Fig. 1A). Conversely, blocking all 3 nAChR subtypes resulted in significantly reduced hippocampal Ca^{2+} activity, the opposite effect of oAβ42 treatment (αBTx + DhβE + αCTx AuIB, 0.50 ± 0.08 $\Delta F/F_{min}$, p = 0.0003) (Fig. 8A). This suggests oAβ42 effects may be due to selective inhibition of both α7 and α4β2 nAChR subtypes.

Next, we measured the effects of the nAChR antagonists on Ca^{2+} activity in hippocampal interneurons by using Dlx-GCaMP6f as shown in Fig. 3B. In contrast to excitatory neurons (Fig.

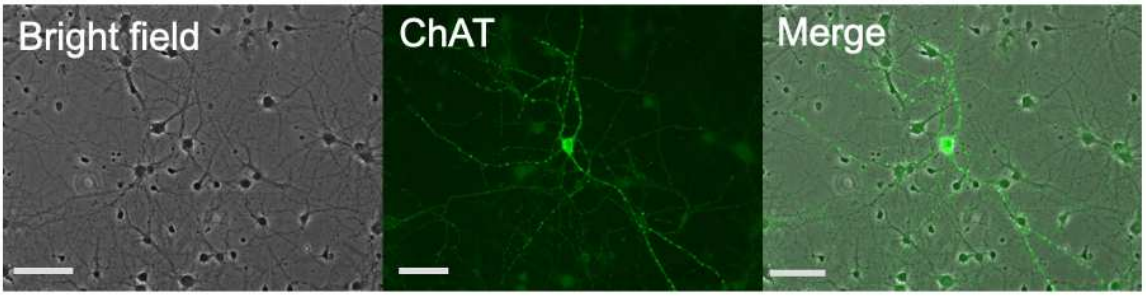

Figure 7. Non-selective inhibition of nAChRs is unable to reduce oAβ42-induced hyperactivity. Representative images of a bright field, immunocytochemistry staining using an anti-ChAT antibody (green) and a merge image show that cholinergic neurons are present in mouse hippocampal culture. A scale bar indicates 100μm.

4A), acute treatment of 50 nM αBTx and 1 mM DHβE significantly reduced interneuron-specific GCaMP6f signals (CTRL, 1.00 ± 0.09 $\Delta F/F_{min}$ and αBTx + DHβE, 0.57 ± 0.06 $\Delta F/F_{min}$, p = 0.041) (Fig. 4B), mimicking the oAβ42 effects in interneurons (Fig. 4B). Moreover, treating neurons with all 3 antagonists showed significant elevation of interneuron Ca^{2+} activity, the opposite effect of oAβ42 treatment (αBTx + DhβE + αCTx AuIB, 1.64 ± 0.16 $\Delta F/F_{min}$, p = 0.0003) (Fig. 4B). Notably, each antagonist by themselves had no effect on GCaMP6f activity (αBTx, 1.07 ± 0.11 $\Delta F/F_{min}$, p = 0.997; DHβE, 0.98 ± 0.14 $\Delta F/F_{min}$, p > 0.999; and αCTx AuIB, 0.94 ± 0.11 $\Delta F/F_{min}$, p = 0.999) (Fig. 4B). Taken together, selective inhibition of α7 and α4β2 nAChRs induces hyperexcitability and hypoactivity in hippocampal excitatory and inhibitory neurons, respectively, as seen in oAβ42 treatment (Figs. 1A and 3B).

Combination treatment of selective nAChR agonists is required to abolish oAβ42-induced hyperexcitation via elevation of inhibitory neuronal activity

Because inhibition of α7 and α4β2 nAChRs mimicked the oAβ42-induced effects seen in both hippocampal excitatory and inhibitory neurons (Fig. 4), we hypothesized that concurrent activation of both receptor types would abolish the oAβ42-induced effects. Indeed, when we treated neurons with 250 nM oAβ42 and concurrently activated α7 and α4β2 nAChRs using 1

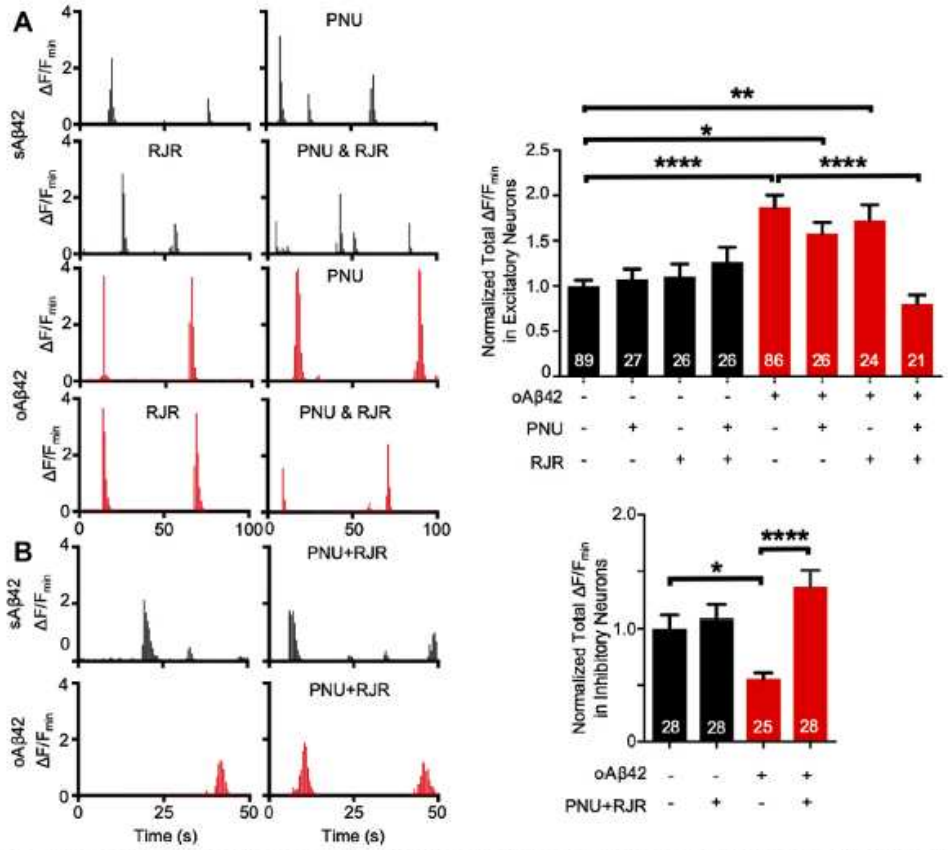

Figure 8. Combination treatment of α7 and α4β2 nAChRs abolishes oAβ42-induced hyperexcitation in hippocampal pyramidal and inhibitory cells. (A) Representative traces of GCaMP5 fluorescence intensity and a summary graph of normalized average of total Ca^{2+} activity in each condition showing that treatment of 1 mM PNU-282987 (PNU), an α7 agonist, and 2 mM RJR-2403 oxalate (RJR), an α4β2 agonist, together significantly decreases oAβ42-induced Ca^{2+} hyperactivity. Notably, activation of either α7 or α4β2 singularly does not decrease oAβ42-induced Ca^{2+} hyperactivity (n = number of neurons, *p < 0.05, **p < 0.01, ****p < 0.0001, one-way ANOVA, Tukey Test). (B) Representative traces of GCaMP6f fluorescence intensity and a summary graph of normalized average of total Ca^{2+} activity in each condition showing that treatment of 1 mM PNU and 2 mM RJR together significantly increases oAβ42-induced Ca^{2+} hypoactivity in interneurons (n = number of neurons, *p < 0.05, ****p < 0.0001, one-way ANOVA, Tukey Test). Abbreviations: α BTX, α-bungarotoxin; DHβE, dihydro-β-erythroidine hydrobromide; nAChR, acetylcholine receptor; oAβ42, soluble Aβ42 oligomer; sAβ42, scrambled Aβ42.

mM PNU-120596 (PNU) and 2 mM RJR-2403 oxalate (RJR), oAβ42-induced Ca^{2+} hyperexcitation was significantly reduced in pyramidal cells (sAβ42, 1.00 ± 0.06 $\Delta F/F_{min}$; oAβ42, 1.87 ± 0.13 $\Delta F/F_{min}$, $p < 0.0001$; oAβ42 + PNU + RJR, 0.81 ± 0.09 $\Delta F/F_{min}$, $p < 0.0001$) (Fig. 8A). Importantly, activation of either α7 or α4b2 nAChR singularly had no effect on oAβ42-induced hyperexcitation (oAβ42 + PNU, 1.58 ± 0.12 $\Delta F/F_{min}$, $p = 0.786$ and oAβ42 + RJR, 1.72 ± 0.17 $\Delta F/F_{min}$, $p = 0.996$) (Fig. 8A). Next, we examined whether combination treatment of α7

and α4β2 nAChR agonists was capable of rescuing the oAβ42 effects in GABAergic interneurons. Notably, stimulation of both α7 and α4β2 nAChRs was sufficient to rescue oAβ42-induced Ca^{2+} hypoactivity in interneurons (sAβ42, 1.00 ± 0.11 $\Delta F/F_{min}$; oAβ42, 0.56 ± 0.05 $\Delta F/F_{min}$, $p = 0.0436$; oAβ42 + PNU + RJR, 1.36 ± 0.15 $\Delta F/F_{min}$, $p < 0.0001$) (Fig. 8B). This suggests that combinatorial activation of α7 and α4β2 nAChRs is required to rescue the oAβ42 effects in both hippocampal excitatory and inhibitory neurons.

Combined application of α7 and α4β2 nAChR antagonists mimicked oAβ42 effects, whereas simultaneous inhibition of all 3 nAChRs showed the opposite results (Fig. 4). This suggests it is possible that inhibition of α3β4 nAChRs can reverse oAβ42 effects in both excitatory and inhibitory cells. To test this idea, we first treated neurons with 250 nM oAβ42 and 3 mM αCTx AulB and measure GCaMP5 activity (Fig. 9A). As seen before, oAβ42 treatment was sufficient to induce Ca^{2+} hyperexcitation (sAβ42, 1.00 ± 0.10 $\Delta F/F_{min}$, and oAβ42, 2.14 ± 0.27 $\Delta F/F_{min}$, $p < 0.0001$) (Fig. 9A). However, inhibition of α3β4 nAChRs had no significant effect on Aβ42-induced Ca^{2+} hyperexcitation in excitatory neurons (oAβ42, 2.14 ± 0.27 $\Delta F/F_{min}$ and oAβ42 + αCTx AulB, 1.68 ± 0.25 $\Delta F/F_{min}$, $p = 0.3309$) (Fig. 9A). Next, we measured Ca^{2+} activity in inhibitory neurons by using mDlx-GCaMP6f (Fig. 9B). As seen before, oAβ42 treatment decreased GCaMP6f activity significantly (sAβ42, 1.00 ± 0.01 $\Delta F/F_{min}$, and oAβ42, 0.55 ± 0.06 $\Delta F/F_{min}$, $p = 0.0012$) (Fig. 9B). However, inhibition of α3β4 nAChRs had no significant effect on Ca^{2+} activity in the presence or absence of oAβ42 treatment (sAβ42 + αCTx AulB, 0.91 ± 0.10 $\Delta F/F_{min}$, $p = 0.8817$, and oAβ42 + αCTx AulB, 0.67 ± 0.07 $\Delta F/F_{min}$, $p = 0.7633$) (Fig. 9B). This suggests inhibition of α3β4 nAChRs by itself is unable to reverse oAβ42 effects.

Of clinical relevance, currently the U.S. Food and Drug Administration-approved drugs for AD mostly delay the general breakdown of ACh, which potentially stimulates various types of

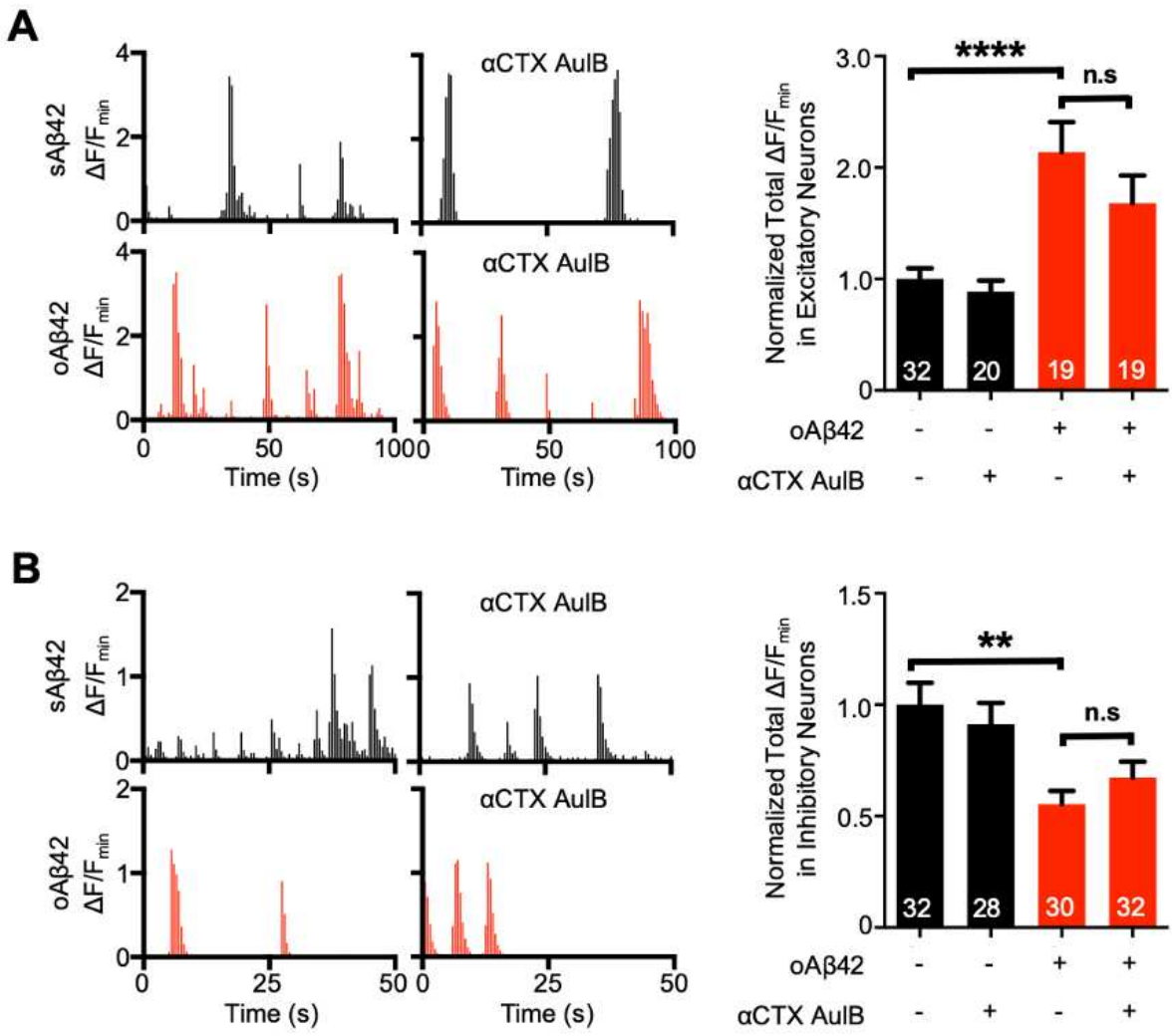

Figure 9. Inhibition of α3β4 nAChRs is unable to reverse the oAβ42 effects in hippocampal pyramidal and inhibitory cells.
(A) Representative traces of GCaMP5 fluorescence intensity and a summary graph of normalized average of total Ca^{2+} activity in each condition showing that treatment of 3μM αCTX AuIB, an α3β4 antagonist, has no effect on oAβ42-induced Ca^{2+} hyperactivity in excitatory neurons (n = number of neurons, ****$p < 0.0001$, one-way ANOVA, Tukey Test). **(B)** Representative traces of GCaMP6f fluorescence intensity and a summary graph of normalized average of total Ca^{2+} activity in each condition showing that inhibition of α3β4 receptors has no effect on oAβ42-induced Ca^{2+} hypoexcitation in inhibitory cells (n = number of neurons, **$p < 0.01$, one-way ANOVA, Tukey Test).

AChRs. To mimic this effect, we used a cholinergic agonist, carbachol. Interestingly, we showed 1 mM carbachol was unable to rescue oAβ42-induced Ca^{2+} hyperexcitation but instead exacerbated the oAβ42 effects in hippocampal neurons (sAβ42, 1.00 ± 0.08 $\Delta F/F_{min}$;

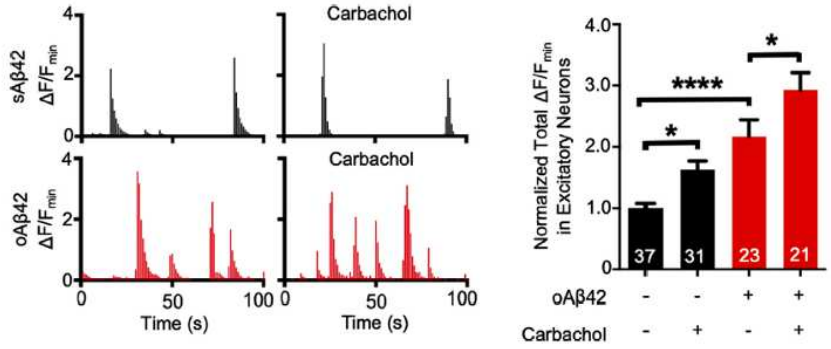

Figure 10. Carbachol is unable to rescue oAβ42-induced Ca^{2+} hyperactivity. Representative traces of GCaMP5 fluorescence intensity and a summary graph of normalized average of total Ca^{2+} activity in each condition showing that application of a nonselective AChR agonist, 1 mM carbachol, does not rescue oAβ42-induced Ca^{2+} hyperactivity and exacerbates Ca^{2+} activity in the presence or absence of oAβ42 (n = number of neurons, *p < 0.05, ****p < 0.0001, one-way ANOVA, Tukey Test). Abbreviations: AChR, acetylcholine receptor; oAβ42, soluble Aβ42 oligomer; sAβ42, scrambled Aβ42.

oAβ42, 2.17 ± 0.28 $\Delta F/F_{min}$, p < 0.0001; oAβ42 + carbachol, 2.93 ± 0.28 $\Delta F/F_{min}$, p = 0.0462) (Fig. 10). We further confirmed that in the absence of Aβ, carbachol significantly elevated Ca^{2+} activity (sAβ42, 1.00 ± 0.08 $\Delta F/F_{min}$, and sAβ42 + carbachol, 1.63 ± 0.14 $\Delta F/F_{min}$, p = 0.04) (Fig. 10). This suggests nonselective stimulation of AChRs may have unintended consequences that limit agonist impact. Taken together, selective coactivation of α7 and α4β2 nAChRs is required to abolish the oAβ42 effects in both inhibitory and excitatory neurons.

Discussion

Although increased epileptiform activity has been shown to occur in the early stages of AD, a cellular mechanism for this aberrant activity has not yet been detailed. We show here a novel cellular mechanism for hippocampal hyperactivity in AD (Fig. 11). Aβ42 induces hypoactivity in hippocampal interneurons and consequent hyperexcitability in pyramidal cells (Figs. 1A and 3B). Furthermore, we show that selective inhibition of α7 and α4β2 nAChRs but not α3β4 receptors in hippocampal interneurons and excitatory neurons mimics oAβ42 effects on neuronal activity (Fig. 4). More importantly, selective coactivation of α7 and α4β2 receptors is

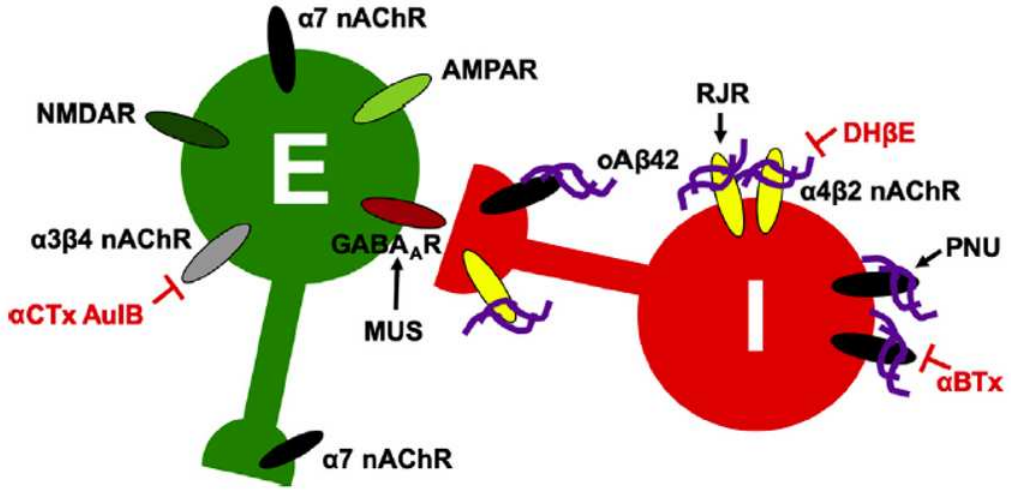

Figure 11. Soluble Aβ42 oligomer-induced hyperexcitability via selective inhibition of nAChRs in hippocampal interneurons. Excitability of hippocampal excitatory neuron (E) is regulated by a balance between AMPAR- (light green) and NMDAR- (dark green) mediated glutamatergic excitation and GABAergic inhibition via $GABA_A$Rs (red). nAChRs are densely expressed in hippocampal inhibitory interneurons (I) and regulated by cholinergic inputs. oAβ42 (purple) selectively inhibits both α7 (black) and α4β2 (yellow) nAChR subtypes in interneurons but not α3β4 receptors (gray) in excitatory cells to reduce neuronal activity in interneurons, leading to hyperexcitation in hippocampal pyramidal neurons. Therefore, combination treatment of α7 and α4β2 nAChR agonists, PNU and RJR, in the hippocampus can be neuroprotective in AD. Abbreviations: α BTX, α -bungarotoxin; DHβE, dihydro-β-erythroidine hydrobromide; AD, Alzheimer's disease; nAChR, acetylcholine receptor; oAβ42, soluble Aβ42 oligomer; sAβ42, scrambled Aβ42.

required for a rescue of both Aβ42-induced hypoactivity in interneurons and hyperactivity in excitatory cells (Fig. 8). However, we show that general activation of AChRs by carbachol does not lessen pyramidal cell hyperactivity and instead exacerbates hyperactivity further (Fig. 10). Congruently, current AD medications are only mildly effective at treating symptoms and slowing disease progression, possibly due to nonselective stimulation of receptors (71). Therefore, the idea that AB42 selectively affects α7 and α4β2 nAChRs in hippocampal inhibitory interneurons to induce hyperexcitation is a fundamentally new concept and could have impactful implications on drug discovery.

It can be difficult to reconcile hyperexcitability in the context of reduced surface AMPAR expression in the presence of oAβ42. A large body of studies have confirmed that Aβ oligomers cause synaptic depression at specific excitatory synapses in the hippocampus as evidenced by

impaired synaptic plasticity, reduced synaptic transmission, and a decrease in surface AMPAR expression (19,20,72–76). However, at the network level, Aβ oligomers cause epileptiform activity and seizures (6,15,77). Cellular mechanisms of these contradictory Aβ-dependent effects have not been completely determined (7). Importantly, in addition to excitatory synaptic inputs, neural activity is dependent on inhibition, which regulates overall activity level and shapes the temporal pattern of activity (78,79). In fact, loss of the tuberous sclerosis complex (TSC) 1 in CA1 pyramidal cells of the hippocampus results in disrupted inhibitory synaptic function, which alters the balance of excitatory and inhibitory synaptic transmission, leading to hippocampal hyperexcitability (80). More importantly, such hyperexcitation in the hippocampus persists when surface AMPAR expression is reduced (80), consistent with our findings. Thus, neural activity can be enhanced by repressing inhibitory synapses onto excitatory neurons even if glutamatergic synapses on excitatory cells are depressed. Another hypothesis is that hyperexcitability can be driven by the Aβ-induced suppression of glutamate reuptake. It has been shown that there is reduction of glutamate clearance rates in synapses close to amyloid deposits, and chronic states of elevated glutamate levels are found near amyloid plaques (81). Moreover, a recent study using two-photon imaging to measure in vivo Ca^{2+} and glutamate transients shows that soluble human Aβ dimers are sufficient to induce hyperexcitation in the hippocampus (60). As glutamate is the major excitatory neurotransmitter, it is possible that an increase in glutamate levels can induce hippocampal hyperexcitation. Indeed, elevation of glutamate uptake alleviates nerve root-mediated pain-induced neuronal hyperexcitability (82). Another possible explanation of this inconsistency is the different kinetics of oAβ42 effects on neuronal hyperexcitability. One study shows that 300 nM oAβ42 in cultured neurons causes a gain of NMDAR function within seconds after application (83), whereas prolonged (>45 minutes) exposure of high concentration (500 nM-5 mM) oAβ42 in cultured neurons is sufficient to induce GluA1 and NR1 internalization (84,85). Thus, it is possible that Ca^{2+} hyperexcitation can be induced by acute treatment of 250 nM oAβ42. It is also possible that chronic exposure (~1 hour)

of 250 nM oAβ42 is sufficient to reduce surface expression of AMPA receptors. Although we started recording Ca^{2+} activity within seconds after oAβ42 treatment, we continued to record more than one hour under the same condition, yet we have not found any significant differences in Ca^{2+} activity throughout the duration of each experiment. This thus rules out the possibility that our findings can be caused by the different kinetics of oAβ42 effects. Taken together, it remains to be determined if Aβ-induced synaptic depression and network abnormality are mechanistically related.

A large body of studies support that Aβ can physically interact with α7, α4, and β2 receptors in various different model systems (25,44,86,87), whereas Aβ is unable to affect α3 and β4 receptor function when heterologously expressed in Xenopus oocytes (46). This suggests Aβ may not be able to interact with α3β4 receptors. Interestingly, one study shows Aβ40 inhibits α3β4 receptors in human embryonic kidney (HEK) cells (88). We used a soluble oligomeric form of Aβ42 rather than Aβ40, which may lend to the different response. In fact, much of literature describes that different forms of Aβ interact with different receptors (89). Thus, the discrepancy observed in our data and the study by Nery et al. may be due to different forms of Aβ used in the experiments. Although α7 and α4β2 nAChRs are expressed in both pyramidal cells and inhibitory neurons in the hippocampus and are able to modulate hippocampal synaptic plasticity (90,91), α7- and β2-containing nAChRs are mainly expressed in hippocampal GABAergic interneurons, demonstrated by double in situ hybridization with glutamate decarboxylase 67 (GAD67) and nAChRs (27). However, α3 and β4 subunits are rarely detected in GABAergic cells (27). It has also been suggested that low levels of α3β4 receptors are present in hippocampal glutamatergic neurons (92). This supports the idea that soluble Aβ42 oligomers reduce neuronal activity in inhibitory neurons via selective inhibition of α7 and α4β2 receptors, but not α3β4 nAChRs.

This poses the question: Why do soluble Aβ42 oligomers predominantly affect interneurons but not excitatory cells? GABAergic cells contain both presynaptic α7 receptors

and somatodendritic expression of α7 and α4β2 nAChRs (93,94), whereas excitatory neurons have mainly presynaptic α7 nAChRs (26,95,96). Importantly, somatodendritic α7 nAChRs in rodent hippocampal interneurons are functionally coupled with $GABA_A$Rs and as it follows, stimulation of α7 receptors downregulates GABA currents (97). This suggests $GABA_A$R activity can be elevated when α7 nAChRs are inhibited. However, inhibition of α7 nAChRs by itself is not sufficient to reduce neuronal excitability in GABAergic neurons possibly due to the presence of functional α4β2 nAChRs. Accordingly, coinhibition of α7 and α4β2 receptors is sufficient to decrease neuronal activity in inhibitory cells, leading to hyperexcitation in pyramidal neurons (Fig. 4). In contrast to GABAergic neurons, the direct cholinergic modulation of tonic firing in excitatory neurons is notably mediated by muscarinic AChRs, although α7 nAChRs can contribute to pyramidal cell activity through potential interaction with NMDARs in presynaptic terminals (98). This suggests that nAChR-mediated cholinergic activity in the hippocampus may mainly affect excitability in inhibitory interneurons. More importantly, nearly all of ACh responsive neurons in rat hippocampal cultures are GABAergic neurons (43), consistent with previous findings that GABAergic interneurons in hippocampal slices are extremely sensitive to Ach (99–101), further implicating predominant cholinergic effects on neuronal activity in hippocampal interneurons. Taken together, these previous studies and our current findings led us to the idea that soluble Aβ42 oligomers inhibit α7 and α4β2 receptors primarily in interneurons, contributing to hyperexcitation via disinhibition.

Cholinergic interneurons intrinsic to the hippocampus have been found and may contribute to a hippocampal source of ACh (43,70). However, cellular function of intrinsic hippocampal cholinergic neurons has not been fully understood yet. Importantly, our study focuses on the contribution of intrinsic hippocampal cholinergic inputs to disrupted neuronal activity in AD. Nonetheless, the majority of cholinergic inputs to both pyramidal cells and interneurons in the hippocampus originate from the basal forebrain, which have crucial roles in

cognition by modulating properties of the hippocampal network (102,103). Moreover, many studies indicate the strong correlation between dysfunction of basal forebrain cholinergic neurons and cognitive deficits in patients with AD (104). Importantly, Aβ has adverse effects on the basal forebrain cholinergic systems in cultured neuron and animal models that could be crucial for understanding AD pathogenesis (104). Thus, we are still unable to rule out the possibility that Aβ can differentially affect basal forebrain-originated cholinergic function in the hippocampus.

In the presymptomatic stages of AD, neuronal hyperexcitability may play a role in increased network and epileptiform activity leading to eventual cognitive decline, yet current medications may act to increase hyperexcitability. In fact, there are discrepancies involving the use of nicotine treatment to stimulate nAChRs to alter cognitive function. For example, nicotine agonists have been found to improve performance in a variety of memory tasks in rodents and nonhuman primate studies (105), whereas several other studies have failed to find significant enhancement of learning and memory by nicotine treatment (106). Furthermore, some results show that stimulating one type of nAChR by using a specific agonist enhances cognitive performance, but other studies find no beneficial effect. For instance, selective α7 nAChR agonists have recently been reported to improve cognition in a variety of animal models (107–109), whereas another study has found almost no beneficial effect on learning and memory in mice (110). Moreover, an α4β2 nAChR agonist alone can improve working memory only in young rats but not older animals (111). Notably, we reveal that inhibition of α3β4 receptors has no effect on oAβ42-induced alteration of Ca^{2+} transients in both excitatory and inhibitory cells (Fig. 9). This suggests oAb42 may affect different subtypes of nAChRs other than the α7, α4β2, and α3β4 subtypes and possibly receptors other than nAChRs to alter neuronal activity. In fact, it has been shown that Aβ can interact with α7β2, α2β2, and α4 α5β2 nAChRs (31,40). Notably, nAChR agonists have consistently suggested promising approaches in the treatment of AD. However, clinical trials thus far have been challenged by adverse effects

or minimal improvement (112). Interestingly, many drugs that have been used in clinical trials target either the α7 receptor or a broad range of nAChRs, including α7, α4β2, α6β2, and α3β4 (112). Our finding that nonselective stimulation of nAChRs has adverse effects (Fig. 10) may explain why these drugs are failed. Importantly, we have confirmed combination treatment of c nAChR agonists is required to restore normal Ca^{2+} activity in Aβ-treated cells (Fig. 8). Thus, combination treatment of selective agonists leads to innovative and novel therapeutic strategies. Nonetheless, further studies are needed to better understand the role of each receptor agonist or combination treatment of agonists in cognitive function to develop more effective pharmacological treatments for AD.

Currently, there are 5 Alzheimer's drugs approved by U.S. Food and Drug Administration that treat the symptoms of AD, temporarily improving memory and cognitive processing concerns. However, these medications do not treat the underlying causes of the disease or slow its progression. Markedly, there are several drugs in development for AD with billions of dollars invested. Despite the massive investment in AD drugs targeting Aβ, there have been exponentially more failures than treatment successes, suggesting that the amyloid hypothesis can no longer be used in AD therapeutics (113). However, an argument has been made against whether these trials failed because Aβ actually is the wrong target by countering that the interventions were started too late in the progression of the disease (114). One possible reason is that the pharmacological intervention may be too late for the patients because the pathophysiological process of AD is thought to begin decades before the diagnosis (115). Therefore, there is a need to establish valid early AD biomarkers. Importantly, Aβ-induced hyperexcitability has interesting implications especially for seizure-like activity and epilepsy at the early stage of the disease pathogenesis, which are potentially linked to AD-associated cognitive impairment (6,7,15,116). In fact, in people at high risk of developing AD, abnormal activation of specific networks during memory processing can be detected decades before the predicted onset of clinical disease (117–120). This suggests hyperexcitation may be a

preclinical AD biomarker. Thus, our data provide a potential cellular mechanism underlying Aβ-induced hyperexcitability, which may lead to a novel therapeutic target for preclinical AD. Moreover, in the AD mouse model, Aβ can negatively affect GABAergic interneuron function in the hippocampus, which can lead to network hyperexcitability and eventual cognitive decline (17). Nonetheless, the mechanism of how Aβ disrupts interneuron function has not been fully understood. The present study provides not only a previously unidentified cellular mechanism underlying Aβ-induced dysfunction in interneurons but also a novel early therapeutic approach of combination treatment of α7 and α4β2 nAChR agonists.

REFERENCES

1. Selkoe DJ. Alzheimer's disease. Vol. 3, Cold Spring Harbor Perspectives in Biology. 2011.

2. Querfurth HW, LaFerla FM. Alzheimer's disease. N Engl J Med. 2010 Jan 28;362(4):329–44.

3. Holtzman DM, Mandelkow E, Selkoe DJ. Alzheimer disease in 2020. Cold Spring Harbor Perspectives in Medicine. 2012;2(11).

4. S.F. K, S.-C. C, W. Z, R.K.S. W, R. B, K. I. Early-onset network hyperexcitability in presymptomatic Alzheimer's disease transgenic mice is suppressed by passive immunization with anti-human APP/Aβ antibody and by mGluR5 blockade. Frontiers in Aging Neuroscience. 2017;

5. Noebels J. A perfect storm: Converging paths of epilepsy and Alzheimer's dementia intersect in the hippocampal formation. Epilepsia. 2011;52(SUPPL. 1).

6. Palop JJ, Chin J, Roberson ED, Wang J, Thwin MT, Bien-Ly N, et al. Aberrant Excitatory Neuronal Activity and Compensatory Remodeling of Inhibitory Hippocampal Circuits in Mouse Models of Alzheimer's Disease. Neuron. 2007;55(5).

7. Palop JJ, Mucke L. Epilepsy and cognitive impairments in alzheimer disease. Vol. 66, Archives of Neurology. 2009.

8. Friedman D, Honig LS, Scarmeas N. Seizures and Epilepsy in Alzheimer's Disease. Vol. 18, CNS Neuroscience and Therapeutics. 2012.

9. Brown JT, Chin J, Leiser SC, Pangalos MN, Randall AD. Altered intrinsic neuronal excitability and reduced Na+ currents in a mouse model of Alzheimer's disease. Neurobiology of Aging. 2011;32(11).

10. Busche MA, Eichhoff G, Adelsberger H, Abramowski D, Wiederhold KH, Haass C, et al. Clusters of hyperactive neurons near amyloid plaques in a mouse model of Alzheimer's disease. Science (1979). 2008;321(5896).

11. Busche MA, Chen X, Henning HA, Reichwald J, Staufenbiel M, Sakmann B, et al. Critical role of soluble amyloid-β for early hippocampal hyperactivity in a mouse model of Alzheimer's disease. Proc Natl Acad Sci U S A. 2012;109(22).

12. Harris JA, Devidze N, Verret L, Ho K, Halabisky B, Thwin MT, et al. Transsynaptic Progression of Amyloid-β-Induced Neuronal Dysfunction within the Entorhinal-Hippocampal Network. Neuron. 2010;68(3).

13. Hartley DM, Walsh DM, Ye CP, Diehl T, Vasquez S, Vassilev PM, et al. Protofibrillar intermediates of amyloid β-protein induce acute electrophysiological changes and progressive neurotoxicity in cortical neurons. Journal of Neuroscience. 1999;19(20).

14. Kuchibhotla K v., Goldman ST, Lattarulo CR, Wu HY, Hyman BT, Bacskai BJ. Aβ Plaques Lead to Aberrant Regulation of Calcium Homeostasis In Vivo Resulting in Structural and Functional Disruption of Neuronal Networks. Neuron. 2008;59(2).

15. Minkeviciene R, Rheims S, Dobszay MB, Zilberter M, Hartikainen J, Fülöp L, et al. Amyloid beta-induced neuronal hyperexcitability triggers progressive epilepsy. J Neurosci. 2009 Mar 18;29(11):3453–62.

16. Roberson ED, Halabisky B, Yoo JW, Yao J, Chin J, Yan F, et al. Amyloid-β/fyn-induced synaptic, network, and cognitive impairments depend on tau levels in multiple mouse models of alzheimer's disease. Journal of Neuroscience. 2011;31(2).

17. Verret L, Mann EO, Hang GB, Barth AMI, Cobos I, Ho K, et al. Inhibitory interneuron deficit links altered network activity and cognitive dysfunction in alzheimer model. Cell. 2012;149(3).

18. Puzzo D, Privitera L, Leznik E, Fà M, Staniszewski A, Palmeri A, et al. Picomolar amyloid-beta positively modulates synaptic plasticity and memory in hippocampus. J Neurosci. 2008 Dec 31;28(53):14537–45.

19. Hsieh H, Boehm J, Sato C, Iwatsubo T, Tomita T, Sisodia S, et al. AMPAR Removal Underlies Aβ-Induced Synaptic Depression and Dendritic Spine Loss. Neuron. 2006;52(5).

20. Kamenetz F, Tomita T, Hsieh H, Seabrook G, Borchelt D, Iwatsubo T, et al. APP Processing and Synaptic Function. Neuron. 2003;37(6).

21. DM W, I K, JV F, WK C, R A, MS W, et al. Naturally secreted oligomers of amyloid beta protein potently inhibit hippocampal long-term potentiation in vivo. Nature. 2002;416(6880).

22. Kadir A, Almkvist O, Wall A, Långström B, Nordberg A. PET imaging of cortical 11C-nicotine binding correlates with the cognitive function of attention in Alzheimer's disease. Psychopharmacology (Berl). 2006;188(4).

23. Nordberg A. Nicotinic receptor abnormalities of Alzheimer's disease: Therapeutic implications. Vol. 49, Biological Psychiatry. 2001.

24. Dani JA, Bertrand D. Nicotinic acetylcholine receptors and nicotinic cholinergic mechanisms of the central nervous system. Vol. 47, Annual Review of Pharmacology and Toxicology. 2007.

25. Jürgensen S, Ferreira ST. Nicotinic receptors, amyloid-β, and synaptic failure in Alzheimer's disease. In: Journal of Molecular Neuroscience. 2010.

26. Ji D, Lape R, Dani JA. Timing and location of nicotinic activity enhances or depresses hippocampal synaptic plasticity. Neuron. 2001;31(1).

27. Son JH, Winzer-Serhan UH. Expression of neuronal nicotinic acetylcholine receptor subunit mRNAs in rat hippocampal GABAergic interneurons. Journal of Comparative Neurology. 2008;511(2).

28. Arora K, Alfulaij N, Higa JK, Panee J, Nichols RA. Impact of sustained exposure to β-amyloid on calcium homeostasis and neuronal integrity in model nerve cell system expressing α4β2 Nicotinic acetylcholine receptors. Journal of Biological Chemistry. 2013;288(16).

29. Auld DS, Kar S, Quirion R. β-amyloid peptides as direct cholinergic neuromodulators: A missing link? Trends in Neurosciences. 1998;21(1).

30. Lambert MP, Barlow AK, Chromy BA, Edwards C, Freed R, Liosatos M, et al. Diffusible, nonfibrillar ligands derived from Aβ1-42 are potent central nervous system neurotoxins. Proc Natl Acad Sci U S A. 1998;95(11).

31. Liu Q, Huang Y, Xue F, Simard A, DeChon J, Li G, et al. A novel nicotinic acetylcholine receptor subtype in basal forebrain cholinergic neurons with high sensitivity to amyloid peptides. Journal of Neuroscience. 2009;29(4).

32. McLean CA, Cherny RA, Fraser FW, Fuller SJ, Smith MJ, Beyreuther K, et al. Soluble pool of Abeta amyloid as a determinant of severity of neurodegeneration in Alzheimer's disease. Ann Neurol. 1999 Dec;46(6):860–6.

33. Albuquerque EX, Pereira EFR, Alkondon M, Rogers SW. Mammalian nicotinic acetylcholine receptors: From structure to function. Vol. 89, Physiological Reviews. 2009.

34. Clementi F, Fornasari D, Gotti C. Neuronal nicotinic receptors, important new players in brain function. In: European Journal of Pharmacology. 2000.

35. Lindstrom JM. Nicotinic acetylcholine receptors of muscles and nerves: Comparison of their structures, functional roles, and vulnerability to pathology. In: Annals of the New York Academy of Sciences. 2003.

36. Hahm ET, Nagaraja RY, Waro G, Tsunoda S. Cholinergic Homeostatic Synaptic Plasticity Drives the Progression of Aβ-Induced Changes in Neural Activity. Cell Reports. 2018;24(2).

37. Wang HY, Lee DHS, D'Andrea MR, Peterson PA, Shank RP, Reitz AB. β-Amyloid1–42 Binds to α7 Nicotinic Acetylcholine Receptor with High Affinity. Journal of Biological Chemistry. 2000;275(8).

38. Wang HY, Lee DH, Davis CB, Shank RP. Amyloid peptide Abeta(1-42) binds selectively and with picomolar affinity to alpha7 nicotinic acetylcholine receptors. J Neurochem. 2000 Sep;75(3):1155–61.

39. Cecon E, Dam J, Luka M, Gautier C, Chollet AM, Delagrange P, et al. Quantitative assessment of oligomeric amyloid β peptide binding to α7 nicotinic receptor. British Journal of Pharmacology. 2019;176(18).

40. Lamb PW, Melton MA, Yakel JL. Inhibition of neuronal nicotinic acetylcholine receptor channels expressed in Xenopus oocytes by β-amyloid1-42 peptide. Journal of Molecular Neuroscience. 2005;27(1).

41. Liu Q, Huang Y, Shen J, Steffensen S, Wu J. Functional α7β2 nicotinic acetylcholine receptors expressed in hippocampal interneurons exhibit high sensitivity to pathological level of amyloid β peptides. BMC Neuroscience. 2012;13(1).

42. Wu J, Kuo YP, George AA, Xu L, Hu J, Lukas RJ. beta-Amyloid directly inhibits human alpha4beta2-nicotinic acetylcholine receptors heterologously expressed in human SH-EP1 cells. J Biol Chem. 2004 Sep 3;279(36):37842–51.

43. Liu Q, Kawai H, Berg DK. beta -Amyloid peptide blocks the response of alpha 7-containing nicotinic receptors on hippocampal neurons. Proc Natl Acad Sci U S A. 2001 Apr 10;98(8):4734–9.

44. Lombardo S, Maskos U. Role of the nicotinic acetylcholine receptor in Alzheimer's disease pathology and treatment. Vol. 96, Neuropharmacology. 2015.

45. Pettit DL, Shao Z, Yakel JL. beta-Amyloid(1-42) peptide directly modulates nicotinic receptors in the rat hippocampal slice. J Neurosci. 2001;21(1).

46. Pym L, Kemp M, Raymond-Delpech V, Buckingham S, Boyd CAR, Sattelle D. Subtype-specific actions of beta-amyloid peptides on recombinant human neuronal nicotinic acetylcholine receptors (alpha7, alpha4beta2, alpha3beta4) expressed in Xenopus laevis oocytes. Br J Pharmacol. 2005 Dec;146(7):964–71.

47. Kim S, Titcombe RF, Zhang H, Khatri L, Girma HK, Hofmann F, et al. Network compensation of cyclic GMP-dependent protein kinase II knockout in the hippocampus by Ca2+-permeable AMPA receptors. Proc Natl Acad Sci U S A. 2015;112(10).

48. Kim S, Violette CJ, Ziff EB. Reduction of increased calcineurin activity rescues impaired homeostatic synaptic plasticity in presenilin 1 M146V mutant. Neurobiology of Aging. 2015;36(12).

49. Kim S, Ziff EB. Calcineurin Mediates Synaptic Scaling Via Synaptic Trafficking of Ca2+-Permeable AMPA Receptors. PLoS Biology. 2014;12(7).

50. Sztukowski K, Nip K, Ostwald PN, Sathler MF, Sun JL, Shou J, et al. HIV induces synaptic hyperexcitation via cGMP-dependent protein kinase II activation in the FIV infection model. PLoS Biology. 2018 Jul 27;16(7).

51. Stine WB, Dahlgren KN, Krafft GA, LaDu MJ. In vitro characterization of conditions for amyloid-beta peptide oligomerization and fibrillogenesis. J Biol Chem. 2003 Mar 28;278(13):11612–22.

52. Sztukowski K, Nip K, Ostwald PN, Sathler MF, Sun JL, Shou J, et al. HIV induces synaptic hyperexcitation via cGMP-dependent protein kinase II activation in the FIV infection model. PLoS Biology. 2018;

53. Akerboom J, Chen TW, Wardill TJ, Tian L, Marvin JS, Mutlu S, et al. Optimization of a GCaMP calcium indicator for neural activity imaging. Journal of Neuroscience. 2012;32(40).

54. Chen TW, Wardill TJ, Sun Y, Pulver SR, Renninger SL, Baohan A, et al. Ultrasensitive fluorescent proteins for imaging neuronal activity. Nature. 2013;499(7458).

55. Dimidschstein J, Chen Q, Tremblay R, Rogers SL, Saldi GA, Guo L, et al. A viral strategy for targeting and manipulating interneurons across vertebrate species. Nature Neuroscience. 2016;19(12).

56. Newman RH, Zhang J. Visualization of phosphatase activity in living cells with a FRET-based calcineurin activity sensor. Molecular BioSystems. 2008;4(6).

57. Morris GP, Clark IA, Vissel B. Inconsistencies and Controversies Surrounding the Amyloid Hypothesis of Alzheimer's Disease. Vol. 2, Acta Neuropathologica Communications. 2014.

58. Jarosz-Griffiths HH, Noble E, Rushworth J v., Hooper NM. Amyloid-β receptors: The good, the bad, and the prion protein. Vol. 291, Journal of Biological Chemistry. 2016.

59. Hooper NM, Rushworth J v. Lipid rafts: Linking Alzheimer's amyloid-β production, aggregation, and toxicity at neuronal membranes. International Journal of Alzheimer's Disease. 2011.

60. Zott B, Simon MM, Hong W, Unger F, Chen-Engerer HJ, Frosch MP, et al. A vicious cycle of β amyloid−dependent neuronal hyperactivation. Science (1979). 2019;365(6453).

61. Ferreira ST, Klein WL. The Aβ oligomer hypothesis for synapse failure and memory loss in Alzheimer's disease. Vol. 96, Neurobiology of Learning and Memory. 2011.

62. Walsh DM, Selkoe DJ. Manuscript A beta oligomers - a decade of discovery. J Neurochem. 2007;101(5).

63. Gleichmann M, Mattson MP. Neuronal calcium homeostasis and dysregulation. Vol. 14, Antioxidants and Redox Signaling. 2011.

64. Diering GH, Huganir RL. The AMPA Receptor Code of Synaptic Plasticity. Vol. 100, Neuron. 2018.

65. Lee HK, Kameyama K, Huganir RL, Bear MF. NMDA induces long-term synaptic depression and dephosphorylation of the GluR1 subunit of AMPA receptors in hippocampus. Neuron. 1998;21(5).

66. Sanderson JL, Gorski JA, Gibson ES, Lam P, Freund RK, Chick WS, et al. Akap150-anchored calcineurin regulates synaptic plasticity by limiting synaptic incorporation of Ca2+-permeable AMPA receptors. Journal of Neuroscience. 2012;32(43).

67. Jones EG, Huntley GW, Benson DL. Alpha calcium/calmodulin-dependent protein kinase II selectively expressed in a subpopulation of excitatory neurons in monkey sensory-motor cortex: Comparison with GAD-67 expression. Journal of Neuroscience. 1994;14(2).

68. Ochiishi T, Terashima T, Yamauchi T. Specific distribution of Ca2+/calmodulin-dependent protein kinase II alpha and beta isoforms in some structures of the rat forebrain. Brain Res. 1994 Oct 3;659(1–2):179–93.

69. Benson DL, Cohen PA. Activity-independent segregation of excitatory and inhibitory synaptic terminals in cultured hippocampal neurons. Journal of Neuroscience. 1996;16(20).

70. Yi F, Catudio-Garrett E, Gábriel R, Wilhelm M, Erdelyi F, Szabo G, et al. Hippocampal “cholinergic interneurons” visualized with the choline acetyltransferase promoter: Anatomical distribution, intrinsic membrane properties, neurochemical characteristics, and capacity for cholinergic modulation. Frontiers in Synaptic Neuroscience. 2015;7(MAR).

71. H. Ferreira-Vieira T, M. Guimaraes I, R. Silva F, M. Ribeiro F. Alzheimer’s disease: Targeting the Cholinergic System. Current Neuropharmacology. 2016;14(1).

72. Chapman PF, White GL, Jones MW, Cooper-Blacketer D, Marshall VJ, Irizarry M, et al. Impaired synaptic plasticity and learning in aged amyloid precursor protein transgenic mice. Nature Neuroscience. 1999;2(3).

73. Hsia AY, Masliah E, Mcconlogue L, Yu GQ, Tatsuno G, Hu K, et al. Plaque-independent disruption of neural circuits in Alzheimer’s disease mouse models. Proc Natl Acad Sci U S A. 1999;96(6).

74. Jürgensen S, Antonio LL, Mussi GEA, Brito-Moreira J, Bomfim TR, de Felice FG, et al. Activation of D1/D5 dopamine receptors protects neurons from synapse dysfunction induced by amyloid-β oligomers. Journal of Biological Chemistry. 2011;286(5).

75. Shankar GM, Bloodgood BL, Townsend M, Walsh DM, Selkoe DJ, Sabatini BL. Natural oligomers of the Alzheimer amyloid-beta protein induce reversible synapse loss by modulating an NMDA-type glutamate receptor-dependent signaling pathway. J Neurosci. 2007 Mar 14;27(11):2866–75.

76. Whitcomb DJ, Hogg EL, Regan P, Piers T, Narayan P, Whitehead G, et al. Intracellular oligomeric amyloid-beta rapidly regulates GluA1 subunit of AMPA receptor in the hippocampus. Scientific Reports. 2015;5.

77. Sperling RA, LaViolette PS, O’Keefe K, O’Brien J, Rentz DM, Pihlajamaki M, et al. Amyloid Deposition Is Associated with Impaired Default Network Function in Older Persons without Dementia. Neuron. 2009;63(2).

78. Isaacson JS, Scanziani M. How inhibition shapes cortical activity. Vol. 72, Neuron. 2011.

79. Kullmann DM. Interneuron networks in the hippocampus. Vol. 21, Current Opinion in Neurobiology. 2011.

80. Bateup HS, Johnson CA, Denefrio CL, Saulnier JL, Kornacker K, Sabatini BL. Excitatory/Inhibitory Synaptic Imbalance Leads to Hippocampal Hyperexcitability in Mouse Models of Tuberous Sclerosis. Neuron. 2013;78(3).

81. Hefendehl JK, LeDue J, Ko RWY, Mahler J, Murphy TH, MacVicar BA. Mapping synaptic glutamate transporter dysfunction in vivo to regions surrounding Aβ plaques by iGluSnFR two-photon imaging. Nature Communications. 2016;7.

82. Nicholson KJ, Gilliland TM, Winkelstein BA. Upregulation of GLT-1 by treatment with ceftriaxone alleviates radicular pain by reducing spinal astrocyte activation and neuronal hyperexcitability. Journal of Neuroscience Research. 2014;92(1).

83. de Felice FG, Velasco PT, Lambert MP, Viola K, Fernandez SJ, Ferreira ST, et al. Aβ oligomers induce neuronal oxidative stress through an N-methyl-D-aspartate receptor-dependent mechanism that is blocked by the Alzheimer drug memantine. Journal of Biological Chemistry. 2007;282(15).

84. Guntupalli S, Jang SE, Zhu T, Huganir RL, Widagdo J, Anggono V. GluA1 subunit ubiquitination mediates amyloid-β-induced loss of surface α-amino-3-hydroxy-5-methyl-4-isoxazolepropionic acid (AMPA) receptors. Journal of Biological Chemistry. 2017;292(20).

85. Sinnen BL, Bowen AB, Gibson ES, Kennedy MJ. Local and use-dependent effects of β-Amyloid oligomers on NMDA receptor function revealed by optical quantal analysis. Journal of Neuroscience. 2016;36(45).

86. Dineley KT, Pandya AA, Yakel JL. Nicotinic ACh receptors as therapeutic targets in CNS disorders. Vol. 36, Trends in Pharmacological Sciences. 2015.

87. Parri HR. Nicotinic Acetylcholine Receptor Interaction with ß-Amyloid: Molecular, Cellular, and Physiological Consequences. Current Alzheimer Research. 2009;999(999).

88. Nery AA, Magdesian MH, Trujillo CA, Sathler LB, Juliano MA, Juliano L, et al. Rescue of Amyloid-Beta-Induced Inhibition of Nicotinic Acetylcholine Receptors by a Peptide Homologous to the Nicotine Binding Domain of the Alpha 7 Subtype. PLoS ONE. 2013;8(7).

89. Smith LM, Strittmatter SM. Binding Sites for Amyloid-β Oligomers and Synaptic Toxicity. Cold Spring Harb Perspect Med. 2017 May 1;7(5).

90. Jones S, Yakel JL. Functional nicotinic ACh receptors on interneurones in the rat hippocampus. Journal of Physiology. 1997;504(3).

91. Vizi ES, Lendvai B. Modulatory role of presynaptic nicotinic receptors in synaptic and non-synaptic chemical communication in the central nervous system. Vol. 30, Brain Research Reviews. 1999.

92. Feduccia AA, Chatterjee S, Bartlett SE. Neuronal nicotinic acetylcholine receptors: Neuroplastic changes underlying alcohol and nicotine addictions. Frontiers in Molecular Neuroscience. 2012.

93. Alkondon M, Albuquerque EX. Nicotinic acetylcholine receptor alpha7 and alpha4beta2 subtypes differentially control GABAergic input to CA1 neurons in rat hippocampus. J Neurophysiol. 2001 Dec;86(6):3043–55.

94. Zarei MM, Radcliffe KA, Chen D, Patrick JW, Dani JA. Distributions of nicotinic acetylcholine receptor alpha7 and beta2 subunits on cultured hippocampal neurons. Neuroscience. 1999;88(3):755–64.

95. Alkondon M, Albuquerque EX. A non-alpha7 nicotinic acetylcholine receptor modulates excitatory input to hippocampal CA1 interneurons. J Neurophysiol. 2002 Mar;87(3):1651–4.

96. Gray R, Rajan AS, Radcliffe KA, Yakehiro M, Dani JA. Hippocampal synaptic transmission enhanced by low concentrations of nicotine. Nature. 1996;383(6602).

97. Zhang J, Berg DK. Reversible inhibition of GABAA receptors by alpha7-containing nicotinic receptors on the vertebrate postsynaptic neurons. J Physiol. 2007 Mar 15;579(Pt 3):753–63.

98. Bali ZK, Nagy L v, Hernádi I. Alpha7 Nicotinic Acetylcholine Receptors Play a Predominant Role in the Cholinergic Potentiation of N-Methyl-D-Aspartate Evoked Firing Responses of Hippocampal CA1 Pyramidal Cells. Front Cell Neurosci. 2017;11:271.

99. Alkondon M, Pereira EF, Barbosa CT, Albuquerque EX. Neuronal nicotinic acetylcholine receptor activation modulates gamma-aminobutyric acid release from CA1 neurons of rat hippocampal slices. J Pharmacol Exp Ther. 1997 Dec;283(3):1396–411.

100. Frazier CJ, Buhler A v, Weiner JL, Dunwiddie T v. Synaptic potentials mediated via alpha-bungarotoxin-sensitive nicotinic acetylcholine receptors in rat hippocampal interneurons. J Neurosci. 1998 Oct 15;18(20):8228–35.

101. McQuiston AR, Madison D v. Nicotinic receptor activation excites distinct subtypes of interneurons in the rat hippocampus. Journal of Neuroscience. 1999;19(8).

102. Frotscher M, Léránth C. Cholinergic innervation of the rat hippocampus as revealed by choline acetyltransferase immunocytochemistry: A combined light and electron microscopic study. Journal of Comparative Neurology. 1985;239(2).

103. Frotscher M, Vida I, Bender R. Evidence for the existence of non-GABAergic, cholinergic interneurons in the rodent hippocampus. Neuroscience. 2000;96(1).

104. Mattson MP, Pedersen WA. Effects of amyloid precursor protein derivatives and oxidative stress on basal forebrain cholinergic systems in Alzheimer's disease. International Journal of Developmental Neuroscience. 1998;16(7–8).

105. Levin ED, Simon BB. Nicotinic acetylcholine involvement in cogitive function in animals. Vol. 138, Psychopharmacology. 1998.

106. Vicens P, Carrasco MC, Redolat R. Effects on early training and nicotine treatment on the performance of male NMRI mice in the water maze. Neural Plasticity. 2003;10(4).

107. Bitner RS, Bunnelle WH, Anderson DJ, Briggs CA, Buccafusco J, Curzon P, et al. Broad-spectrum efficacy across cognitive domains by alpha7 nicotinic acetylcholine receptor agonism correlates with activation of ERK1/2 and CREB phosphorylation pathways. J Neurosci. 2007 Sep 26;27(39):10578–87.

108. Cincotta SL, Yorek MS, Moschak TM, Lewis SR, Rodefer JS. Selective nicotinic acetylcholine receptor agonists: Potential therapies for neuropsychiatric disorders with cognitive dysfunction. Vol. 9, Current Opinion in Investigational Drugs. 2008.

109. Redrobe JP, Nielsen E, Christensen JK, Peters D, Timmermann DB, Olsen GM. α7 nicotinic acetylcholine receptor activation ameliorates scopolamine-induced behavioural changes in a modified continuous Y-maze task in mice. European Journal of Pharmacology. 2009;602(1).

110. Vicens P, Ribes D, Torrente M, Domingo JL. Behavioral effects of PNU-282987, an alpha7 nicotinic receptor agonist, in mice. Behavioural Brain Research. 2011;216(1).

111. Levin ED, Christopher NC. Persistence of nicotinic agonist RJR 2403-induced working memory improvement in rats. Drug Development Research. 2002;55(2).

112. Hoskin JL, Al-Hasan Y, Sabbagh MN. Nicotinic acetylcholine receptor agonists for the treatment of Alzheimer's dementia: An update. Nicotine and Tobacco Research. 2019;21(3).

113. Huang YM, Shen J, Zhao HL. Major Clinical Trials Failed the Amyloid Hypothesis of Alzheimer's Disease. J Am Geriatr Soc. 2019;67(4).

114. McDade E. Reply to: Major Clinical Trials Failed the Amyloid Hypothesis of Alzheimer's Disease. J Am Geriatr Soc. 2019;67(4).

115. Mehta D, Jackson R, Paul G, Shi J, Sabbagh M. Why do trials for Alzheimer's disease drugs keep failing? A discontinued drug perspective for 2010-2015. Expert Opinion on Investigational Drugs. 2017;26(6).

116. Bakker A, Krauss GL, Albert MS, Speck CL, Jones LR, Stark CE, et al. Reduction of Hippocampal Hyperactivity Improves Cognition in Amnestic Mild Cognitive Impairment. Neuron. 2012;74(3).

117. Bateman RJ, Xiong C, Benzinger TLS, Fagan AM, Goate A, Fox NC, et al. Clinical and Biomarker Changes in Dominantly Inherited Alzheimer's Disease. New England Journal of Medicine. 2012;367(9).

118. Filippini N, MacIntosh BJ, Hough MG, Goodwin GM, Frisoni GB, Smith SM, et al. Distinct patterns of brain activity in young carriers of the APOE-ε4 allele. Proc Natl Acad Sci U S A. 2009;106(17).

119. Mondadori CRA, Buchmann A, Mustovic H, Schmidt CF, Boesiger P, Nitsch RM, et al. Enhanced brain activity may precede the diagnosis of Alzheimer's disease by 30 years. Brain. 2006;129(11).

120. Reiman EM, Quiroz YT, Fleisher AS, Chen K, Velez-Pardo C, Jimenez-Del-Rio M, et al. Brain imaging and fluid biomarker analysis in young adults at genetic risk for autosomal dominant Alzheimer's disease in the presenilin 1 E280A kindred: A case-control study. The Lancet Neurology. 2012;11(12).

121. Sun JL, Stokoe SA, Roberts JP, Sathler MF, Nip KA, Shou J, et al. Co-activation of selective nicotinic acetylcholine receptors is required to reverse beta amyloid-induced Ca2+ hyperexcitation. Neurobiology of Aging. 2019 Sep;